Investigation of Close Proximity Underwater Explosion Effects on a Ship-Like Structure Using the Multi-Material Arbitrary Lagrangian Eulerian Finite Element Method

Keith G. Webster

A thesis submitted to the Faculty of

Virginia Polytechnic Institute and State University

in partial fulfillment of the requirements for the degree of

MASTER OF SCIENCE

in

Ocean Engineering

Dr. Alan J. Brown, Chairman
Dr. Wayne L. Neu
Dr. Owen F. Hughes

January 29, 2007
Blacksburg, Virginia

Keywords: UNDEX, Proximity, Fluid/Structure Interaction, MMALE, US Navy Blast Test, Sandwich Plate System (SPS)

Investigation of Close Proximity Underwater Explosion Effects on a Ship-Like Structure Using the Multi-Material Arbitrary Lagrangian Eulerian Finite Element Method

Keith G. Webster

Abstract

This thesis investigates the characteristics of a close proximity underwater explosion and its effect on a ship-like structure. Finite element model tests are conducted to verify and validate the propagation of a pressure wave generated by an underwater explosion through a fluid medium, and the transmission of the pressure wave in the fluid to a structure using the Multi-Material Arbitrary Lagrangian/Eulerian method. A one dimensional case modeling the detonation of a spherical TNT charge underwater is investigated. Three dimensional cases modeling the detonation of an underwater spherical TNT charge, and US Navy Blast Test cases modeling a shape charge and a circular steel plate, and a shape charge and a Sandwich Plate System (SPS) are also investigated. This thesis provides evidence that existing tools and methodologies have some capability for predicting early-time/close proximity underwater explosion effects, but are insufficient for analyses beyond the arrival of the initial shock wave. This thesis shows that a true infinite boundary condition, a modified Gruneisen equation of state near the charge, and the ability to capture shock without a very small element size is needed in order to provide a sufficient means for predicting early-time/close proximity underwater explosion effects beyond the arrival of the initial shock wave.

Dedication

To

My fiancée Kathleen C. Brittain, my mother Jeneane S. Webster, and my father Larry G. Webster for their love and support. Without it, none of this would have been possible.

Acknowledgements

I would like to thank Dr. Alan J. Brown and Dr. John A. W. Sajdak for their assistance, guidance, and expertise. Your patience and understanding is greatly appreciated.

TABLE OF CONTENTS

TABLE OF FIGURES

CHAPTER 1 INTRODUCTION

1.1 Motivation and Background For Total Ship Survivability

1.1.1 Definition of Survivability

To understand the study of ship vulnerability and explosion analysis it is important to have an overall perspective of the larger system problem that is total ship survivability. The standard OPNAV instruction definition for survivability is: "the capacity of the total ship system to avoid and withstand damage and maintain and/or recover mission integrity [1]". There are three key elements in the OPNAV definition of survivability as shown by Equation (1),

$$S = 1 - P_h P_{k/h} \left(1 - P_{r/k}\right) \tag{1}$$

where S is the probability of survival of a naval ship, P_h is the probability of being hit by a weapon (susceptability), $P_{k/h}$ is the probability of a kill or loss of mission capability given a hit (vulnerability), and $P_{r/k}$ is the probability of recovery given a specific kill or loss (recoverability). Figure 1 shows a Survivability Time-line that illustrates the survivability processes and how the mission capability of the ship is affected over time.

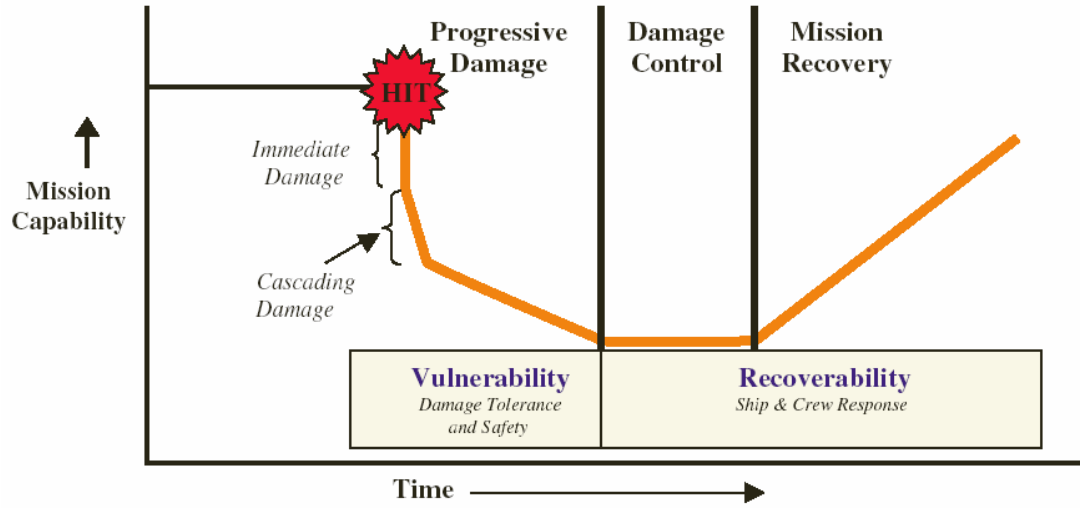

Figure 1 - Survivability Time-line [32]

The first important element of total ship survivability is susceptability, P_h. Susceptability is the probability of a ship being hit by a threat weapon [1]. There are active and passive methods to avoid hits. Passive methods depend on the ability of the ship not to be detected. Passive methods include minimizing the ships' signatures (radar cross-section, acoustic, magnetic, and

thermal signatures). Active methods include Electronic Warfare (SEW) (early detection of threats, radar jamming techniques), maneuvering (the ability to get out of the way), the ability to strike the attacker, and the ability to intercept potential weapon threats after the weapon has been launched, but before it hits the ship. These final capabilities fall under the category of combat systems and Ship Self Defense Systems (SSDS). Shipboard combat systems may include Anti-Air Warfare (AAW), Anti-Submarine Warfare (ASW), Anti-Surface Ship Warfare (ASUW), Electronic Warfare (SEW) using Decoy Launching Systems (DLS), and Mine Countermeasures (MCM). In the Survivability Time-line in Figure 1, susceptability involves the period of time before a hit occurs.

The second important element of total ship survivability is vulnerability, $P_{k/h}$. Vulnerability is the conditional probability given a hit that some level of damage will occur or capability will be lost [1]. This probability must consider the full range of threat weapons, energies, and strike or stand-off locations. Examples of different threats are covered in Section 1.1.2. Vulnerability is the passive capability of the ship structure and system designs to withstand and minimize the physical damage associated with being hit by an enemy weapon. It assumes that the ship has already been hit, P_h, and that the ship has some ability to withstand damage, $(1-P_{k/h})$. Figure 1 shows that once the ship is hit, there is some immediate damage followed by cascading damage. Cascading damage results from the immediate damage and can include fire, progressive flooding and various progressive explosions. The extent to which the cascading damage occurs is categorized as progressive damage.

The ability to withstand damage and continue to perform the ship's mission capabilities is very important for a naval ship. Mission capabilities are typically categorized as primary mission capabilities and secondary mission capabilities. Some of a naval ships primary capabilities are: ship control and propulsion; command and control; navigation; surface, air, and underwater surveillance; countermeasures; launch, recover, fuel, rearm aircraft and small craft; essential maintenance of aircraft and ordnance; weapons stowage, control, launch, and guidance; replenish at sea; minehunting and sweeping; combat payload transport; casualty and damage control; collective protection system. All of these are essential and required operational capabilities associated with the various missions of a particular ship. There are different extents of loss for the ships mission capabilities. There are categories of loss and degrees of loss given in standard naval casualty reports for loss of mission capabilities. The loss of any of these capabilities is considered a casualty, and all are integrated in the definition of ship vulnerability.

The third important element of total ship survivability is recoverability, $P_{r/h}$. Recoverability is the probability given a particular damage or hit of a ship to recover from this damage [1]. At this point the ship has been struck by an enemy weapon and the destructive effects of the weapon have already occurred. Recoverability measures the ability of the ship to control, stop, and recover from the damage caused by an enemy weapon and save itself in terms of mission capability, not sinking, and minimizing loss of life. The recoverability phase in Figure 1, includes damage control, initial repair of the ship, and gradual mission recovery.

1.1.2 Threats

There are many different types of threats a naval ship can encounter. The number of possibilities of different types of weapons systems and different types of damage each weapon can inflict on a ship are large. Figure 2 shows a summary of some of the major casualties due to weapons that have been encountered by US Navy ships in the recent past. Figure 2 shows that the main threat has been due to mines. Explosive threats can be categorized as underwater explosions (UNDEX) and air explosions (AIREX). They can also be categorized by whether they are internal or external to the ship and if external, how far away they are from the ship. The main threat that this thesis is concerned with are external close proximity underwater explosions and the resulting damage.

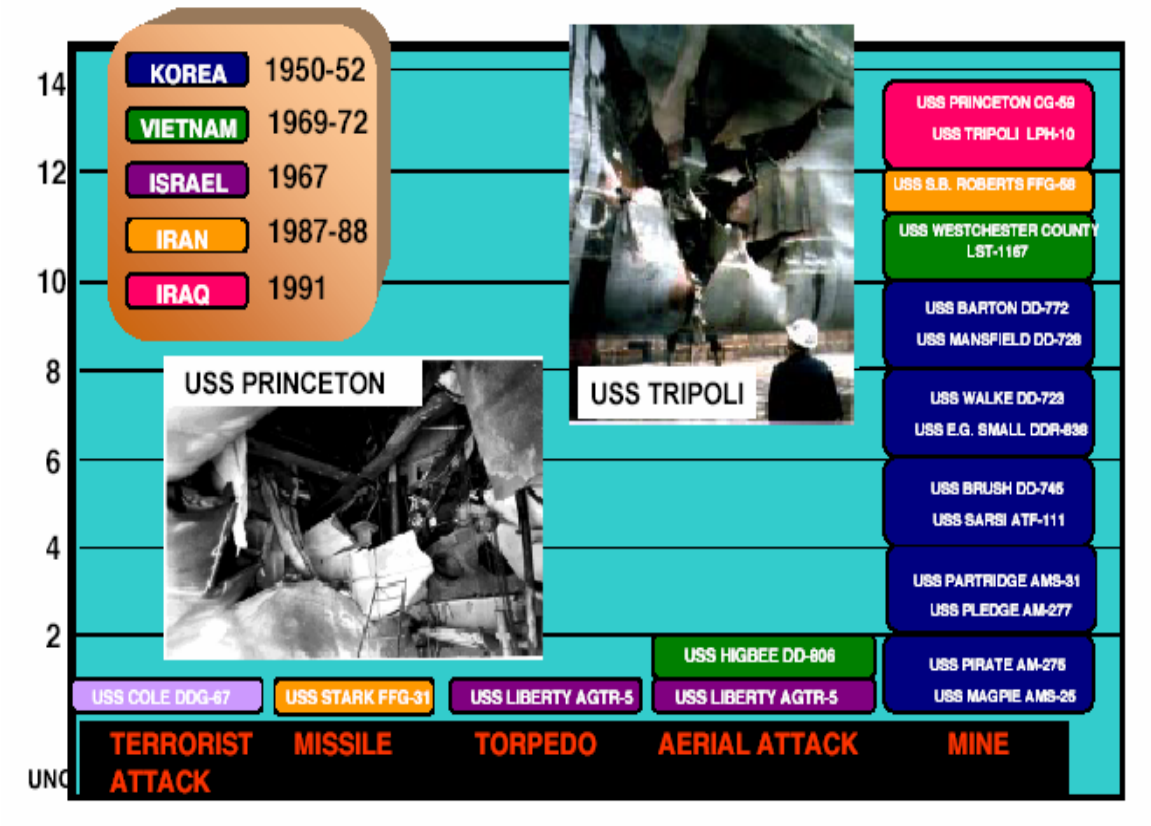

Figure 2 - US Navy Ship Casualties Since 1950 [32]

Some of the ship casualties in Figure 2 that were a result of UNDEX events due to various types of mines are discussed in more detail in Section 1.1.2.1 through Section 1.1.2.3. Figure 3 shows different types of mine threats and how they are used at various depths underwater. Section 1.1.2.5 discusses the attack on the USS Cole. This attack was unique in that the damage was caused by an AIREX and UNDEX event. Section 1.1.2.6 discusses the AIREX events that occurred in the attack on the USS Stark. Damage on a ship caused by an AIREX and UNDEX event can be a result of an internal or external explosion. Damage can also by caused by fragmentation. Section 1.1.2.7 discusses internal explosions and fragmentation.

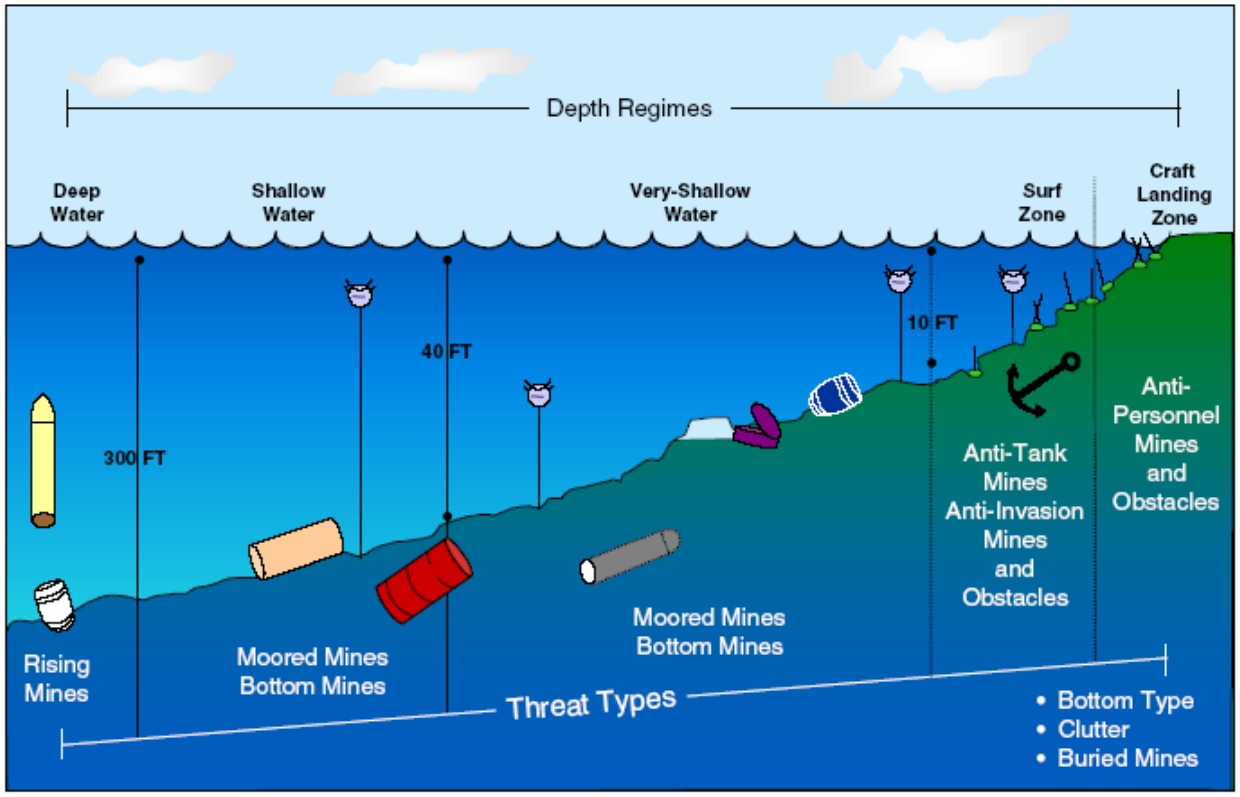

Figure 3 - Sea Mine Threats By Water Depth [2]

1.1.2.1 USS Tripoli – Contact Mines - Blast

The USS Tripoli was a helicopter carrier used in the Persian Gulf War in the 1990's. The damage shown in Figure 4 and Figure 5 was caused by an Iraqi Pattern 1908 contact mine. The local extent of damage was a 20 by 30 foot hole in the side shell plating on the starboard bow of the ship and minimal interior damage. Figure 4 and Figure 5 show the classic petal pattern typically found in plate rupture. The side shell of the ship ruptured as a result of the material fatigue caused by the high temperatures involved in the chemical reaction of the high explosive material and the impact load generated by the shock wave. There was no bubble pulse loading since the explosive gas bubble was vented out through the free surface of the water.

Figure 4 - USS Tripoli – Contact Mine [34]

Figure 5 - USS Tripoli – Contact Mine [3]

1.1.2.2 USS Princeton – Bottom Mines [4] – Shock and Bubble Pulse

At 07:16 on February 18th, 1991, the USS Princeton detonated an Italian-made MRP acoustic mine (not a Manta as has often been reported - MRP is a much heavier and more dangerous weapon) on the seabed 16 feet under the ship's stern. The gas bubble from the explosion spread underneath the ship's keel, lifting the fantail nearly out of the water. The bubble pulse vibrated

against the ship's hull, striking repeated blows and transferring large volumes of energy into the structure. The shock waves traveled from stern to bow, whipping the ship along its longitudinal axis so that the bow and stern shuddered, heaved and fell in a very rapid cycle. Crewmen were hurled off their feet into bulkheads and into the overhead. The blast also detonated another MRP-80 mine three hundred yards off the starboard beam. This added a horizontal component to the vertical shockwaves buffeting Princeton.

Some idea of the ship's gyrations at this point can be judged by the fact that a gunner on a 25 mm mount amidships looked up at the mooring chocks on the fantail as it arched upwards. The decks in the forward superstructure had vertical and horizontal deflections of four to six feet on a cycle of six to seven seconds. Spring bearings on both prop shafts were knocked out of alignment. Fuel tank covers were thrown loose and the aft five inch magazine was flooded with fuel oil.

The structural damage was devastating. At frame 72, forty feet from the stern, the shock had snapped steel girders. The main deck heaved upward twenty degrees, nearly severing the fantail from the rest of the ship. At frame 260, a six-inch crack opened in the Princeton's aluminum superstructure, running from the doorway to the Aegis radar room on the main deck, up through the radio room and down the other side of the ship. More than ten percent of the ship's superstructure separated from the main deck. There was major hull plate buckling all along the ship's length.

Steel teeth snapped from the elevation drive on the aft gun mount. Restraining bolts broke from several missile launchers on the fantail and four Harpoons burst through their membrane coverings before sliding back into the launcher tubes. In the crypto vault, where the ship's classified documents were stored, the shock sheared away 22 bolts fastening the door frame to a bulkhead, tossing the frame and its thick steel door twenty feet down a corridor.

Unlike the USS Tripoli, hit earlier by a Pattern 1908 contact mine, the Princeton's hull was not holed, but the ship still began flooding through fractures, burst welds, split seals etc. The shock had severed a six-inch fire main at Frame 472, spraying tons of sea water into the stern and swamping number 3 electrical switchboard. The ship's chill-water pipes, used to cool radar and other equipment, also ruptured. Within minutes the overheated Aegis system shut down, blinding the ship and leaving her without AAW warfare capability. Contrary to some reports, the ship was incapable of any significant combat functions at this point. It would be two hours before the AAW systems could be brought back on line.

Princeton had been turning to starboard, and the blast jammed the port rudder, leaving the ship out of control. A damage control team tried without success to manually crank the damaged rudder back to center line but their efforts were disrupted by an urgent order to abandon the after steering room because of fears that the fantail was about to tear away from the ship. Other damage teams clamped the ruptured fire mains and began pumping out flooded compartments while repairmen cut through a steel deck with torches, patched the leaks, and restored the Aegis system less than two hours after the explosions. The rudder problem was corrected by wrapping a long chain around the rudder post and yanking the port rudder into proper alignment by brute force.

The USS Princeton was left dead in the water, able (just) to fight but incapable of movement. Any further stress on her fragile hull and fractured superstructure, either from another mine or simply the vibration of her engines, could be catastrophic. Eighty percent of the structural strength of the ship had been destroyed, raising the possibility that the stern could suddenly fill with water and drag the cruiser to the bottom. The ship's propulsion system was so badly damaged that it was feared that it would detonate additional mines if the engines were started. Although all four gas turbines were functional, it was decided to tow her out of danger. A year later, both main reduction gears failed due to damage from the mines. The small picture in the lower left side of Figure 2 shows some of the damage done to the USS Princeton.

The damage to the USS Princeton is very different from the USS Tripoli (Section 1.1.2.1). The dynamic effects of the bubble pulse loading greatly increased the total damage to the ship. The combination of bubble pulse loading and the shock load from a proximity mine can generate significantly more damage than the shock and blast load from a side impacting contact mine.

1.1.2.3 USS Samuel B. Roberts – Contact Mine - Blast

On April 14, 1988 in the Persian Gulf, the USS Samuel B. Roberts hit a mine while using auxiliary-propulsion units to back down its original wake. The mine contained an estimated 250 pounds of TNT, which lifted the ship 10 feet and blew a hole under the starboard main engine (Figure 6). That hole measured 9 feet in diameter. Figure 7 shows the mine also tore a gash 22 feet long in the ship's port side. The blast knocked both main-propulsion gas turbines off their foundations. It also shoved the 40-ton main-reduction gear up and back, pulling the turbine shaft back and eliminating ship's propulsion. Pieces of auxiliary machinery that had been bolted and welded in the bilges were impaled in the overhead. Other damage included buckled and cracked

decks above the main engine room and a bent, twisted keel. Figure 8 shows the ship in drydock for repairs. The damage to the USS Samuel B. Roberts is a combination of the previous 2 involving blast, rupture and bubble effects from an under keel contact mine.

Figure 6 - USS Samuel B. Roberts – Contact Mine Damage Under Keel [35]

Figure 7 - USS Samuel B. Roberts – Close-up of Contact Mine Damage [34]

Figure 8 - USS Samuel B. Roberts – Contact Mine [32]

Figure 9 illustrates how the size and cost of the explosive weapon is not as important as where the weapon impacts the ship by comparing the cost of the mine that impacted the ship to the cost of repairing the ship.

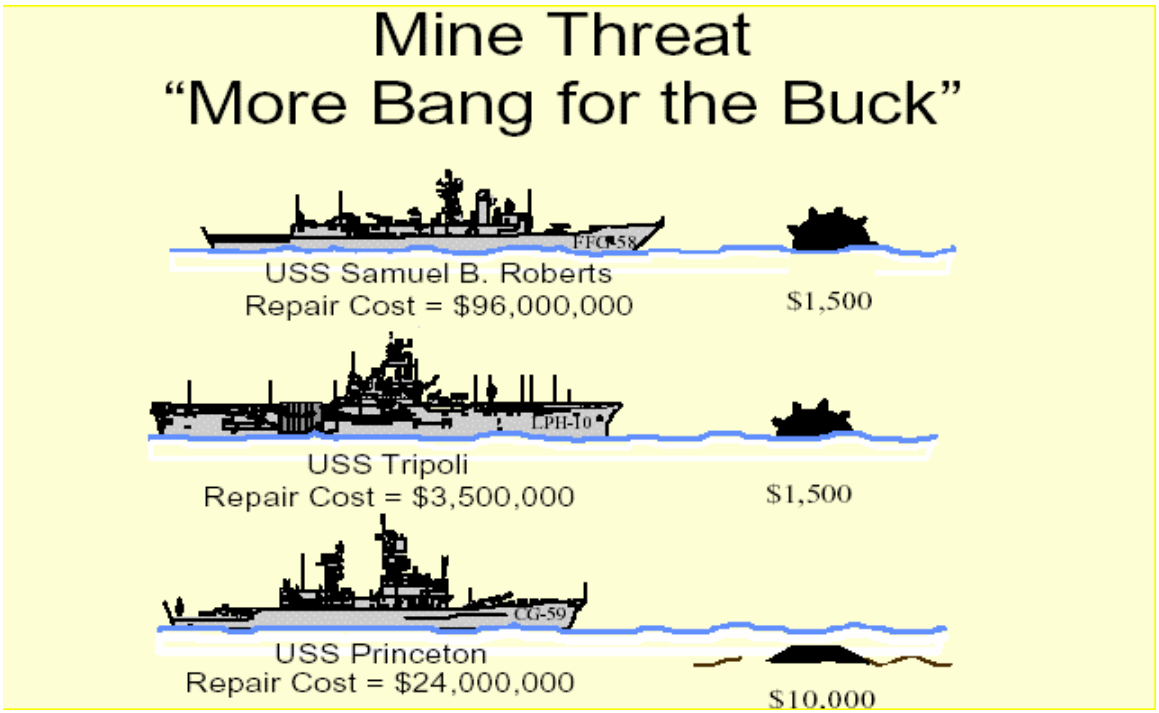

Figure 9 - Comparison of Threat Cost to Damage Repair Cost [32]

1.1.2.4 Australian Naval Ship – Gas Bubble

The Australian Navy conducted an underwater explosion test on one of its ships. The test consisted of a MK 46 torpedo detonated under the keel of the ship. Figure 10 shows the

sequence of events of the under keel torpedo test. Figure 10 shows the dramatic effect the under keel explosion has on lifting the ships hull out of the water in a hogging motion and then crashing down in a sagging motion and ultimately breaking the ship in half. The shockwave and the gaseous bubble generated by the underwater explosion both contribute to the damage of the ship. The interaction of the shockwave, bubble, and structure are discussed in Section 1.2.

Figure 10 - Australian Navy MK 46 Torpedo Test (Under Keel) [32]

1.1.2.5 USS Cole – AIREX and UNDEX Contact Explosion

The USS Cole was attacked in Aden Harbor, Yemen, on October 12, 2000. While the ship was refueling offshore, a small craft approached the ship and exploded. The small boat is believed to have been packed with 400-700 pounds of explosives, and the blast blew a 40-foot by 60-foot hole in the side of the USS Cole. Figure 11, Figure 12, and Figure 13 show the damage caused by the explosion that occurred at the waterline of the USS Cole. This type of explosion is unique in that it is an air explosion and an underwater explosion. The physics involved in such an event are complex and trying to predict the structural response to this type of problem is difficult.

Figure 12 shows that the area of damage below the ships waterline is larger than the area of damage above the waterline.

Figure 11 - USS Cole – AIREX and UNDEX Contact Explosion [32]

Figure 12 - USS Cole – AIREX and UNDEX Contact Explosion Showing Damage Above and Below the Waterline [32]

Figure 13 - USS Cole AIREX and UNDEX Contact Explosion [32]

1.1.2.6 USS Stark – AIREX Penetrating Internal Explosion

The USS Stark was struck by two Anti-Shipping AM-39 Exocet Missiles. The first missile punched through the port side hull, eight feet above the waterline (Figure 14). The missile severed the firefighting water main for the forward part of the ship. It then split into two pieces and tore through the ship on a 35-degree diagonal filling the crew sleeping quarters with burning rocket fuel and throwing shrapnel throughout. The shrapnel had a devastating affect on the internal structure of the ship. The warhead did not explode but tore through seven bulkheads and came to rest at the starboard hull. Thirty seconds later, a second missile hit the port hull eight feet forward of the previous missiles entry point. The warhead exploded and ignited an inferno that flashed through the sleeping quarters, burning over 3500 degrees. Figure 15 and Figure 16 show the 11.5 degree portside list caused by flooding as a result of the broken water main.

Figure 14 - USS Stark – Penetrating Internal Air Explosion [32]

Figure 15 - USS Stark Shown with a List Due to Compartment Flooding [32]

Figure 16 - USS Stark Damaged by 2 Exocet Missiles [32]

1.1.2.7 Internal Blast and Fragmentation Damage

The effects of a weapon threat penetrating and exploding internally are demonstrated in the USS Stark case in Section 1.1.2.6. Internal explosions can have a significant impact on the damage to a ship. Figure 17 shows an internal explosion test on a ship-like structure that is designed to minimize or withstand damage caused by an internal explosion. It shows that the effects are still significant. A method to determine limits and extent of damage caused by an internal explosion are shown in Figure 18. This method accounts for multiple compartment damage based on the hole size generated by the penetration of the weapon.

Figure 17 - Hardened Structure Test [32]

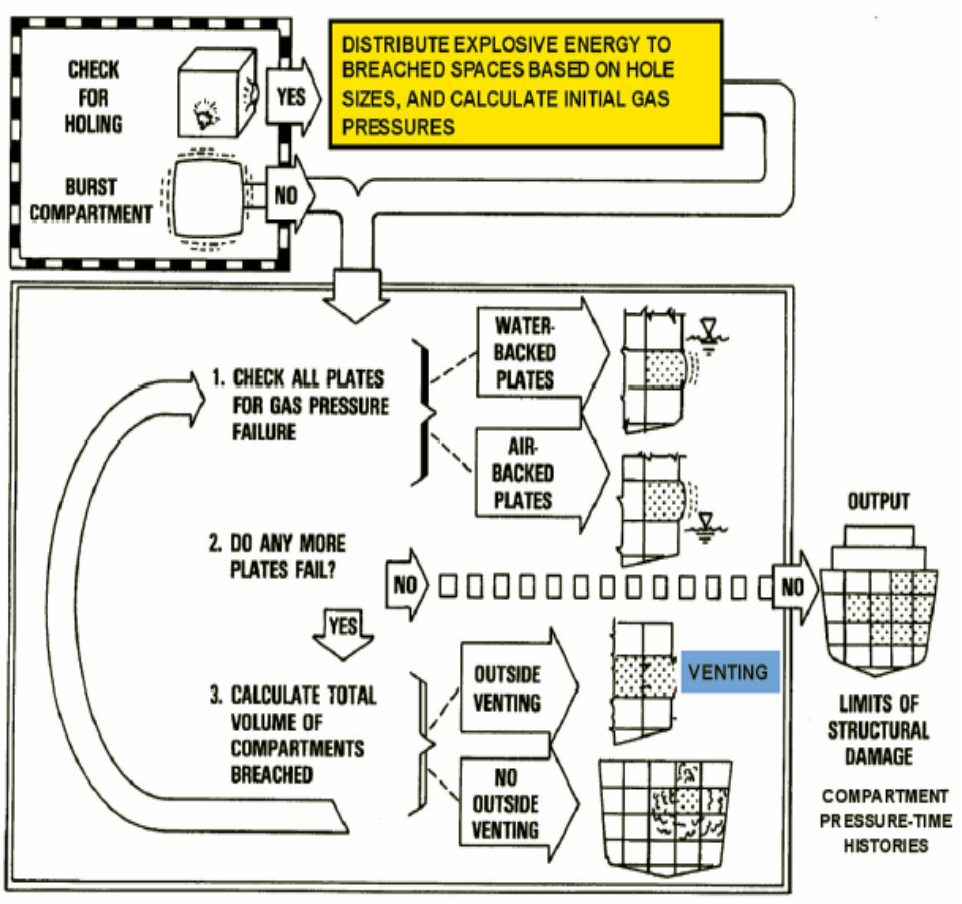

Figure 18 - Internal Blast Damage Diagram [32]

Fragmentation can have a devastating affect on the ship structure, equipment, and personal. This is described in the USS Stark case in Section 1.1.2.6. Fragmentation damage can be significant from both internal and external explosive bursts. Figure 19 shows a diagram fragmentation and of assessing the affect of fragmentation in the overall vulnerability of a ship.

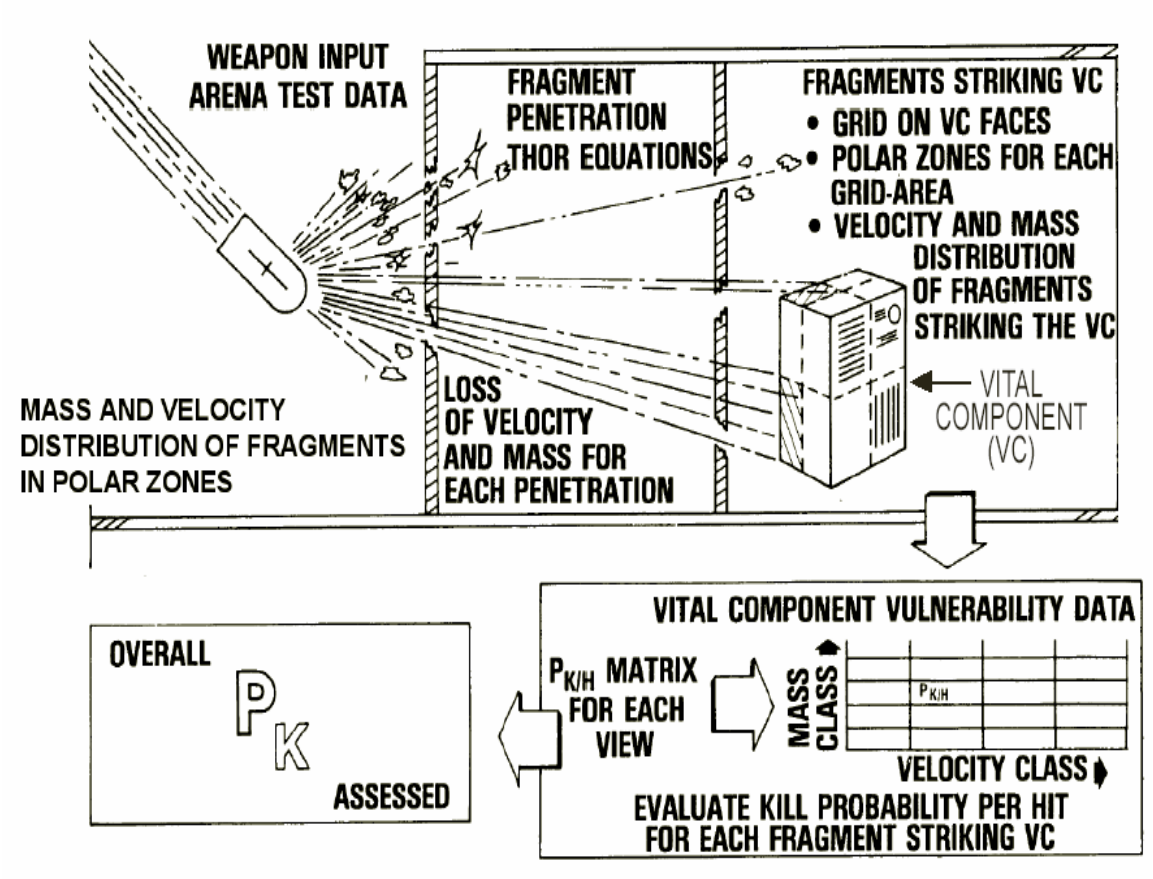

Figure 19 - Fragment Vulnerability Diagram [32]

This indicates the explosion damage is not the only significant form of damage and that damage due to fragmentation and internal explosions needs to be accounted for in the vulnerability assessment.

1.1.3 Probabilistic Vulnerability Analysis

Total ship survivability vulnerability analysis needs to be a probabilistic analysis. The survival/explosion event is a probabilistic event. There are numerous threats (AIREX, UNDEX, Penetrating, Contact), locations (External, Internal, Under-keel), and types of weapons (Mines, Missiles, Torpedo's, Bulk Explosives) that produce different levels of energy that have a different affect on the damage inflicted on a ship. Section 1.1.2 describes some of the possible

scenarios that a ship may likely encounter. There are many other scenarios that can cause major damage. A method that can analyze and quantify various threat scenarios for a particular ship design is needed. Figure 20 is a diagram of the process of developing a Measure of Performance (MOP) for vulnerability of a ship that would be used in a ship design optimization code. Figure 20 shows the elements and the complexity involved in the problem of assessing the vulnerability of a ship.

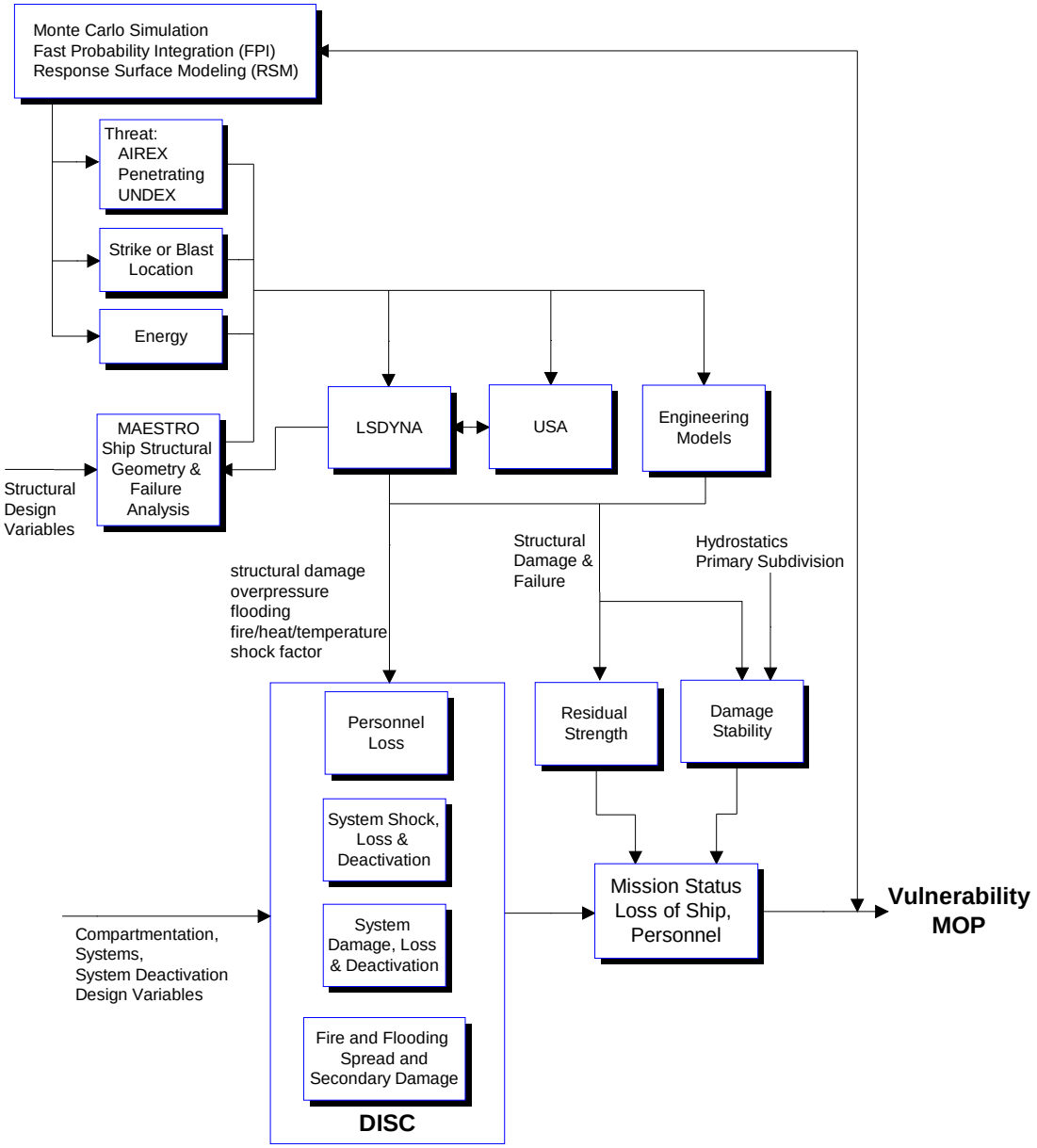

Figure 20 - Development of Vulnerability Measure of Performance [32]

1.1.4 Conclusions from Recent Casualties

Sections 1.1.2.1 through 1.1.2.7 discuss specific cases of damage caused by different types of underwater explosions. This thesis will focus on proximity underwater explosions.

1.2 Underwater Explosion Event

The general underwater explosion problem begins with an explosive charge of a certain size and material located at a depth below the free surface of the water surrounding it. The water is assumed to behave as a compressible fluid that is incapable of supporting significant tension. The ship is on the free surface of the water, and depending on the location of the explosive relative to the ship, the explosive may be classified as a near-field or far-field explosion. The important result of the explosion are the ship's early and late time response. The definition of a far-field underwater explosion and a near-field underwater explosion is given at the conclusion of this section; however it is important to first understand the phenomena of a generic underwater explosion.

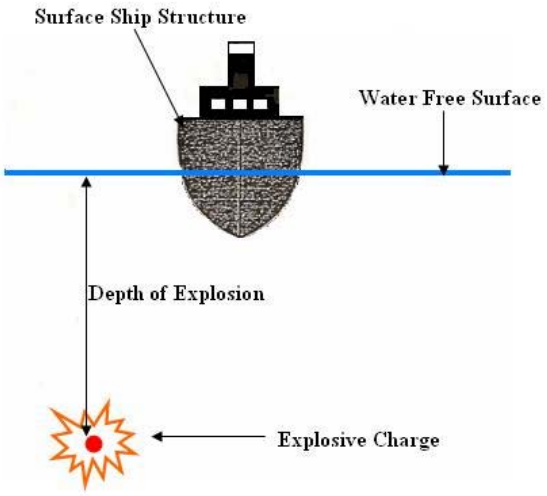

Figure 21 - General Setup of Underwater Explosion Problem [33]

The general sequence of events of an underwater explosion begins with the chemical reaction of the explosive material. This chemical reaction takes place in two parts: the initial chemical reaction and the detonation process. Prior to the start of the explosive process the explosive material is an unstable chemical substance in a gas, solid, or liquid state [5]. An initial chemical reaction both exothermic and rapid in nature is started by the transfer of energy (most commonly heat energy) to the explosive material [5]. The mechanism that initially transfers energy to the

explosive material is called the “detonator” or “igniter”. The detonator is made from a more sensitive explosive material than the primary explosive material in the charge. As the explosive material is ignited, it reacts and releases energy, and is transformed into a more stable state. The product of the reaction is a hot gas at a very high pressure [6]. This chemical reaction is called an explosion or explosive reaction.

If the pressure created by the initial chemical reaction is large enough a thermo-mechanical shock wave, referred to as the “detonation wave”, is created. In the detonation process, the detonation wave propagates at a supersonic speed through the explosive material still in its original state generating intense heat. The intense heat sets off new explosive reactions in the unreacted material as the wave passes through, making the detonation process self-sustaining [5].

The gaseous products (the converted gas behind the detonation wave) generated by the detonation process have no time to expand due to the high propagation speed of the detonation wave. As a result the gaseous products are continually heated and cannot relieve pressure through expansion. Therefore the pressures in the gas behind the detonation wave reach magnitudes in the range of 2 to 4 million psi [5, 6]. The pressure reached in the gaseous products is termed the “detonation pressure” or the “Chapman-Jouguet” pressure. This pressure is a constant, dependent on the type of explosive material used [5]. These extreme pressures are the driving force behind the rapid propagation of the detonation wave. Because of this the chemical reactions of the detonation process can be assumed to occur instantaneously for engineering purposes [5].

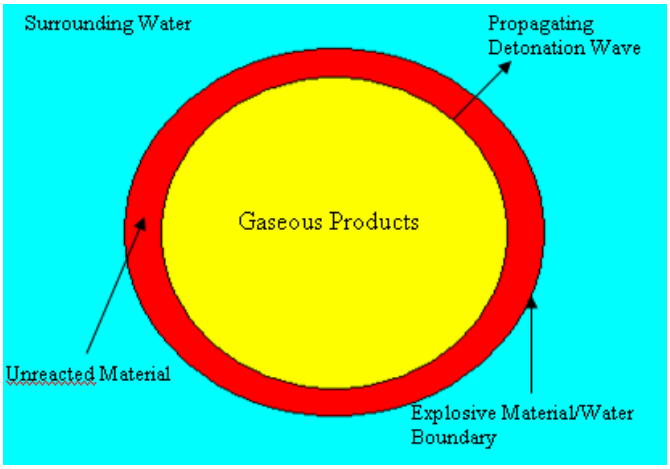

Figure 22 - Underwater Explosion During Detonation Process [31]

When the detonation wave reaches the explosive material/water boundary all unreacted material has been converted to gas. The gaseous products now make up a very dense, superheated, and

spherical gas bubble. At this time the detonation process of the underwater explosion is complete.

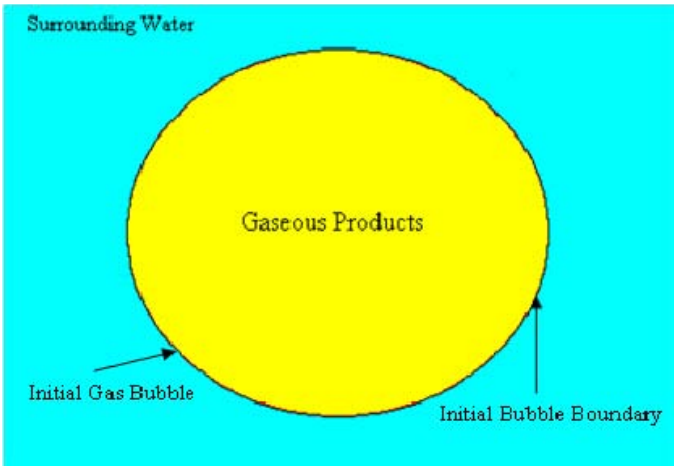

Figure 23 - Underwater Explosion at Instant of Detonation Process Completion [31]

The immense pressure inside the initial gas bubble is initially alleviated by the generation of a large compressive pressure wave and a resulting outward flow of water. This pressure wave created by the arrival of the detonation wave at the boundary is termed the "shock wave".

The shock wave shape is characterized by a nearly discontinuous rise in pressure followed by a brief period (a few milliseconds) of exponential decay [6]. The maximum pressure reached by the shock wave is termed the "peak" pressure and plays an important role in calculating structural responses resulting from an underwater explosion. The shock wave propagates in water as a spherical wave, initially traveling faster than the speed of sound. As the shock wave moves further from the origin of the explosion its propagation speed falls to the speed of sound in water, where it remains constant [7]. In addition to losing speed, the peak pressure reduces and the shape of the shock wave becomes more elongated as it moves further from the explosion origin. Figure 24 shows the initial shape and the shape of a shock wave that has propagated away from the explosion origin.

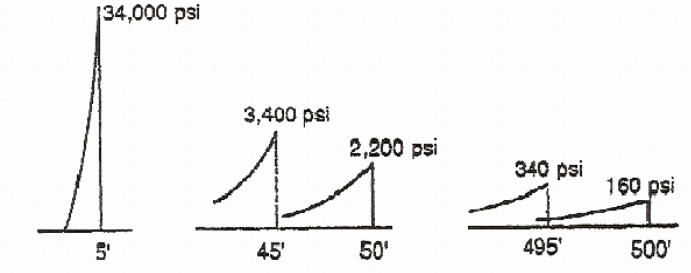

Figure 24 - Shock Wave Profiles Measured at Varying Distances from Explosion Origin [6]

As the shock wave propagates it approaches three types of boundaries: the rigid bottom boundary (seafloor), the free surface of the water, and fluid-structure interface. At the bottom boundary the shock wave is reflected as a compression wave much smaller in magnitude than the original shock wave [6, 7]. If the explosion occurs in shallow water then the wave reflected from the bottom can combine with the incident shock wave and the free surface reflected wave to change the pressure field of the surrounding water significantly. However for analysis in most near and far field cases the explosion is considered to occur in deep enough water that the bottom reflected wave does not interact with the other shock waves.

The first significant boundary the shock wave encounters is the fluid-structure interface of the water and the ship's hull. At this boundary the shock wave creates pressure loading on the hull that is characterized as an instantaneous rise to peak pressure followed by an exponential decay. For a far-field explosion it is often assumed that this load is applied to the hull as a whole and the hull response is assumed to be elastic [7].

For surface ships the initial pressure loading gives the hull an upward acceleration regardless of where the shock wave originates [7]. The upward acceleration continues until the hull begins to move faster than the surrounding water. When this point is reached the loading drops to zero and the water at the hull is exposed to tension [7]. Because water cannot sustain tension a cavitation region develops at the interface between the hull and water [10]. This cavitation region is termed "local" or "hull" cavitation. At the onset of local cavitation the hull has reached its maximum upward velocity, called the "kickoff" velocity, due to the shock wave loading [7].

After reaching the kickoff velocity the hull begins to slow down and the local cavitation region closes. This causes the hull to be reloaded. Reloading occurs because prior to the closure of the local cavitation region the hull is not in contact with the water. When the cavitation region closes the water impacts the hull, causing it to be reloaded [11]. The form of the reloading pressure on the hull is similar to the shock wave induced pressure, although the loads imposed on the hull from reloading are not as large as those created by the shock wave impact [7].

The second boundary the propagating shock wave encounters is the free surface of the water. The arrival of the shock wave on the free surface is visible in two separate phenomena. The first is an expanding ring of darkened water called the "slick". The darkness of the slick is a result of the rippled water created in the slick region by cavitation when contrasted to the surrounding water that is actually smoothed by the reflection of the shock wave. The slick lasts only a matter

of milliseconds due to its rapid velocity and serves as an indication of the points the shock wave has reached on the surface [6].

Following the slick is an upheaval of white water called the "spray dome" [6]. The spray dome is created by the vertical velocity given to the water surface when the incident shock wave is reflected. Once the vertical velocity of the spray dome reaches zero it collapses. The time at which this occurs depends on the charge size and depth of the explosion [6, 8].

Underneath the free surface the incident shock wave is reflected back into the water as a tensile wave. Due to the large density difference between water and air, the pressure of the reflected wave is almost the pressure of the incident shock wave. A schematic of the shock wave reflection is given in Figure 25.

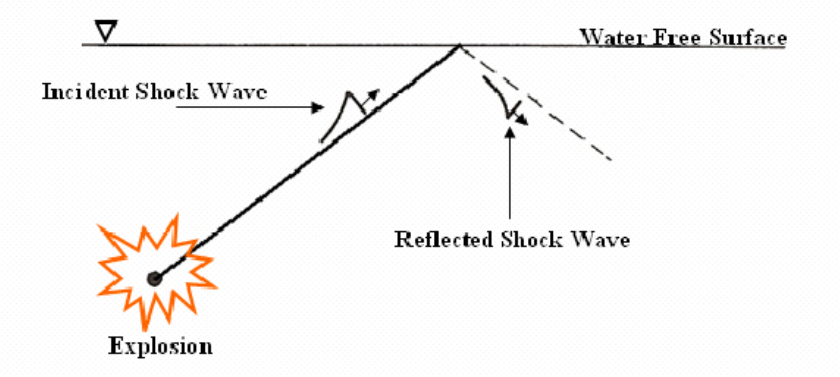

Figure 25 - Reflection of Incident Shock Wave at Free Surface [8]

The closeness of the incident and reflected wave pressures creates a cavitation "surface cutoff" effect at locations in the surrounding water where the incident and reflected shock wave meet. At these points the pressures of the shock and reflected wave cancel each other out reducing the pressure at that point to a negative pressure causing cavitation. When surface cut off occurs at the hull, the exponentially decaying loading from the incident shock wave impact experiences a rapid drop to hydrostatic pressure [7]. The surface cutoff effect and the resulting pressure-time history of an arbitrary point P is show in Figure 26 and Figure 27 respectively.

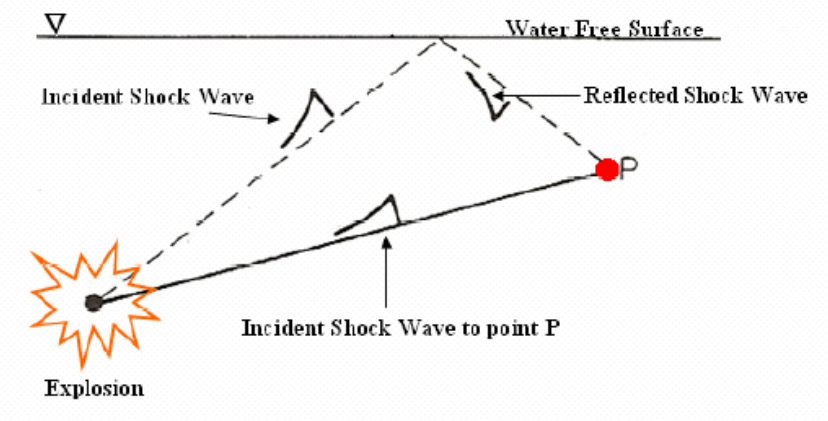

Figure 26 - Shock Wave Interaction at Point P due to Free Surface Effects [8]

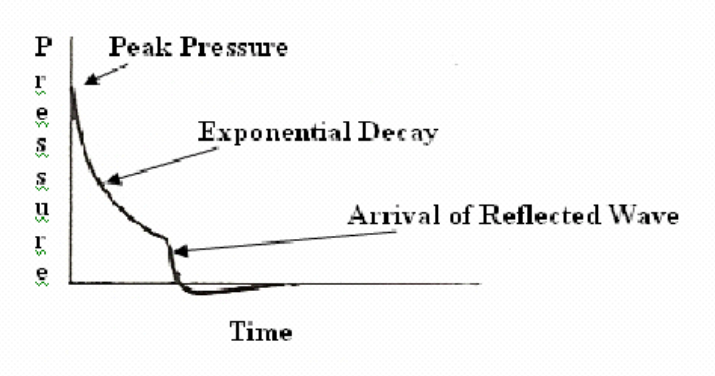

Figure 27 - Pressure-time History due to Surface Cutoff of Point P [8]

In addition to creating the surface cutoff effect, the reflected wave also generates a large or "bulk" cavitation region near the surface of the water. Because water cannot sustain tension and the reflected wave is a tensile wave the pressure around the water surface drops below the vapor pressure and cavitation occurs [10]. The region stays cavitated until the pressure in the region returns a value that is above the vapor pressure of water.

The size of the bulk region is dependent on the location of the explosion origin and the size of explosive used [10]. This region is symmetric about the vertical axis of the explosion origin and is bounded by an upper and lower boundary. Figure 28 depicts a bulk cavitation region.

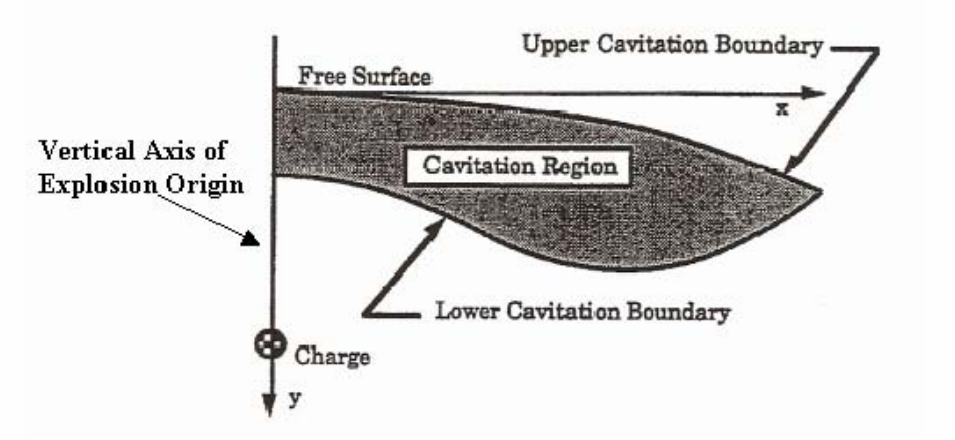

Figure 28 - A Bulk Cavitation Region [10]

The points that make up the upper cavitation boundary are generated when the reflected wave lowers the absolute pressure at these points to below vapor pressure. The absolute pressure at the upper cavitation boundary is defined as a combination of the atmospheric, hydrostatic, incident shock wave, and reflected wave pressures [10].

The points that make up the lower cavitation boundary are determined by the increase in the absolute pressure and the decay of the "breaking" pressure. The breaking pressure is the pressure of the reflected wave needed to cause cavitation at a point in the surrounding water [10]. When the decay of the breaking pressure reaches a minima (equals zero), the lower cavitation boundary is formed. This boundary represents the line beyond which the pressure of the reflected wave is no longer large enough to reduce the absolute pressure in the water to a point where cavitation occurs.

After some time, the bulk cavitation region begins to close in a zipper like manner. As it closes the water above the upper cavitation boundary crashes down on the water below the lower cavitation boundary. This causes a pressure wave, called the cavitation pulse, to radiate from the region. Much like the closing of the local cavitation region causes reloading on the ship's hull, the closure of the bulk cavitation region also causes reloading to occur. Depending on the ship's proximity to the point of closer of the cavitation region, the impact of the water on the hull can cause pressure loads more damaging than the loads created by the initial shock wave impact [7].

The combination of the initial shock impact loading, the local cavitation reloading, and the bulk cavitation reloading account for the early time or shock response of the ship to the underwater explosion. The following paragraphs detail the explosion phenomena that account for the late time response of the ship structure.

Recall that at the conclusion of the detonation process what remains is a very dense, superheated, and spherical gas bubble. While the release of the shock wave significantly lowers the pressure inside this gas bubble, it still exceeds the hydrostatic pressure of the surrounding water [6]. The gas internal to the bubble seeks to return to the hydrostatic pressure of the surrounding water to restore equilibrium. These gases begin to expand, reducing the internal pressure of the bubble and creating a large flow of water away from the bubble. Once the pressure of the internal gaseous products reaches hydrostatic equilibrium the expansion of the gas bubble continues due to the large inertia of the outwardly flowing water surrounding the bubble. As the inertia driven expansion continues the pressure of the gaseous products falls below hydrostatic pressure [5]. Expansion continues until the pressure differential between the hydrostatic pressure and the internal gas bubble pressure becomes large enough to cause the outward flow of water to stop [6]. At this instant the internal gas bubble pressure is at its minimum and the diameter is at its largest. The bubble begins to contract. As it does this the internal gas bubble pressure grows larger and the diameter of the bubble gets smaller. It continues to contract until the compression of the gaseous products stop the contraction and force the bubble to expand again [6]. The process of expansion and contraction repeats throughout the duration of the gas bubble, making it an oscillating system. With each period, the time it takes the bubble to go through a single expansion/contraction cycle, the size of the bubble expands to decreases and the minimum size it contracts to increases. Figure 29 illustrates this and is a result of energy loss during the oscillation process.

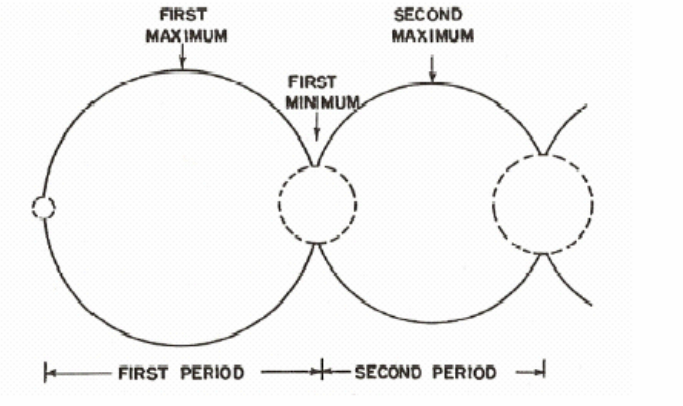

Figure 29 - Gas Bubble Oscillation [6]

The oscillation of the gas bubble causes new pressure waves, called “secondary” or “bubble” pulses, to be radiated outward from the bubble. The manner in which the bubble pulses are created is very similar to the manner in which the shock wave is created. Like the shock wave,

the bubble pulses are a result of the high pressure inside the gas bubble attempting to return to the hydrostatic pressure of the surrounding water. Therefore the bubble pulses are emitted when the pressure internal to the bubble is greatest which occurs at the bubble minimums [6, 7]. The velocity of the bubble pulses is also similar to the shock wave. The pulses propagate at the speed of sound in water [8]. The rise and decay of the peak shock wave pressure roughly occurs on the order of microseconds, where the rise and decay of the bubble pulse occurs on the order of milliseconds.

Unlike the shock wave the bubble pulses do not display a discontinuous rise in pressure followed by an exponential decay. If the bubble is assumed to remain stationary at the origin of the explosion the general shape of a bubble pulse is a gradual rise to the peak pressure that is concave in form followed by a concave shaped decay to hydrostatic pressure. This general shape is shown in Figure 30. The peak pressure achieved by the bubble pulses is between 10% and 20% less than the peak of the shock for the first bubble pulse. This percentage increases for every pulse that is emitted [6, 7].

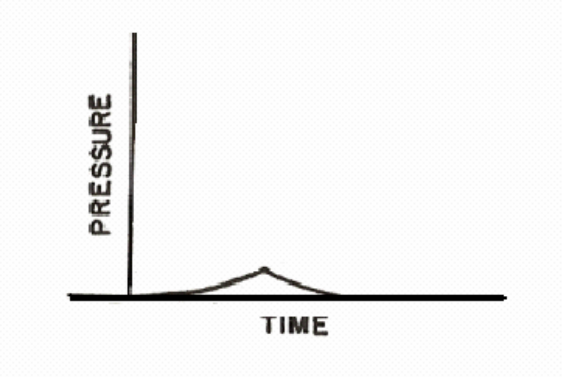

Figure 30 - Typical Bubble Pulse Shape [6]

Occurring concurrently with the oscillation of the gas bubble and pulse generation is the migration of the bubble towards the surface of the water. The bubble migration is created by the buoyancy of the gaseous products and is influenced by the oscillation of the bubble. At larger gas bubble sizes the inertia of the outward flowing water balances out a majority of the buoyancy force causing the bubble to rise minimally. When the gas bubble is close to or at minimum size the inertia of the outwardly flowing water is greatly reduced. This allows the buoyancy force of the gaseous products to have a greater effect on the net upward force acting on the gas bubble accounting for the much higher rate of ascent of the bubble at its smallest sizes. The migration phenomenon is represented in Figure 31 [7].

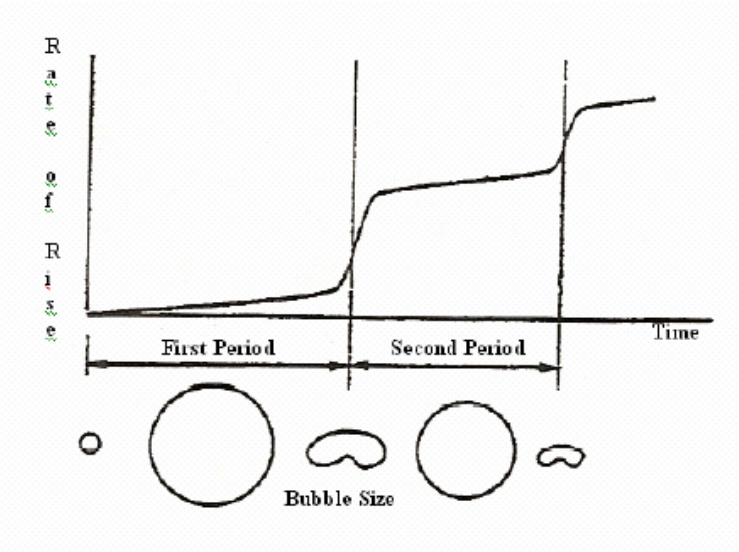

Figure 31 - Bubble Migration Compared to Bubble Size [7]

Earlier the shape of a bubble pulse was defined with the assumption that the bubble did not migrate. However the migration of the bubble has a significant effect on the shape of the bubble pulse. When the bubble has large vertical velocity, as it does around its minimums, the pressure of the bubble pulse is significantly reduced. This causes the bubble pulse to assume a more triangular shape as shown in Figure 32. The triangular shape is a result of the impulse of the bubble pulse being unaffected by the motion of the bubble. Therefore as the peak pressure of the pulse reduces, the pulse develops a much more gradual rise and decay keeping the area under the pressure-time curve the same as in the higher pressure bubble pulse curve.

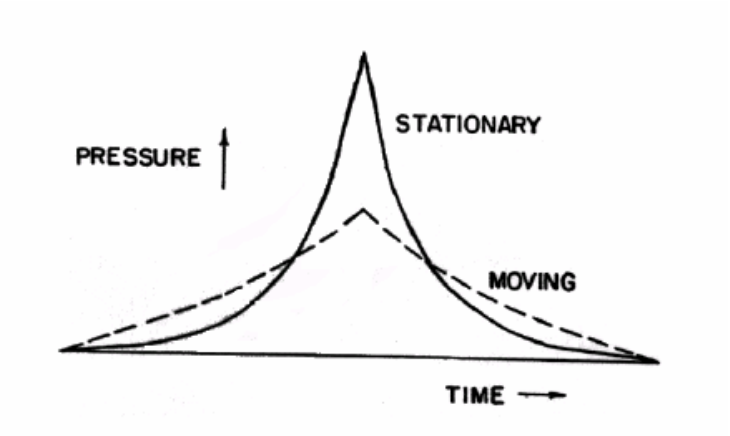

Figure 32 - Bubble Pulse Shape with and without Migration [6]

If the explosion occurs at the bottom boundary (sea floor), the bubble form changes into a hemispherical bubble. The hemispherical bubble initially sits on the bottom eventually breaking away due to buoyancy. After breaking away the hemispherical bubble oscillates and migrates in the same manner as the spherical gas bubble [8].

The bubble pulses are the second phenomena of an underwater explosion to reach the ship's hull. Because the bubble pulses are so much weaker than the shock wave only the first bubble pulse is considered in most cases. Although this is the strongest bubble pulse it does not always create a damaging response. The response it generates in the ship is largely dependent on the wave's frequency, phase, and the proximity of the pulse to the hull when the gas bubble generates it [7].

The bubble pulse contributes to the shock wave damage depending on its phase when it strikes the hull. No additional local cavitation occurs from the bubble pulse loading so the loading due to the bubble pulse is due only to initial impact.

If the bubble pulse is generated at a close proximity to the hull then it can rupture the hull as almost all of its energy impacts the hull. If the explosion occurs far enough away from the free surface, the bubble pulses will damp out and have little effect on the ship's response.

When the frequency of the shock response and bubble pulse response matches the resonant frequency of the ship, whipping occurs. The whipping motion of the ship can break the ship's hull girder or cause other types of severe structural damage [7].

The last underwater explosion phenomenon to reach the free surface or the ship is the gas bubble itself. As the bubble approaches the free surface and the ship it experiences an attraction force to the ship and a repulsion force from the free surface [6, 8]. If the bubble migrates such that it is close to the hull at the time it reaches the free surface, two types of loading can occur.

The first type of gas bubble loading is created by the outwardly flowing water around the bubble impacting the hull of the ship. Pressures loaded on the hull in this manner are quite high and the duration of the loading period is much longer than the loading period of the shock wave. These loads are capable of creating significant damage to the hull in localized areas. Damage that in some cases is greater than the shock wave induced damage to the hull.

The second type of gas bubble loading occurs when the bubble actually collapses onto the hull of the ship. This occurs as the bubble contracts in close proximity to the hull, creating a pressure differential that results in both the collapsing bubble and a high-speed water jet [7]. The impact of the water jet can be forceful enough to puncture the hull. In other cases the water jet causes

an initial pressure loading like that of the shock wave and gives the hull a secondary kickoff velocity.

The ship response created by the bubble pulse and gas bubble loading make up the late time response of the ship. In circumstances where the water jet impacts the hull it is estimated that 60% of the total damage results from the late time response and only 40% comes from the early time (shock wave impact) response [8].

If the bubble is close to the surface during its initial motion and at a sufficient distance away from the hull then on arrival at the free surface it vents into the atmosphere in the form of a "plume". The plume is comprised of white water mixed with the explosive gas products. This mixture is thrown vertically into the air and once its maximum height is reached it crashes back down to the water surface. A typical plume is shown Figure 33. Note that both the slick and what remains of the dome are also visible.

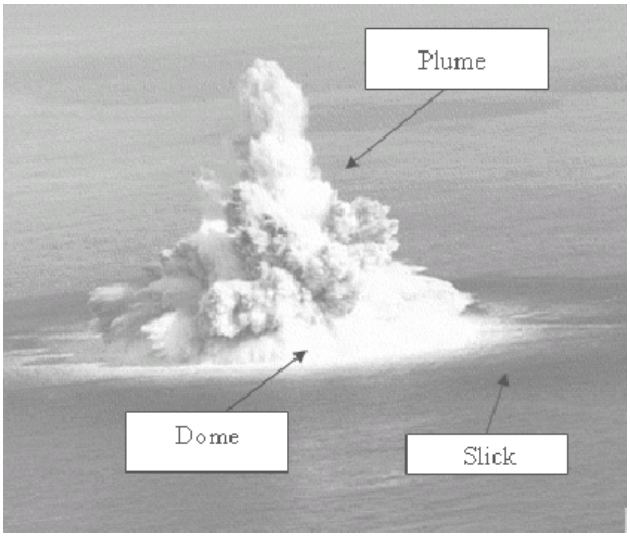

Figure 33 - Plume, Spray Dome, and Slick [9]

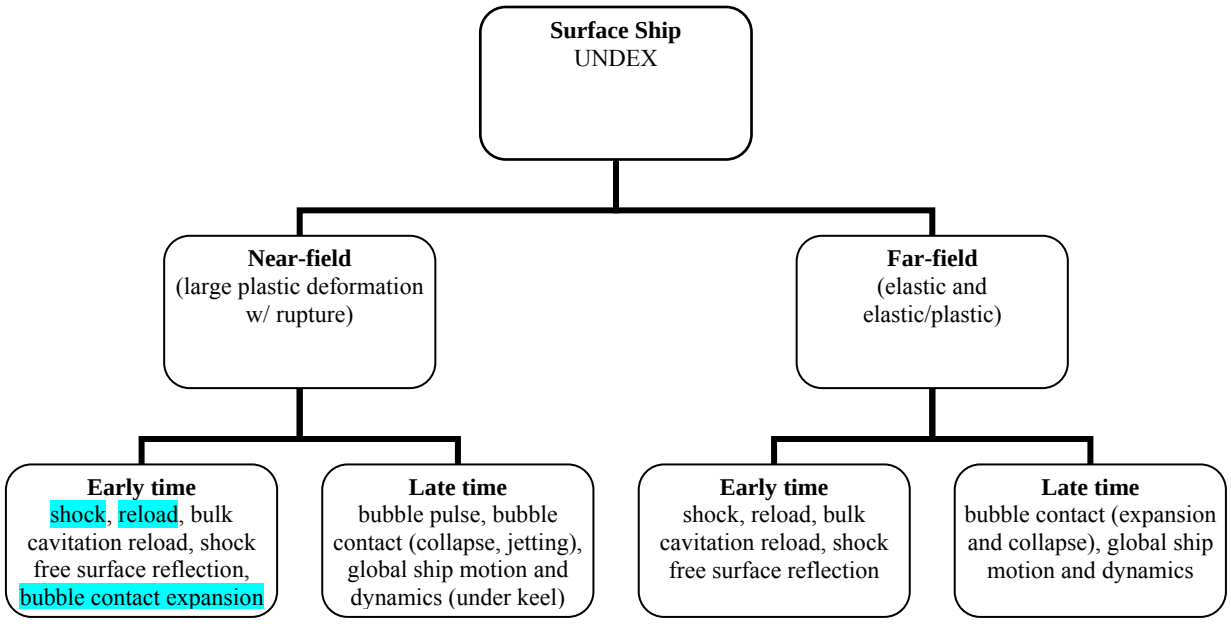

Figure 34 - Near-field and Far-field Definition Based on Structural Response and Deformation

1.2.1 Far Field Underwater Explosion

Considering the underwater explosion phenomena detailed above, the definition of a near vs. far-field explosion based on hydrodynamic phenomena is difficult. Instead, it can be based on the structural response as illustrated in Figure 34.

In most cases, a charge that detonates close to the ship's hull causes significant plastic deformation and rupture. A charge detonated close to the ship also causes further damage to the ship from the fragmentation of the charge housing [7]. As the distance of the charge is increased, a point is reached where the hull no longer ruptures, but significant plastic hull deformation still occurs. Further increasing the charge distance, reaches a point where only elastic deformation occurs [7, 12].

A far field underwater explosion affects primarily the global response of the ship, but can cause significant shock damage to systems inside the ship. The affect of an explosion can be divided into response due to the shock wave and response due to the gas bubble [12].

Taking into account the above characteristics, a far field underwater explosion is defined for this report as an underwater explosion that meets the following two criteria. The first criterion is that the depth of the explosion is large enough that neither the shock wave or bubble effects cause hull rupture. Second, a far field explosion occurs at a large enough depth that the bubble pulses

damp out before reaching the ship structure; hence the pulses do not affect the late time response of the ship.

1.2.2 Near Field/Proximity Underwater Explosion

The response of a structure to a near-field underwater explosion involves every aspect of the underwater explosion event. A near field/proximity underwater explosion can cause global and local damage to the ship structure. Structural response includes both the early time and late time events of an underwater explosion. Early time response involves plate and/or panel deformation and rupture due to the shockwave. Late time response involves plate and/or panel deformation and rupture due to the subsequent bubble pulses and possible bubble jetting. Figure 34 shows the near-field underwater explosion definition based on structural response. This thesis investigates the highlighted early time phenomena in Figure 34.

1.2.3 Similitude Equations

Analytical equations describing the physics of underwater explosions (UNDEX) are very complex. The method of similitude offers a simplified way to calculate characteristics of an underwater explosion. Similitude relations yield information on properties such as pressure, impulse, and energy associated with each of the three major events of an underwater explosion [6]: the shock wave (Section 1.2.3.1), the gas bubble (Section 1.2.3.2), and the secondary pressure pulses (Section 1.2.3.3).

Developed mainly by A.B. Arons in the 1940s [6], the similitude equations use experimentally determined constants and a set of generic equations in three variables, the charge weight, explosion depth, and a point of interest in the explosive field. The method assumes that if the variables of two separate explosions are different by some ratio, the characteristics of the explosions are the same at two corresponding points of interest scaled by the same ratio [6]. This is referred to by Cole as the “principle of similarity”.

While the similitude equations give a good understanding of the general behavior of underwater explosions they are limited because they are experimentally based, and they only apply to a certain range for the variables (Table 1) of charge weight, explosion depth, and point of interest location [15].

Table 1 Validity Range for Similitude Equation Variables

Parameter	**Variable**	**Validity Range**
Peak Pressure (P_{peak})	P_{peak}	3.4-138 MPa
Peak Pressure Decay	$t-t_{peak}$	$<2\tau$
Decay Time Constant (θ)	P_{peak}	3.4-138 MPa
Shock Wave Impulse (I)	P_{peak}	3.4-138 MPa
Shock Wave Energy Flux (E)	P_{peak}	3.4-138 MPa
Gas Bubble Periods (T_n)	----------	Always Valid
Gas Bubble Max Radii ($A_{max\ n}$)	----------	Always Valid
Bubble Pulse Max Pressure (P_{bp})	Z_o	152-1219 m
Bubble Pulse Duration (τ_{bp})	Z_o	198 m-???

In addition to these limitations a number of assumptions (Table 2) are required. The major assumptions made in the similitude equations are that there are no effects from boundary surfaces, termed a "freewater" explosion [15], and no migration of the gas bubble takes place [16].

Table 2 Assumptions Required for Similitude Equations

Assumption	Characteristic Affected	Impact
No boundary surface effects	Shock Wave, Gas Bubble, Bubble Pulse	No reflection of shock wave or bubble pulse. No cavitation or free surface effects. All similitude equations based on explosions that took place significantly far away from boundary surfaces.
Freewater (infinite fluid) explosion	Gas Bubble	Bubble reaches its maximum before it reaches surface.
No gas bubble migration	Gas Bubble, Bubble Pulse	Shape of bubble pulse unaffected by moving bubble.[1]
Spherical gas bubble	Gas Bubble	Allows bubble radius to be found using similitude. Effects volume of bubble used in energy equations.
Only first bubble pulse significant	Pressure-time History	Other pressure pulses that reach point R are ignored.
Water at point R does not go into tension	Bubble Pulse Shape	Allows graphs given by Arons and Yennie[8] to be used to predict bubble pulse shape.
Incompressible fluid/no energy losses in bubble oscillation	Gas Bubble	Creates error in hydrodynamic bubble energy calculations.
Irrotational fluid	Gas Bubble	Allows potential to be used to develop energy equations

Table 3 provides the similitude equation constants for TNT used in this thesis. The similitude equations are presented in Sections 1.2.3.1 through 1.2.3.3.

Table 3 TNT Constants for Similitude Equations

Calculation	Constant	Source
Peak Pressure	K_1=23800, A_1=1.16	Cole[6]/Shin[17,36,37]
Shock Wave Time	K_2=0.058, A_2=-0.185	Cole[6]/Shin[17,36,37]
Shock Wave Impulse	K_3=1.798, A_3=0.98	Cole[6]
Shock Wave Energy Flux Density	K_4=3034.9, A_4=2.155	Cole[6]
Jones Constant for Bubble Dynamics	K_J=2712.28 $m^{11/4}/s^2$	Cole[6]
Secondary Pressure Pulse	K_{bp}=12.148, A_{bp}= -1/6	Cole[6]

1.2.3.1 Shock Wave

There are four characteristics associated with the shock wave that are of primary interest when using similitude. These are, the peak pressure, the pressure-time history, the shock wave impulse, and the shock wave energy flux density. The peak pressure is given by both Cole [6] and Swisdak [15] as:

$$P_{\max} = K_1 \left(\frac{W^{\frac{1}{3}}}{R} \right)^{A_1} \tag{2}$$

where R is the radius to the point of interest from the center of the charge in ft., and W is the charge weight in pounds-force. To determine the pressure-time history of point R for the shock wave portion of the explosion an exponential decay of peak pressure is assumed [15]. The time constant, θ, is the time it takes for the pressure to fall to 36.8% of the peak pressure [15].

$$\theta = (W)^{\left(\frac{1}{3}\right)} \cdot K_2 \left[\frac{(W)^{\left(\frac{1}{3}\right)}}{R} \right]^{A_2} \tag{3}$$

With the time constant from Equation (3) and the peak pressure from Equation (2), the pressure-time history at a point R is given by Equation (4).

$$P(t) = P_{\max} \cdot e^{\frac{-t-t_1}{\theta}} + P_D \tag{4}$$

where P_D is the hydrostatic pressure at charge depth D. t_1, Equation (5), is the time it takes the shock wave to reach the point of interest R and C is the speed of sound in the fluid.

$$t_1 = \frac{R}{C} \tag{5}$$

Two other properties, impulse (I) and energy flux density (E), of the shock wave are also calculated using similitude methods. These properties are calculated using Equations (6) and (7).

$$I = K_3 \cdot W^{\frac{1}{3}} \left(\frac{W^{\frac{1}{3}}}{R} \right)^{A_3} \tag{6}$$

$$E = K_4 \cdot W^{\frac{1}{3}} \left(\frac{W^{\frac{1}{3}}}{R} \right)^{A_4} \tag{7}$$

Impulse is in units of (lbm-sec)/in^2 and energy flux density is in units of (lbm-in)/in^3.

1.2.3.2 Gas Bubble Dynamics

The dynamics of the gas bubble associated with an underwater explosion have many parameters which can be found through coupling similitude equations with hydrodynamic methods [6, 16]. The first of these parameters is the radius-time history of the gas bubble. To find the radius-time history using similitude and energy equations the first step is to find the first period of oscillation and the radius at the first bubble maximum using Equations (8) and (9).

$$t_{b1} = 1.14(\rho_0)^{\frac{1}{2}} \frac{Y_0^{\frac{1}{3}}}{(\rho_0 \cdot g \cdot z_0)^{\frac{5}{6}}} \tag{8}$$

$$A_{M1} = \left[\left(\frac{4\pi}{3} \rho_0 \cdot g \cdot z_0 \right)^{-1} \cdot Y_0 \right]^{\frac{1}{3}} \tag{9}$$

where ρ_0 is the initial density of the fluid, g is the gravitational constant, z_0 is the initial depth from level of zero pressure change, $z_0 = D + 33\,ft$. The constant Y_0 is found using Equations (10) and (11).

$$Q_0 = \frac{K_J}{\gamma - 1} \left(\frac{4\pi}{3} \cdot \frac{W}{\rho_{TNT} \cdot g} \right)^{1-\gamma} \tag{10}$$

$$Y_0 = \frac{W}{g} \cdot Q_0 + \frac{4\pi}{3} \cdot \rho_0 \cdot \frac{W}{\rho_{TNT}} \cdot z_0 \tag{11}$$

where Q_0 is the initial energy per mass for the TNT explosive charge, γ is the ratio of specific heats for TNT gas products (equal to 1.25 in this thesis). K_J is the Jones constant given in Table 3. Equation (8) gives the approximate time at which the gas bubble is at its first minimum. Equation (9) is the approximate gas bubble maximum radius.

The last step in finding the radius-time history is to calculate the second period of oscillation and the second bubble maximum. This is accomplished by scaling Equation (10) and (11) by a factor of 0.34. This scale factor represents the percentage of energy that is lost after the first bubble pulse [6].

$$Q_1 = 0.34 \cdot Q_0 \tag{12}$$

$$Y_1 = 0.34 \cdot Y_0 \tag{13}$$

Repeating the steps for the first period of oscillation and the first bubble maximum gives the second period of oscillation and the second bubble maximum:

$$t_{b2} = 1.14(\rho_0)^{\frac{1}{2}} \frac{Y_1^{\frac{1}{3}}}{(\rho_0 \cdot g \cdot z_0)^{\frac{5}{6}}} \tag{14}$$

$$A_{M2} = \left[\left(\frac{4\pi}{3} \rho_0 \cdot g \cdot z_0 \right)^{-1} \cdot Y_1 \right]^{\frac{1}{3}} \tag{15}$$

Equation (14) gives the approximate time at which the gas bubble is at its second minimum. Equation (15) is the approximate gas bubble second maximum radius. The approximate time when the gas bubble is at its first maximum and second maximum can be calculated using Equations (16) and (17).

$$t_{bM1} = \frac{1}{2} \cdot t_{b1} \tag{16}$$

$$t_{bM2} = t_{b1} + \frac{1}{2}(t_{b2} - t_{b1}) \tag{17}$$

The bubble periods of oscillation can now be determined.

$$T_1 = t_{b1} \tag{18}$$

$$T_2 = (t_{b2} - t_{b1}) \tag{19}$$

1.2.3.3 Secondary Pressure Pulse

Associated with the secondary pressure pulse or bubble pulse, are five major characteristics: The time of arrival at point R, the peak pressure, the impulse, the duration. There is no direct similitude relation for the time of arrival of the bubble pulse. Figure 35 shows the bubble pulse begins to propagate when the gas bubble reaches its first minimum and is assumed to reach point R at the first bubble period, T_1 [6, 16]. The estimated pulse velocity is found by

$$u = \frac{\pi}{2} \left(\frac{A_{M1} - \left(\frac{W}{\rho_{TNT} \cdot g} \right)^{\frac{1}{3}}}{t_{bM1}} \right) \tag{20}$$

and the arrival time of the maximum secondary pressure pulse at location R is given as

$$t_{2p} = \frac{R}{u} \tag{21}$$

where, in Equation (20), A_{M1} is calculated in Equation (9) and t_{bM1} is calculated in Equation (16). The maximum pressure of the secondary pulse, in lb./in.^{2}, at location R is

$$P_{2\max} = \left[2.26 \cdot 10^{-6} \cdot k \left(4.19 \cdot 10^{7} rQ \frac{(\gamma - 1)}{k} \right)^{1+\frac{2}{3(\gamma-1)}} \cdot \frac{(W)^{\frac{1}{3}}}{R} \right] - P_0 \tag{22}$$

where, for TNT, $\gamma = 1.25$, $k = 7.83 \times 10^9$, and the fraction of the detonation energy $rQ = 440$ [6]. Impulse becomes a more important characteristic when studying the bubble pulse as the bubble pulse is a more prolonged wave when compared to the shock wave [6]. The impulse of the secondary pressure pulse is calculated using Equation (23).

$$I_2 = K_{bp} \cdot z_0^{A_{bp}} \left(\frac{W^{\frac{2}{3}}}{R} \right) \tag{23}$$

The values for K_{bp} and A_{bp} are given in Table 3. The duration of the pressure impulse is found by calculating the secondary pressure pulse period. This is done by dividing Equation (23) by Equation (22). Equation (24) is the duration of the secondary pressure pulse.

$$T_2 = \frac{I_2}{P_{2\max}} \tag{24}$$

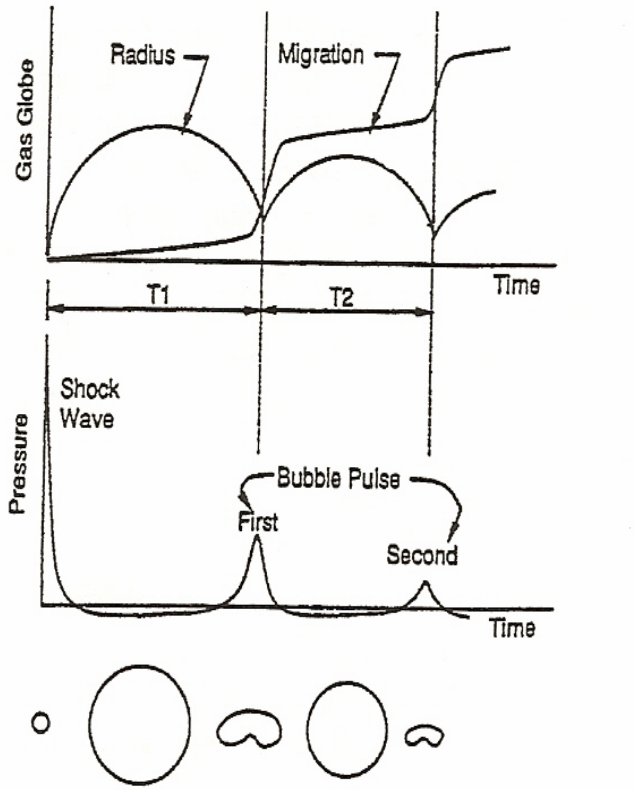

Figure 35 - Bubble Pulse Arrival Time Compared with Bubble Oscillation [15]

1.3 Literature Survey

1.3.1 UNDEX Models

The ability to predict and assess the global and local damage of a ship due to an underwater explosion event is of great interest in naval ship design. A method that is capable of analyzing the coupled dynamic response of the structure and the fluid is needed. There are two ways of solving these types of problems: analytically, and numerically.

1.3.1.1 Analytical Models

A possible analytical solution approach is to discretize the solution into a series of solutions that represent "response modes," which are used to approximate the total solution. Discretization of space and time result in simple solutions that are pieced together to approximate a continuous solution. Surface approximations give an approximate solution to a large surface by obtaining simple solutions to small surfaces that are pieced together [18]. Analytical solutions for such large scale and complex problems like those discussed in this paper, are not practical. A more feasible approach to assessing the dynamic response of a structure to an undex event is needed.

1.3.1.2 Finite Element and Computational Models

Numerical solutions offer various methods of assessing the dynamic response of a fluid and a structure. Numerical solvers are typically grouped into three categories; Doubly Asymptotic Approximation (DAA) codes (boundary element method codes), Computational Fluid Dynamics (CFD) codes, and Hydrocodes.

1.3.1.2.1 DAA CODES

DAA codes are structural dynamics codes that use the Doubly Asymptotic Approximation. The DAA is a structure-medium interaction (SMI) approximation that is asymptotically exact at the low-frequency and high-frequency limits. In F.E. response calculations, DAA provides a set of ODE's for the SMI that are solved in tandem with the response ODE's for the dry structure. [18] DAA codes do not include bubble dynamics calculations or cavitation, and are not accurate in the mid-frequency range.

1.3.1.2.2 CFD CODES

Traditional Computational Fluid Dynamics (CFD) codes are often used in conjunction with structural response codes to obtain a solution. CFD codes do not calculate structural response, they are purely fluid codes. The fluid response is obtained in a CFD code possibly as a pressure-time history, and then is used as input load for the structural code. CFD codes include Boundary Element Method (BEM) codes, which treat the fluid as irrotational and/or incompressible, requiring discretization of material interfaces only. CFD codes may also include Eulerian or Arbitrary Lagrangian/Eulerian (ALE) formulations for the fluid calculations.[18]

1.3.1.2.3 HYDROCODES

Hydrocodes are computational mechanics tools that simulate the response of both solid and fluid material under highly dynamic conditions (e.g., detonation and impact) where shock wave propagation is a dominant feature. Hydrocodes make fewer approximations than either of the more special-purpose Computational Fluid Dynamics (CFD) or Computational Solid Mechanics (CSM) methods. They numerically solve the more fundamental time-dependent equations of continuum mechanics that CFD and CSM do not. Hydrocodes are tools for simulation of multi-material, compressible, transient continuum mechanics [18]. There are four main types of

hydrocodes; Lagrangian, Eulerian, Coupled Eulerian-Lagrangian (CEL), and Arbitrary Lagrangian Eulerian (ALE). [18]

The computational mesh of a Lagrangian model remains fixed on the material. Since the mass in each element remains fixed, no mass flux at inter-element boundaries must be computed. Material distortions correspond to Lagrangian mesh distortions. Large distortions may result in reductions in time-steps and/or stoppage of the calculation. The general limitation of most Lagrangian hydrocodes to relatively low-distortion computations limits their applicability to shock-structure interaction analysis. Some Lagrangian methods that have potential application to UNDEX-SMI analysis but are not as mature include the Free Lagrange Method (FLM), Smoothed Particle Hydrodynamics (SPH), and the Total Lagrangian formulation. [18]

Eulerian hydrocodes advance solutions in time on a mesh fixed in space, thus avoiding the Lagrangian mesh distortions problems. Eulerian hydrocodes include material strength (flow of solids) and multi-material capabilities, unlike Eulerian CFD codes. Eulerian hydrocodes are strictly transient dynamics solvers. They are not designed to solve steady-state fluid flow problems. Eulerian hydrocodes are computationally expensive, compared to CFD codes, due to their ability to have elements that contain more than one material (i.e., multi-material elements). Numerical algorithms are required that prevent artificial material diffusion (the mixing of materials across a material interface) in mixed elements. The convergence to a common state parameter (e.g., pressure) in a multi-material element can also result in considerable expense. [18]

Coupled Eulerian-Lagrangian (CEL) hydrocodes use both Eulerian and Lagrangian methods in separate regions of the domain. A recommended practice concerning the application of the CEL method is to discretize solids (materials in which the material strength plays a dominant role) in a Lagrangian frame, and materials exhibiting primarily fluid behavior (little or no strength) in an Eulerian frame. The Eulerian and Lagrangian regions continuously interact with each other, allowing coupling of a fluid and structure. A typical CEL code comprises three modules: Eulerian, Lagrangian, and Coupling. The Coupling module handles the two-way flow of information between the Eulerian and Lagrangian modules using “interface elements”. Interface elements are employed that coincide with the exterior surfaces of the Lagrangian model, forming a surface in a three dimensional model. The interface elements determine the volume of the Eulerian elements partially covered by the Lagrangian mesh. The presence of an arbitrarily shaped Lagrangian model usually creates some very small volumes in partially covered Eulerian

elements; these are “blended” with neighboring cells to avoid the severe time step restrictions on small elements [18]. Eulerian hydrocode passes the loads (nodal forces) on the surface structural nodes while the Lagrangian code passes the node locations and velocities back at the end of each computational step [20].

Arbitrary Lagrangian Eulerian (ALE) hydrocodes share aspects with both Lagrangian and Eulerian hydrocodes; Lagrangian motion is computed every time step, followed by a remap phase in which the spatial mesh is either rezoned (Lagrangian), rezoned to its original shape (Eulerian) or rezoned to some “advantages” shape (between Lagrangian and Eulerian). ALE mesh motions are based primarily on the preservation of a uniform mesh, not the capture of physical phenomena. The ALE method couples the fluid dynamics with the structural dynamics directly, without interfacing two separate coordinate systems as is done in the CEL method. Structural elements can be incorporated directly in the ALE framework [19]. The Arbitrary Lagrangian Eulerian method is the preferred method for assessing structural response due to an underwater explosion for large deformations. The method provides the capabilities to model the fluid dynamics and the structural dynamics most efficiently.

Section 1.3.1.2.1 discusses how Doubly Asymptotic Approximation (DAA) codes do not account for the explosive gas bubble, cavitation, or any of their effects on a structure and only accounts for elastic structural responses. DAA codes are not applicable for solving the close-in underwater explosion fluid-structure problem. Section 1.3.1.2.2 discusses how CFD codes, alone, are not capable of solving the close-in underwater explosion fluid-structure problem. Section 1.3.1.2.3 discusses the different solution methodologies of hydrocodes. Table 4 lists prominent hydrocodes and the solution method capability of each code.

Table 4 Comparison of Prominent Hydrocode Solution Methods [19]

CODE	Lagrangian	Smoothed Particle Hydrodynamics (SPH)	Free-Lagrange Method (FLM)	Eulerian	Coupled Eulerian/ Lagrangian (CEL)	Single-Material Arbitrary Lagrangian Eulerian (SALE)	Multi-Material Arbitrary Lagrangian Eulerian (MALE)
ALE3D	*			*		*	*
ALEGRA	*			*		*	*
AUTODYN-3D	*					*	
CTH				*			
CTH-EPIC	*			*	*		
DYNA3D	*						
DYSMAS/ELC	*			*	*		
EPIC	*	*					
HULL	*			*	*		
LS-DYNA	*			*		*	*
MESA				*			
MSC/DYTRAN	*			*	*	*	*
PRONTO3D	*	*					

The Arbitrary Lagrangian/ Eulerian solution method is chosen here for its ability to handle both the shock wave and bubble dynamics effects of an underwater explosion and for its ability to directly couple the fluid and structural dynamics.

1.3.2 UNDEX Problems and Model Validation

Three test cases are used in this thesis to demonstrate the use of the ALE method in LS-DYNA for UNDEX problems.

A one dimensional case is used to show that the ALE method will propagate a pressure wave through the fluid, demonstrating velocity and stress information is passed correctly from node to node. The 1-D case modeling the detonation of a spherical TNT charge underwater, (Section 3.1), is compared to the Naval Postgraduate School Thesis [17,36,37] Deep Spherical Bubble Problem 1-D results.

A three dimensional case is used to show that the shock wave pressure is propagated correctly in three dimensions. This includes the decay of shock pressure profile due to the dispersion of a radiating wave, and the pressure profile of the first bubble pulse.

The Deep Spherical Bubble Problem, (Chapter 3) from the Naval Postgraduate School Thesis [17,36,37] is reproduced to show the ability of the multi-material ALE (MMALE) method in LS-DYNA to handle the interaction of the explosive products in the fluid medium.

1.4 Objectives

The primary objectives of this thesis are: to assess existing methods and tools for predicting UNDEX damage in proximity underwater explosion problems. Underwater blast loading from proximity explosions and bubble pulses are of particular interest. This thesis will attempt to show that simply applying a pressure-time history load calculated using similitude equations to a structure is insufficient for a close-in underwater explosion where the shockwave, explosive gas bubble, and structure all interact together. The Arbitrary Lagrangian Eulerian Finite Element method is used to show that results from the FE analysis are different than the results given by the similitude equations and for the simple cases studied, provide a more sufficient and correct analysis.

1.5 Thesis Outline

This paper investigates the ability of the Multi-material Arbitrary Lagrangian/Eulerian method in LS-DYNA to simulate the non-linear dynamic response of a ship-like structure to a near-field underwater explosion. The sequence of undex events can be separated into two phases: explosive/fluid interaction and fluid/structure interaction. Chapter 1 provides an introduction and motivation for the need to accurately model and simulate underwater explosion events to evaluate the vulnerability element of a total ship survivability assessment. A description of the sequence of underwater explosion events and current methods and their limitations are reviewed. Chapter 2 provides a description of analysis tools used in this thesis and the LS-DYNA ALE method theory. The one dimensional and three dimensional validations for the explosive/fluid interaction phase are described and analyzed in Chapter 3. Chapter 4 provides the three dimensional case studies involving the explosive/fluid and the fluid/structure interaction phases of an underwater explosion event. Chapter 5 discusses the conclusions of this paper and future work.

CHAPTER 2 ANALYSIS TOOLS

2.1 LSDYNA

LS-DYNA 970 explicit finite element code is used to model the early-time and the late-time response of an underwater explosion. This chapter describes previous methods [21,22] and methods used in this thesis for using LS-DYNA's ALE method.

2.1.1 Description of LS-DYNA

LS-DYNA is a general purpose finite element code for analyzing the large deformation dynamic response of structures including structures coupled to fluids. The main solution methodology is based on explicit time integration. A contact-impact algorithm allows difficult contact problems to be treated with heat transfer included across the contact interfaces. Spatial discretization is achieved using four node tetrahedron and eight node solid elements, truss elements, membrane elements, discrete elements, and rigid bodies. Material behavior is handled with constitutive models and equation of state models. [23]

2.1.2 VT Study Uses

Prediction of the behavior and damage to a ship subjected to an underwater explosion requires a thorough understanding of the physics and hydrodynamics of an underwater explosion. The development of an integrated and validated explosive and fluid model is necessary for modeling a near field explosive-fluid-structure interaction problem such as a ship subjected to the explosion of a contact mine or sub-keel torpedo where cavitation, material deformation, material rupture, internal compartment overpressure and secondary and tertiary bubble pulses are significant effects. Finite element models for the explosive-fluid dynamics are evaluated and compared to actual explosive tests and to the peak pressure approximation. Finite element models for the fluid-structure interaction are evaluated and compared to analytical solutions. The finite element models are developed using the Arbitrary Lagrangian Eulerian (ALE) method of explicit finite element analysis (FEA) in the LSDYNA version 970 program.

2.1.3 LS-DYNA Arbitrary Lagrangian/Eulerian (ALE) Finite Element Solution Methodology

LS-DYNA has the capability to obtain solutions using three different FE methodologies; Lagrangian, Eulerian, or Arbitrary Lagrangian Eulerian (ALE).

Purely Lagrangian methods are typically used only for structural deformation. The mesh moves in space. The computational expense of this method is determined by the amount of mesh deformation that occurs. If large deformations occur and mesh distortion is high, the calculation will terminate and the mesh will need to be repaired manually in order to continue the calculation. This process is necessary every time the mesh becomes too distorted for the calculations to continue. Obtaining solutions to the fluid dynamics portion of underwater explosion fluid/structure interaction event is not feasible using a purely Lagrangian method due to the high deformation of the fluid mesh caused by the shock wave.

Purely Eulerian methods are typically used for fluid calculations. The mesh is fixed in space. The Eulerian method is not suitable for modeling structural deformation since the mesh is not allowed to deform. Obtaining solutions to the structural dynamics portion of underwater explosion fluid/structure interaction event is not feasible using a purely Eulerian method due to the deformation of the structural mesh caused by the shock wave.

The Arbitrary Lagrangian/Eulerian (ALE) method is able to solve the fluid dynamics calculations and handle the structural deformations by using a combination of the Lagrangian method and the Eulerian method.

2.1.3.1 GOVERNING EQUATIONS FOR ALE METHOD

The governing equations in LS-DYNA's ALE method are the conservation equations used in a finite element formulation as discussed in Sections 2.1.3.1.1 - 2.1.3.10. Energy, mass, and momentum are conserved and advected from element to element. The ALE method in LS-DYNA can solve the conservation equations using a Lagrangian formulation, an Eulerian formulation, or the Arbitrary Lagrangian/Eulerian (ALE) formulation. LSDYNA uses a Split Operator Technique to solve the conservation equations using the Eulerian formulation and the ALE formulation.

2.1.3.1.1 CONSERVATION EQUATIONS

Conservation equations are used to solve for the fluid mesh velocities and displacements [25]. The conservation of mass, momentum, and energy are given in Equations (25), (26), and (27).

$$\frac{\partial \rho}{\partial t} = (-\rho) div(v) - (v_i - u_i)\frac{\partial \rho}{\partial x_i} \tag{25}$$

$$\rho \frac{\partial v_i}{\partial t} = \sigma_{i,j} - \rho(v_i - u_i)\frac{\partial v_i}{\partial x_j} \tag{26}$$

$$\rho \frac{\partial e}{\partial t} = \sigma_{ij}\varepsilon_{ij} - \rho(v_i - u_i)\frac{\partial e}{\partial x_j} \tag{27}$$

where v is the fluid velocity and u is the mesh velocity.

The default formulation for LS-DYNA is the Lagrangian reference frame. The Lagrangian formulation for the conservation equations sets the mesh velocity equal to the particle velocity, (u = v) in Equation 25, 26, and 27, and will give a deformed mesh solution. If the mesh becomes too distorted, the calculation is terminated and a manual rezone of the mesh nodes (adjusting the distorted mesh by hand) will need to be performed in order to carry out the rest of the calculation.

The Eulerian formulation for the solution of the conservation equations sets the mesh velocity, u = 0 in Equation 25, 26, and 27. This gives a fixed mesh solution. In the Eulerian formulation, the Split Operator Technique uses a two step process. The first step of the formulation begins with a Lagrangian calculation making the mesh velocity equal to the particle velocity. The mesh moves with the fluid, thus mass is conserved. The mesh velocities and displacements are solved for, then the mesh nodal characteristics are updated. As long as mesh distortion is acceptable, the Lagrangian calculation is continued. When mesh deformation is highly distorted, such that time-step size decreases, a second step is conducted. The second step is the Eulerian mesh rezoning calculation, where the mesh velocity equals zero and the deformed element nodes return to their original location. The Eulerian mesh rezone is followed by an advection step that transports material flux from one element to another. The amount of material flux is determined by the mesh rezoning. Section 2.1.3.4 discusses the advection process in more detail. Figure 36 shows the Lagrangian formulation and the two step process for the Eulerian formulation. Figure 36 illustrates how the Eulerian formulation begins with a Lagrangian calculation and ends with an Eulerian calculation and material flux between adjacent elements resulting from the Eulerian mesh rezone.

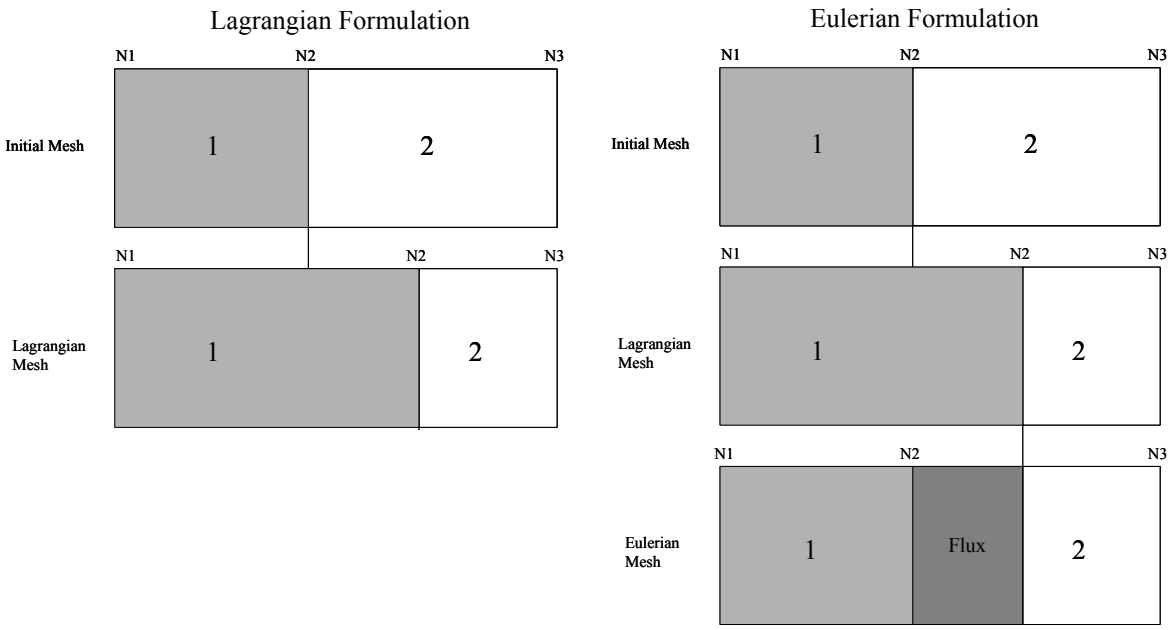

Figure 36 - Illustration of 1-D Lagrangian and 1-D Eulerian Formulation [25]

Figure 37 shows the how flux is determined in the ALE formulation. LSDYNA uses a Split Operator Technique to solve the conservation equations. Unlike the Eulerian formulation, where mesh nodes are rezoned to their original locations, the ALE formulation rezones element nodes to an optimal position determined by a mesh rezoning algorithm (Section 2.1.3.3). The amount of material flux is determined by the ALE rezoning algorithm. The ALE formulation keeps the mesh distortion and the computationally expensive advection calculation to a minimum.

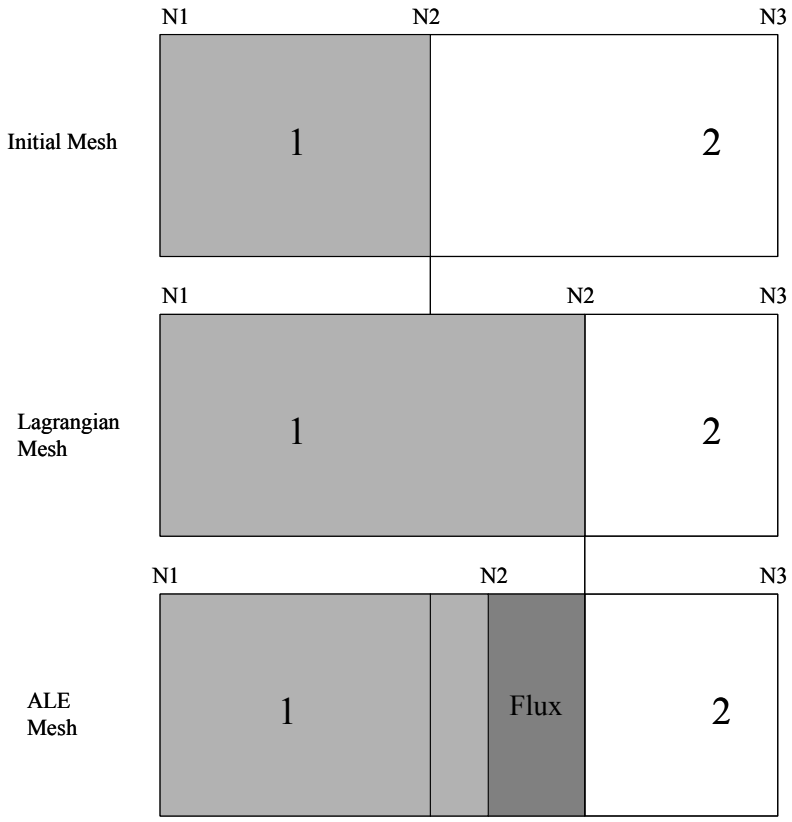

Figure 37 - Illustration of 1-D ALE Formulation [25]

2.1.3.2 TIME INTEGRATION ALGORITHM FOR ALE METHOD

LS-DYNA uses the Central Difference Method to advance the position of the Lagrangian mesh in time [25]. The stability requirement for the explicit integration is controlled by the element velocity, u, the speed of sound, c, and the characteristic length of the element, x [25].

$$\Delta t = \frac{\Delta x}{(c+u)} \tag{28}$$

$$f^{n} = f^{n+1/2} - f_{,t}\left(t_{n+1/2}\right)\frac{\Delta t^{n+1/2}}{2} + f_{,tt}\left(t_{n+1/2}\right)\left(\frac{\Delta t^{n+1/2}}{2}\right)^{2} + O\left(\Delta t^{n+1/2}\right)^{3} \tag{29}$$

$$f^{n+1} = f^{n+1/2} + f_{,t}\left(t_{n+1/2}\right)\frac{\Delta t^{n+1/2}}{2} + f_{,tt}\left(t_{n+1/2}\right)\left(\frac{\Delta t^{n+1/2}}{2}\right)^{2} + O\left(\Delta t^{n+1/2}\right)^{3} \tag{30}$$

Subtracting Equation (29) from Equation (30) gives a second order accurate integration rule [25].

$$f^{n+1} = f^{n} + f_{,t}\left(t_{n+1/2}\right)\Delta t^{n} + O\left(\Delta t^{n+1/2}\right)^{3} \tag{31}$$

where f is the nodal force function at each time step.

The energy equation, defined as

$$\dot{E} = Vs_{ij}\dot{\varepsilon}_{ij} - (p+q)\delta_{ij} \tag{32}$$

where V is the element volume, is integrated in time and is used for equation of state evaluations and a global energy balance. s_{ij} and p represent the deviatoric stresses and pressure where the deviatoric stress is

$$s_{ij} = \sigma_{ij} + (p+q)\delta_{ij} \tag{33}$$

and the pressure is defined by the material and equation of state models. q is the bulk viscosity, δ_{ij} is the kronecker delta ($\delta_{ij} = 1$ if i = j; otherwise $\delta_{ij} = 0$) and $\dot{\varepsilon}_{ij}$ is the strain rate tensor. The stress, σ_{ij}, in each material is obtained through the material and equation of state models for each time step. The mesh is updated after each iteration by defining a nodal force function

$$f_n = f_{\text{int}}^n + f_{ext}^n \tag{34}$$

where the internal nodal force function is

$$f_{\text{int}} = \int_V B^t \sigma_{ij} \cdot dx \tag{35}$$

where B^t is the transpose of the strain-displacement matrix. The external nodal force function, f_{ext}, is obtained from body forces, boundary forces, contact forces and non-reflecting boundary conditions. Boundary conditions are discussed in section 2.1.3.9. The nodal velocities are updated by

$$u^{n+1/2} = u^{n-1/2} + \frac{1}{2}\frac{f_n}{M}\left(\Delta t^n + \Delta t^{n+1}\right) \tag{36}$$

where M is the nodal mass. The nodal locations (displacements) are updated by

$$x^{n+1} = x^n + u^{n+1/2}\Delta t^n \tag{37}$$

The process is repeated for each time-step. Staggering the displacement and velocity allows for a second order accurate time algorithm. [21]

2.1.3.3 MESH REZONING FOR THE ALE METHOD

Mesh rezoning algorithm's (smoothing algorithm's) are used to keep the fluid (solid element) mesh from becoming too distorted so computation times do not increase. Rezoning transforms a non-uniform mesh into a uniform mesh [25]. The Lagrangian formulation does not use rezoning techniques. The Eulerian formulation uses an Eulerian rezone technique that returns the displaced nodes to their original location. The ALE formulation uses algorithms for mesh

rezoning. In this thesis the equipotential algorithm is used to control mesh rezoning and material flux.

The equipotential algorithm transforms a non-uniform mesh into a uniform mesh by maintaining the location of the boundary nodes at their lagrangian location and iterating the internal nodes to converge to a uniform mesh by solving the equipotential equation for the nodal displacement,

$$\nabla^2 u = 0 \tag{38}$$

where ∇^2 is the Laplacian operator and u in the nodal displacement [25].

2.1.3.4 ADVECTION ALGORITHM

Advection algorithms are used to track the transport of material flux from one element to another. The amount of material transported is determined by the mesh rezoning techniques for each formulation. The algorithms are stable, monotonic, and conservative. Mass, momentum, and internal energy are advected for fluid materials. Mass, momentum, internal energy, stress components, and plastic strain are advected for solid materials. This paper is only concerned with advection for fluid materials. In general, the advection algorithm uses the equation

$$s_e \cdot V_e = s_l \cdot V_l + \sum_{faces} s_l^j \cdot Flux_j \tag{39}$$

$$\Delta M = \sum_{faces} s_l^j \cdot Flux_j \tag{40}$$

where s_e is the property of the Eulerian element receiving the advected quantity, V_e is the volume of the Eulerian element, s_l is the property of the Lagrangian element being advected, V_l is the volume of the Lagrangian element, s_l^j is the property being advected in the j^{th} face of Lagrangian element, and $Flux_j$ is the volume flux through the adjacent element j. ΔM is the change in momentum resulting from advection in the x, y, or z direction. The variable s is defined for internal energy, mass, and momentum advection as

$$s = \frac{E}{V} \tag{41}$$

$$s = \rho \tag{42}$$

$$s = \rho \cdot U \tag{43}$$

where V is the element volume, the momentum advection variable U, in Equation (43), is the element velocity in the x, y, and z directions. The element velocities (u, v, w) are calculated by taking an average of the nodal velocities in the corresponding direction.

$$U^{elem} = \frac{1}{8} \sum_{node=1,8} U^{node} \tag{44}$$

Momentum advection is done directly through the nodes [25]. LSDYNA uses a Half Index Shift which constructs a staggered mesh, where the staggered mesh nodes are located at the elements center. This will allow for the momentum flux to be calculated through the element faces. In this thesis a Second Order Van Leer algorithm is used for advection. Equations (39-44) describe a first order accurate advection algorithm. The Van Leer algorithm uses Equation (45) instead of Equation (43) in the advection calculation.

$$s = \rho_0 + \frac{1}{2}(x_1 - x_0)\frac{\partial \rho}{\partial x}(x_1) \tag{45}$$

Figure 38 shows an illustration of the how the second order accurate Van Leer algorithm, Equation (45), uses a parabolic fit to transition the amount of material flux flowing across element faces. The Van Leer algorithm allows for a gradual change in material flux at the element face, as opposed to an abrupt change at the element face. The amount of material flux through the element faces is a result of the amount of mesh distortion that occurs, which is controlled by the mesh rezoning method that is applied. Flux is the volume of material moving from element 1 to element 2 [25]. Figure 36 shows how the material flux is obtained in an Eulerian formulation where the mesh nodes are rezoned back to their original locations (fixed mesh). Figure 37 shows how the material flux is obtained in an ALE formulation where the mesh nodes are rezoned to an optimal location. In this thesis all formulations use the second order accurate Van Leer advection algorithm.

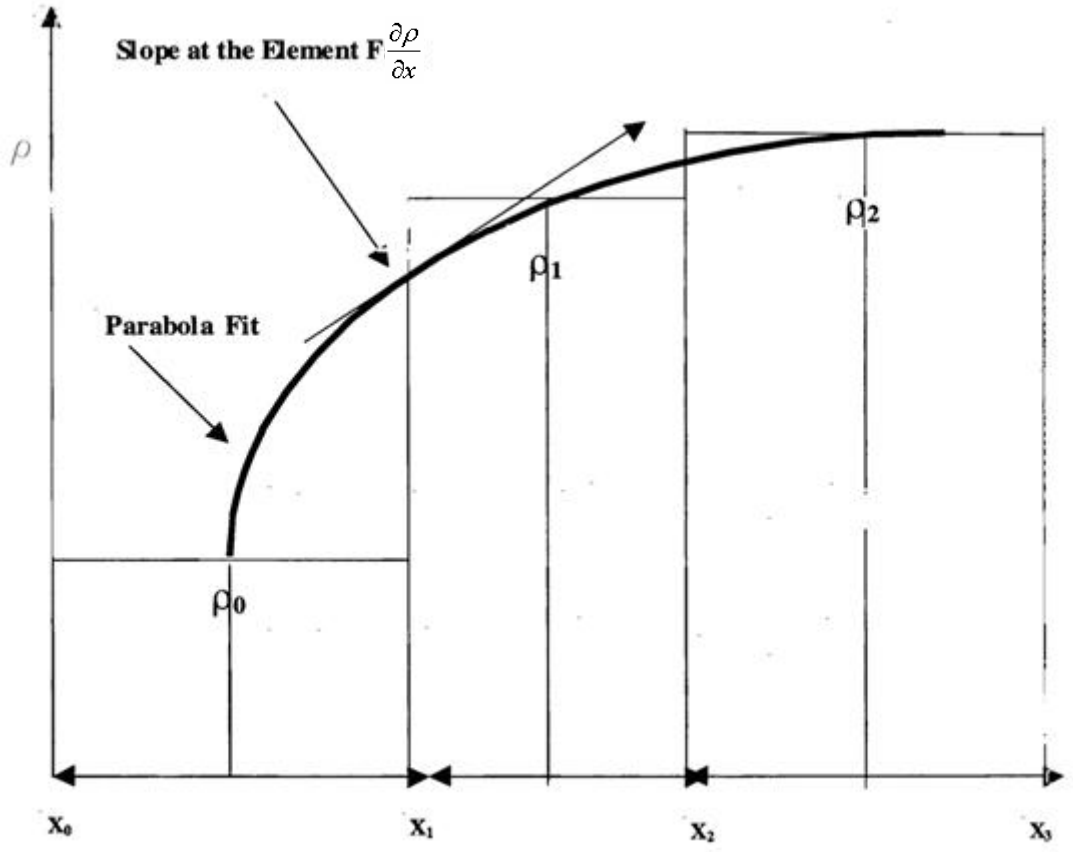

Figure 38 - Illustration of Second Order Van Leer Algorithm [25]

2.1.3.5 FLUID/STRUCTURE COUPLING METHOD

When determining the vulnerability of a ship to an underwater explosion it is important to be able to translate the fluid dynamics to the structure. Underwater explosions can generate large amounts of energy. It is important to ensure the energy is properly transferred to the to a structure with minimal loss. One way to accomplish this is by having one to one nodal alignment of the fluid and structure, capable of transferring the data directly from the fluid to the structure.

To have proper transfer of information from fluid mesh domain to structural mesh domain, it is necessary to have an adequate fluid/structure coupling algorithm. The *CONSTRAINED_LAGRANGE_IN_SOLID card in LSDYNA allows for a Lagrangian "slave" mesh to be coupled with an Eulerian "master" mesh. The Lagrangian structural mesh is always the slave mesh. There are several types of coupling methods allowed in this command. This paper uses type 4, penalty coupling without erosion, for all test cases since energy is conserved.

Penalty coupling tracks the relative displacement, d, between the Lagrangian node and the fluid material location in the Eulerian material [25] and applies a coupling force proportional to d using the Equation (46)

$$F = -K \cdot d \tag{46}$$

where K is a spring constant and is calculated based on the constitutive material properties of the model. The coupling force is distributed to the Eulerian fluid nodes and the Lagrangian structural nodes.

2.1.3.6 MULTI-MATERIAL ARBITRARY LAGRANGIAN/EULERIAN

The ability to track different materials in an underwater explosion event is important. In the fluid domain there are usually two different materials before detonation of the explosive; the high explosive material, and the fluid. There are at least three different materials in the fluid domain after the initial detonation; the unburned portions of the high explosive, the burned gaseous products of the high explosive (which grows to become the explosive bubble), and the fluid. After the shockwave has been released and is traveling through the fluid medium, cavitation poses another material difference that exists. It is necessary to have the ability to track these materials in order to capture the interaction between them. In a close-in underwater explosion there are interactions between the shockwave, the gaseous bubble, the structure, and the cavitation regions formed by the shockwave and the reflected shockwave. In LS-DYNA material is tracked by density. Eulerian methods are not capable of handling more than one material in an element.

The multi-material ALE formulation uses the same governing equations as the ALE formulation except that for each element the calculations are performed iteratively for each material group in the element. For material group i, the strain rate is ε_i, the internal energy is E_i, deviatoric or shear stress is τ_i, pressure from the equation of state is P_i, the stress is given by

$$\sigma_i = -P_i + \tau_i \tag{47}$$

the internal nodal force is calculated by

$$F = \alpha_i \cdot \int_V B^T \sigma_i \tag{48}$$

where α_i is the volume fraction in the element and has the requirement

$$\sum_{i=1}^{Ngroups} \alpha_i = 1 \tag{49}$$

where Ngroups is the number of different materials in the element. After each calculation the volume fractions need to be recomputed using a pressure relaxation calculation in each element. The pressure relaxation calculation is given by

$$P_1 - K_1 \frac{\partial V_1}{V_1} = P_2 - K_2 \frac{\partial V_2}{V_2} \tag{50}$$

$$\delta V_1 + \delta V_2 = \delta V \tag{51}$$

where δV is the amount of material (volume) flux in the element after the lagrangian calculation and the subscripts refer to adjacent elements. The amount of total material to be advected can now be calculated. In LS-DYNA a volume fraction method is used to produce rules to determine how the materials in the element are advected.

Rule 1:

Material common to both neighboring elements are transported in proportion to the volume fraction of the acceptor element, with the restriction that no more than the total donor element volume may be transported [25].

Rule 2:

If there are no remaining materials common to both elements, the remaining transport volume is proportional to the remaining donor volume [25].

The process is repeated for each material at every time-step. As the number of materials to be tracked in each element increases the computational expense will increase.

2.1.3.7 EQUATION OF STATE MODELS

Equation of state models are used in LS-DYNA to relate the internal element energy, pressure, density, and volume of specified materials. Equations of state can be used to initialize internal characteristics of elements. In this thesis air, water, and the high explosive material are modeled using equations of state. Equations of state are used with material models (Section 2.1.3.8) in determining the internal force function of each element.

The linear polynomial equation of state is used for air in this thesis. The linear polynomial EOS is linear in internal energy [21]. The pressure is defined as

$$P = C_0 + C_1\mu + C_2\mu^2 + C_3\mu^3 + (C_4 + C_5\mu + C_6\mu^2)E \tag{52}$$

where μ is

$$\mu = \frac{\rho}{\rho_0} - 1 \tag{53}$$

The linear polynomial equation of state can also be used to model gas with the gamma law equation of state [21]. Setting $C_0 = C_1 = C_2 = C_3 = C_6 = 0$ and $C4 = C5 = \gamma - 1$, where γ is the ratio of specific heats. The pressure is given as

$$p = (\gamma - 1)\frac{\rho}{\rho_0}E \tag{54}$$

The units of E are the units of pressure [21].

Equation of state models can have a significant influence on the results of a finite element analysis. Pressure, energy, and density changes are non-linear in an underwater explosion event. The linear polynomial equation of state is linear in internal energy and is not a good means to model the water in an underwater explosion event, where capturing the propagation of pressure and energy is important. It is a good means of modeling air, since this thesis is not concerned with tracking the propagation of energy and pressure in air. The gamma law version of the linear polynomial EOS is used for air since it is computationally inexpensive and is able to handle air in tension and compression.

The Gruneisen equation of state is used to calculate the internal characteristics of water in this thesis. This equation of state can properly handle shock wave propagation in an underwater explosion event due to its ability to incorporate a nonlinear shock velocity-particle velocity relationship and the ability to handle a fluid in tension and compression, which is important when attempting to capture cavitation phenomena in water.

The Gruneisen equation of state with cubic shock velocity-particle velocity defines pressure for compressed material as

$$p = \frac{\rho_0 C^2 \mu\left[1 + \left(1 - \frac{\gamma_0}{2}\right)\mu - \frac{a}{2}\mu^2\right]}{\left[1 - (S_1 - 1)\mu - S_2\frac{\mu^2}{\mu+1} - S_3\frac{\mu^3}{(\mu+1)^2}\right]^2} + (\gamma_0 + a\mu)E \tag{55}$$

where E is the internal energy per unit volume, C is the intercept of the u_s-u_p curve, S_1, S_2, and S_3 are the coefficients of the slope of the u_s-u_p curve, γ_0 is the Gruneisen gamma, and a is the first order volume correction to γ_0. Constants C, S_1, S_2, S_3, γ_0, and a are all input parameters [21].

The compression is defined in terms of the relative volume, V, as:

$$\mu = \frac{1}{V} - 1 \tag{56}$$

For expanded materials the pressure is defined by Equation (57) [21].

$$p = \rho_0 C^2 \mu + (\gamma_0 + a\mu)E \tag{57}$$

The Jones-Wilkins-Lee equation of state is used to model the detonation products of high explosives. The pressure is defined as

$$p = A\left(1 - \frac{\omega}{R_1 V}\right)e^{-R_1 V} + B\left(1 - \frac{\omega}{R_2 V}\right)e^{-R_2 V} + \frac{\omega E}{V} \tag{58}$$

where E is the initial internal energy and V is the initial relative volume [21]. The JWL equation of state is used with the high explosive burn material (Section 2.1.3.8) to calculate the internal force function and the energy of the explosive material.

2.1.3.8 MATERIAL MODELS

Material models use pressure calculated in equation of state models to determine the internal characteristics of material in an element.

Null material is used to model fluids (air and water) in this thesis. The null material model is chosen for its ability to: define dynamic viscosity; the incorporation of strain rate, finite in a fluid, instead of strain, infinite in a fluid; and for its ability to calculate stresses in a fluid. For solid elements, equations of state can be called through this model to avoid deviatoric stress calculations. This model is very useful when material strength, the ability to sustain finite deformation under the action of constant shear stress, is neglected. An optional viscous stress of the form

$$\sigma_{dij} = 2\mu\dot{\varepsilon}'_{ij} \tag{59}$$

is computed for nonzero μ where $\dot{\varepsilon}'_{ij}$ is the deviatoric strain rate.

Pressure in null material is calculated by using the Gruneisen equation of state. Stress in the null material is then calculated by Equation (60),

$$\sigma_{ij} = -P_{EOS} \cdot I_d + \sigma_{dij} \tag{60}$$

where I_d is the identity matrix [21]. The element stress from Equation (60) is used is Equations (33) and (35) to solve for the internal force function.

The high explosive burn material is used in the modeling of explosive materials. The pressure in the explosive material is calculated using the JWL equation of state and a burn fraction. The burn fraction is defined by Equations (61) through (63),

$$F_1 = \frac{\rho V^2}{P_{cj}}\left(1 - \frac{v}{v_0}\right) \tag{61}$$

$$\frac{v}{v_0} = \frac{\rho}{\rho_0} \tag{62}$$

$$F_2 = (t - t_b)V\frac{2}{3\Delta x} \tag{63}$$

where t_b is the burn time of the element ($t_{bj} = d_j/V$), where d_j is the distance from the detonation point to the center of the j^{th} high explosive element. (d_j is used to obtain a spherical pressure distribution). Δx is the characteristic element length. V is the initial relative volume in the high explosive element. P_{cj} is the Chapman-Jouguet pressure. The overall pressure in the high explosive material is then defined by Equation (64).

$$P = F \cdot P_{JWL} \tag{64}$$

After detonation, $S_{ij} = 0$ and the energy equation becomes

$$\dot{E} = -(p + q)\dot{V} \tag{65}$$

and the material behaves like a gas. Defining the beta burn flag for the high explosive material is key in how the material will be treated. Beta = 1, beta burn, is used to detonate the high explosive by means of volumetric compression. The burn fraction used in this option is F_1 (Equation 61). Beta = 2, programmed burn, the detonation is controlled by the lighting time if each element. The burn fraction F_2, Equation (63), is used. This option allows the explosive material to behave as an elastic plastic material and allows compression without detonation [25].

Beta = 0, beta + programmed burn, is the option used in this thesis. The burn fraction is then calculated by Equation (66):

$$F = \max(F_1, F_2) \tag{66}$$

and the final pressure is calculated by Equation (64) for all beta options. The final pressure is input into Equation (65) to calculate the energy of the high explosive material.

The material model *MAT_PLASTIC_KINEMATIC is used with shell elements to model non-failing steel structures in this paper. This is material type 3 in LS-DYNA. It models the isotropic and kinematic hardening plasticity and includes a Cowper Symonds strain rate model. This material model is more cost effective compared to the linear plasticity model.

The material model *MAT_PIECEWISE_LINEAR_PLASTICITY is an elasto-plastic material with an arbitrary stress strain curve and an arbitrary strain rate. It allows for material failure based on a plastic strain rate and includes a Cowper Symonds strain rate model. This material model allows for a more thorough representation of the material than the Plastic-Kinematic material model. The piecewise linear plasticity model is used to model failing steel structures in this thesis.

2.1.3.9 BOUNDARY CONDITIONS

Boundary conditions are applied to the FEA model to simulate various conditions. In this paper, the Euler Boundary condition and the Non-Reflecting Boundary condition are used in the FE fluid analysis to simulate model symmetry conditions and to reduce the overall size of the mesh model.

The Euler boundary condition defines velocity constraints at the boundaries of the fluid. The EBC variable is located in the *CONTROL_ALE card. There are three options available; off, on with stick condition, on with slip condition. The off option allows unconstrained velocities at the boundaries. The stick condition sets the normal component of the nodal velocity at the boundary equal to zero. The slip condition sets the material velocity equal to zero for all boundary nodes.

The Non-Reflecting Boundary Condition or transmitting boundary condition is applied to the fluid model exterior boundaries where an infinite or semi-infinite domain is required. The boundary condition prevents artificial stress wave reflections from reentering the model domain. Internally, LS-DYNA computes an impedance matching function for all non-reflecting boundary segments based on an assumption of linear material behavior [21]. This method applies viscous normal and shear stresses (Equation 67 and 68) to the boundaries:

$$\sigma_{normal} = -\rho c_d V_{normal} \tag{67}$$

$$\sigma_{shear} = -\rho c_s V_{\tan} \tag{68}$$

where ρ is the material density, c_d is the dilatational wave speed, and c_s is the shear wave speed of the fluid. V_{normal} and V_{tan} are the normal and tangential components of the particle velocity at the boundaries. The constants c_d, c_s, and ρ are assigned values during initialization based on the material properties of the non-reflecting boundaries.

2.1.3.10 INITIAL VOLUME FRACTION GEOMETRY

The *INITIAL_VOLUME_FRACTION_GEOMETRY card in LS-DYNA allows the initialization of different materials in a single element of a multi-material ALE model. This is achieved by using a volume fraction method where specific geometric shapes or mesh parts are defined and either the inside or outside of those shapes are filled with the specified material. This method treats the material defined by the boundary of the geometry the same as if it were modeled with a mesh.

CHAPTER 3 DEVELOPMENT OF EXPLOSIVE CHARGE/FLUID MODEL

It is important to understand how mesh modeling and the use of the LS-DYNA input cards affect the results of the ALE finite element analysis. Chapter 3 discusses the development of a modeling and simulation technique, with a 1-D and 3-D model, that will produce acceptable results for the ALE method in LS-DYNA. Section 3.1 discusses the 1-D model, a reproduction of the NPS Deep Spherical Bubble Problem [17,36,37], that displays the early-time and late-time behavior of an underwater explosion. Section 3.2 discusses the 3-D modeling approach, based on the NPS model [17,36,37], that displays the early-time and late-time behavior of an underwater explosion.

A basic understanding of a few key effects that different modeling techniques have on a FEA solution is needed. The first effect is how a stress (pressure) wave propagates through a FEA fluid model. It is important that there is orthogonality between all the fluid elements. Any region in the fluid model where elements are not orthogonal to the previous set of elements will produce numerical reflections when the stress (pressure) wave passes over that transition region (orthogonal elements to non-orthogonal elements). The second effect is when the stress (pressure) wave exits the fluid model mesh, in the case of a small model that uses an infinite boundary (Section 2.1.3.9) to simulate a larger region. The outer element boundary, where the stress wave exits, needs to be orthogonal to the previous elements. A rectangular mesh and/or a cylindrical mesh will accomplish both of these key points.

In order to properly model the explosive charge, such that when the shock wave is emitted from the charge it propagates in the proper shape, the charge must be modeled in the correct shape. For instance, if a spherical shaped charge is modeled using rectangular model the shock wave will have a step shape to it and will not have the spherical spreading shape it should. In order to prevent the improper shape it is necessary to model the charge in spherical coordinates. This poses a new problem. In a spherical coordinate mesh all the radial direction mesh lines converge onto a single point at the center of the sphere. The angles between the converging mesh lines become very small. LS-DYNA cannot handle these small angles and will give an error message and terminate. The way to handle the small angle problem is to begin the explosive charge mesh model as a rectangular mesh and transition it into a spherical mesh. It is important that the transition region remain inside the bounds of the explosive charge and not be in the fluid mesh

region, or the complications discussed above will occur. Figure 49 and Figure 50 show the modeling technique necessary to model a spherical charge.

3.1 Deep Spherical Bubble (DSB) Problem: 1-D Analysis

This analysis is based on a Deep Spherical Bubble (DSB) problem originally studied in a Naval Post Graduate School thesis by Chisum[17,36,37]. Results using an LSDYNA ALE model are compared to Chisum's results using a finite volume method.

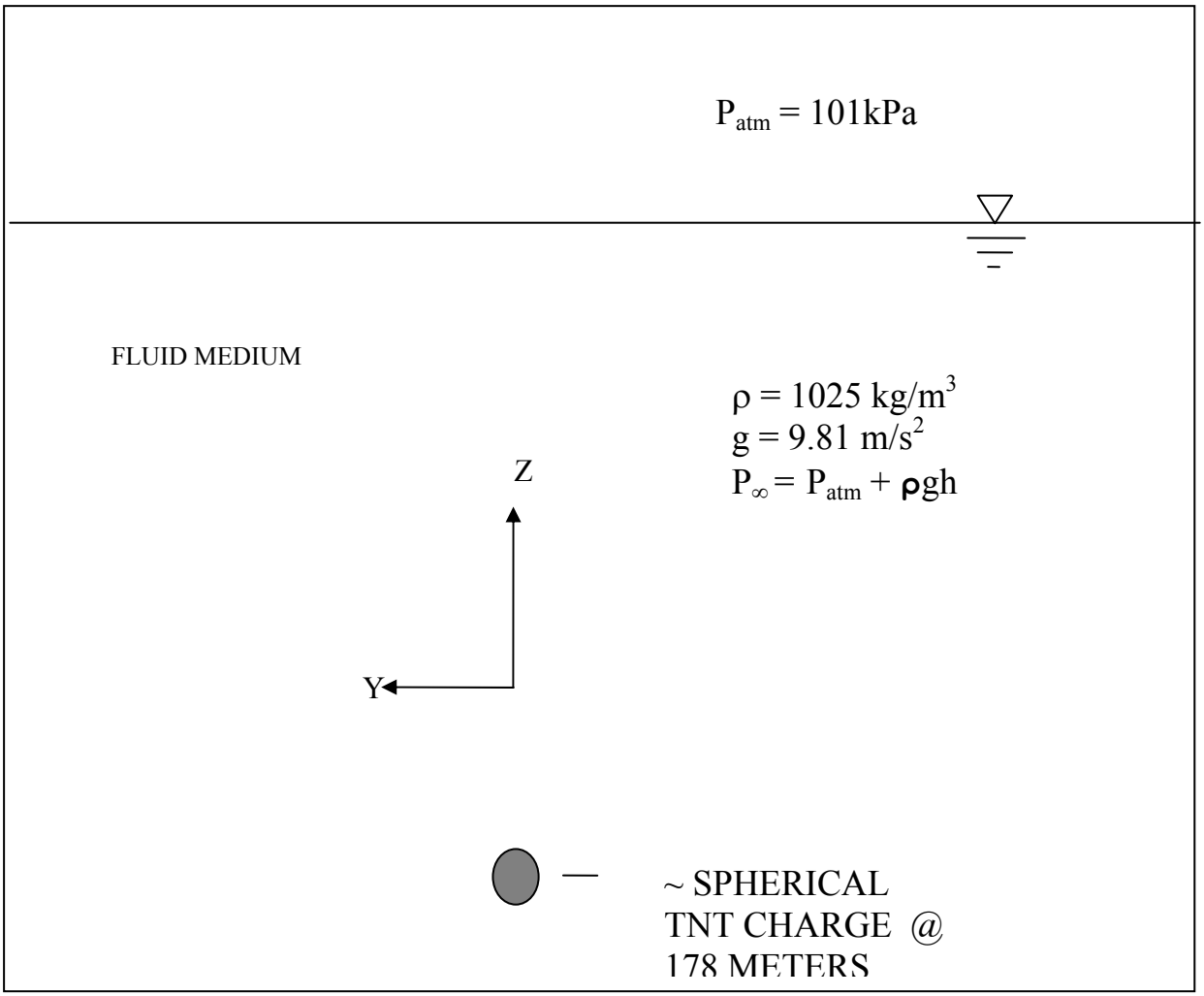

Figure 39 - Illustration of Spherical TNT Charge Detonated in Seawater[17,36,37]

3.1.1 Description

A spherical TNT charge is detonated at a depth (178m) in seawater with an initial density (ρ) equal to 1025 kg/m^3 as illustrated in Figure 39. The 1-D DSB problem[17,36,37] uses an adjusted charge of TNT to reproduce three dimensional results. The TNT charge size is adjusted

so that the peak pressure matches the analytical result from the peak pressure approximation. Figure 40 shows the horizontal finite element mesh, a 1-D expanding rectangle with the fluid (seawater) extending 178 meters from the center of the explosive charge to the free surface. The entire model is hydrostatically initiated for a charge depth (h) equal to 178 meters where the gravitational constant and atmospheric pressure are assumed to be 9.81m/s^2 and 101 kPa respectively. The colored regions of the fluid mesh correspond to varying mesh sizes and mesh densities as shown in Figure 41 and Figure 42. Table 5 shows the mesh variations.

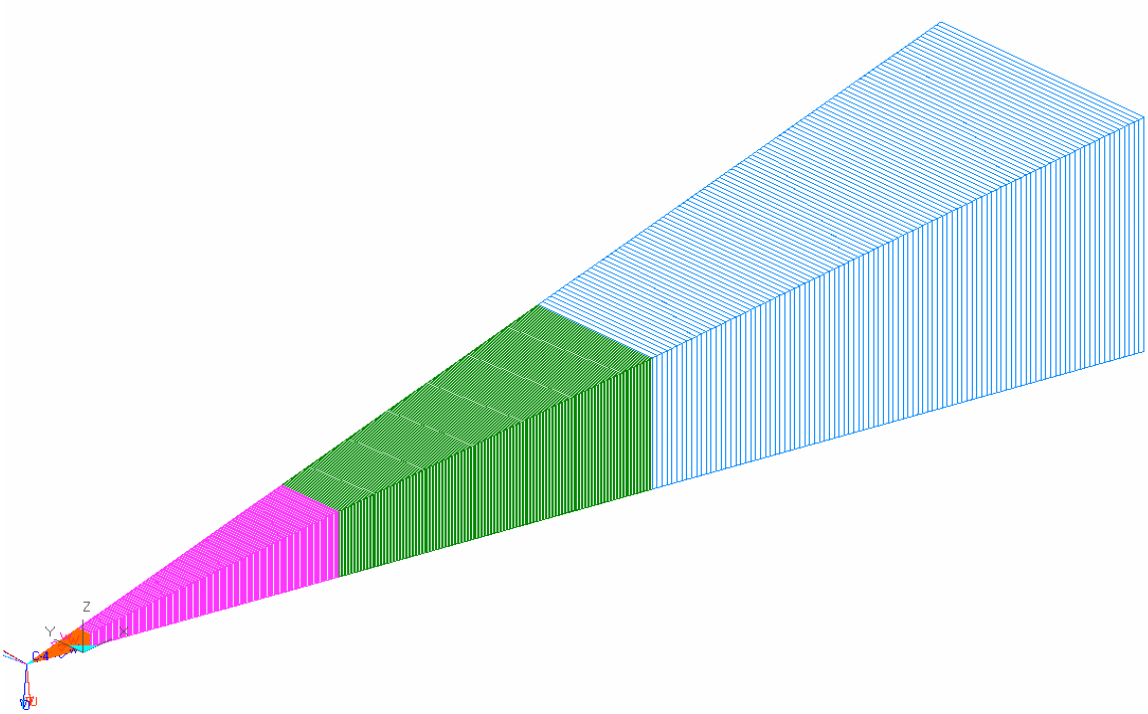

Figure 40 - Illustration of 1-D Deep Spherical Bubble Horizontal FE Model

3.1.2 Problem Setup in LSDYNA

The explosive is modeled using LSDYNA 1 point ALE multi-material elements and the MAT_HIGH_EXPLOSIVE_BURN material model with the Jones-Wilkens-Lee equation of state. Table 6 provides values of the constant parameters for the TNT charge used in all evaluations in this thesis. The charge mass is scaled, as in the NPS thesis, for the 1-D analysis.

The fluid (seawater) is modeled using LSDYNA 1 point ALE multi-material elements and the Null material model with the Gruneisen equation of state. Table 7 provides values of the constant parameters for the TNT charge used in all evaluations in this thesis.

The Pressure-time history is collected at a point 0.8 meters from the center of the adjusted charge. The outer most boundary face of the model, segment 607 as shown in Figure 43, is modeled using the Non-Reflecting Boundary Condition (Section 2.1.3.9) in order to allow the pressure wave to continue through the end of the fluid model without reflections, as if the fluid where modeled out to infinity. Additional analyses are conducted to determine the effect moving the outer fluid domain boundary, where the Non-Reflecting Boundary Condition is applied, has on the early-time and late-time pressure-time history results. The outer fluid domain boundary is modeled out to; 10, 25, 50, 65, 70, 74, 100, and 352.6 meters, and is compared to the 178.6 meter model as shown in Figure 48.

Table 5 DSB 1D Mesh Model Components

Part Number	**Number of Elements**	**Length of Elements (m.)**	**Part Domain (m.)**	**Part Type**
100	3	0.117	0 ~ 0.353	Explosive
200	199	0.003	0.353 ~ 1.0	Fluid
300	199	0.045	1.0 ~ 10	Fluid
400	199	0.2	10 ~ 50	Fluid
500	100	0.5	50 ~ 100	Fluid
600	100	0.786	100 ~ 178.6	Fluid

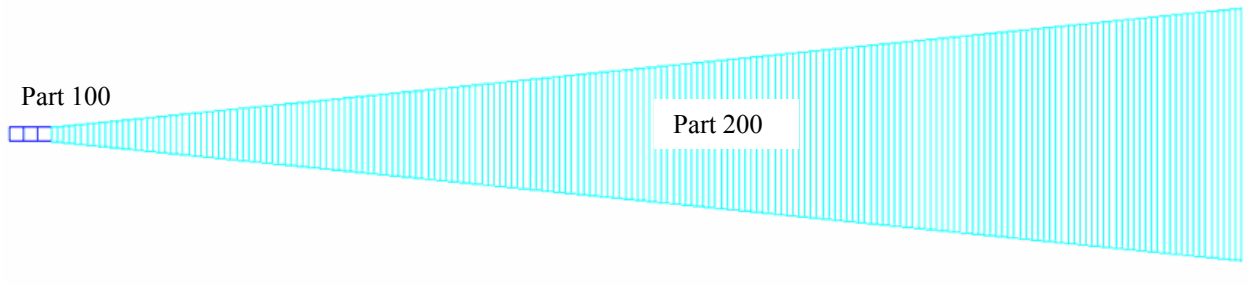

Figure 41 - Close-up of Explosive Charge Region of 1D DSB Model

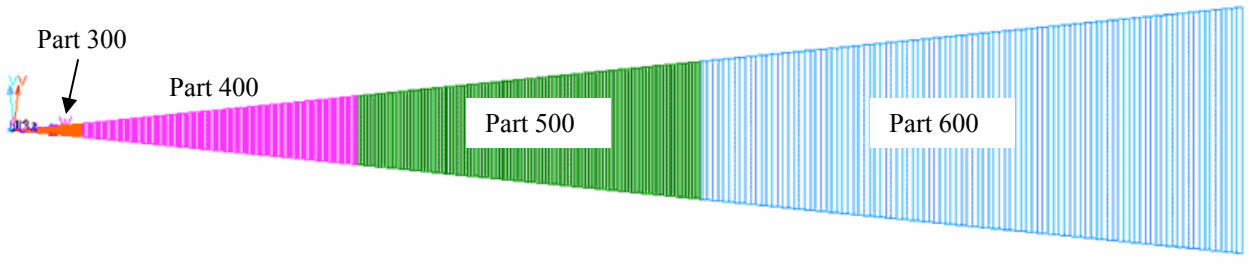

Figure 42 - Illustration of 1-D Deep Spherical Bubble FE Model

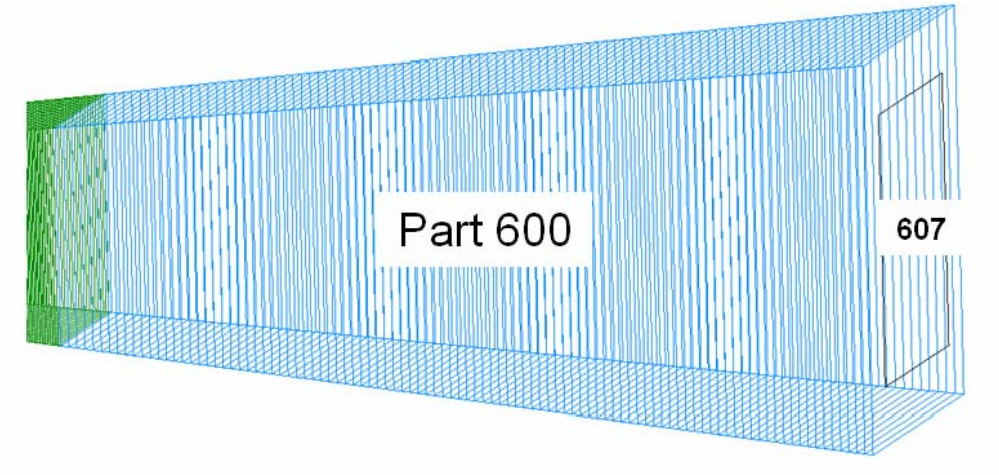

Figure 43 - Illustration of 1D Model Non-Reflecting Boundary Condition

Figure 44 and Figure 45 illustrate the local coordinate system and nodal constraints imposed on the charge portion and fluid portion of the 1-D model. A local coordinate system is created on the model to constrain the nodal motion to the radial only direction. This action is necessary in a 1-D model to capture the bubble dynamics that occur in the late time response of an underwater explosion.

The FEA results of the 1-D DSB problem are compared to bubble radius versus time data from the NPS Deep Spherical Bubble [17,36,37]. All analysis are performed on Pentium III or Pentium IV desktop PC's.

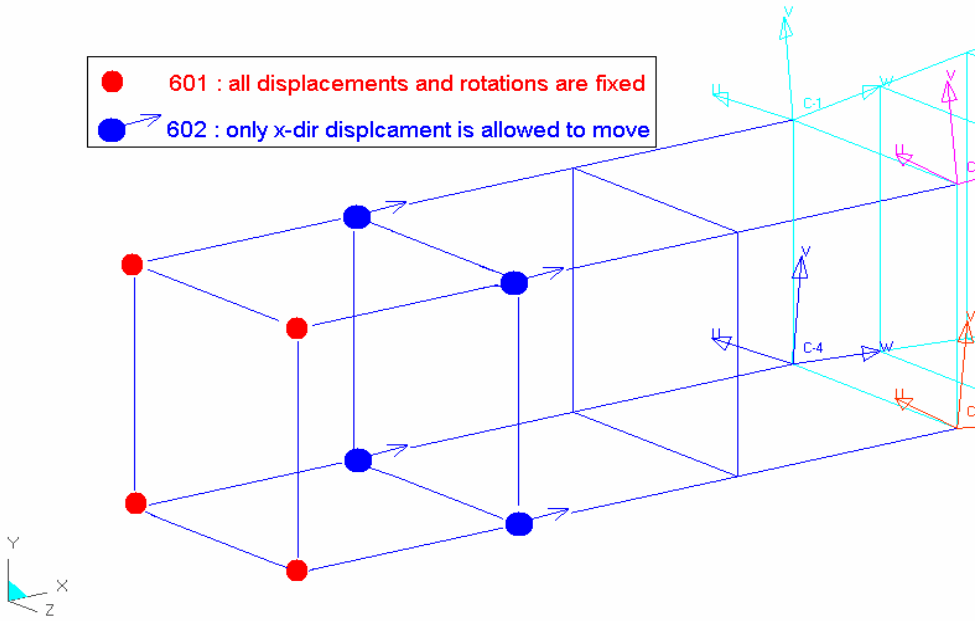

Figure 44 - Illustration of Charge Model Boundary Conditions

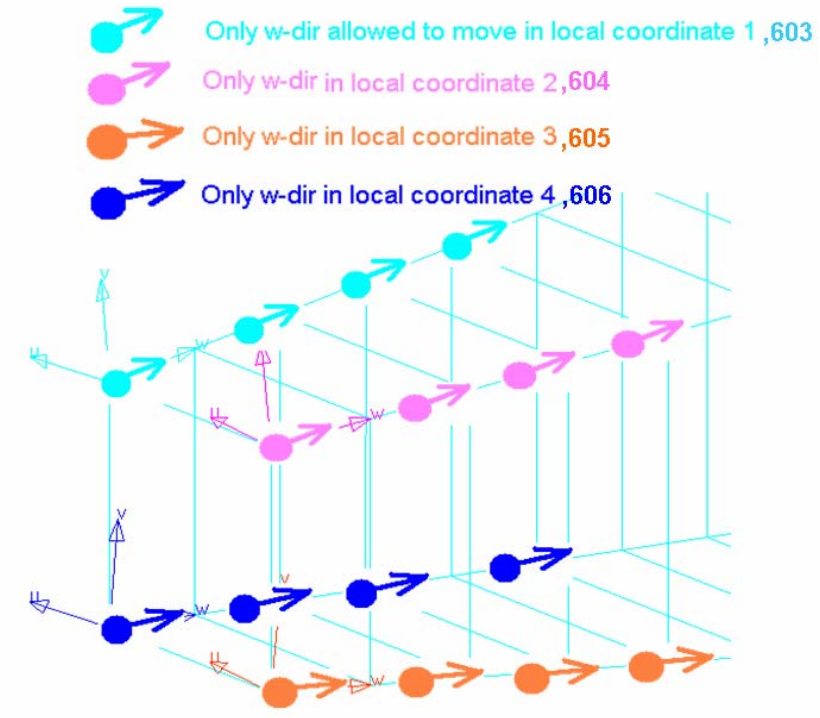

Figure 45 - Illustration of Fluid Model Boundary Conditions

3.1.3 Results

The 1-D FEA analysis bubble radius results are compared to the bubble radius results from the NPS Deep Spherical Bubble 1-D Problem [17,36,37]. Bubble radius data cannot be directly output from LS-DYNA. This data must be extracted from the analysis, at every time step, by displaying the density versus time data in the LS post-processor and measuring the bubble growth. The bubble wall is assumed to be located at the interface between the fluid and gas. This method ignores the thickness of bubble and results in possible errors in measurement. Figure 46 shows the bubble radius results comparison between the LS-DYNA 1-D FEA analysis and the reported NPS Deep Spherical Bubble 1-D Problem [17,36,37] bubble radius results.

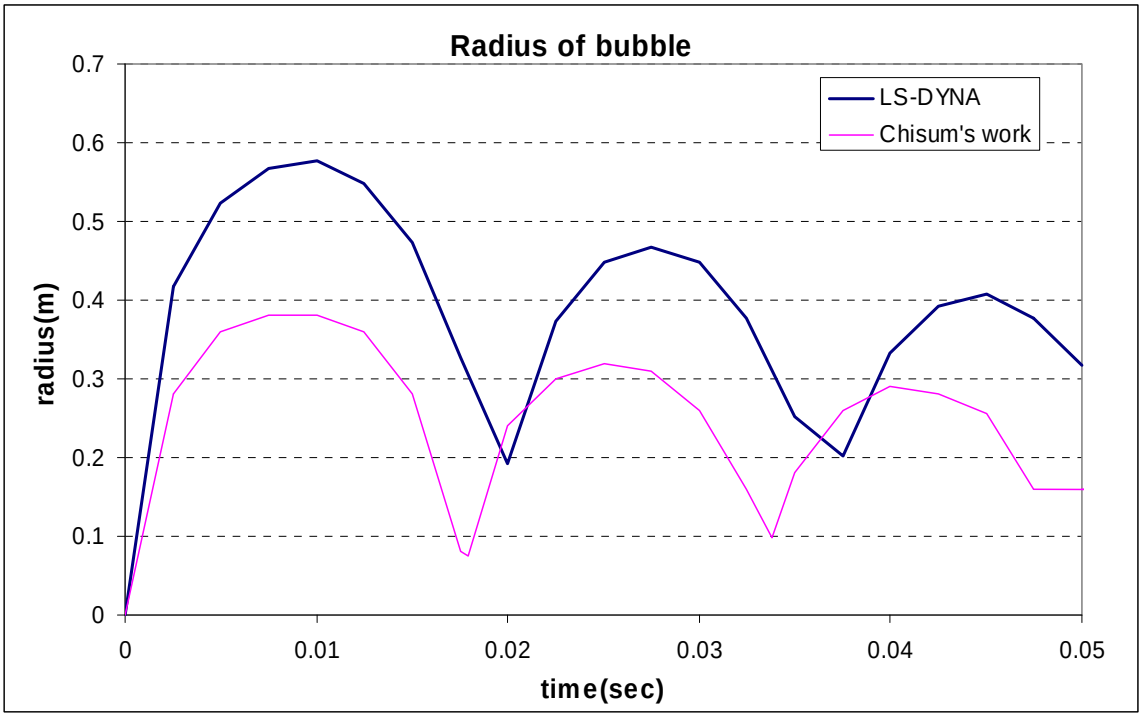

Figure 46 - Bubble Radius vs. Time for 1-D Deep Spherical Bubble Problem

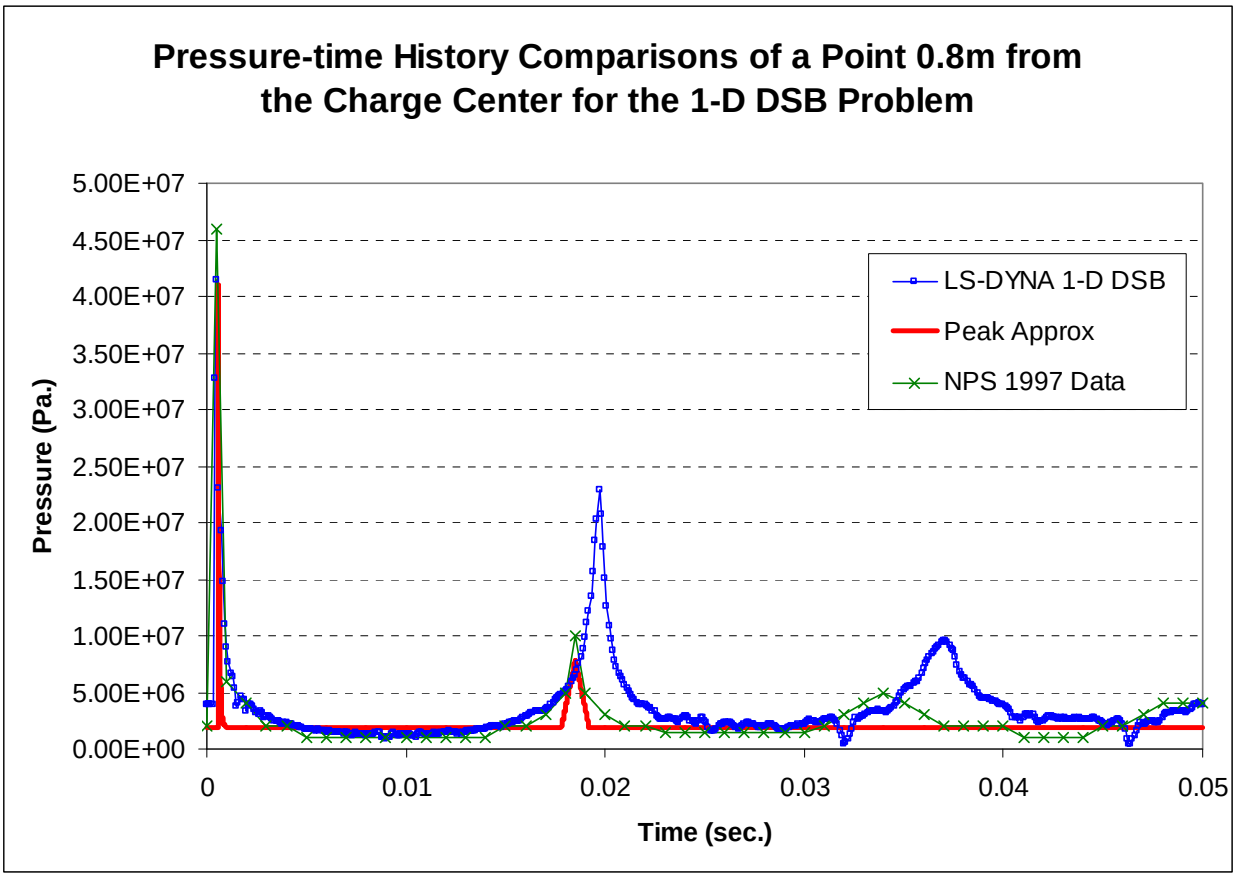

Figure 47 - Pressure-time History Comparison of 1-D DSB Problem, the Peak Approximation, and NPS 1997 Data [17,36,37].

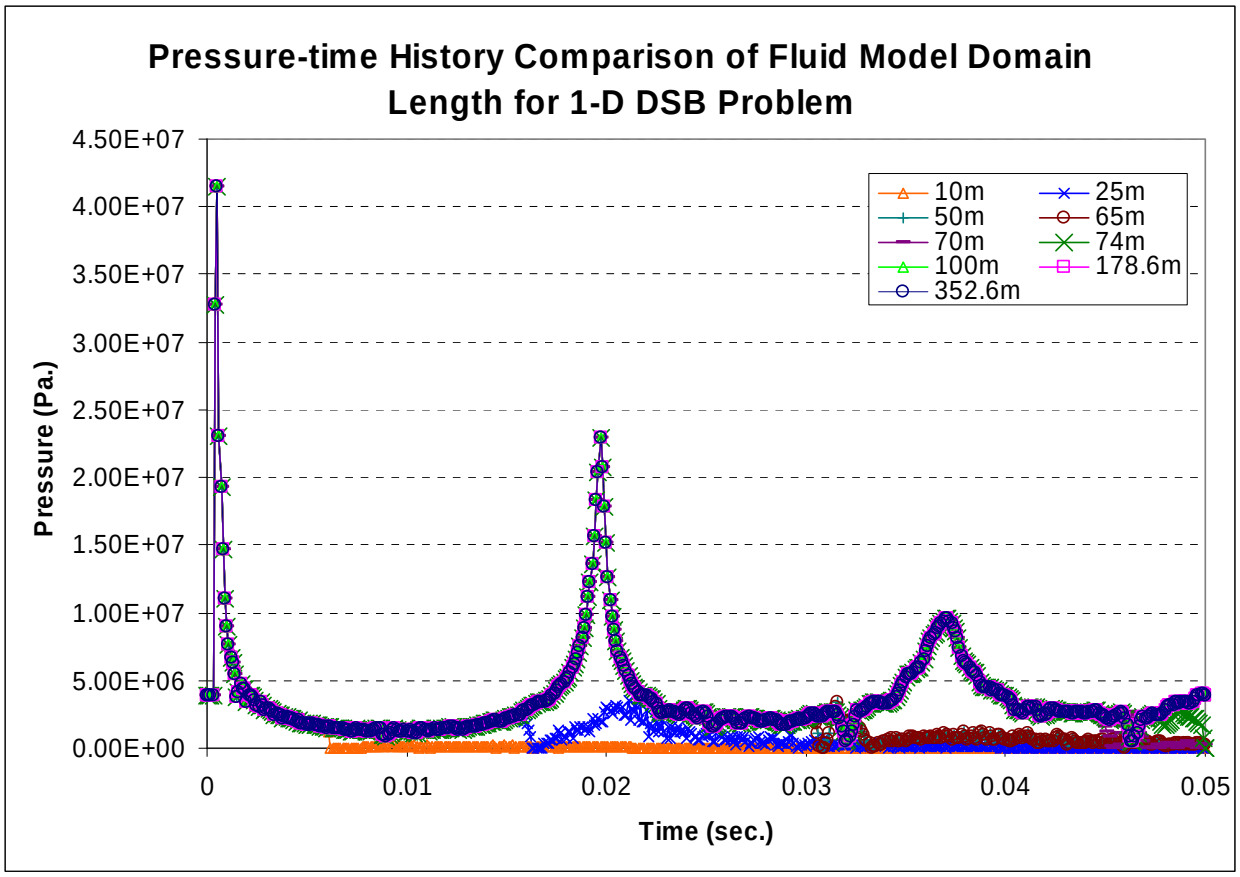

Figure 48 - Pressure-time History Comparison of Fluid Model Domain Length for 1-D Deep Spherical Bubble Problem

3.1.4 Discussion

The following conclusions can be made about the LS-DYNA 1-D analysis:

1. The length of fluid domain directly impacts the late-time response as shown in Figure 48. The Non-Reflecting Boundary Condition does not simulate an "infinite" boundary. A true infinite boundary condition is needed in order to minimize mesh model size.

2. To simulate the axisymmetric bubble motions in LS-DYNA, the radial constraints are needed by configuring new local coordinate systems in order to simulate a true 1-D problem in LS-DYNA.

3. The variation between the FEA results and the NPS results can be the differences in LS-DYNA(finite element code) and MSC/Dytran(finite volume code).

3.2 Deep Spherical Bubble Problem: 3-D Analysis

The ability to capture the propagation of a pressure wave and bubble dynamics in a three dimensional model of an underwater explosion is an important component in the process of developing a method for predicting damage to a ship caused by an underwater explosion. The 3-D Deep Spherical Bubble (DSB) Problem [17,36,37] is a cylindrical TNT charge detonated at a depth of 178m. The maximum pressure (peak pressure) and the first bubble pulse are key phenomena that need to be captured. Comparing the pressure-time history at a fixed location in the fluid to the pressure-time history given by the similitude equations' peak approximation (Section 1.2.3) will show if the pressure wave propagation phenomena is captured. Reproducing the early-time pressure results using the input data from the 3-D Deep Spherical Bubble Problem from the Naval Postgraduate School [17,36,37] is attempted first (Section 3.2.2.1). The results are analyzed (Section 3.2.2.1) and a determination that a need for a modified method that will capture the pressure wave phenomena is made and an investigation to properly capture the shock phenomena is conducted in Section 3.2.2.2. Once the early-time results are obtained, a two part sensitivity analysis is conducted on the DSB problem to gain an understanding of the FEA code and to develop a method that will capture the pressure wave characteristics accurately. The first part, Matrix #1 (Section 3.2.2.3.1), investigates the sensitivity of the pressure wave characteristics to varying element size and configuration, time-step size, and the number of time-step cycles between material advection. The second part, Matrix #2 (Section 3.2.2.3.2), investigates the sensitivity of the pressure wave characteristics to different boundary conditions.

Section 3.2.1 gives a description of the 3-D Deep Spherical Bubble problem.

3.2.1 Description

A spherical TNT charge is detonated at a depth (178m) in seawater with an initial density (ρ) equal to 1025 kg/m^3 as illustrated in Figure 39. The 3-D DSB problem [17,36,37] uses a 0.66-lb. charge of TNT with a charge radius of 0.03525 meters for most analysis unless otherwise noted. The finite element meshes are one octant of a sphere with the fluid (seawater) extending in most cases to 1.5 meters from the center of the explosive charge unless otherwise noted. The entire model is hydrostatically initiated for a charge depth (h) equal to 178 meters where the gravitational constant and atmospheric pressure are assumed to be 9.81m/s^2 and 101 kPa respectively. Figure 49 and Figure 50 show illustrations of the FEA models used. The FEA model mesh configuration in Figure 49 and Figure 50 is used since the transition region, where

the rectilinear mesh becomes a spherical mesh, is inside the high explosive charge mesh model region. Artificial pressure wave reflections occur when the transition region is in the fluid mesh domain. A purely rectilinear mesh configuration and a purely spherical mesh configuration were considered. Having a purely rectilinear mesh poses difficulties when trying to produce a spherical pressure wave from a non-spherical charge shape. The purely spherical mesh causes difficulties in the FEA calculation due to the convergence of the radial lines at the charge center. The convergence of the radial lines at the location of the charge center produces very small angles in an element. LS-DYNA cannot handle such small angles between element edges and a run-time error will occur.

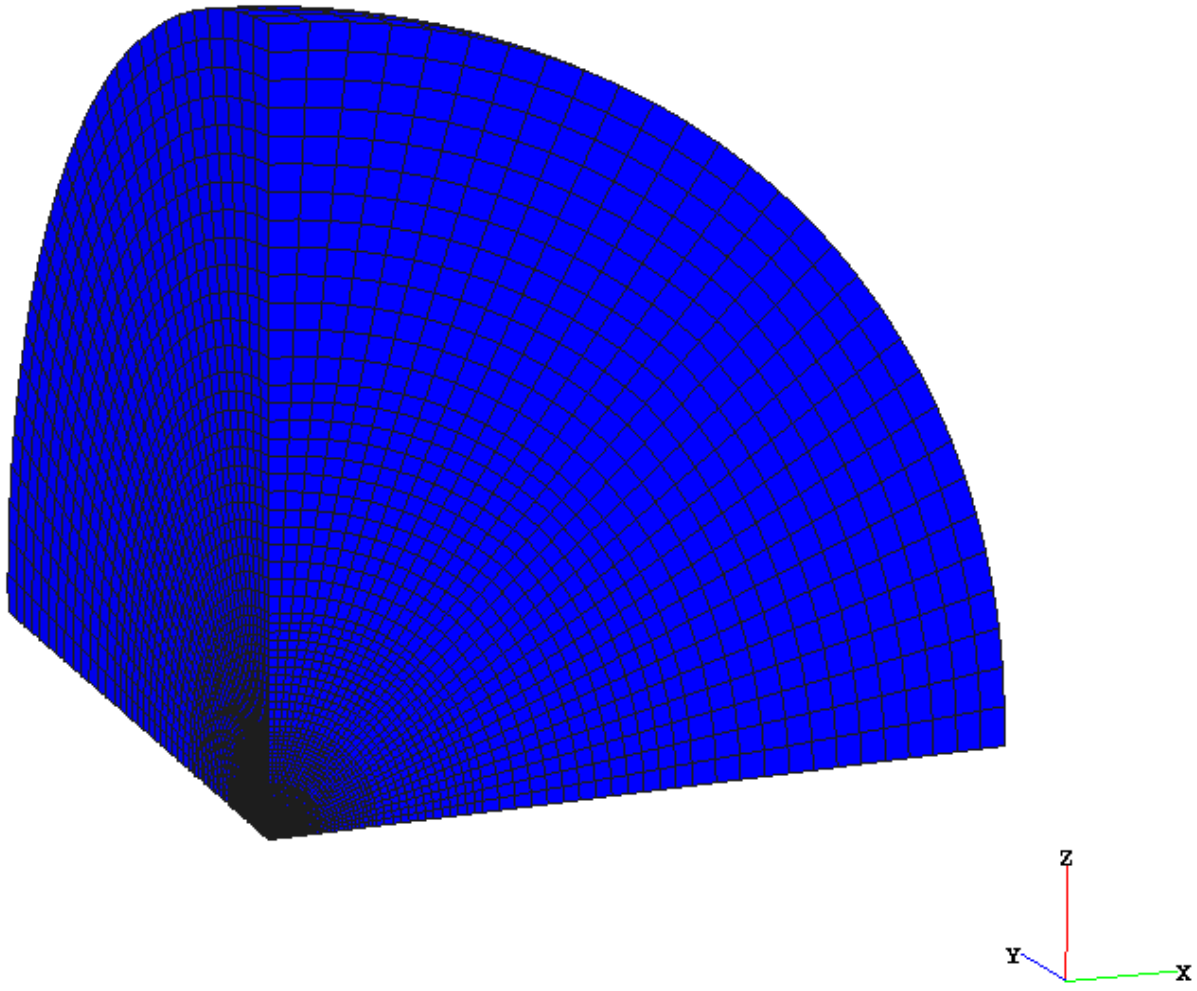

Figure 49 - Illustration of 3-D Deep Spherical Bubble FE Model

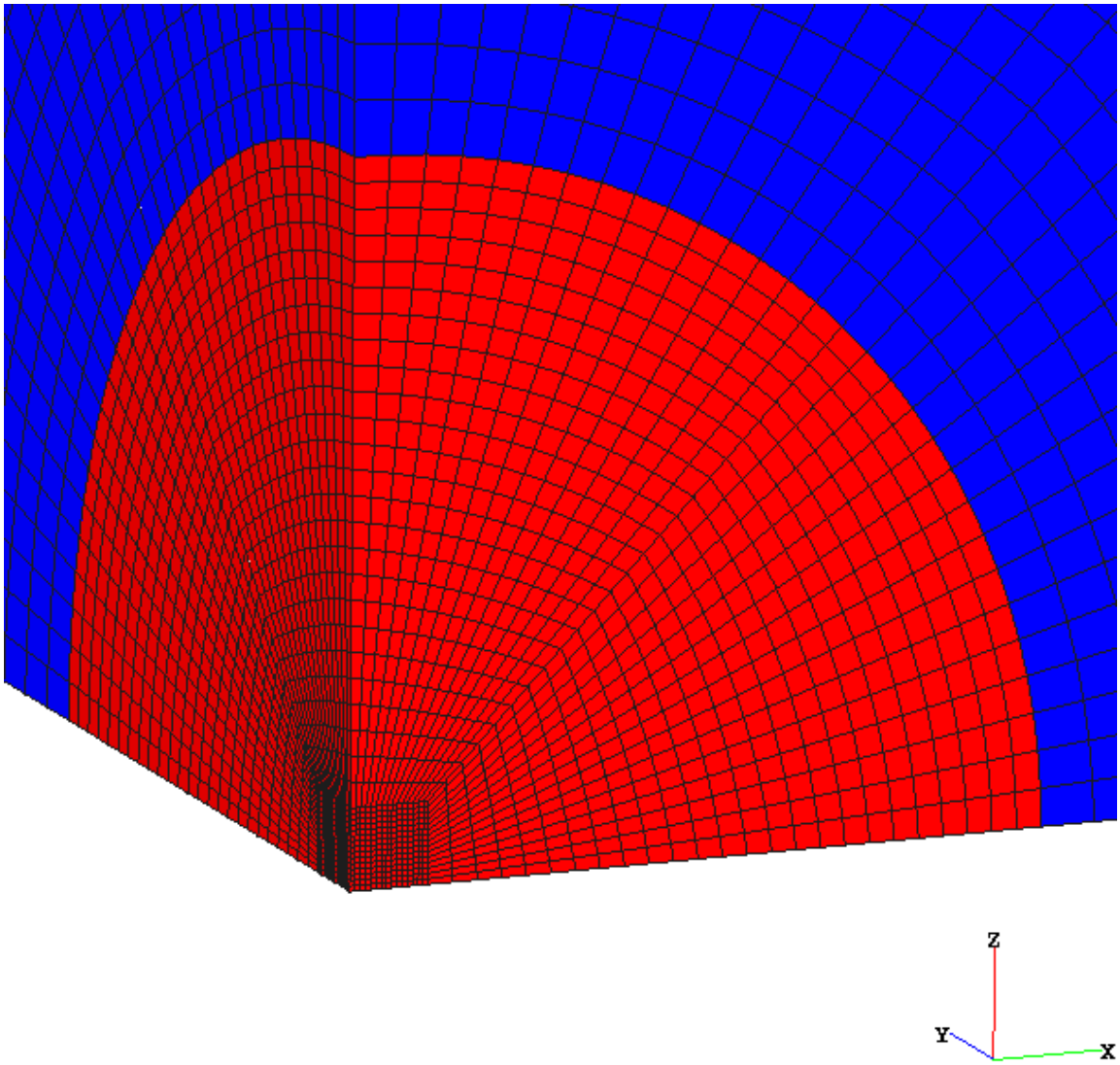

Figure 50 - Illustration of Charge Region for 3-D Deep Spherical Bubble FE Model

3.2.2 Problem Setup in LSDYNA

The explosive is modeled using LSDYNA 1 point ALE multi-material element type elements and the MAT_HIGH_EXPLOSIVE_BURN material model with the Jones-Wilkens-Lee equation of state. Table 6 provides values of the constant parameters for the TNT charge used in all evaluations in this thesis. Appendix APPENDIX D shows the LS-DYNA input file for case Reproduction Test case shown in Figure 53 and Table 8.

Table 6 Constant Parameters for TNT Charge

Parameter	***Value***	***Units***
Charge Type	TNT	--
Charge Mass	0.299	kg
Charge Density	1630	kg/m^3
Charge Depth	178.6	m
Charge Detonation Velocity	6930	m/s
Chapman-Jouguet Pressure	2.10E+10	N/m^2
Jones-Wilkens-Lee Coefficient A	3.71E+11	N/m^2
Jones-Wilkens-Lee Coefficient B	3.21E+09	N/m^2
Jones-Wilkens-Lee Coefficient R1	4.15	--
Jones-Wilkens-Lee Coefficient R2	0.95	--
Jones-Wilkens-Lee Omega	0.3	--
Internal Energy of Explosive per Reference Specific Volume	6.99E+09	J/m^3

The fluid (seawater) is modeled using LSDYNA 1 point ALE multi-material type elements and the Null material model with the Gruneisen equation of state. Table 7 provides values of the constant parameters for the TNT charge used in all evaluations in this thesis.

Table 7 Constant Parameters for Seawater

Parameter	*Value*	*Units*
Water Type	Sea	--
Water Density	1025	kg/m^3
Speed of Sound in Water	1415	m/s
Dynamic Viscosity Coefficient	1.13E-03	Ns/m^2
Intercept of vs-vp Curve	1415	m/s
Gruneisen Coefficient S1	2.56	--
Gruneisen Coefficient S2	-1.986	--
Gruneisen Coefficient S3	0.2268	--
Water Temperature	20	Degrees Celsius
Gruneisen Gamma	0.4934	--
First Order Volume Correction to Gamma	1.3937	--
Internal Energy of Water per Reference Specific Volume	3.85E+06	J/m^3
Relative Volume at Time 0 to Reference Specific Volume	1	--

Specific FEA resultant data of interest is the pressure-time history collected at a point 0.8 meters from the center of the 0.66-lb. charge. The data is collected using tracer particles that are fixed in space. This is done with the *DATABASE_TRHIST and the *DATABASE_TRACER cards

in LSDYNA. The outer most spherical boundary faces of the model are given the Non-Reflecting Boundary Condition (Section 2.1.3.9) in order to allow the pressure wave to continue through the end of the fluid model, no reflections, as if the fluid where modeled out to infinity.

The FEA results of the 0.66-lb. charge of TNT at h = 178 meters are compared to data generated by the Peak Approximation (Section 1.2.3 and Appendix APPENDIX A) shown in Figure 51 and Figure 52. The peak approximation is the most widely used method of analytically determining the pressure-time history of an underwater explosion. The peak approximation uses empirical relations that describe the peak pressure and the decay at a point in space some radial distance (R) outward from the center of the explosive charge. All analysis are performed on Pentium III or Pentium IV desktop PC's.

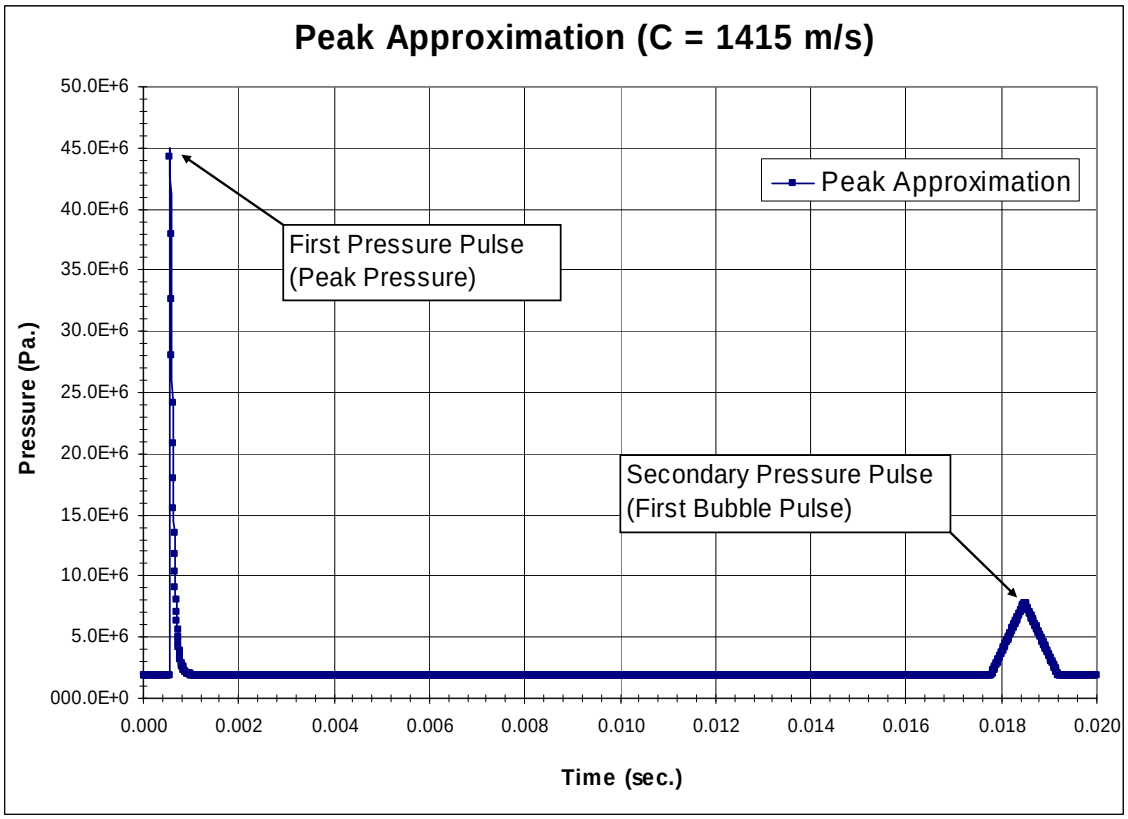

Figure 51 - Peak Approximation for 0.66-lb. TNT at 178 meters to 0.025 seconds

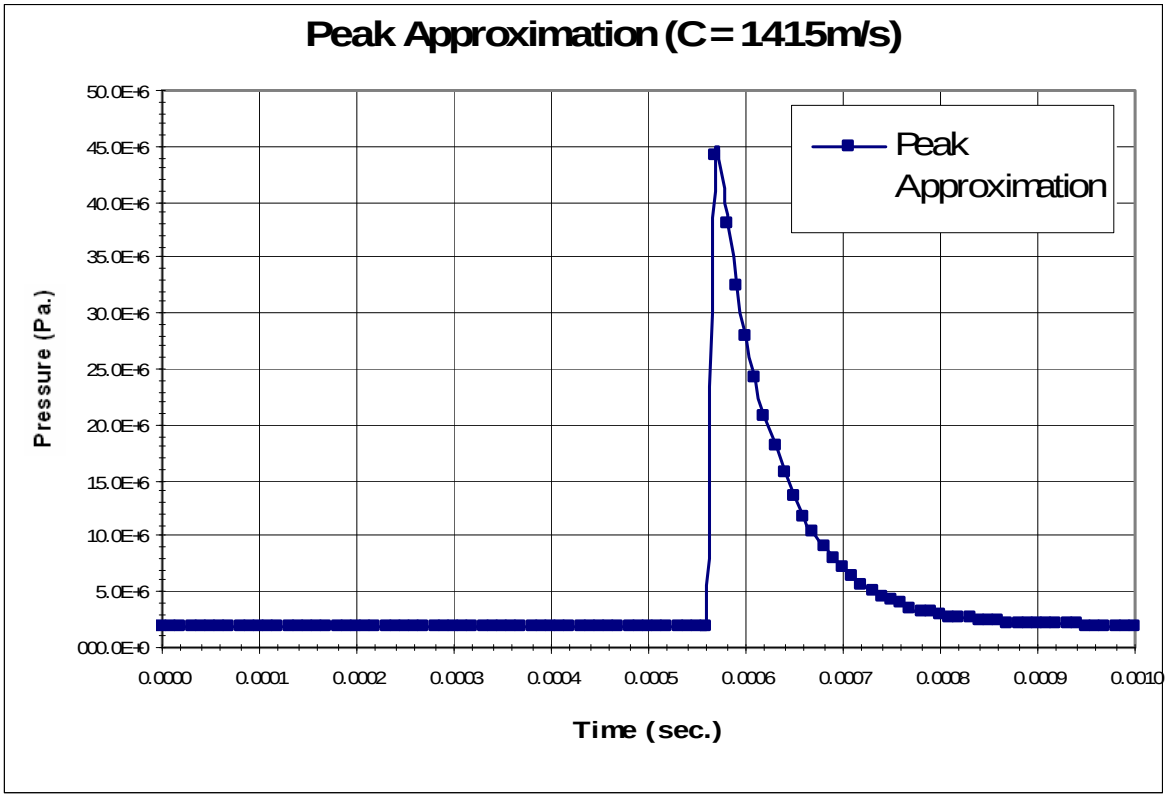

Figure 52 - Peak Approximation for 0.66-lb. TNT at 178 meters to 0.001 seconds

3.2.2.1 Reproducing NPS Early-time Pressure Results

3.2.2.1.1 Problem Setup

The Reproduction Test problem set up is the same as above. The Gruneisen Equation of State input data, Table 7, from the Naval Postgraduate School thesis [17,36,37] is used. Element size and configuration type ES15_25, discussed in Section 3.2.2.3.1 page 94, is used. This element size is similar to the element size used in the NPS thesis [17,36,37]. In the NPS thesis [17,36,37], the FEA termination time is 0.05 seconds. The FEA termination time for the Reproduction test is 0.001 seconds. The termination time is decreased for the Reproduction Test since only the early-time response is to be considered in this text. Section 3.2.2.3 will investigate reproducing the late-time portion of the DSB problem.

3.2.2.1.2 Results

Figure 53 shows the results of the Reproduction Test compared to Extrapolated NPS data [17,36,37] and the Peak Approximation. Table 8 compares the time of occurrence and magnitude peak pressure values. The Extrapolated NPS Data plot is taken from the plotted

results for the 3-D Deep Spherical Bubble Problem in the NPS thesis [17,36,37]. The difference in FEA termination time is the reason the Extrapolated NPS Data has few data points and is the cause of the small peak and decay rates. Figure 53 and Table 8 show that the magnitude and time of occurrence of the peak pressure obtained by NPS [17,36,37] Extrapolated NPS Data, is close to the Peak Approximation. Figure 53 and Table 8 show that the magnitude of the peak pressure in the Reproduction Test is smaller than the Peak Approximation value and the time of occurrence is close the Peak Approximation value.

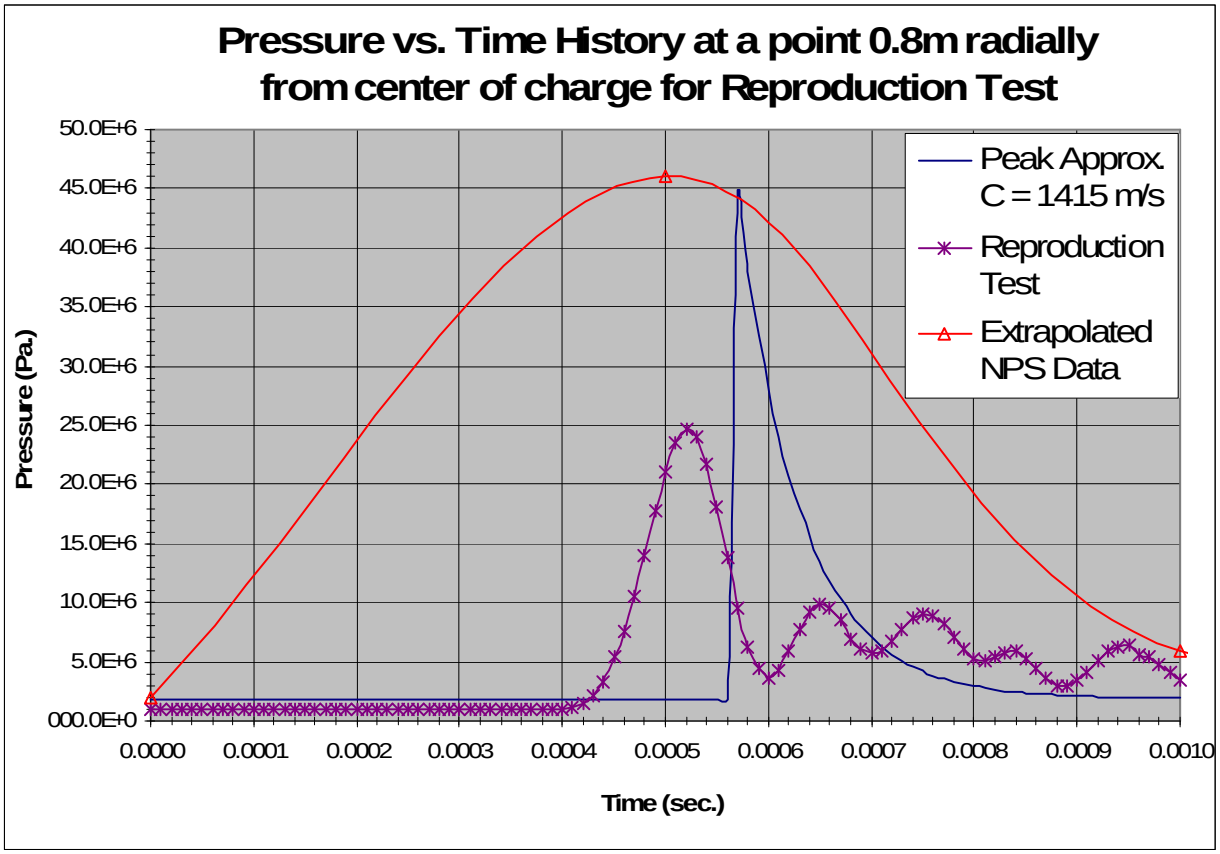

Figure 53 - Pressure-time History Results for Reproduction Test using ES15_25 Configuration

Table 8 Comparison of Time of Occurrence and Magnitude of Peak Pressure for the Reproduction Test

	Peak Pressure Time of Occurrence (sec.)	**Magnitude of Peak Pressure (Pa.)**
Peak Approx.	**0.00057**	**45.0E+06**
Reproduction Test	**0.00052**	**24.6E+06**
Extrapolated NPS Data	**0.0005**	**46.3E+06**

3.2.2.1.3 Conclusions

The time of occurrence of the peak pressure in the Reproduction Test is within an acceptable range of the Peak Approximation value. The magnitude of the peak pressure in the Reproduction Test is not within an acceptable range of the Peak Approximation value. Two possible reasons for this discrepancy might be:

1. The speed of sound, C, used in the Gruneisen equation of state.

2. The fluid medium equation of state used for the ALE explicit FEA models is a 3rd order (cubic) form of the Gruneisen equation of state and may not properly define the pressure density relation of the fluid at every instance. Therefore, the Gruneisen equation of state input values used from the NPS thesis [17,36,37] may not be adequate for use at all times.

Section 3.2.2.2 investigates the effects of a linear form of the Gruneisen equation of state.

3.2.2.2 Non-match of Peak Pressure

Possible causes of the variation in the peak pressure magnitude between the Reproduction Test ALE FEA and the peak approximation is the specified initial acoustic velocity and the Gruneisen equation of state parameters. These input parameters, Table 7, that describe the fluid properties may not adequately capture the pressure-density relationship for the fluid close to the charge, leading to an incorrect calculation of energy. The parameter *C* defined as the speed of sound in water in the peak approximation and in the NPS Thesis [17,36,37] is 1415 m/s.

Section 3.2.2.2.1 describes the process used to determine appropriate Gruneisen input parameters and initial acoustic velocity (y-intercept of the shock velocity/ particle velocity curve for water), C, that will define the correct pressure-density relationship for the fluid.

3.2.2.2.1 Variation of the Gruneisen EOS Parameters

The Gruneisen EOS, in LS-DYNA, defines pressures for compressed material as given by Equation 55 and for expanded material as by Equation 57, where C is the intercept of the v_s-v_p curve, S1 is the linear Gruneisen coefficient of the slope of the v_s-v_p curve, S2 is the quadratic Gruneisen coefficient of the slope of the v_s-v_p curve, S3 is the cubic Gruneisen coefficient of the slope of the v_s-v_p curve, γ_o is the Gruneisen gamma, a is the first order volume correction to γ_o, E is the internal energy per reference specific volume ($1/\rho_o$), and V_0 is the relative volume at time zero to the reference specific volume. Marsh [26] provides the shock data for water (pure H_2O) as shown in Table 9.

Table 9 Los Alamos Scientific Laboratories Shock Hugonoit Data for Water

Hugonoit Data for Water					
Reference: Marsh, LASL Shock Hugoniot Data, University of California Press, 1980					
Material	H20				
Initial Density	0.998	g/cm^3	998	kg/m^3	
Shock Velocity (m/s)	***Particle Velocity (m/s)***	***Pressure (Mpa)***	***Specific Volume (m^3/g)***	***Density (kg/m^3)***	***Volume Fraction***
1.4800E+03	0.0000E+00	0.0000E+00	1.0018E-03	9.9800E+02	1.0000E+00
3.3140E+03	9.0000E+02	2.9770E+03	7.9700E-04	1.3700E+03	7.2800E-01
3.6170E+03	1.1360E+03	4.1010E+03	6.8730E-04	1.4550E+03	6.8600E-01
3.6080E+03	1.1400E+03	4.1050E+03	6.8540E-04	1.4590E+03	6.8400E-01
3.6200E+03	1.1440E+03	4.1330E+03	6.8530E-04	1.4590E+03	6.8400E-01
3.5340E+03	1.1440E+03	4.0350E+03	6.7760E-04	1.4760E+03	6.7600E-01
3.9440E+03	1.3060E+03	5.1410E+03	6.7020E-04	1.4920E+03	6.6900E-01
3.9360E+03	1.3110E+03	5.1500E+03	6.6830E-04	1.4960E+03	6.6700E-01
3.9720E+03	1.3160E+03	5.2170E+03	6.7000E-04	1.4920E+03	6.6900E-01
4.0440E+03	1.3390E+03	5.4050E+03	6.7010E-04	1.4920E+03	6.6900E-01
4.0770E+03	1.3570E+03	5.5230E+03	6.6840E-04	1.4960E+03	6.6700E-01
4.4820E+03	1.6000E+03	7.1580E+03	6.4420E-04	1.5520E+03	6.4300E-01
4.6350E+03	1.6890E+03	7.8130E+03	6.3690E-04	1.5700E+03	6.3600E-01
4.6740E+03	1.7130E+03	7.9910E+03	6.3480E-04	1.5750E+03	6.3400E-01
4.7000E+03	1.7410E+03	8.1680E+03	6.3070E-04	1.5860E+03	6.3000E-01
4.7200E+03	1.7490E+03	8.2400E+03	6.3060E-04	1.5860E+03	6.2900E-01
4.7550E+03	1.7730E+03	8.4150E+03	6.2830E-04	1.5920E+03	6.2700E-01
4.7270E+03	1.7790E+03	8.3930E+03	6.2490E-04	1.6000E+03	6.2400E-01
4.7150E+03	1.7920E+03	8.4320E+03	6.2120E-04	1.6100E+03	6.2000E-01
4.6890E+03	1.8140E+03	8.5060E+03	6.1310E-04	1.6310E+03	6.1300E-01
5.4810E+03	2.2660E+03	1.2395E+04	5.8770E-04	1.7010E+03	5.8700E-01
5.4660E+03	2.2660E+03	1.2361E+04	5.8660E-04	1.7050E+03	5.8500E-01
5.5450E+03	2.2740E+03	1.2584E+04	5.9110E-04	1.6920E+03	5.9000E-01
5.5340E+03	2.2750E+03	1.2567E+04	5.9000E-04	1.6950E+03	5.8900E-01
5.5580E+03	2.2990E+03	1.2752E+04	5.8750E-04	1.7020E+03	5.8600E-01
5.5370E+03	2.3100E+03	1.2767E+04	5.8390E-04	1.7130E+03	5.8300E-01
5.5590E+03	2.3240E+03	1.2896E+04	5.8300E-04	1.7150E+03	5.8200E-01
5.8040E+03	2.4790E+03	1.4359E+04	5.7400E-04	1.7420E+03	5.7300E-01
5.8390E+03	2.5140E+03	1.4650E+04	5.7060E-04	1.7530E+03	5.6900E-01
5.8690E+03	2.5300E+03	1.4819E+04	5.7010E-04	1.7540E+03	5.6900E-01
7.9730E+03	4.0510E+03	3.2240E+04	4.9280E-04	2.0290E+03	4.9200E-01
7.9730E+03	4.1600E+03	3.3108E+04	4.7910E-04	2.0870E+03	4.7800E-01
8.3490E+03	4.5140E+03	3.7620E+04	4.6020E-04	2.1730E+03	4.5900E-01
8.3880E+03	4.6320E+03	3.8793E+04	4.4860E-04	2.2290E+03	4.4800E-01
8.4870E+03	4.6330E+03	3.9249E+04	4.5490E-04	2.1980E+03	4.5400E-01
8.6350E+03	4.7220E+03	4.0701E+04	4.5400E-04	2.2030E+03	4.5300E-01
8.9290E+03	4.9420E+03	4.4000E+04	4.4650E-04	2.2400E+03	4.4700E-01

Figure 54 provides the linear fit to the shock Hugonoit data from LASL used for water, with the y-intercept fixed at the value of the speed of sound C (1480 m/s), and with the y-intercept not fixed.

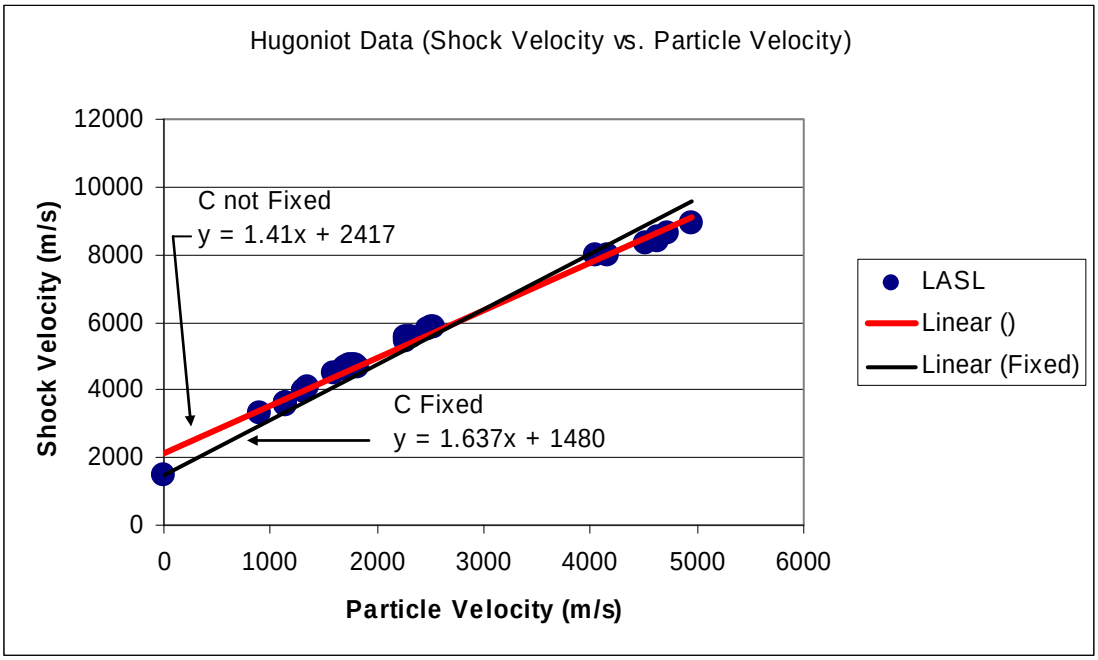

Figure 54 - Plot of Hugonoit Shock Data

Using the linear fit to the Hugonoit Data in the Linear Gruneisen calculation shown in Figure 54, the Pressure Density Curve Fit is formulated as shown in Figure 55 for the non-fixed C case. Figure 56 shows the Pressure Density curve fit for the fixed C case.

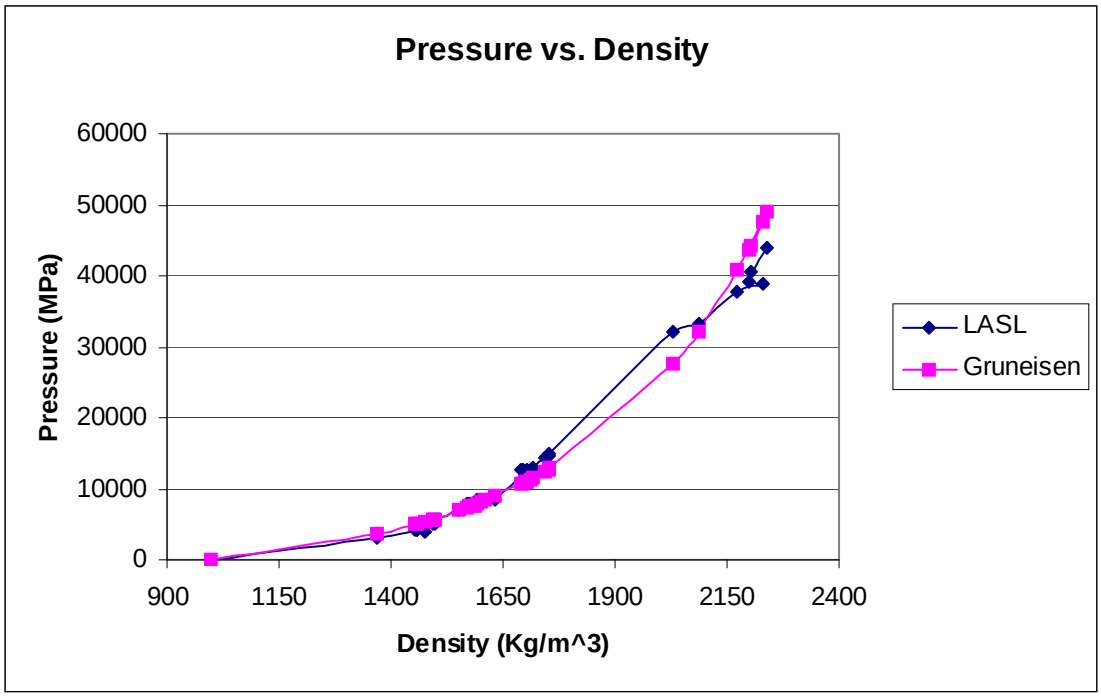

Figure 55 - Pressure Density Curve Fit for Linear Non-fixed C

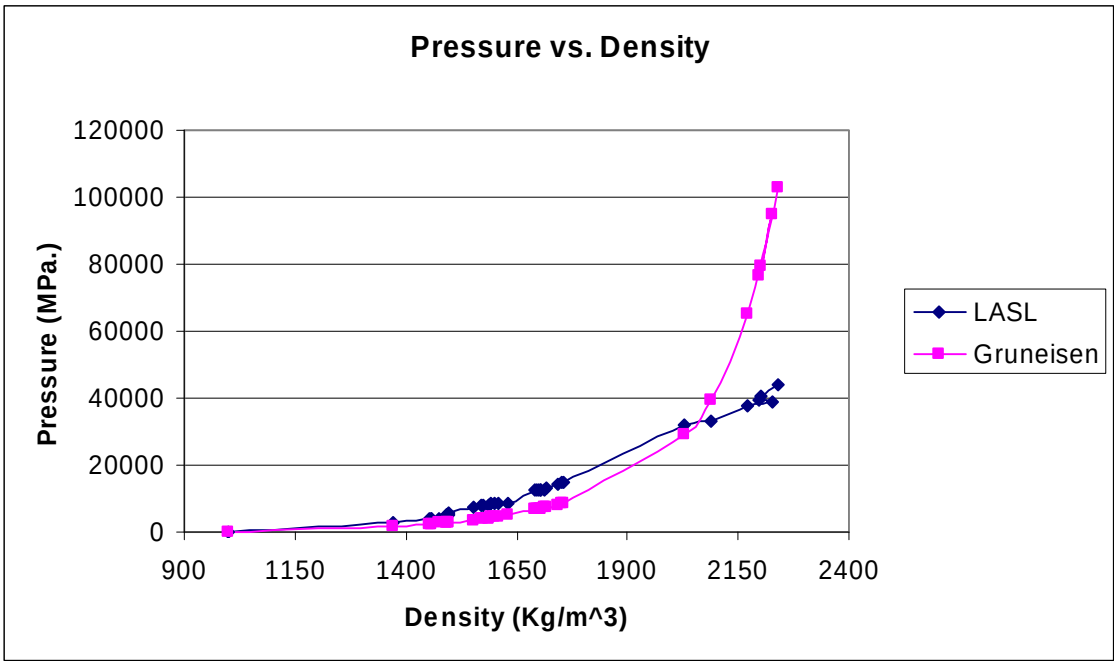

Figure 56 - Pressure Density Curve Fit for Linear Fixed C

Maintaining a linear form of the Gruneisen EOS, the intercept of the shock-particle velocity curve (C) and the linear Gruneisen slope coefficient (S_1) are varied for four analyses in test

Matrix EOS1 as shown in Table 10. These four analyses are then compared to the cubic Gruneisen input data given by the NPS Thesis [17,36,37].

Figure 57 through Figure 66 provide plots of the shock Hugonoit data and pressure density curve fits for the LASL shock data for water [26] against the S1 and C coefficients used in the test cases of Matrix EOS1, as shown in Table 10. Figure 67 and Figure 68 show the plots of the shock Hugonoit data and pressure density curve fits for the LASL shock data for water [26] against the Gruneisen equation of state coefficients used by the NPS in Table 11.

Table 10 Test Matrix EOS1

Run	ES	C	S1
01	15_25	1480 m/s	1.637
02	15_25	1480 m/s	2.2
03	15_25	1480 m/s	2.75
04	15_25	1415 m/s	2.56
05	15_25	2417 m/s	1.41

Table 11 Gruneisen Equation of State Coefficients used by NPS

C	S1	S2	S3	γO	A	E0
1415 m/s	2.56	-1.986	0.2268	0.4934	1.3937	1.847E+06

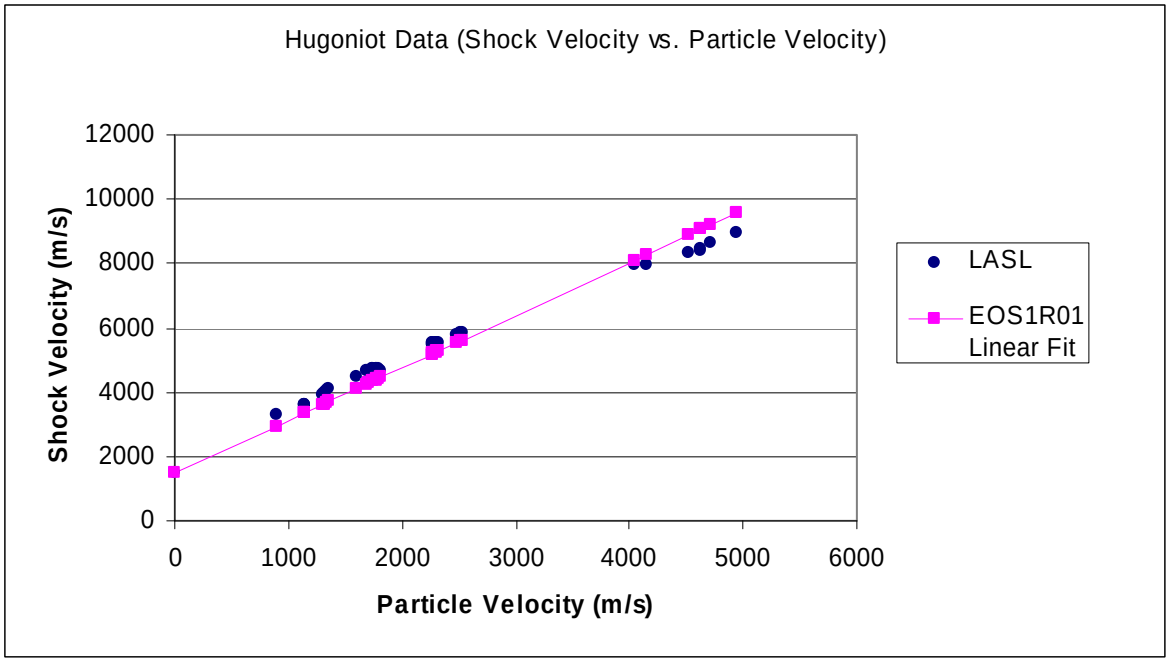

Figure 57 - Hugonoit Shock Data for Test Case EOS1R01

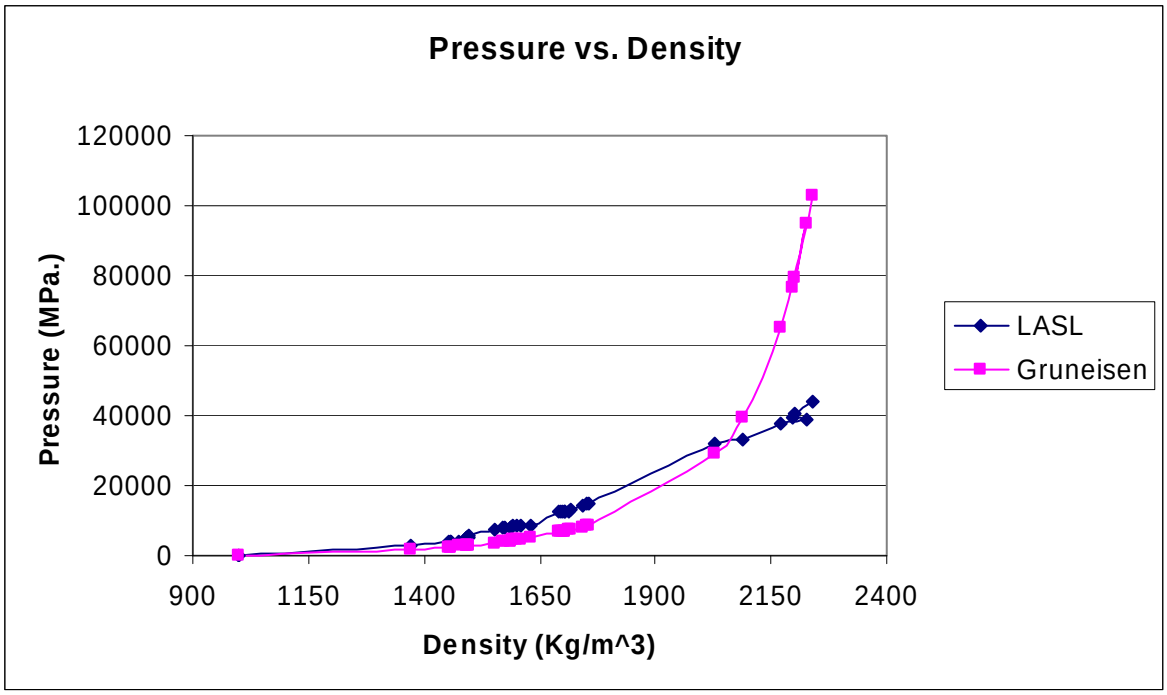

Figure 58 - Pressure Density Curve Fit for Test Case EOS1R01

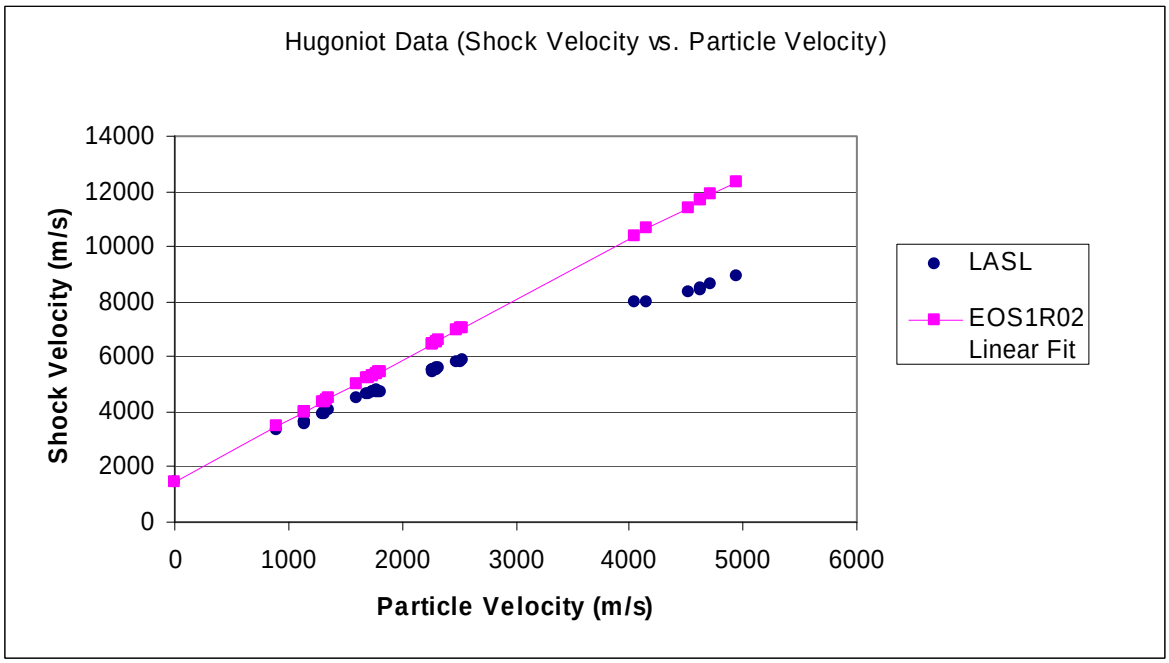

Figure 59 - Hugonoit Shock Data for Test Case EOS1R02

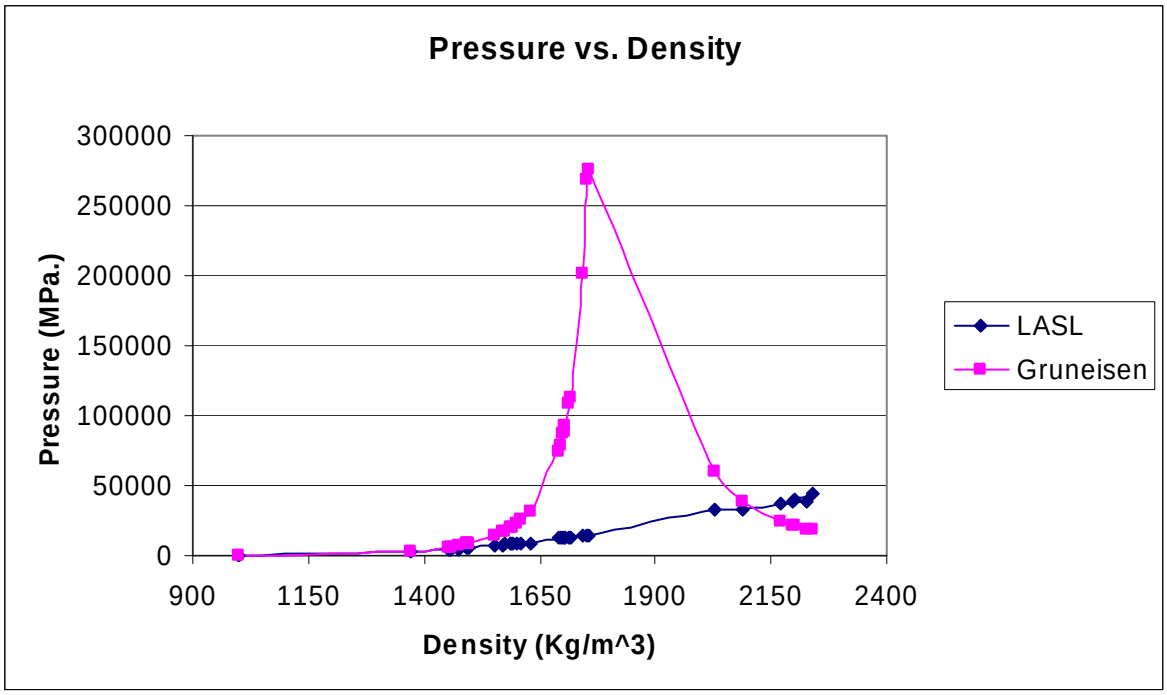

Figure 60 - Pressure Density Curve Fit for Test Case EOS1R02

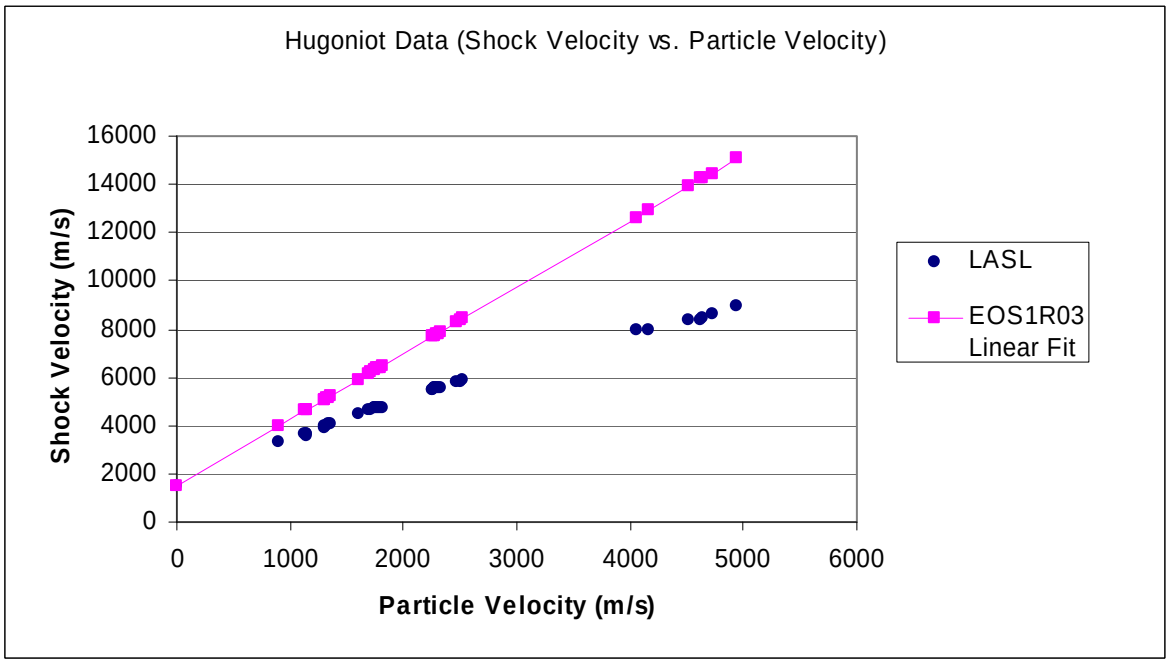

Figure 61 - Hugonoit Shock Data for Test Case EOS1R03

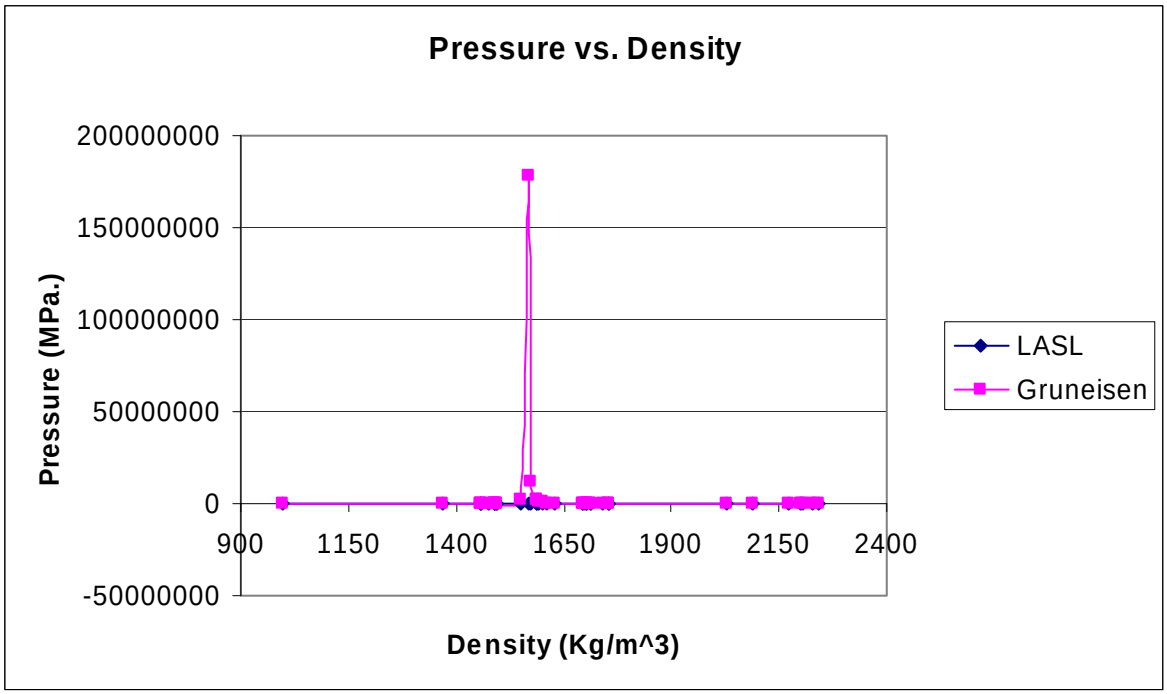

Figure 62 - Pressure Density Curve Fit for Test Case EOS1R03

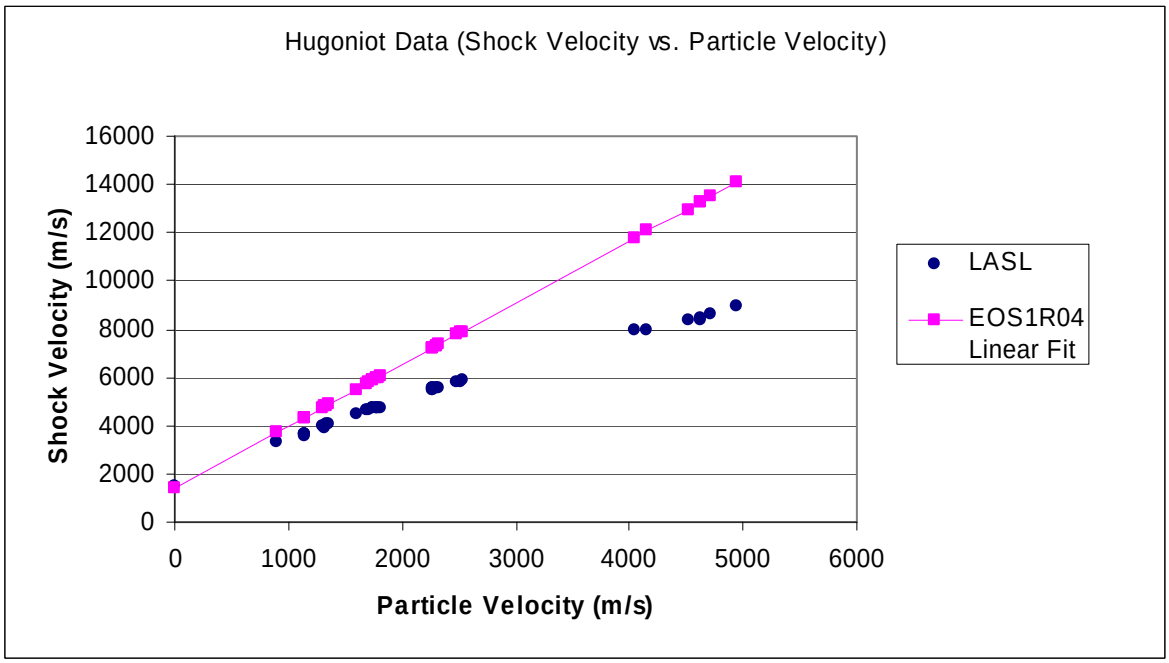

Figure 63 - Hugonoit Shock Data for Test Case EOS1R04

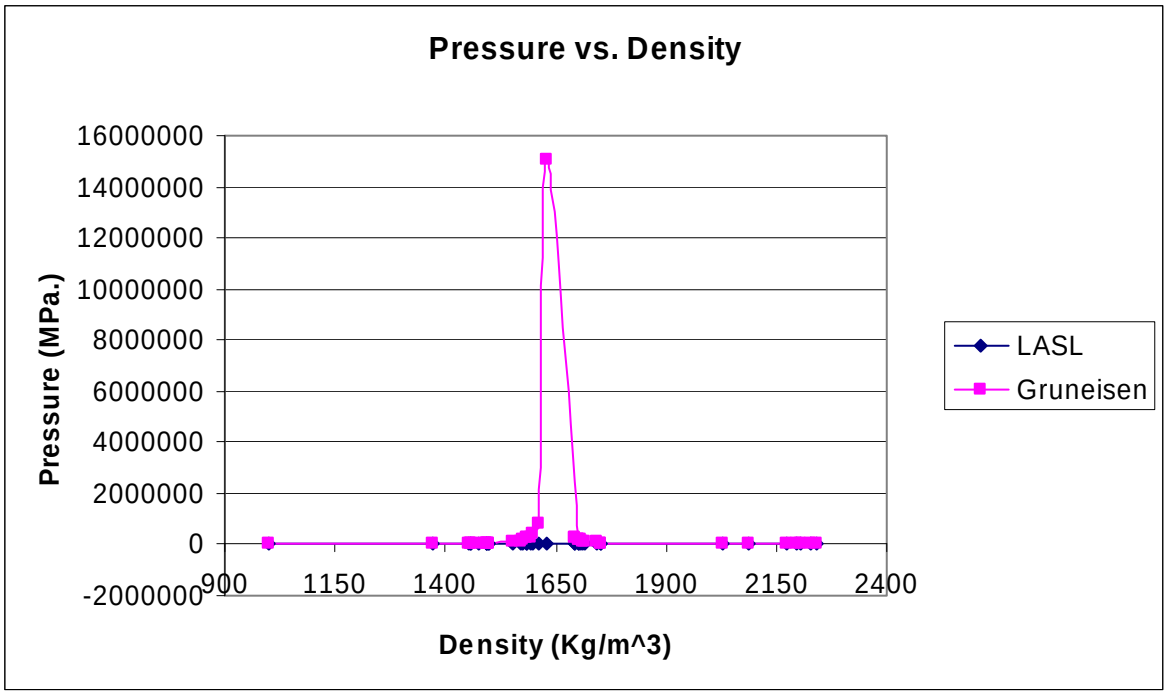

Figure 64 - Pressure Density Curve Fit for Test Case EOS1R04

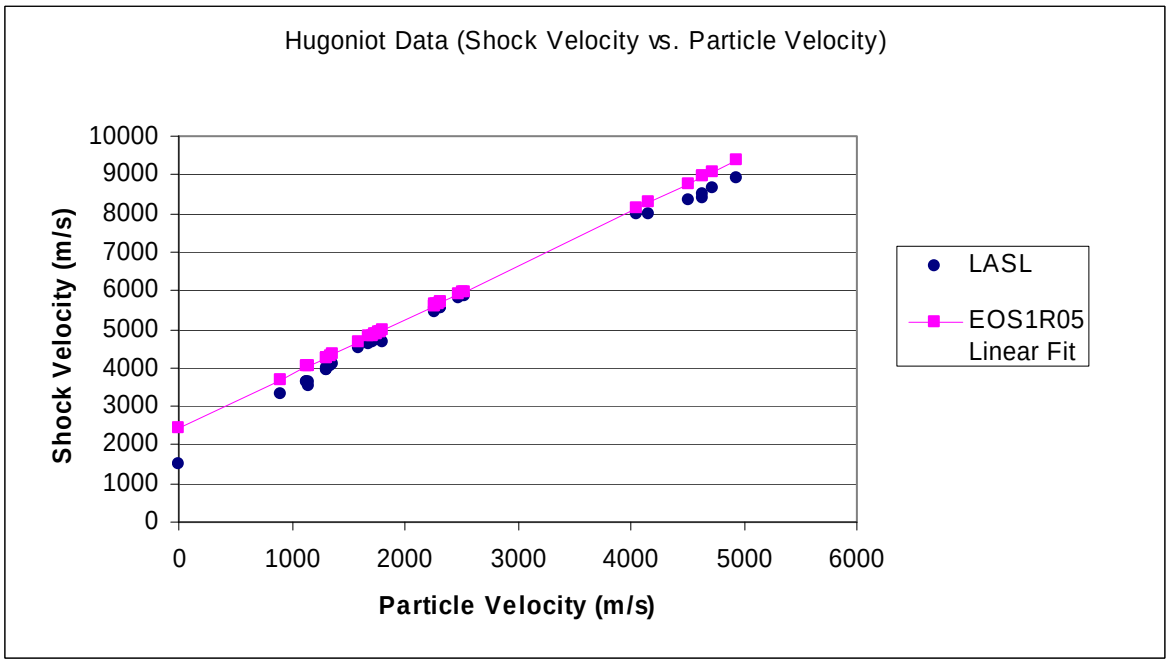

Figure 65 - Hugonoit Shock Data for Test Case EOS1R05

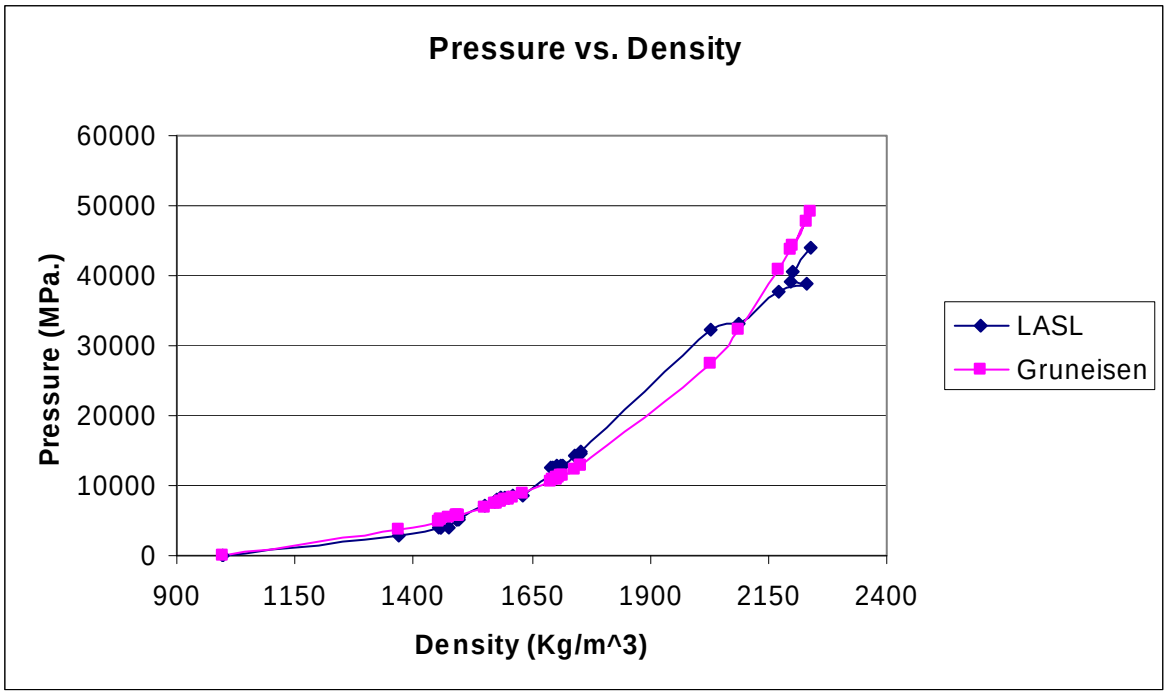

Figure 66 - Pressure Density Curve Fit for Test Case EOS1R05

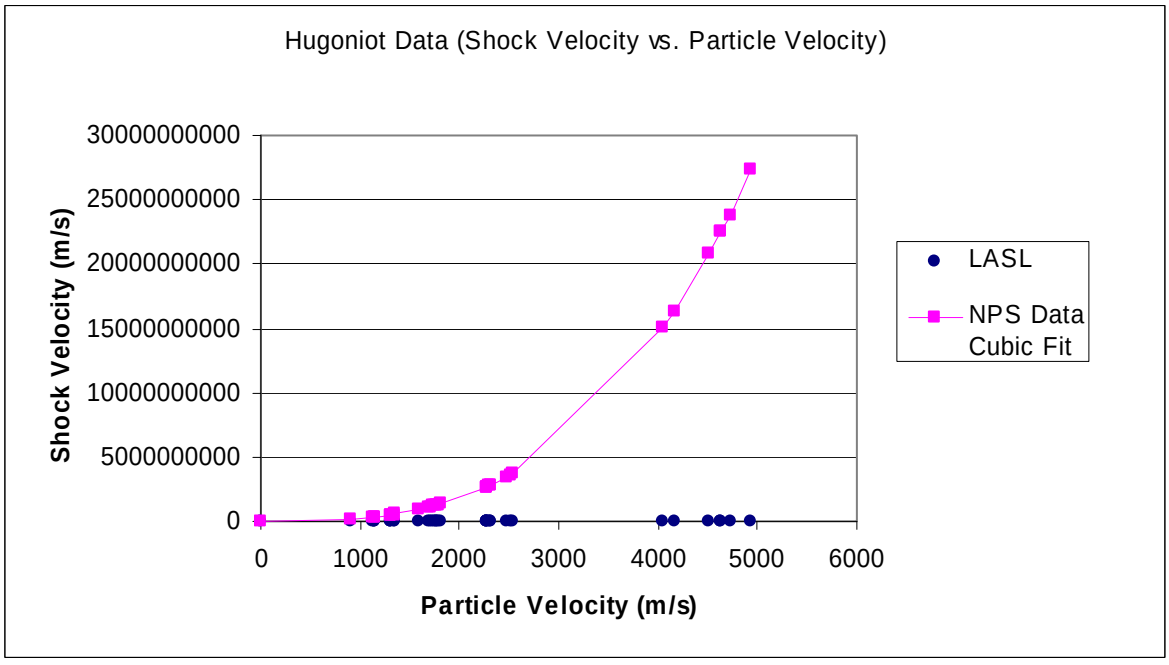

Figure 67 - Pressure Density Curve Fit for NPS Cubic EOS Data

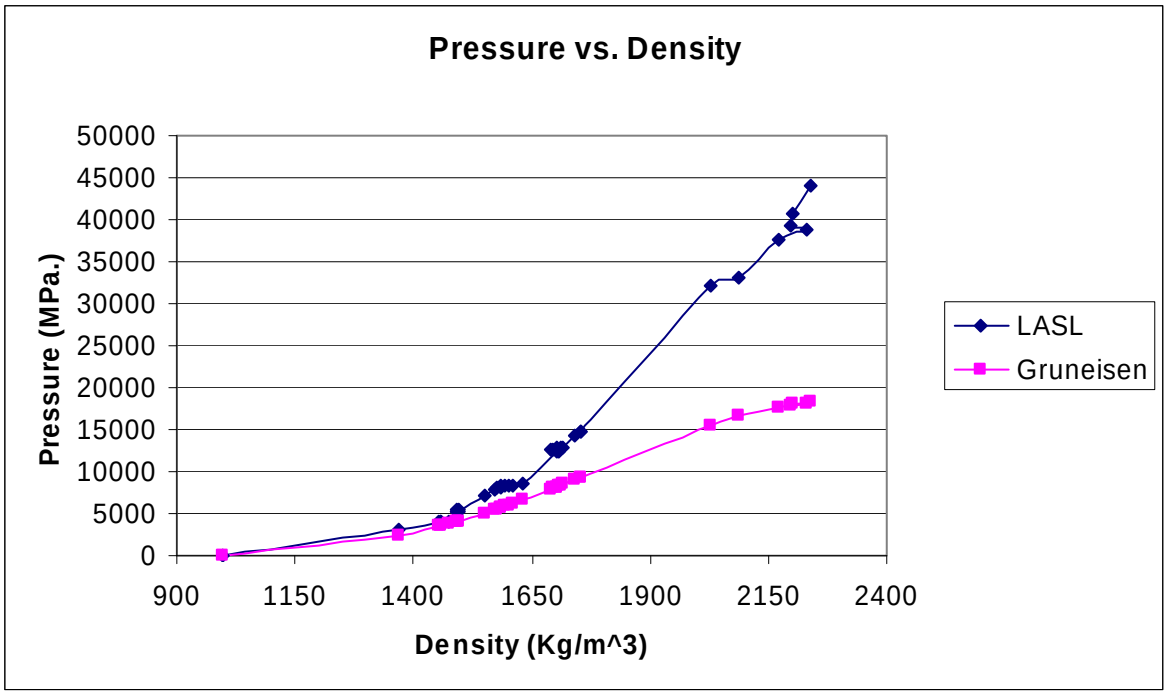

Figure 68 - Pressure Density Curve Fit for NPS Cubic EOS Data

The Peak Approximation is calculated using a value of C = 1480 m/s., to correspond with the LASL Hugonoit Data. The Reproduction Test case and the EOS1 test cases use the same LS-DYNA input deck and have the same mesh configuration. Test Matrix EOS1 runs 01 through 03 use Gruneisen equation of state parameters from the linear fit where the y intercept is fixed at C = 1480 m/s and the corresponding slope value S1 is varied. EOSR05 uses a speed of sound parameter, C = 2417 m/s, and the linear Gruneisen equation of state coefficient, S1 = 1.41, from the linear fit equation with the y-intercept not fixed. Figure 54 shows the plot of the Vs-Vp curve with the linear fit equation where C = 2417 m/s and the linear fit equation where C is fixed at 1480 m/s. Table 11 shows the values of the NPS coefficients for the Gruneisen equation of state [17,36,37] used in EOS1 run 04.

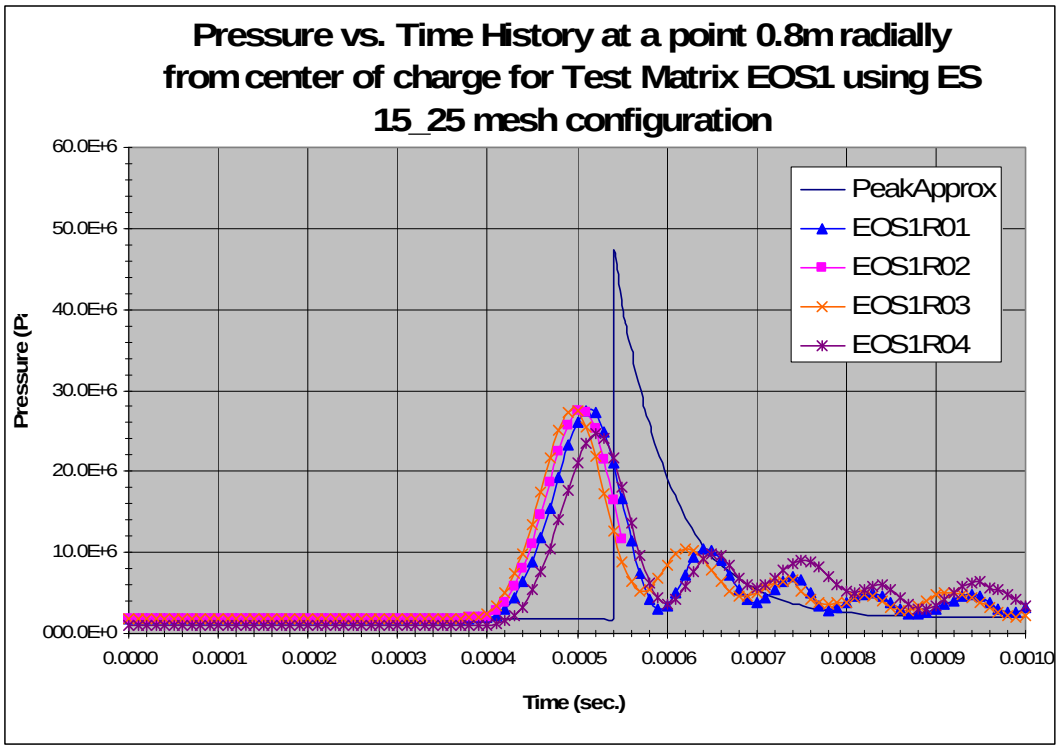

Figure 69 - Pressure-time History for EOS1 Runs 01-04 Compared to Peak Approximation

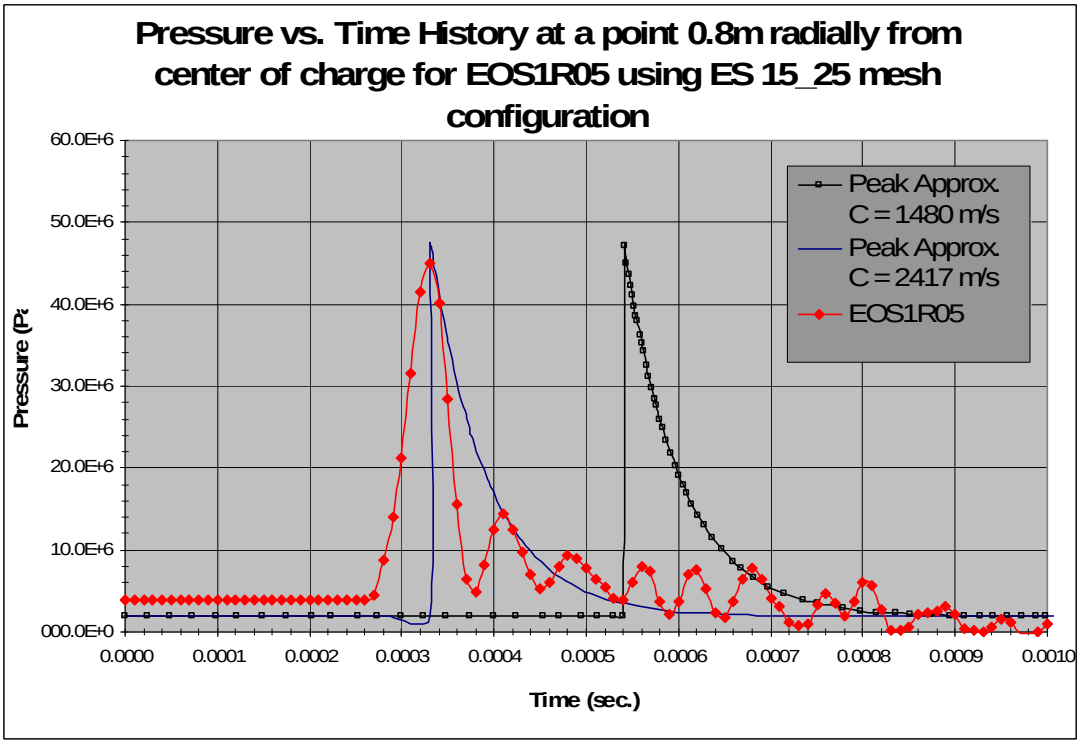

Figure 70 - Pressure-time History for EOS1 Run 05 Compared to Peak Approximation

3.2.2.2.1.1 Results

Figure 69 and Figure 70 give the results from the EOS1 Matrix. The results show the Gruneisen equation of state parameters, C = 1480 m/s and the varied S1 values, used in runs 01-04 will not produce the same peak pressure that the Peak Approximation using the same C value does. Figure 70 shows that the parameters, C = 2417 m/s and S1 = 1.41, used in run 05 will produce the same result as the Peak Approximation using a value of C = 2417 m/s. The results also show that coefficients used by NPS, based on the information available in References 17, 36, and 37, does not produce the correct pressure-density relation for the fluid model near the charge. The Gruneisen equation of state parameters of C = 2417 m/s, the V_S-V_P curve intercept, and S1 = 1.41, slope of the linear fit line, should be used to correctly capture the pressure-density relationship of the fluid in a close proximity UNDEX environment, since the wave speed is greater than the speed of sound in water near the charge (Section 1.2, p23). These results indicate the cause of the time delay between the ALE FEA analysis using C = 1480 m/s and the Peak Approximation using C = 1480 m/s is also due to the less accurate pressure-density relation this value provides. These results suggest that the ALE finite element method is sensitive to the input used to describe the characteristics of the fluid medium. Figure 70 shows the initial hydrostatic pressure is higher in the ALE explicit FEA models, nearly double the Peak Approximation. A possible reason for the variation between the method results and the Peak Approximation is the initial hydrostatic pressure of the ALE explicit FEA models. This may be a result of an improper implementation of the hydrostatic pressure in LS-DYNA. Hydrostatic initialization is addressed in Section 3.2.2.2.2.

3.2.2.2.2 Hydrostatic Initialization of the ALE explicit FEA models

Hydrostatic initialization of the fluid in ALE explicit FEA models is performed through the specification of the internal energy per unit reference volume of the water as shown in Table 7. To determine the proper internal energy per unit reference volume (E) of the water the Gruneisen equation of state for fluid in a compressive state (Equation 69) must be back solved using hydrostatic pressure at the depth of the explosive.

$$p = \frac{\rho_0 C^2 \mu \left[1 + \left(1 - \frac{\gamma_0}{2} \right) \mu - \frac{a}{2} \mu^2 \right]}{\left[1 - (S_1 - 1)\mu - S_2 \frac{\mu^2}{\mu + 1} - S_3 \frac{\mu^3}{(\mu + 1)^2} \right]^2} + (\gamma_0 + a\mu)E \qquad (69)$$

In the initial state of the fluid, μ given by Equation 70 is zero as the density (ρ) is equivalent to the initial density (ρ_0).

$$\mu = \left(\frac{\rho}{\rho_0} \right) - 1 \tag{70}$$

Substituting μ from Equation 70 into Equation 69 and solving for E yields:

$$E = \frac{\rho}{\gamma_0} \tag{71}$$

Where γ_0 is the Gruneisen gamma provided by Table 11 and p is the initial hydrostatic pressure given by Equation 72.

$$p = p_{atm} + \rho_0 \cdot g \cdot h \tag{72}$$

Substituting defined values and the Gruneisen values C = 2417m/s and S1 = 1.41, from EOS1R05 in Table 11, into Equation 69 and 72 then the internal energy per unit reference volume (E) equals 1.891E+06 J/m^3. Figure 71 provides the comparison of the Reproduction Test case using E = 1.891E+06 J/m^3 to the peak approximation.

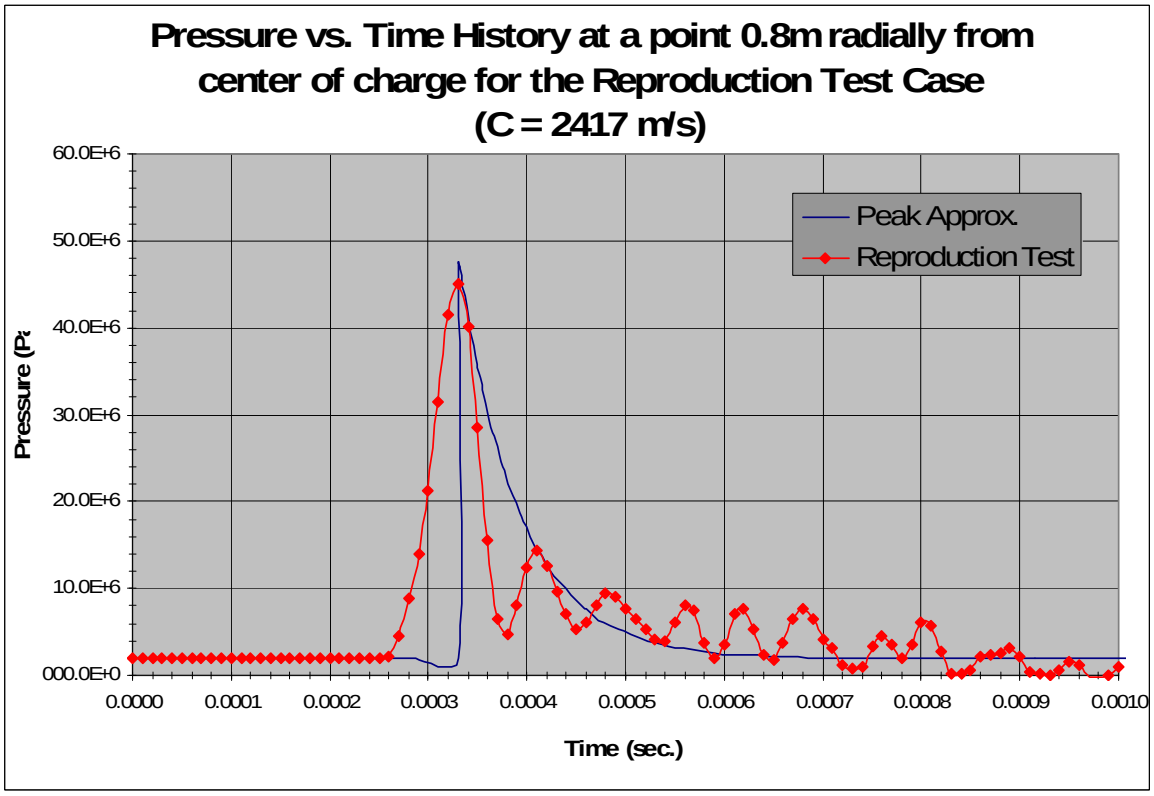

Figure 71 - Pressure-time Histories of the Reproduction Test Case with C = 2417 m/s and E = 1.891E+06 J/m^3 and Peak Approximation.

3.2.2.2.2.1 Results

The results from Figure 71 indicate that the initial internal energy value of 1.891E+06 J/m^3 calculated using the Gruneisen equation of state values, that produced the correct peak pressure and time of occurrence, is the correct value to use to have initial pressure correlation with the Peak Approximation.

The Reproduction Test case model will now capture the correct peak pressure, time of occurrence, and initial pressure when compared to the Peak Approximation when calculated using a value of C = 2417 m/s. Figure 72 shows the extrapolated results obtained by the Naval Postgraduate School [17,36,37] and the Peak Approximation calculated using C = 1415 m/s., compared to the Reproduction Test case that incorporates the Gruneisen equation of state coefficients from EOS1R05 and the initial internal energy that produces matching results to the Peak Approximation calculated using C = 2417 m/s.

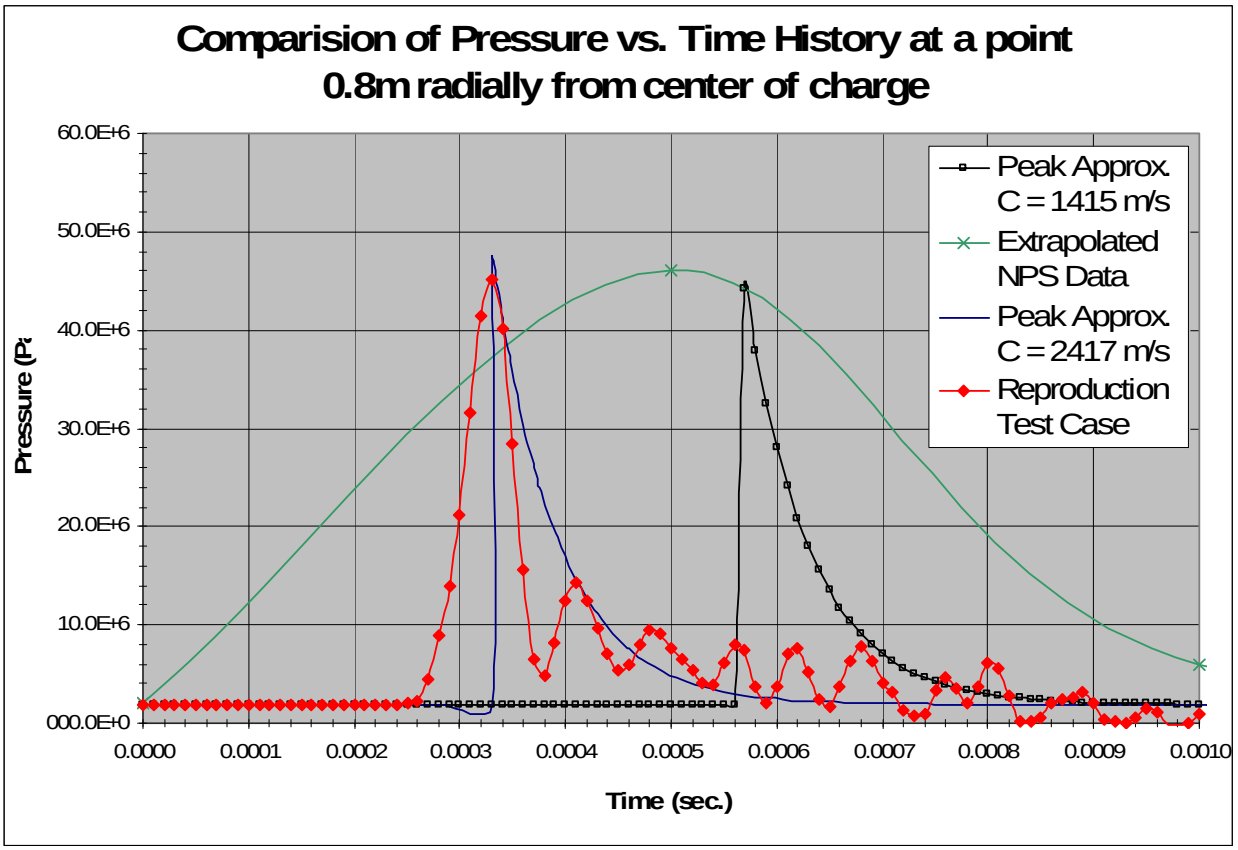

Figure 72 - Comparison of NPS Data, Reproduction Test, and the Peak Approximation using Different Values for C.

Figure 72 shows that the Reproduction Test does not reproduce the same results that the NPS paper [17,36,37] did. It also shows that the peak pressure and time of occurrence results of the analysis are dependant on the fluid equation of state model and the fluid properties.

The finite element model will now produce the desired early-time results, and it has been shown that the model is sensitive to equation of state coefficient variation, attention is given to how sensitive the results are to changes in the element size, timestep size, advection cycles, boundary conditions, and bulk viscosity coefficients of the finite element model.

Section 3.2.2.3 investigates the model sensitivity and determines an appropriate method to obtain both the early-time and late-time results of the 3D DSB problem.

3.2.2.3 Early-time Model Sensitivity Analysis and Late-time Model Method Determination Analysis

The explicit FEA sensitivity analyses are divided into two test matrices. The first test matrix has thirty-two test cases that compare the effect of varying element size, time step size, and number of time steps between ALE advection. The test case from Matrix #1 that best matches the pressure-time history given by the peak approximation is used in Matrix #2 to compare the effect boundary conditions have on capturing the late-time response of the DSB problem. Test Matrix #2 is used to develop a method that will capture both the early-time and late-time responses, the peak pressure of the shock wave and the first bubble pulse.

3.2.2.3.1 Variation of Element Size, Time Step Size and ALE Advection Cycles – Matrix #1

Thirty-two analyses are used to evaluate the sensitivity of the pressure time history to the FEA model element size, time step size and number of cycles before ALE advection. These analyses are listed in Table 12 where the nomenclature M#R# of each test refers to the run number (R#) of the test matrix number (M#). Table 12 is test matrix number M1.

Table 12 Test Matrix M1

Test #	Element Size and Configuration	Time Step Scale Factor	Time Steps between Advection
M1R01	ES3_4	0.67	10
M1R02	ES3_4	0.3	10
M1R03	ES3_4	0.1	10
M1R04	ES3_4	0.67	1
M1R05	ES3_4	0.3	1
M1R06	ES3_4	0.1	1
M1R07	ES6_13	0.67	10
M1R08	ES6_13	0.3	10
M1R09	ES6_13	0.1	10
M1R10	ES6_13	0.67	1
M1R11	ES6_13	0.3	1
M1R12	ES6_13	0.1	1
M1R13	ES9_15	0.67	10
M1R14	ES9_15	0.3	10
M1R15	ES9_15	0.1	10
M1R16	ES9_15	0.67	1
M1R17	ES9_15	0.3	1
M1R18	ES9_15	0.1	1
M1R19	ES12_25	0.67	10
M1R20	ES12_25	0.3	10
M1R21	ES12_25	0.1	10
M1R22	ES12_25	0.67	1
M1R23	ES12_25	0.3	1
M1R24	ES12_25	0.1	1
M1R25	ES15_25	0.67	10
M1R26	ES15_25	0.3	10
M1R27	ES15_25	0.1	10
M1R28	ES15_25	0.67	1
M1R29	ES15_25	0.3	1
M1R30	ES15_25	0.1	1
M1R31	ES18_25	0.67	10
M1R32	ES18_25	0.9	10

The variable TSSFAC in Table 12 denotes the time step size scale factor used in the LS-DYNA FEA to adjust the LS-DYNA calculated time step based on element size. The LS-DYNA Keyword Users Manual [21] suggests a TSSFAC value of 0.67 when using high explosive materials, however the effects of variation from the suggested value is not reported and must be tested and quantified.

The variable NADV in Table 12 denotes the number of time step cycles between ALE advection (Section 2.1.3.4). For test matrix M1 of Table 12 the FE analysis are tested with ALE advections every time step cycle and every 10 time step cycles.

All FEA models of test matrix M1 have a similar topological geometry as shown in Figure 49 and Figure 50. The charge mesh center incorporates rectilinear coordinates and the charge mesh transitions to spherical coordinates to the outer charge boundary. The FE mesh in each model does however vary as the charge element size is changed. The designation for each models charge element size is ES#_# where the first # refers to the number of elements along the x, y and z coordinate axis modeling the cube portion of the charge and the second # refers to the number of elements along the x, y and z coordinate axis modeling the transition portion (from rectangular to spherical coordinates) of the charge. An example of the nomenclature for model ES3_4 is shown in Figure 73.

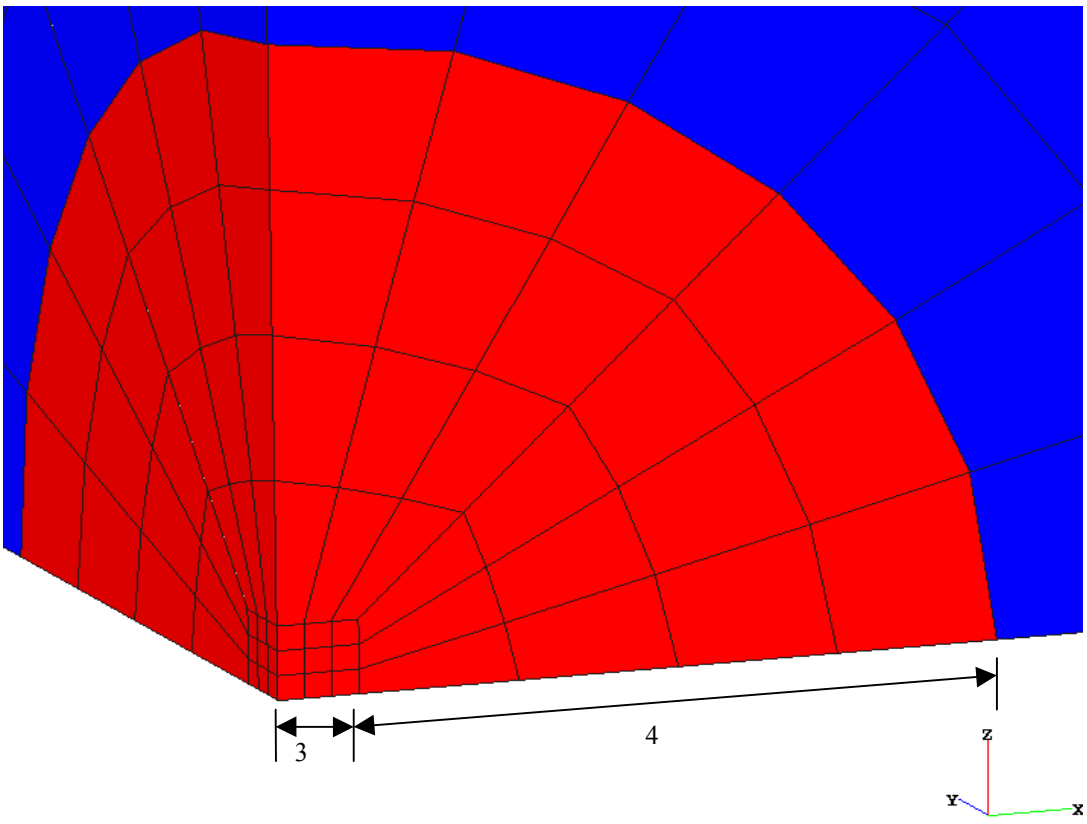

Figure 73 - Example of ES#_# Model Nomenclature for ES3_4

Six mesh configurations are used to determine the sensitivity to element size. Table 13 provides a general description of each mesh configuration. Figure 74 through Figure 79 show each FEA model mesh configuration.

Table 13 Mesh Configuration Description

Model	# Charge Elements	# Fluid Elements	# Total Elements	# Outer Boundary Element Faces
ES3_4	133	434	567	27
ES6_13	1618	3026	4644	108
ES9_15	4372	9236	13608	243
ES12_25	12526	31106	43632	432
ES15_25	20248	48602	68850	675
ES18_25	30130	69986	100116	972

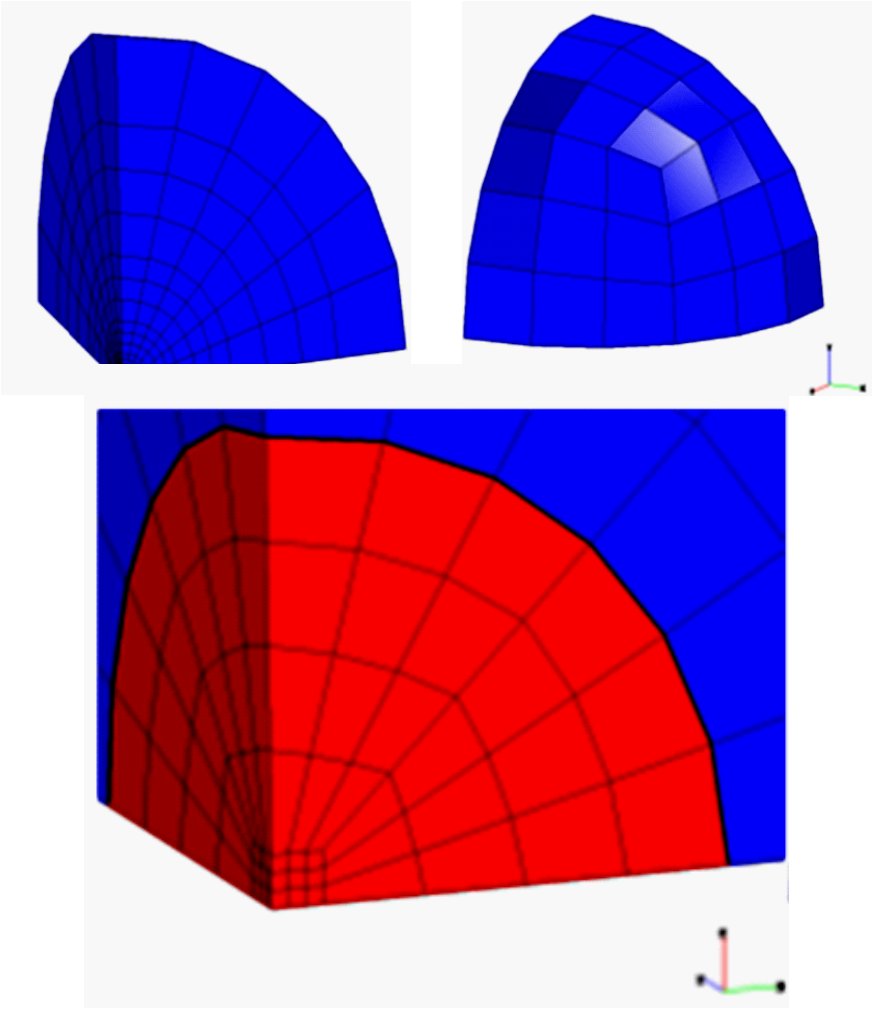

Figure 74 - ES3_4 Mesh Configuration

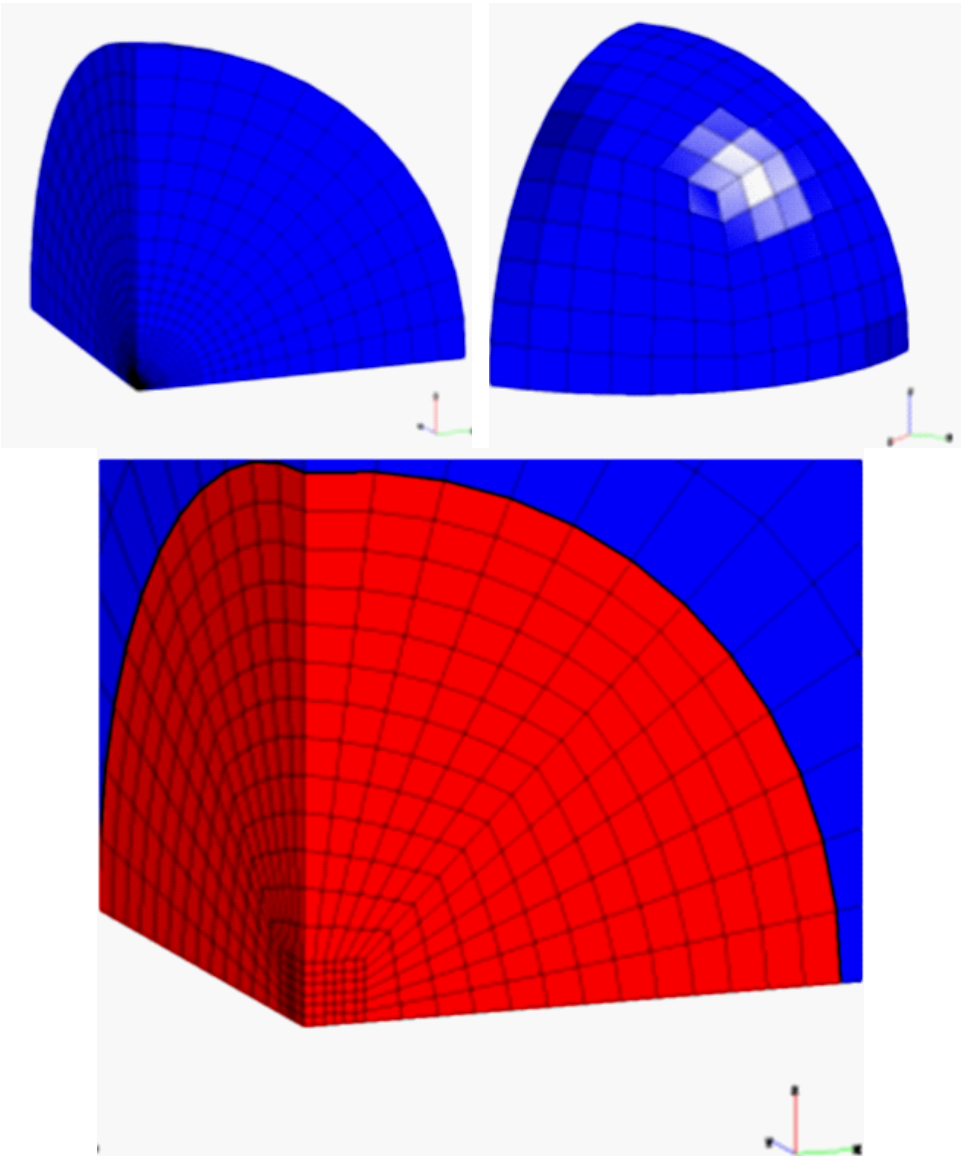

Figure 75 - ES6_13 Mesh Configuration

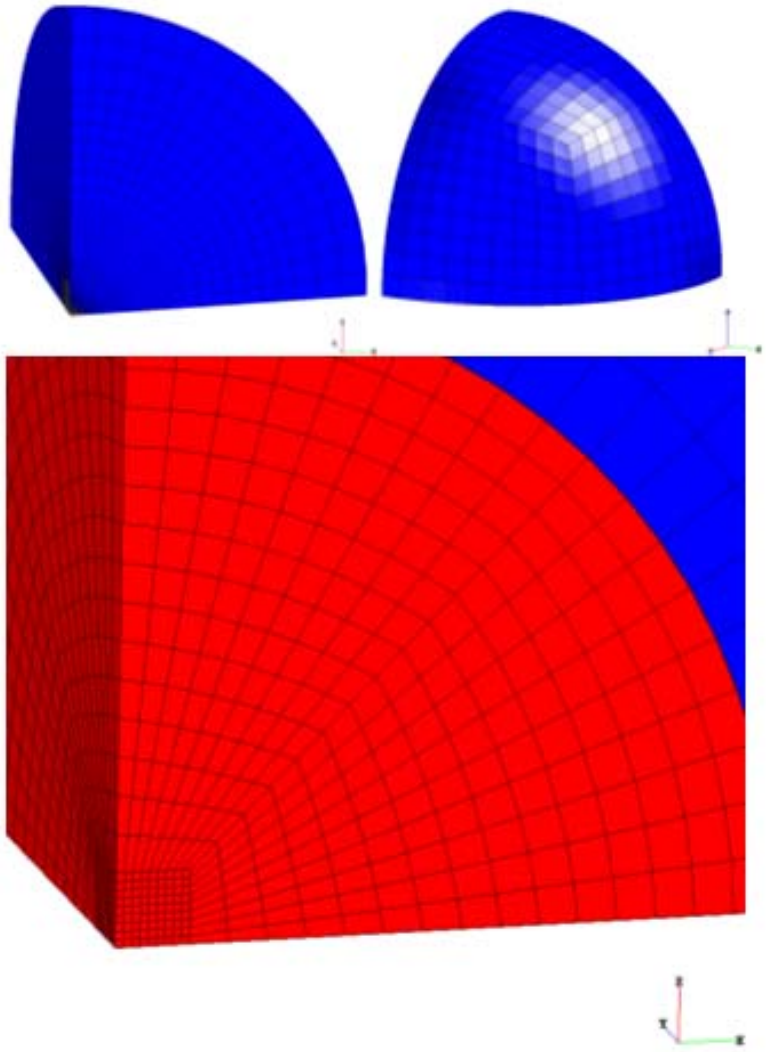

Figure 76 - ES9_15 Mesh Configuration

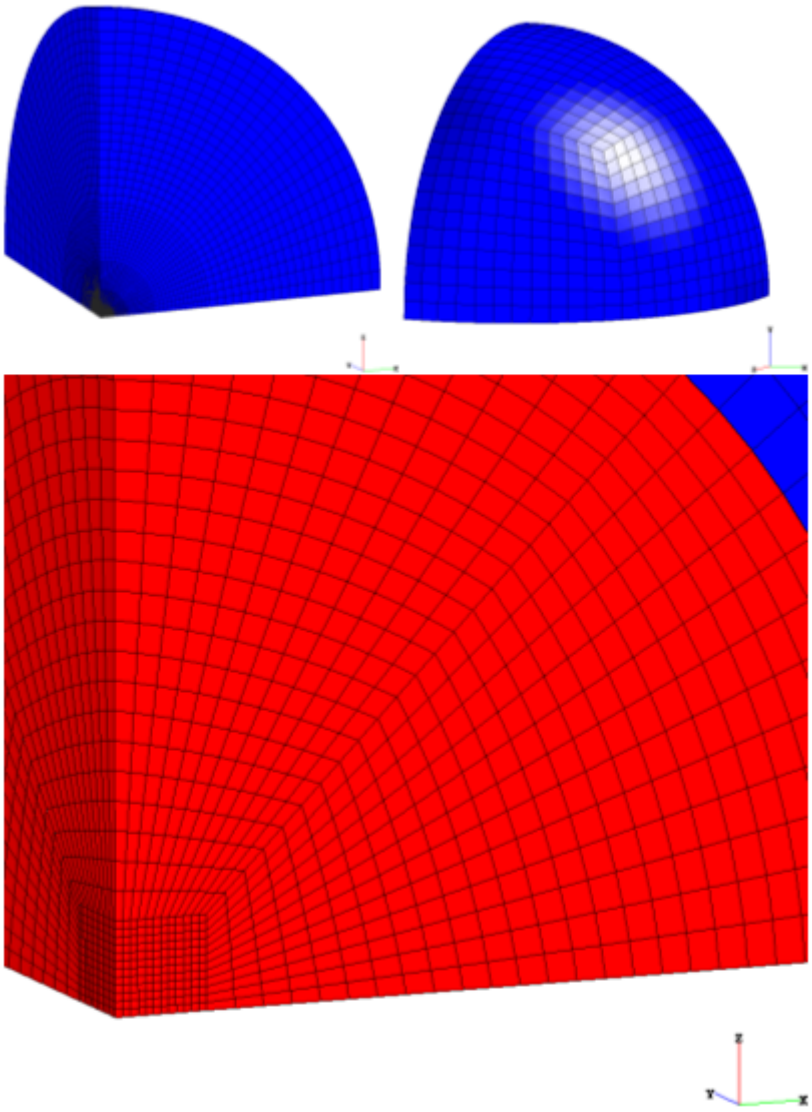

Figure 77 - ES12_25 Mesh Configuration

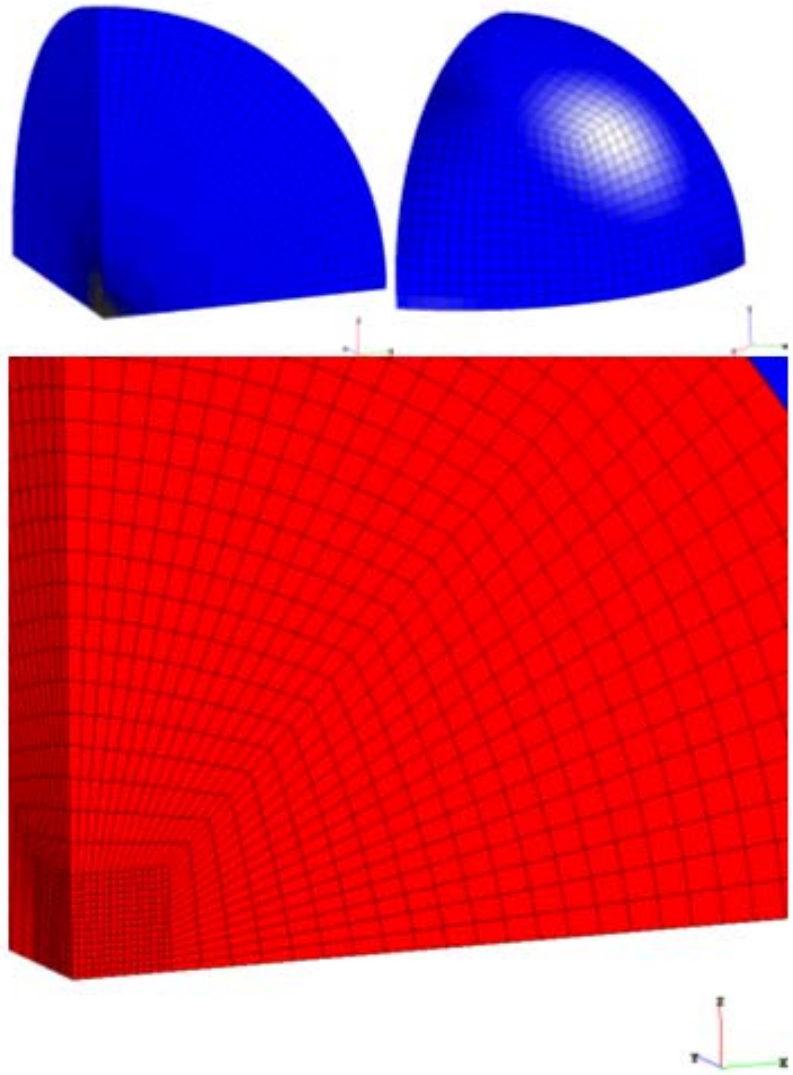

Figure 78 - ES15_25 Mesh Configuration

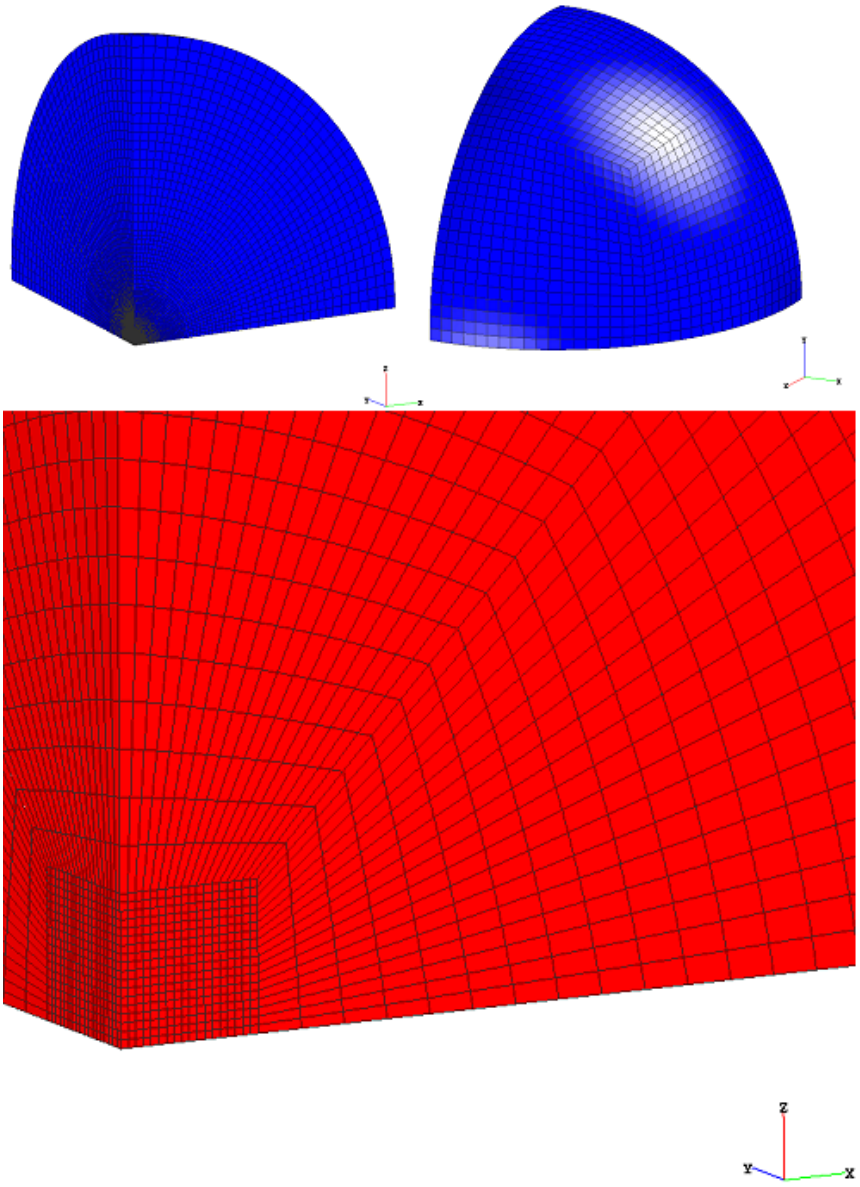

Figure 79 - ES18_25 Mesh Configuration

All runs use a time interval of 0.001 seconds and each mesh configuration has a standard no normal flow Eulerian and Lagrangian boundary conditions on the three planar edges (x-y, x-z and y-z planes) of Figure 74 through Figure 79.

3.2.2.3.1.1 Results of Matrix M1 tests

Table 14 and Figure 80 through Figure 86 provide the results of each test case from Table 12 where cases M1R15, M1R18, M1R21, M1R24, M1R27 and M1R30 were not analyzed because the time to complete the analysis exceeded the permissible 100 hour limit arbitrarily set by the authors. Additionally, test cases M1R26 and M1R28 did not reach the completion analysis time of 0.001 seconds because a negative volume ALE advection error respectively, however, enough data is present in both analyses to determine the characteristics of the peak pressure. Table 14 lists the total analysis run-time (error termination times marked as ***), the peak pressure at 0.8 meters from the center of the 0.66-lb. TNT charge, the analysis time at which the peak occurs for all data from 0.0006 to 0.001 seconds. Figure 80 shows all six analyses with the mesh configuration of ES3_4. Figure 81 shows all six analyses with the mesh configuration of ES6_13. Figure 82 shows the four applicable analyses with the mesh configuration of ES9_15. Figure 83 shows the four applicable analyses with the mesh configuration of ES12_25. Figure 84 shows the four applicable analyses with the mesh configuration of ES15_25 and Figure 85 shows both analyses with the mesh configuration of ES18_25. Examination of Figure 80 through Figure 86 and Table 14 yields the following:

1. Peak Pressure Approximation Convergence

As the mesh is refined, the peak pressure appears to convergence with the peak approximation peak pressure value of 46.3 MPa., and the time of occurrence of the peak pressure is appears to converge with the peak approximation time of occurrence of 0.00033 seconds. The decrease in the time step size scale factor (TSSFAC) increases the value of the peak pressure, this alone will not cause convergence of the peak pressure. For less refined (low density) mesh configurations, the higher the number of time steps between advection cycles (NADV) the higher the peak pressure, but for refined meshes (ES15_25 and ES18_25), the higher NADV the lower the peak pressure. The low density mesh will give a smaller peak pressure value than the peak pressure approximation. If the number of time steps between advection cycles is kept high (less advection cycles), the energy loss due to a less accurate second order advection algorithm is minimized since the amount of material being advected is small relative to the larger element size. This will give a higher peak pressure than having more advection cycles, though with the low density mesh peak pressure convergence is not obtainable. For a more refined mesh, decreasing the number of time steps between advection cycles (increasing the number of advection calculations performed) will increase the peak pressure value. This is due to the large amount of material

being advected relative to the small element size. A greater number of advection calculations are needed to more precisely capture the amount of material moving through the smaller elements.

2. Analysis Time

As the mesh is refined by an order of magnitude, the analysis time is increased by an order of magnitude. As the time step size scale factor (TSSFAC) is lowered, the analysis time is increased by a proportional amount to the decrease of TSSFAC [$TIME_{new} \sim (TSSFAC_{old}/TSSFAC_{new}) \times TIME_{old}$]. As the number of time steps between advection cycles (NADV) is decreased by an order of magnitude, the analysis time is doubled.

Table 14 Test Matrix M1 Results

Test #	Analysis Run-time (hrs)	Peak Pressure (Pa.)	Time of Peak Pressure (sec.)	Fluid Element Size (m.)	Configuration
M1R01	0.22	1.88E+07	3.80E-04		
M1R02	0.38	1.93E+07	3.80E-04		
M1R03	1.38	2.22E+07	3.80E-04		
M1R04	0.067	1.77E+07	3.80E-04		
M1R05	0.18	1.86E+07	3.80E-04		
M1R06	0.53	2.16E+07	3.80E-04	1	ES3_4
M1R07	3.667	2.55E+07	3.40E-04		
M1R08	7	2.77E+07	3.40E-04		
M1R09	39.117	2.77E+07	3.60E-04		
M1R10	5.667	2.34E+07	3.40E-04		
M1R11	13.117	2.68E+07	3.40E-04		
M1R12	27.667	2.72E+07	3.40E-04	~ 0.3	ES6_13
M1R13	13.033	3.30E+07	3.40E-04		
M1R14	33.433	3.36E+07	3.40E-04		
M1R15	N/A	N/A	N/A		
M1R16	23.4	2.94E+07	3.40E-04		
M1R17	50.467	3.26E+07	3.40E-04		
M1R18	N/A	N/A	N/A	~ 0.26	ES9_15
M1R19	54.633	4.53E+07	3.30E-04		
M1R20	***	4.64E+07	3.30E-04		
M1R21	N/A	N/A	N/A		
M1R22	>100	4.48E+07	3.30E-04		
M1R23	N/A	N/A	N/A		
M1R24	N/A	N/A	N/A	0.16	ES12_25
M1R25	35	4.30E+07	3.20E-04		
M1R26	***	4.48E+07	3.30E-04		
M1R27	N/A	N/A	N/A		
M1R28	***	4.79E+07	3.30E-04		
M1R29	***	5.81E+07	3.40E-04		
M1R30	N/A	N/A	N/A	0.16	ES15_25
M1R31	61.85	4.75E+07	3.30E-04		
M1R32	49.2	4.67E+07	3.30E-04	0.16	ES18_25
Peak Approx.	-	4.75E+07	3.40E-04	-	-

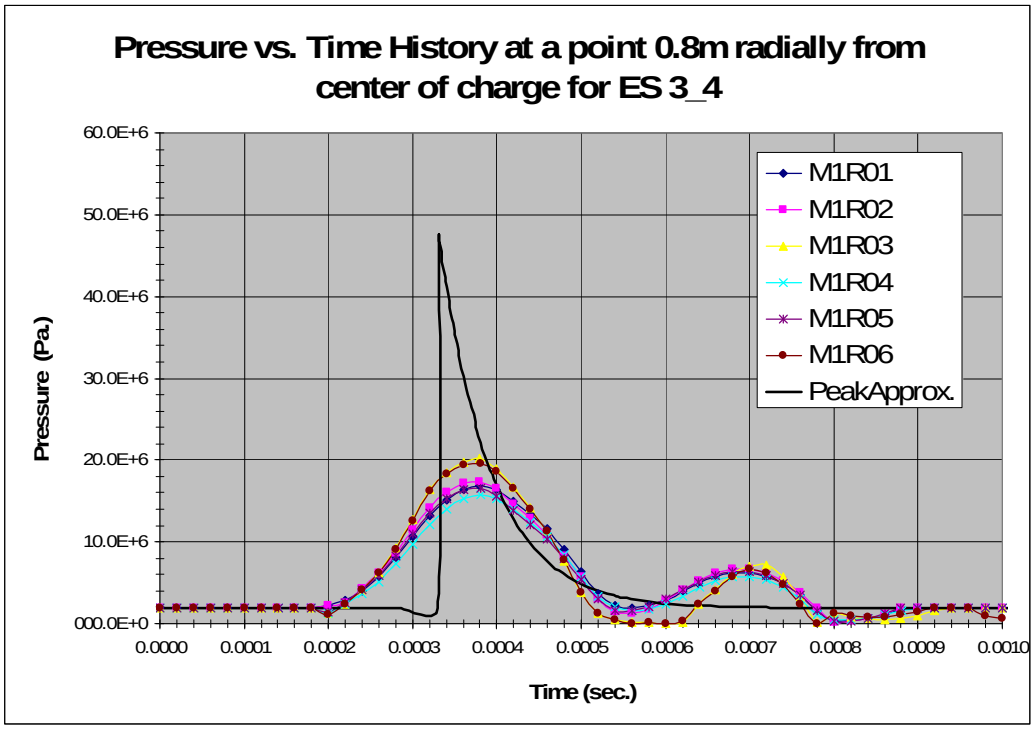

Figure 80 - Pressure-time Histories for Test Cases ES3_4

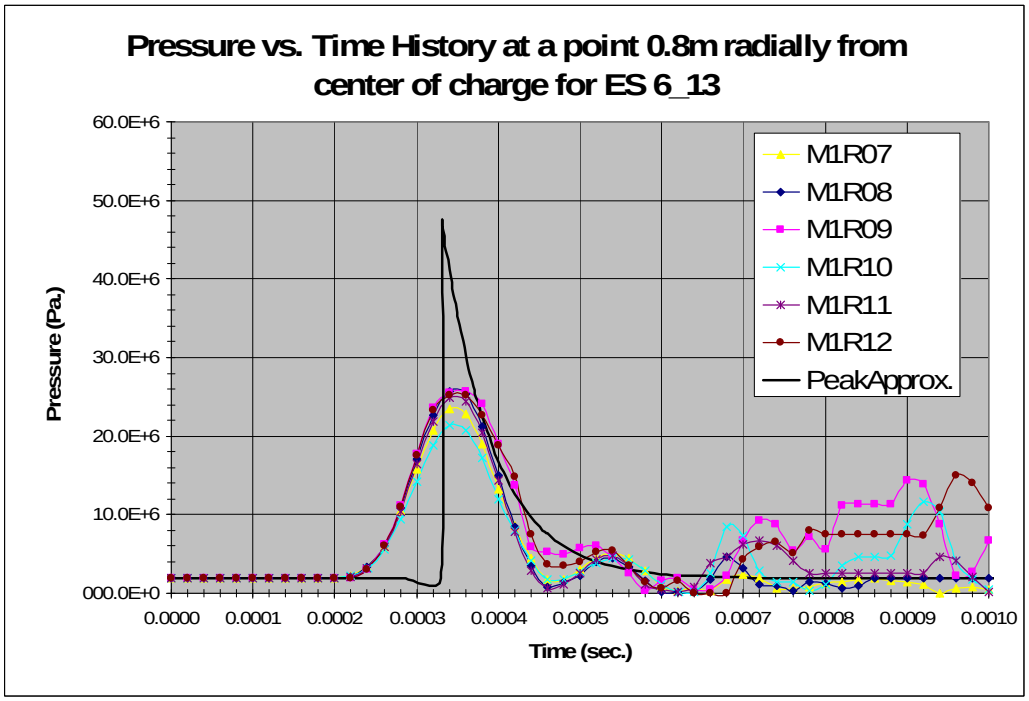

Figure 81 - Pressure-time Histories for Test Cases ES6_13

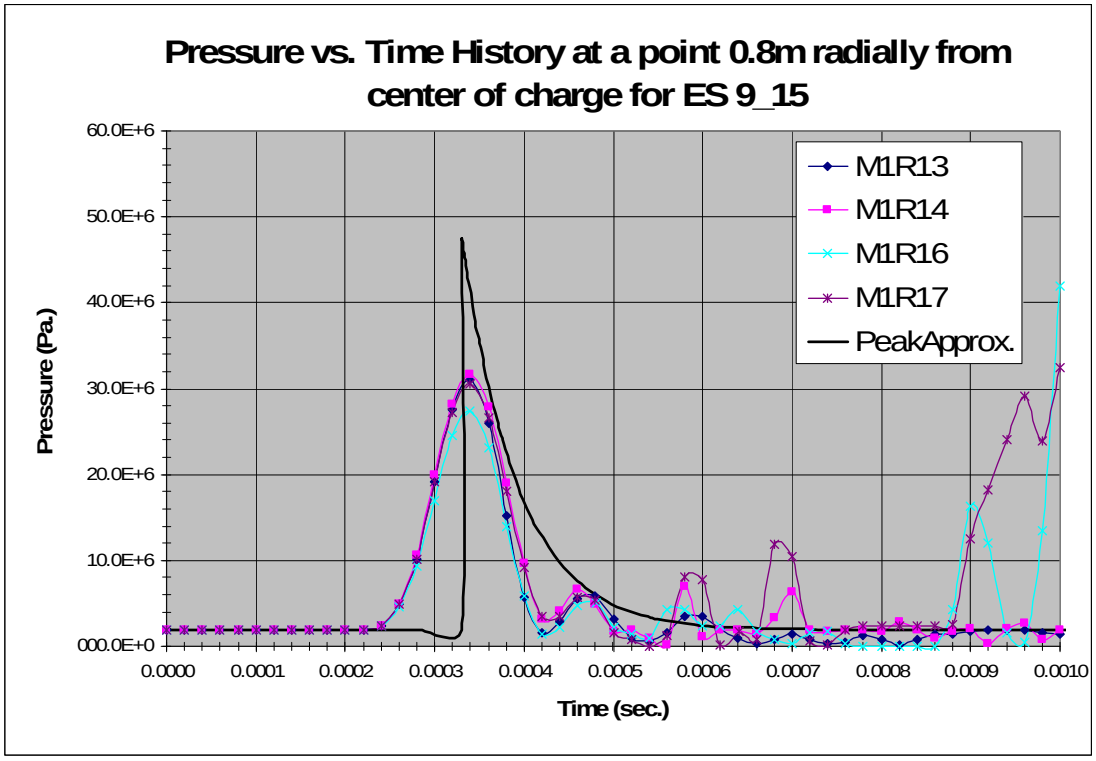

Figure 82 - Pressure-time Histories for Test Cases ES9_15

Again, test case analyses M1R15 and M1R18 of Table 12 exceeded the permissible analysis run-time of 100 hours and as such, results are not reported in Figure 82 or Table 14.

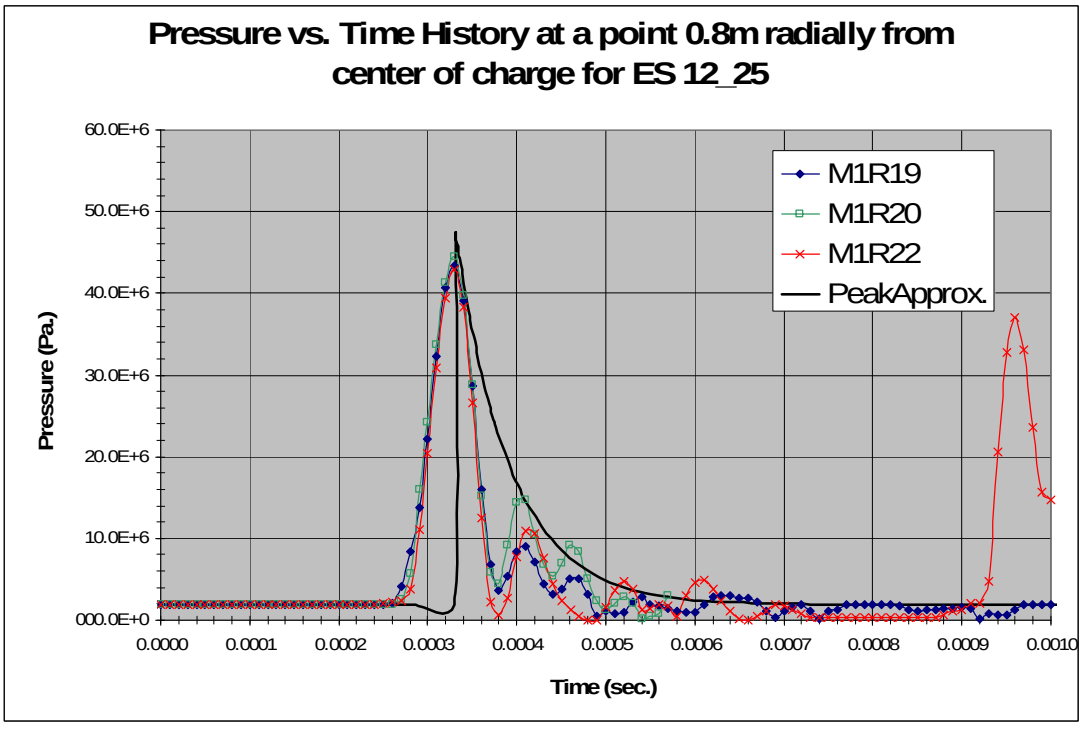

Figure 83 - Pressure-time Histories for Test Cases ES12_25

Test case analyses M1R21, M1R23 and M1R24 of Table 12 exceeded the permissible analysis run-time of 100 hours and as such, results are not reported in Figure 83 or Table 14.

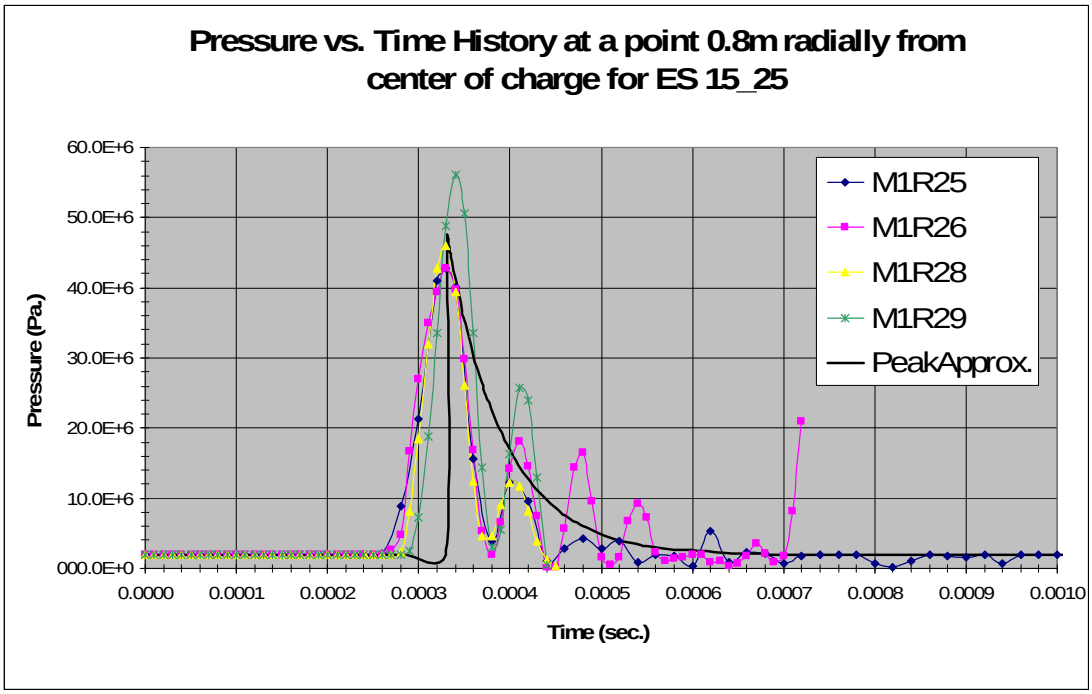

Figure 84 - Pressure-time Histories for Test Cases ES15_25

Again, test case analyses M1R27 and M1R30 of Table 12 exceeded the permissible analysis run-time of 100 hours and as such, results are not reported in Figure 84 or Table 14.

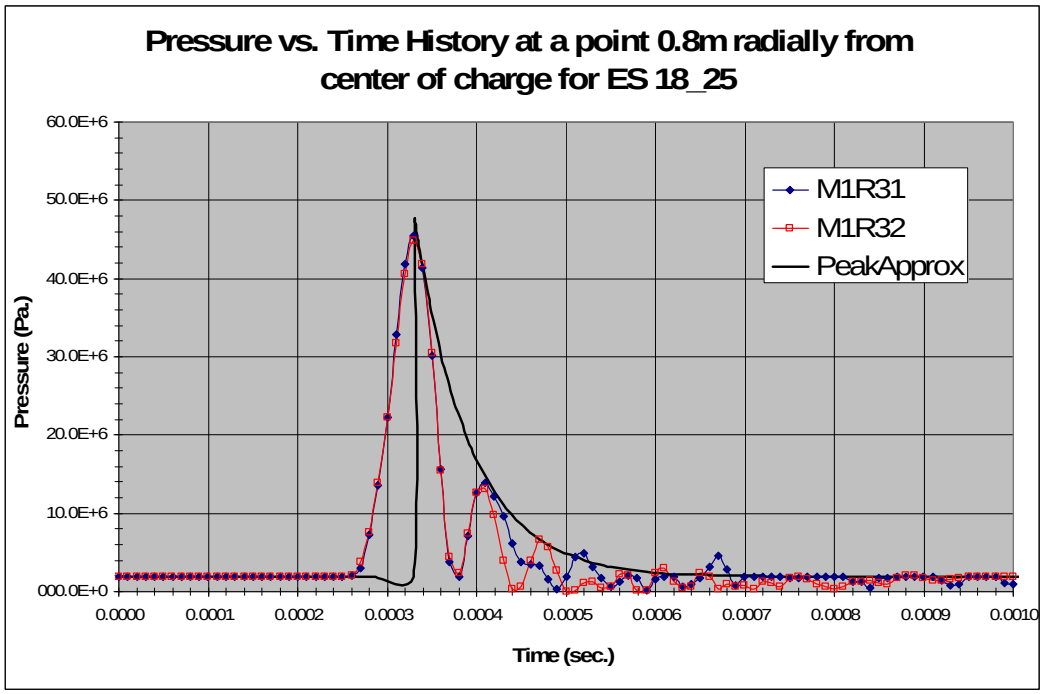

Figure 85 - Pressure-time Histories for Test Cases ES18_25

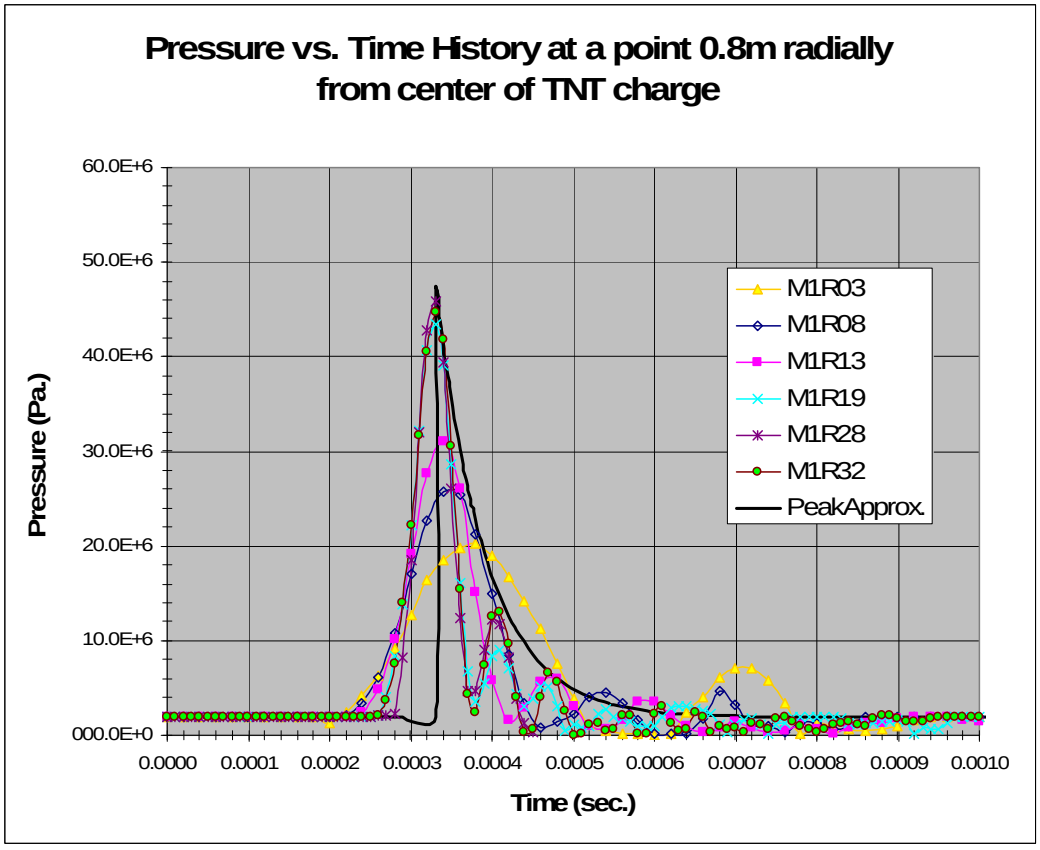

Figure 86 - Convergence of Peak Pressure; Reduced Noise Analyses

Figure 87 provides the comparison of test cases M1R19 (ES12_25), M1R25 (ES15_25) to the peak approximation.

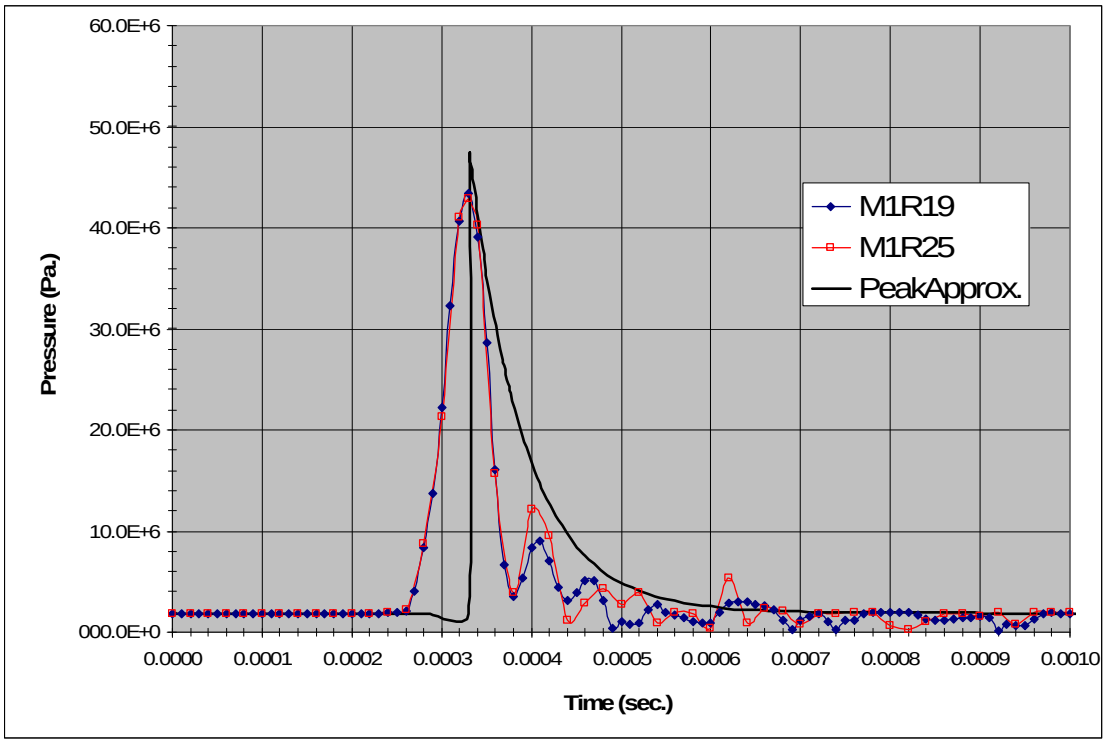

Figure 87 - Pressure-time Histories of M1R19 (ES12_25), M1R25 (ES15_25) and the Peak Approximation

Figure 86 shows that as element size is decreased, the peak pressure appears to converge to the correct value. Figure 87 shows the two mesh configurations for ALE explicit FEA models, M1R19 (ES12_25) and M1R25 (ES15_25), that capture the peak value of the pressure time history and the time of occurrence. In order to prove peak pressure convergence, a more dense mesh is needed. Generating a more dense fluid mesh will cause the transitional charge mesh element size to decrease in order to maintain one to one nodal aligment between the charge and fluid mesh. LS-DYNA computes the initial time-step size based on the smallest element size of the mesh model. Increasing the fluid mesh density will increase the computational expense of the model. Table 14 shows that M1R31 (ES18_25) mesh configuration is more computationally expensive than M1R25 (ES15_25) with a slightly improved peak pressure result. At this time, it is not feasible to construct a more dense fluid mesh than ES18_25 due to computational resourses. Since the early-time pressure response has been captured, it is important to extend

this method so that the late-time response can be captured. Section 3.2.2.3.2 through section 3.2.2.3.5 investigate methods to capture the late-time pressure response of the DSB problem.

3.2.2.3.2 Boundary Condition Analysis for Late-time Response – Test Matrix #2

When an explosive is detonated underwater, a shock wave (1st pressure wave) and explosive gaseous products are given off. These gaseous products rapidly expand, behind the shock wave, forming a gaseous bubble. As the bubble rapidly expands, the high internal pressure of the bubble rapidly reduces to less than the local pressure outside the bubble. Essentially, the internal pressure of the bubble reduces so quickly, due to the rapid expansion of the bubble, it overshoots equilibrium with the local pressure outside the bubble. The local pressure outside the bubble is now greater than the internal pressure. This causes the bubble to rapidly contract. The internal bubble pressure rapidly increases, due to the rapid contraction, and overshoots equilibrium. There is now a high pressure inside the bubble relative to the local pressure external to the bubble. This causes the gaseous bubble to expand rapidly again. As the bubble expands again it produces a 2nd pressure wave (numbering is relative to the shock wave). The bubble oscillates (expands and contracts) around the local (hydrostatic plus dynamic) pressure in the fluid medium until all energy is dissipated or the bubble collapses/bursts. Coincident with the expansions and contractions the bubble migrates slowly, relative to the speed of oscillation, toward the free surface. Each expansion and contraction phase is smaller in pressure magnitude than its predecessor. The dissipation the bubble experiences is due to the resistance acting on the bubble from of all the fluid surrounding the bubble along its path of migration.

To accurately capture the bubble dynamics of an UNDEX event all the surrounding fluid must be modeled or the resistance of the remaining surrounding fluid must be artificially reproduced if use of a smaller model is desired. This resistance can be reproduced by matching the acoustic impedance of the outer boundary of the smaller model to the acoustic impedance produced by the remaining volume of the surrounding fluid.

The Euler Boundary Condition, an Artificial Pressure Boundary Condition (APBC), and the Non-Reflecting Boundary condition are investigated in test Matrix #2.

- The Euler Boundary Condition (EBC) restricts flow through a boundary in the normal direction and allows inviscid motion of the flow parallel to the plane of the boundary (slip condition). The EBC is applied to all nodes on the specified boundary surface.

- The Artificial Pressure Boundary Condition (APBC) produces the pressure of a significantly larger fluid domain that would be generated at a specific location of a smaller fluid domain section of the larger domain. This artificial pressure is necessary to capture the bubble dynamics associated with an underwater explosion. The pressure of the remaining volume of surrounding fluid can be reproduced by calculating the pressure-time history of the explosive/fluid domain at a location equal to the location of the outer boundary of the smaller fluid model (i.e., fluid model boundary located at 1.5m, Pressure-time history of explosive/fluid domain taken at 1.5m) and applying the pressure-time to that boundary. The pressure-time history is generated using the Peak Approximation. All location references are radial distances from the center of the explosive charge.
- The Non-Reflecting Boundary Condition (NRBC) is applied to the exterior boundaries of the analysis model. It allows the modeling of an infinite domain as a finite domain as described in Section 2.1.3.9 and Reference 24. NRBC is used to prevent artificial stress wave reflections generated at the model boundary from reentering the model. Internally LS-DYNA computes the impedance matching function for all non-reflecting boundary segments based on linear material behavior. The finite element mesh needs to be constructed so all significant non-linear events are contained in the discretized model analysis [23].

Since the explosive/fluid interaction has non-linear events occurring throughout the entire space and time domain, it is necessary to couple the NRBC with the Artificial Pressure Boundary Condition (APBC) to capture the non-linear events occurring inside and outside of the modeled domain.

The following are suggestions from the Author for beginning analysis for the boundary conditions to be applied to and run on test analysis M1R13 and M1R25 in test Matrix #2.

1. Apply the Euler Boundary Condition on the spherical boundary (1.5 m from center of charge). Labeled NSIDEBC in the table below.
2. Apply a Non-Reflecting Boundary Condition and apply at the spherical boundary (1.5 m from center of charge). Labeled SSIDNRBC in the table below.
3. Use Pressure vs. Time history from peak approximation (the APBC) and apply at the spherical boundary (1.5 m from center of charge). Have the pressure direction pointing toward the charge. Labeled SSIDPvT in the table below.
4. Apply the EBC and the APBC

5. Perform both 1) and 2) and 3)

6. Perform none

Table 15 shows the case setup for test Matrix #2. NSIDEBC is the Node Set ID to be excluded from Euler Boundary Condition. SSIDNRBC is the Segment Set ID with the Non-Reflecting Boundary Condition applied. SSIDPvT is the Segment Set ID to apply the Pressure vs. Time history load from the Peak Approximation. Node set 17 is the set of nodes the make up the x = 0, y = 0, and z = 0 faces of the model and segment sets 4, 5, and 6 make up the outer spherical faces of the model, the faces are shown in Figure 74 through Figure 79.

Table 15 Test Matrix #2 Boundary Condition Comparisons

Run	ES	TSSFAC	NADV	NSIDEBC	SSIDNRBC	SSIDPvT
01	15_25	0.67	10	17	None	4,5,6
02	15_25	0.67	10	None	None	None
03	15_25	0.67	10	None	None	4,5,6
04	15_25	0.67	10	17	4,5,6	4,5,6

3.2.2.3.2.1 Mesh Density Effect on Overall Run-time

The run-time for the boundary condition tests associated with ES15_25 will be greater than the 100 hour limit. This is due to the increased number of calculations resulting from the FE analysis termination time being increased as needed to capture the late-time response. This is not a practical run time for a small problem like this. Test Matrix #2 runs 01-04 are not performed. Methods are investigated to decrease this run-time while not sacrificing accuracy. Section 3.2.2.3.2.1.1 discusses the methods.

3.2.2.3.2.1.1 Efforts to Decrease Run-time

In an effort to decrease the cost of the ALE FEA analysis, methods are investigated that will allow the overall run-time of the experiment to be in the required 100-hour limit.

3.2.2.3.2.1.1.1 Increase Element Size for Less Dense Mesh

Mesh density is decreased to lower the overall computational run-time of the ALE FEA analyses. Test cases from Matrix 1, seen in Table 12, were run out to a termination time of 0.001 sec. A termination time of 0.02 sec. is required to capture the late time response, the first bubble pulse,

of the UNDEX event. To satisfy the 100 hr. maximum run-time limit test case M1R07, using ES6_13, is chosen. Figure 81 shows the results of M1R07. M1R07 is used in Matrix #2, Table 16, to investigate the boundary conditions needed to accurately capture the late time response.

Table 16 Test Matrix #2 Increased Element Size Boundary Condition Comparisons

Run	ES	TSSFAC	NADV	NSIDEBC	SSIDNRBC	SSIDPvT
05	6_13	0.67	10	17	None	4,5,6
06	6_13	0.67	10	None	None	None
07	6_13	0.67	10	None	None	4,5,6
08	6_13	0.67	10	17	4,5,6	4,5,6

3.2.2.3.2.2 Results of Matrix #2 Increased Element Size Tests

Test cases M2R05 through M2R07 where conducted and the FE analyses all terminated early with errors. Time was not spent investigating the cause of the errors since the boundary conditions used M2R08 seemingly obtained the proper late-time response.

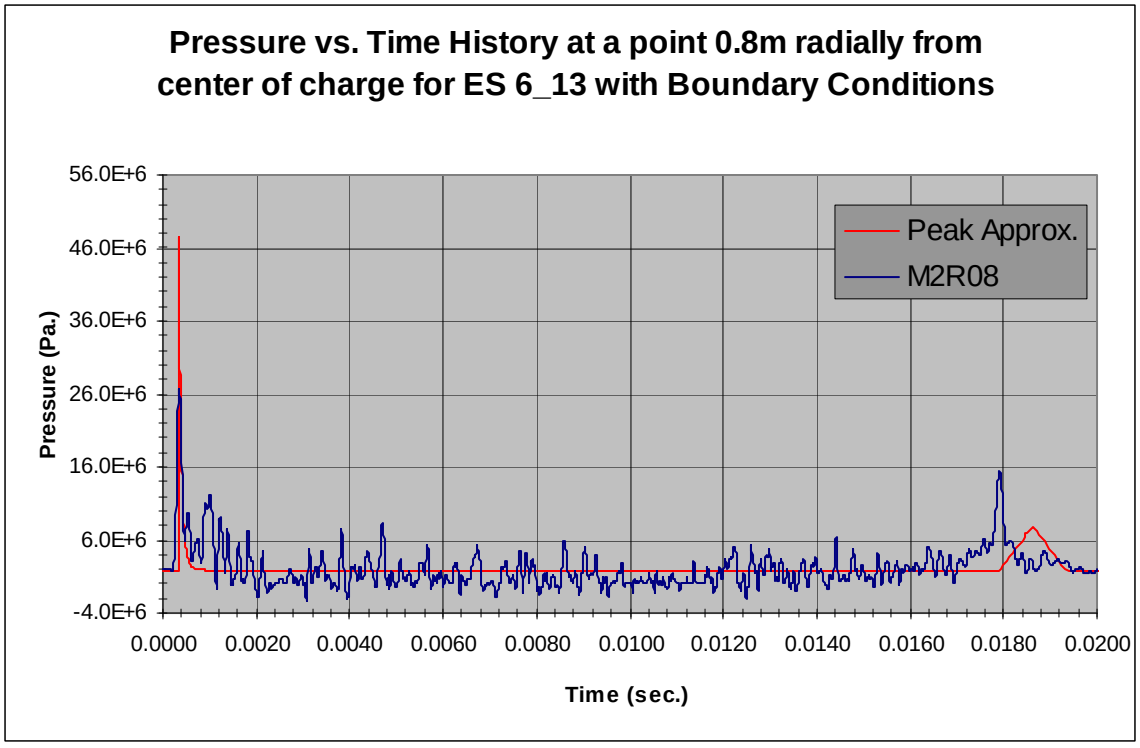

Figure 88 - Pressure-time History of M2R08 Boundary Condition Test Case Compared to the Peak Approximation.

Table 17 Test Matrix 2 Results

Test #	Analysis Run Time (hrs)	Peak Pressure (Pa.)	Time of Peak Pressure (sec.)	1st Bubble Pulse (Pa.)	Time of 1st Bubble Pulse (sec.)
M2R08	130.18	2.68E+07	3.50E-04	1.54E+07	1.7920E-02
Peak Approx.	--	4.75E+07	3.31E-04	7.66E+06	1.82E-02

The results of test case M2R08 show that the use of the Artificial Pressure Boundary Condition, the NRBC and the EBC coupled together will produce the late-time response. It can also be seen that magnitude of the peak pressure is low, as expected, due to the small element size configuration (ES6_13) used. Figure 88 shows that the 1st bubble pulse occurs somewhat earlier than the Peak Approximation predicts and the magnitude of the 1st bubble pulse is larger than the Peak Approximation. These discrepancies can be attributed to the different values of the speed of sound in water used in the ALE FE analysis (C = 2417m/s) and in the coefficients used in the Taylor Approximation for the late-time response portion of the Peak Approximation (C ~ 1500m/s). The coefficients used in the Taylor Approximation are based on test data and cannot be easily adjusted to reflect the change in the speed of sound needed to run the FE analysis. Table 17 shows the magnitudes and time of occurrences of the pressures that are of interest compared to the Peak Approximation calculation.

3.2.2.3.2.2.1 Effect of Boundary Conditions on Peak Pressure

The fluid mesh outer spherical boundary is modeled out to distances of 1m, 1.5m, and 2m. The boundary conditions used in test case M2R08, described in Section 3.2.2.3.2.1.1.1, are applied at these boundary locations for a model using element configuration ES15_25. The ES15_25 model is used since it will capture the correct peak pressure. This is important because it allows the effects of the boundary conditions on the peak pressure to be seen. This FE analysis is run to a termination time of 0.00006 seconds since the effects on the peak pressure are only of interest here. The Artificial Pressure Boundary Condition is calculated by the Peak Approximation using stand-off locations that correspond to the spherical mesh boundary locations. The results of applying the boundary conditions at different locations of the fluid mesh are shown in Figure 89.

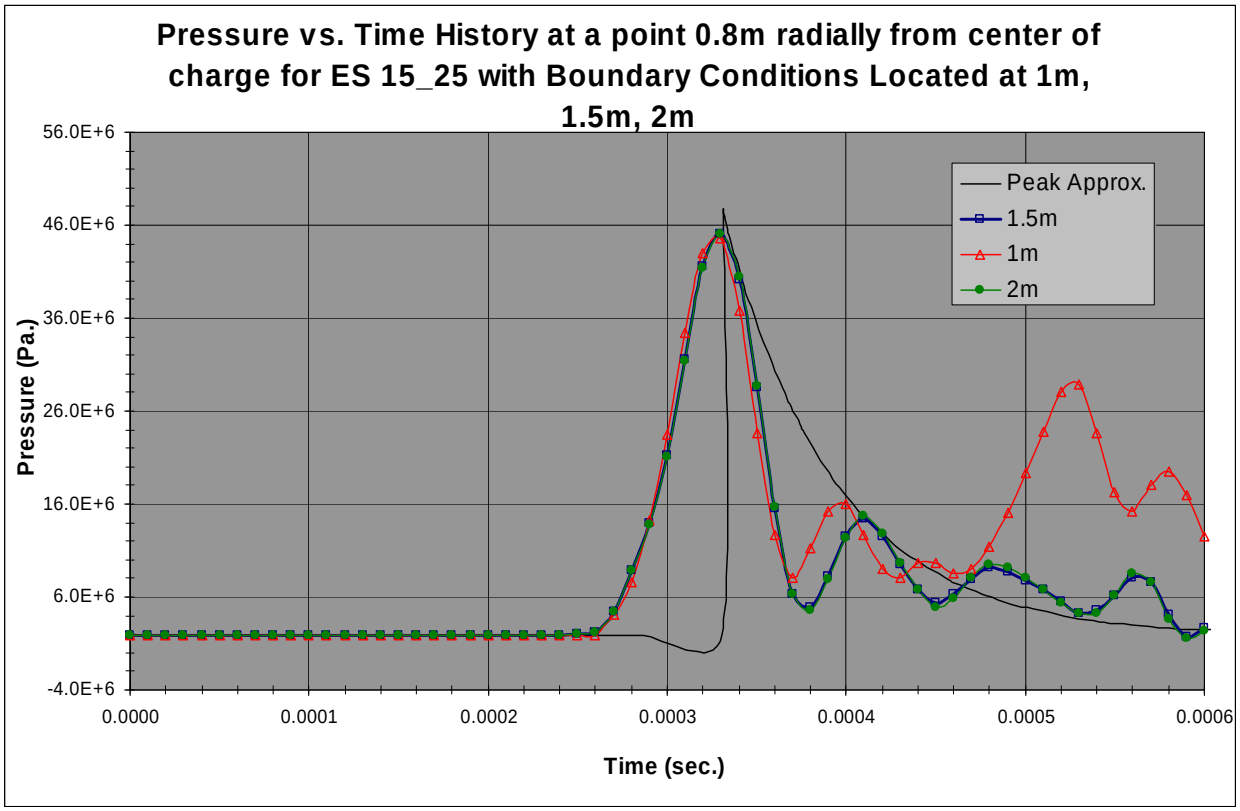

Figure 89 - Pressure-time History of M1R25_BCs Test Case Compared to the Peak Approximation.

Figure 89 shows that placing the boundary conditions at different distances from the charge does effect stability, but does not affect the peak pressure.

3.2.2.3.2.2.2 Effect of Boundary Conditions on Late-time Response

The same tests are conducted on the fluid mesh as in Section 3.2.2.3.2.2.1 except the run times are extended in order to capture the late-time response and a larger mesh size configuration, ES6_13, is used so run times do not exceed 100 hrs. Figure 90 shows the results of these tests.

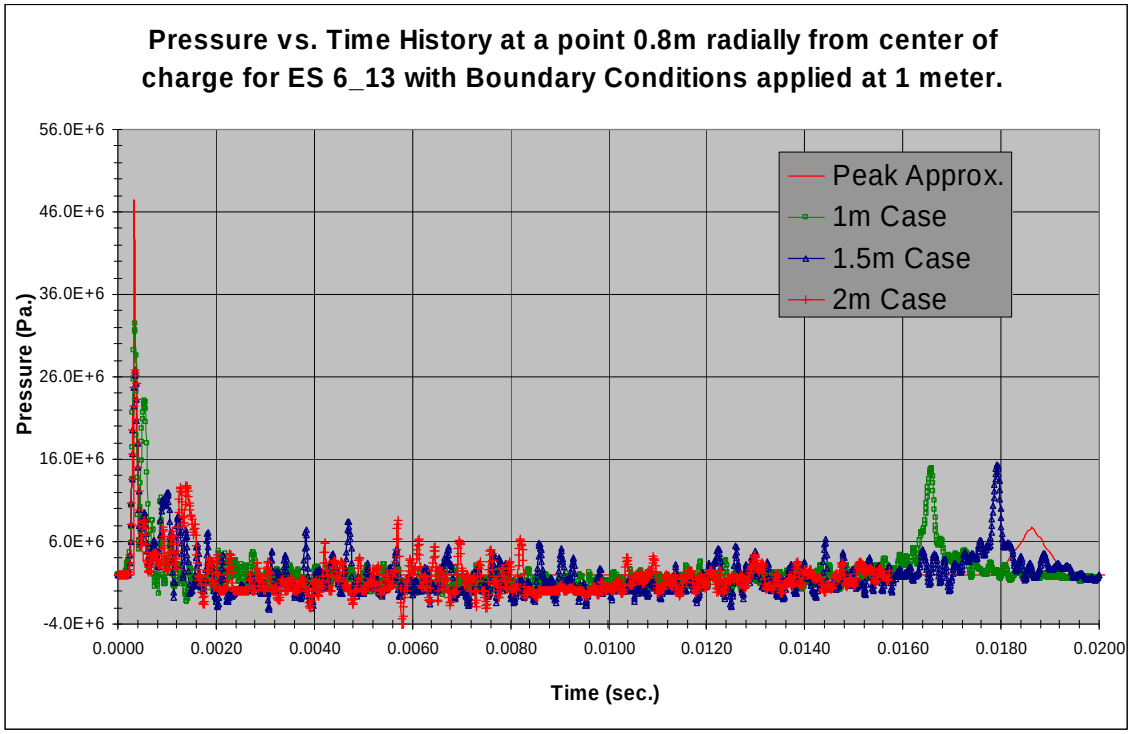

Figure 90 - Comparison of Pressure-time History for ES6_13 with Boundary Conditions applied at 1m, 1.5m, and 2m.

Figure 90 shows the Artificial Pressure Boundary Condition does not correctly capture the late-time response. It has been determined that the secondary pressure peak in Figure 90 is a result of the pressure wave defined by the load curve in the Artificial Pressure Boundary Condition entering the fluid mesh model from the spherical face end. The pressure wave then travels toward the charge and decays until it reaches the point where the pressure data is collected (tracer particle). Figure 90 shows that as the Artificial Pressure Boundary Condition is applied closer to the charge, the secondary pulse reaches the tracer particle more quickly. The secondary pulse is being manufactured by the APBC. The FE analysis is not producing the secondary pulse based on the energy equation calculations of the bubble oscillations. In actuality, the gaseous bubble never collapses in this analysis because the pressure imposed on the bubble by the fluid is not large enough to cause it to collapse. The boundary condition scheme used does not simulate the same conditions as modeling the entire region (out to 178m) of fluid.

It is concluded by the Author that the Artificial Pressure Boundary Condition is appropriate for one point in space at one point in time. It is not accurate for all points in space at any given time. The Artificial Pressure Boundary Condition will not be used in the three dimensional cases in Chapter 4. Section 3.2.2.3.3 discusses modeling the fluid region out to 178m.

3.2.2.3.3 Deep Spherical Bubble Problem Full Model to Capture Late-time Pressure Results

The deep spherical bubble problem cases that are run in Section 3.2.2.1 through Section 3.2.2.3.2.2.2 do not capture the true late-time response. More fluid needs to be modeled or an effective infinite boundary condition be applied to properly match the resistance the fluid imposes on the explosive bubble thus correctly capturing the late-time response. To assess this problem the DSB problem is modeled out to 178m. ES3_4 mesh configuration is used since it will run in the mandated 100 hr. time limit. Two cases are run; the first uses the default bulk viscosity values of Q1 = 1.5 and Q2 = 0.06, the second uses the LS-DYNA [23, 24] suggested bulk viscosity values of Q1 = 4.0 and Q2 = 0.5. Figure 91 shows the results from the default value run.

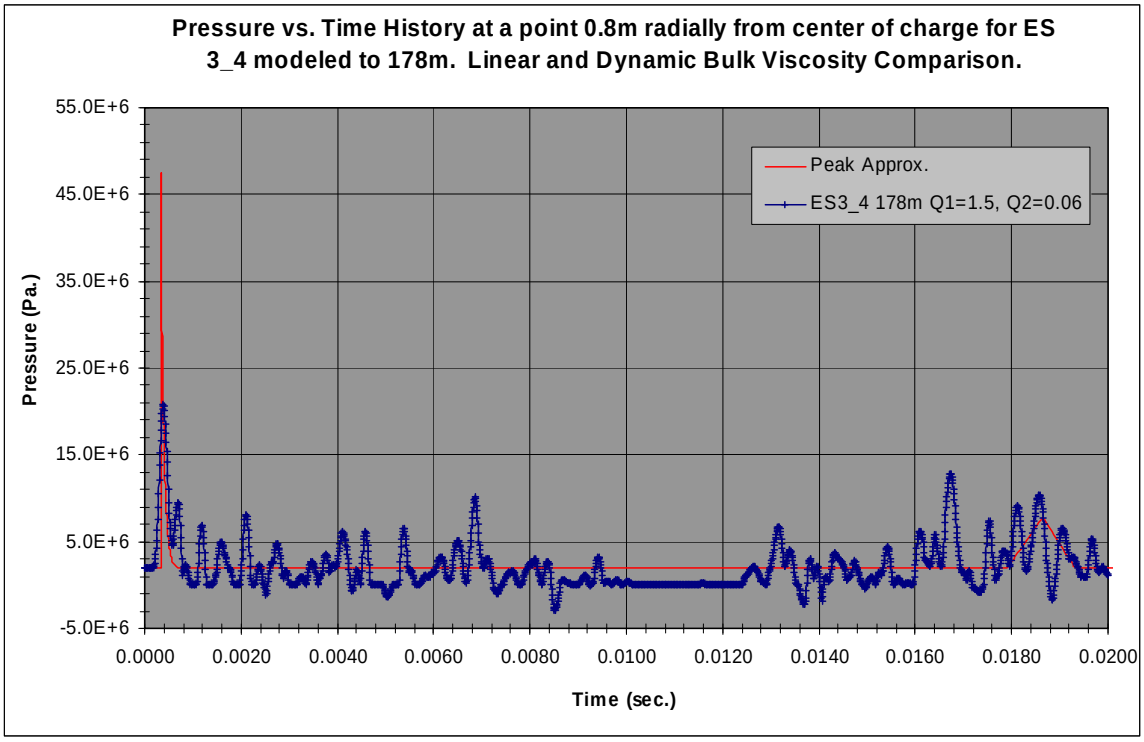

Figure 91 - Pressure-time History for 178m DSB Fluid Model Comparing Default Bulk Viscosity Values to the Peak Approximation

Figure 91 shows the full fluid model captures the late-time response of the deep spherical bubble problem. The correct magnitude of the peak pressure is not captured with the large element size as seen in Figure 91 and discussed in Section 3.2.3. The amount of noise in the results in Figure 91 is a result of the large element volume and an internal bubble spherical shock wave that reflects back and forth off the bubble boundary and off itself at the center of the bubble. These reflected shock waves interact with the gas/water interface. This interface interaction generates a

transmitted shock that travels outward into the water, and a reflected shock that moves inward toward the bubble center. A consequence of this internal bubble structure is a fluctuating gas/water interface pressure, as well as pressure variation at fixed points throughout the flow field [27].

These fluctuations are part of the phenomena that occur during an underwater explosion. It is desirable to include them in the results of the ALE FE analysis. The Q2 coefficient of the artificial bulk viscosity rapidly damps numerical oscillations behind the shock front. Use of a larger Q2 value, than the default value, could potentially damp out a significant portion of the pressure fluctuations due to internal bubble dynamics. Q1 can be varied and increased to attempt to capture the peak pressure and also retain the pressure fluctuations due to internal bubble dynamics.

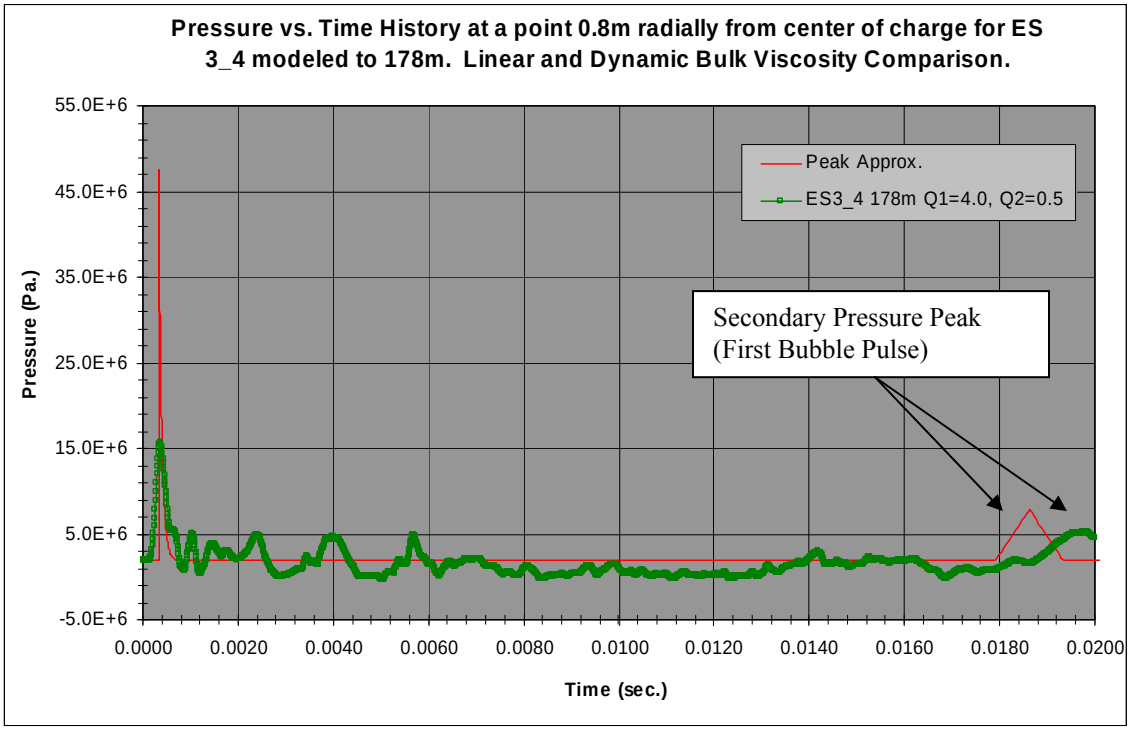

Figure 92 - Pressure-time History for 178m DSB Fluid Model Compared to the Peak Approx.

Figure 92 shows by increasing the bulk viscosity values some of the noise is eliminated and a more distinct peak for the first bubble pulse can be seen occurring around 0.02 seconds.

3.2.2.3.4 Comparison of Kinetic Energy and Pressure Impulse

The inability to capture the correct magnitude of the peak pressure and the secondary pressure pulse in the same model is a problem. The peak pressure depends on the mesh size and may not be captured in larger meshes. The secondary pressure pulse depends on the amount of fluid that the mesh models and a small model may not capture the second pressure pulse. Figure 93 shows the fluid kinetic energy comparison between mesh configuration ES3_4, ES6_13, and ES15_25.

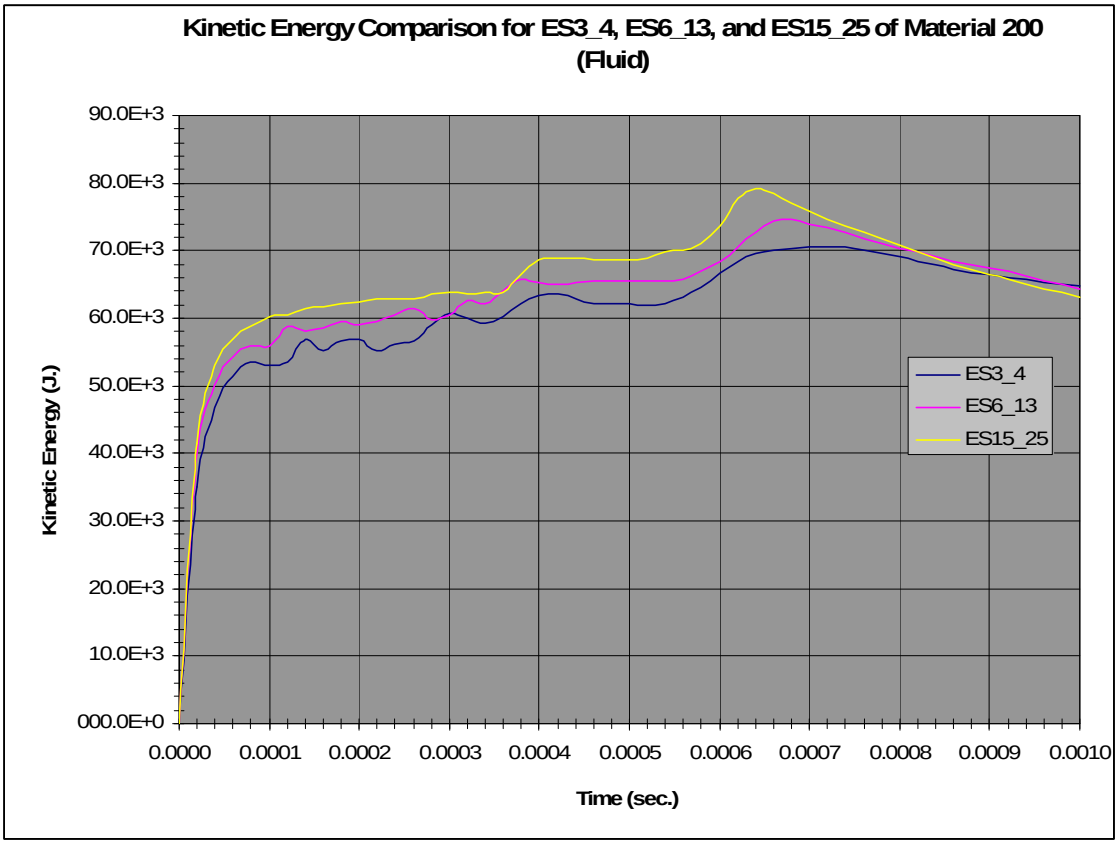

Figure 93 - Kinetic Energy Comparison for DSB Problem Mesh Configurations ES3_4, ES6_13, and ES15_25

Figure 93 shows that for the different mesh configurations the difference in the kinetic energy in the fluid is small. Impulse is the change in momentum produced by a force over a time interval. Figure 94 shows the pressure impulse for mesh configurations ES3_4, ES6_13, and ES15_25.

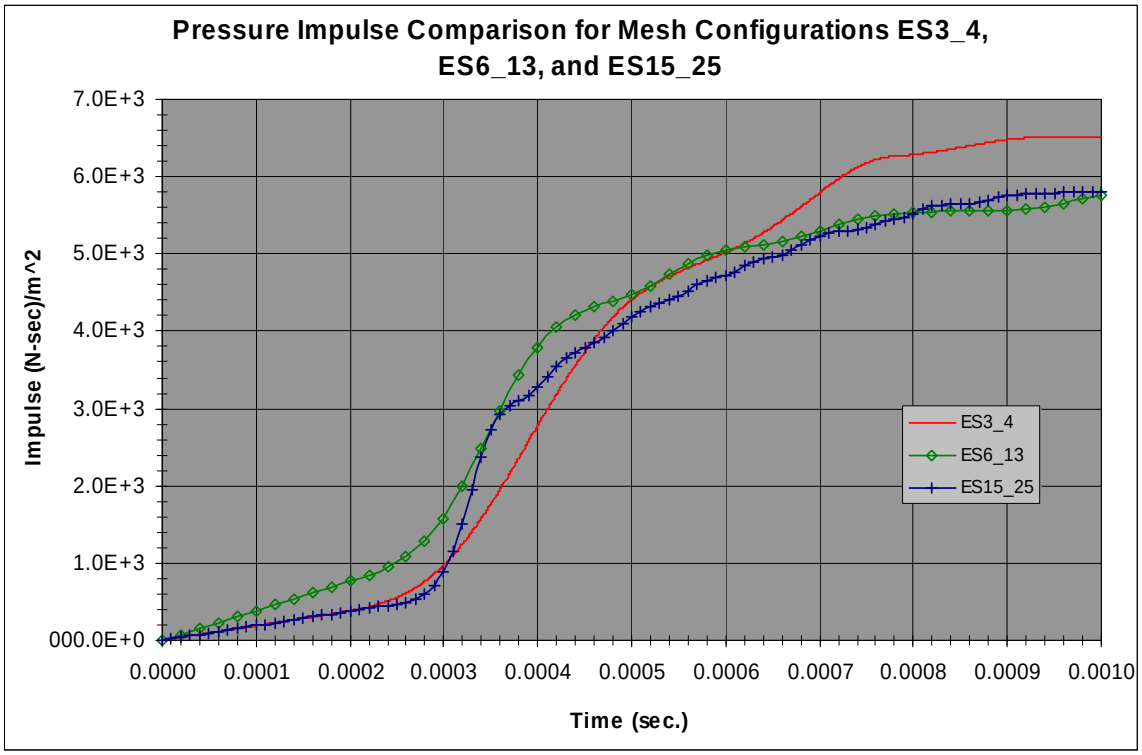

Figure 94 - Comparison of Pressure Impulse for DSB Problem Mesh Configurations ES3_4, ES6_13, and ES15_25

Figure 93 and Figure 94 show that momentum and energy from the detonation of the underwater explosion is conserved through the fluid mesh independent of the mesh configuration even though the element pressure may not capture the peak pressure accurately.

3.2.2.3.5 Modeling Explosive Charge as Initial Volume Fraction Geometry

The ability to capture the energy and momentum associated with an underwater explosive charge without having to model the explosive with a mesh is desirable. This would allow one large fluid mesh to be created for multiple explosive charge locations. Section 2.1.3.10 discusses the *INITIAL_VOLUME_FRACTION_GEOMETRY card in LS-DYNA. Figure 95 shows the pressure impulse for the volume fraction case compared to the cases shown in Figure 94. Figure 96 shows the peak pressure of the volume fraction case compared to the peak pressures from cases ES3_4, ES6_13, and ES15_25.

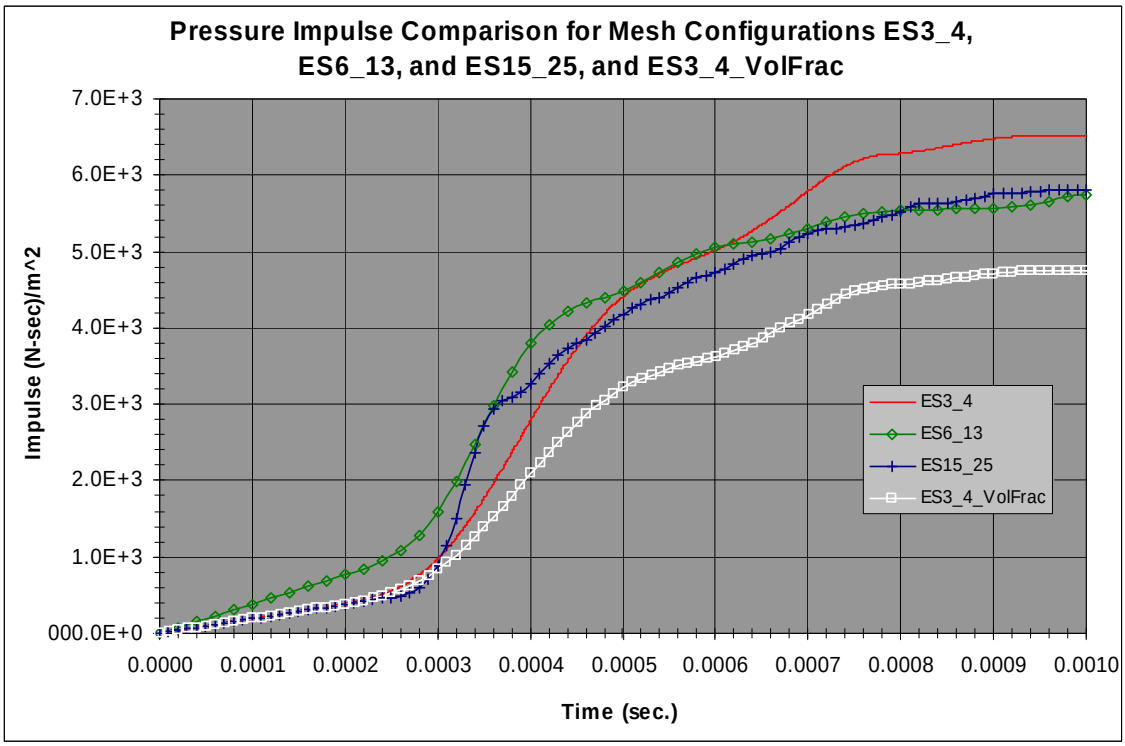

Figure 95 - Pressure Impulse Comparison of ES3_4, ES6_13, ES15_25, and ES3_4_VolFrac

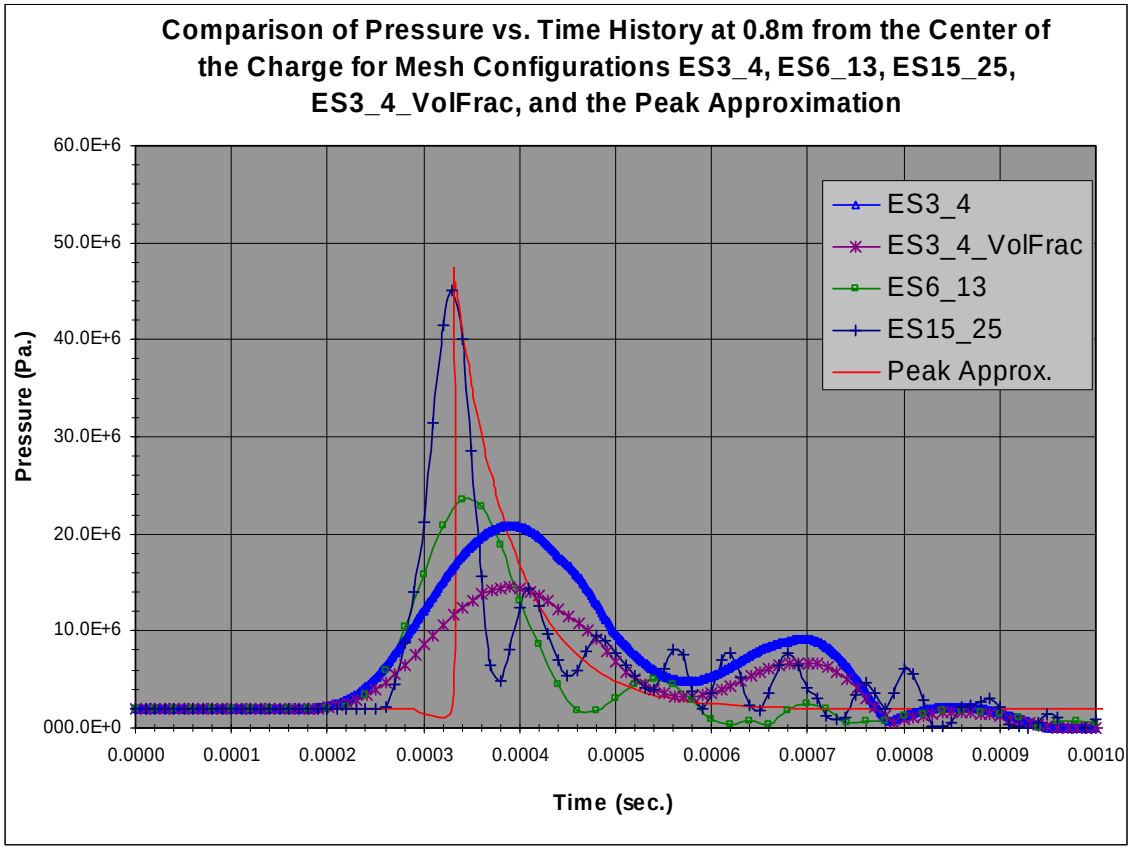

Figure 96 - Pressure-time History Comparison of ES3_4, ES6_13, ES15_25, ES3_4_VolFrac, and the Peak Approximation

Figure 95 and Figure 96 show that modeling the explosive charge with the *INITIAL_VOLUME_FRACTION_GEOMETRY card in LS-DYNA gives approximately the same response as the ES3_4 case only with a small difference in magnitude.

3.2.3 Results

The results of the test matrices show that capturing the peak pressure is dependant on the fluid mesh element size. Figure 97 shows as the mesh element size decreases, thus decreasing element volume, the peak pressure converges to the Peak Approximation solution.

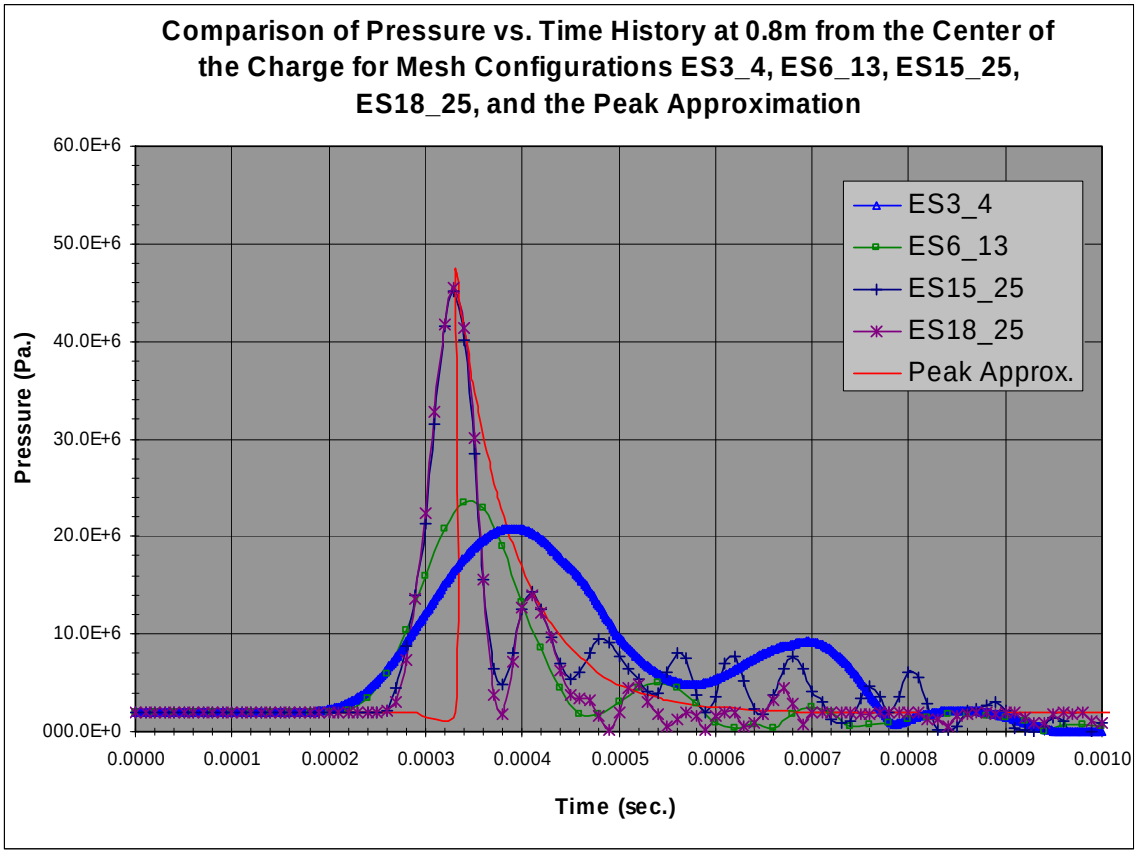

Figure 97 - Comparison of Pressure-time History for ES3_4, ES6_13, ES15_25, ES18_25, and Peak Approx.

Smaller element size will capture the early-time response (peak pressure response of the shock wave) of the Deep Spherical Bubble problem. In order to capture the late-time response (bubble pulse effects) it is necessary to model more fluid to match infinite impedence and for reasonable computation time. It is not feasible to use the smaller mesh size models. It is concluded in Section 3.2.2.3.2 that the Artificial Pressure Boundary Condition does not produce the correct late-time response. Figure 92 in Section 3.2.2.3.3 shows that the full fluid model (modeled to 178m) gives the late-time response when the bulk viscosity values Q1 and Q2 are used to dampen oscillations due to the internal bubble dynamics. Figure 93 through Figure 95 show the pressure impulse in the fluid. Tracking the pressure impulse as a means of validating a fluid model is not recommended for fluid/structure problems. Capturing the correct pressure is necessary since pressure derermines the cavitation behavior. The cavitation regions' behavior impacts the response of the structure in an UNDEX fluid/structure interaction problem.

3.2.4 Discussion

The process and results of the 3-D Deep Spherical Bubble Problem are described in Sections 3.2.1 through 3.2.3. The use of Finite Element Analysis to track the peak pressure pulse from the shock wave and the pressure pulse(s) from the bubble oscillation(s) due to an underwater explosion is limited by computation resources and time. In order to capture the correct peak pressure the mesh elements must be sufficiently small to have a small element volume. This causes longer run times. Since the shockwave and the bubble pulse(s) occur at different orders of magnitude (Section 1.3, pg. 28) of time, the FE analysis must be run long enough to capture the bubble pulse. The time-step size, O(1.0E-08) seconds, due to small mesh size plus the added runtime due to a large termination time, O(1.0E-01) seconds, causes overall computational runtimes to become to expensive. Test case M1R25 results, from Table 14, show the overall runtime is 35 hours on a Pentium IV desktop PC. The termination time is 0.001 seconds. The time step size ranges from 3.33E-08 to 7.76E-10 seconds. The fluid mesh is modeled to 1.5 meters and has 68850 elements (Table 13). Test case M1R25 captures the peak pressure within 9% of the actual value. Figure 91 shows that a modeling a larger fluid volume captures the late time bubble pulse. To use M1R25 test case to capture the bubble oscillation phenomena it would need to be modeled out to 178m, adding approximately 31000 elements for an approximate total of 100000 elements. The overall run time would need to be extended from 0.001 seconds to 0.02 seconds. Just looking at the time step size and the extended run time, it would take approximately 1,170,000 hours (133 years) to complete. More work needs to be done to find a method to decrease the model size, but still capture the late-time responses of the bubble. The application of an impedance matching infinite boundary condition is required. Section 2.1.3.9 discusses how LSDYNA's Non-Reflecting boundary condition uses a linear material model to create an impedance matching function. A linear material model is inadequate for the non-linear material behavior of a near-field underwater explosion event.

3.3 Summary and Resulting Charge/Fluid Model

Chapter 3 describes the models and results for the 1-D and 3-D Deep Spherical Bubble (DSB) problem based on a Naval Postgraduate School's thesis [17,36,37]. Different FE analysis techniques using the Arbitrary Lagrangian-Eulerian (ALE) method in LS-DYNA are investigated. Section 3.2.2.1 discusses reproducing the early-time portion of the DSB problem and shows that the results do not reproduce the peak pressure approximation or NPS results. Section 3.2.2.2 discusses and investigates the causes and solutions to why the early-time pressure response of the DSB problem was incorrect. Specifically, Section 3.2.2.2.1 dicusses the need for a fluid equation of state that can accurately capture the effects of the shock wave on the fluid near the charge and away from the charge. Section 3.2.2.3 investigates the sensitivity of the of the early-time model to element size changes, time-step size changes, and ALE advection cycle changes. Section 3.2.2.3 also investigates developing a method for obtaining the late-time pressure response by using different boundary conditions, as described in Section 3.2.2.3.2. Section 3.2.2.3.3 investigates using the extended (178m) fluid model to capture both the early-time and late-time pressure result. Section 3.2.2.3.5 discusses simulating the explosive charge using the Initial Volume Fraction Geometry option in the ALE method instead of modeling the charge with a mesh. The results show that there is a small difference in the pressure when using the volume fraction to simulate the charge when compared to modeling the charge with a mesh. This small difference is acceptable when you consider the complications of trying to model the explosive charge with a mesh and then have one to one nodal connectivity between the charge, fluid, and structure. This complication is increased if multiple charge locations are going to be considered for a single structure.

The result of the investigations performed in Section 3.1 shows techniques for modeling an underwater explosion and a technique for modeling an underwater explosion involving a structure. If investigating the early-time pressure response of an underwater explosion, follow the technique used for the Reproduction Test case in Section 3.2.2.2.2.1. If you are investigating both the early-time and late-time results of an underwater explosion, follow the technique used in Section 3.2.2.3.3. For fluid/structure interaction problems involving underwater explosions, follow the Initial Volume Fraction Geometry techniques used in Section 3.2.2.3.5 with the exception that the fluid mesh model will be built starting with the structure and going outward, not by starting with the charge and going outward.

The Initial Volume Fraction Geometry modeling and simulation techniques used in Section 3.2.2.3.5 are used in Chapter 4 to investigate fluid/structure interaction problems.

CHAPTER 4 FLUID/STRUCTURE INTERACTION

4.1 1-D Plate Problem

A simple one dimensional problem of a plane wave impacting an infinite steel plate is necessary to check the validity of fluid/structure interaction portion of an ALE FE analysis. The purpose for a problem of this type is to check the propagation of a pressure wave in the fluid, the interaction of the pressure wave with a structure (fluid-structure interaction), and the dynamic response of the structure are behaving correctly. Since the problem is small and one dimensional it can be completed with minimal pc power resulting in short run times. The x-displacement results are compared to the analytic solution [38,39,40] in Appendix APPENDIX F.

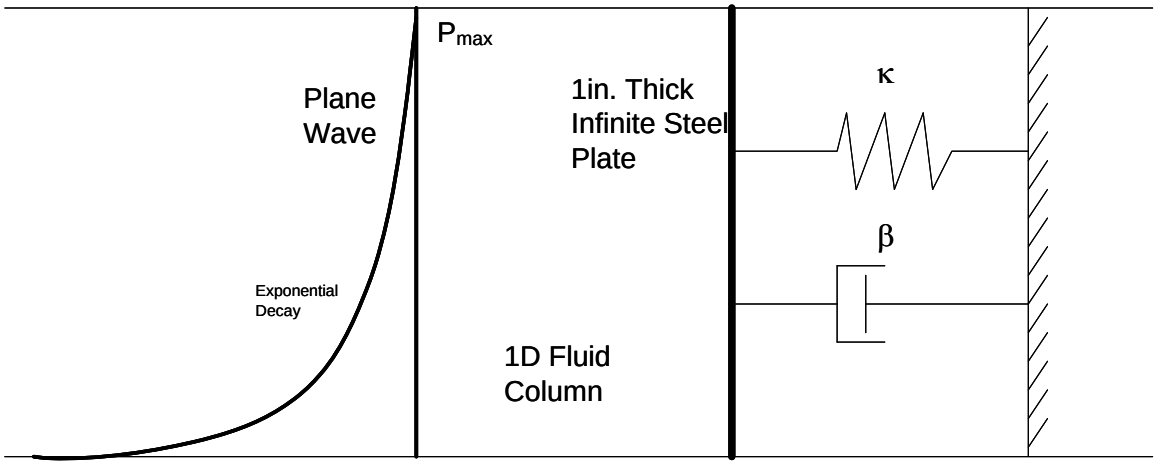

Figure 98 - Illustration of 1-D Plate Problem

4.1.1 Description

The 1-D Plate problem is the interaction of a plane wave, propagating from an initial disturbance, with an infinite plate supported by a spring-damper system. The 1-D plate problem in this thesis is based on the G.I. Taylor analysis of an infinite plate supported by a spring-damper system [40]. For this test case the magnitude of the 1-D Plane wave (P_{max}) is 47.5E+06 Pa. and a 1 inch thick steel plate is used.

4.1.2 Problem Setup in LSDYNA

The 1-D Plate problem fluid is modeled using LS-DYNA 1 point ALE single material element type with a Null Material and the Gruneisen equation of state. The unconstrained infinite steel plate is modeled using Belytschko-Tsay shell elements and the isotropic and kinematic hardening plasticity material model. Table 18 below gives the constants for the Gruneisen equation of state. Table 19 gives the constants used for the *MAT_PLASTIC_KINEMATIC card. Figure 99

and Figure 100 show the FEA model setup of the 5 x 0.5 x 0.5 meter horizontal fluid mesh with an element size equal to 0.1m and the 1 inch thick steel plate used for this problem. The Steel Plate is located at x = 2.5 meters of fluid mesh. Appendix APPENDIX E shows the LS-DYNA input file for this case.

Table 18 Constant Parameters for Seawater

Parameter	*Value*	*Units*
Water Type	Sea	--
Water Density	1025	kg/m^3
Speed of Sound in Water	1480	m/s
Dynamic Viscosity Coefficient	1.13E-03	Ns/m^2
Intercept of vs-vp Curve	2417	m/s
Gruneisen Coefficient S1	1.41	--
Gruneisen Coefficient S2	0	--
Gruneisen Coefficient S3	0	--
Water Temperature	20	Degrees Celsius
Gruneisen Gamma	1	--
First Order Volume Correction to Gamma	0	--
Internal Energy of Water per Reference Specific Volume	0	J/m^3
Relative Volume at Time 0 to Reference Specific Volume	1	--

Table 19 Constants for Steel Plate

Parameter	*Value*	*Units*
Plate Type	Steel	--
Plate Density	7780	kg/m^3
Young's Modulus	2.06E+11	Pa
Poisson's Ratio	0.281	
Yield Stress	3.55E+08	Pa
Tangent Modulus	0.0	Pa
Hardening parameter	0.0	--
Cowper Symonds strain rate parameter, C	0	--
Cowper Symonds strain rate parameter, P	0	
Failure Strain	0	--
Plate thickness	0.0254	m

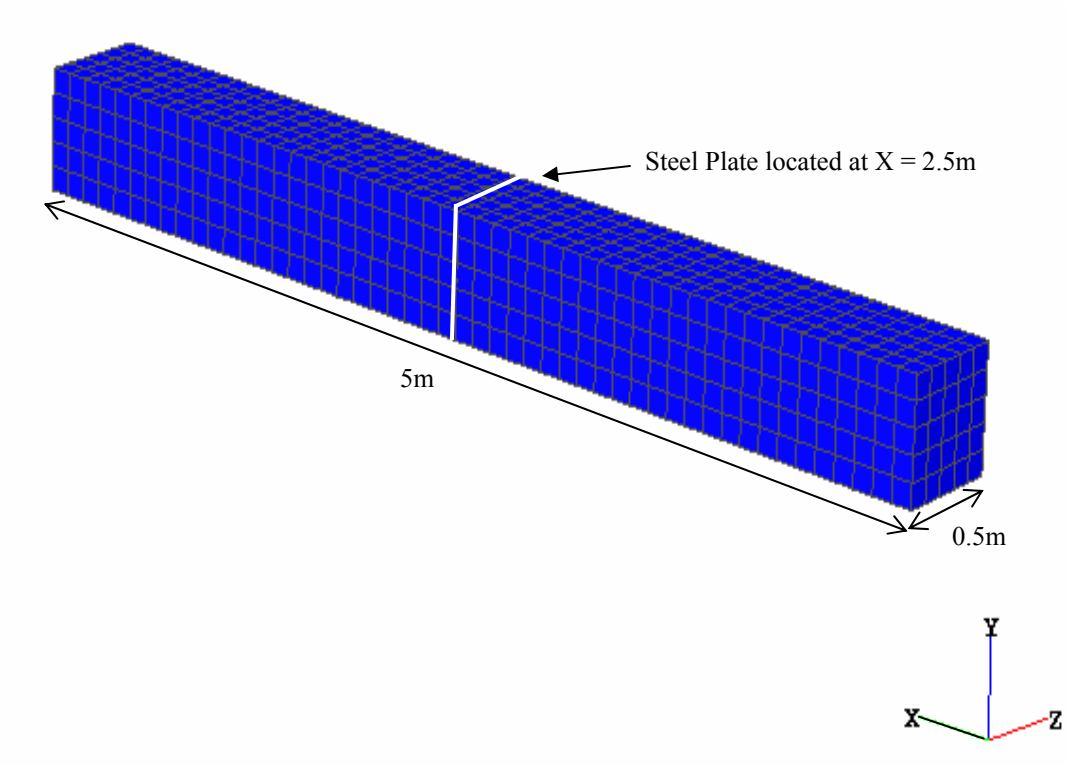

Figure 99 - 1-D Plate Problem FEA Fluid Model Setup

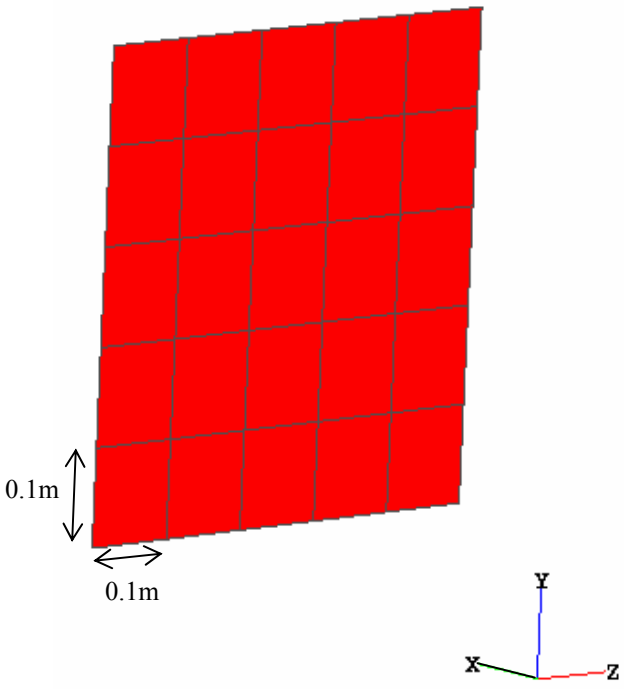

Figure 100 - 1-D Plate Problem FEA Steel Plate Model Setup

The fluid has translational constraints in the y and z directions and is constrained against rotation in all directions. The fluid is given an initial hydrostatic pressure of 0 Pa. and the Euler Boundary Condition (Section 2.1.3.9) is applied to the fluid boundaries. A Non-Reflecting Boundary Condition (Section 2.1.3.9) is applied to the x = 5m fluid boundary. The plane wave is applied to the x = 0m boundary of the fluid. The plane wave is defined by the load curve (Appendix APPENDIX E) and is applied to the boundary by the *LOAD_SEGMENT_SET card. The load curve is used to initialize the fluid as well as in the transient analysis.

4.1.3 Results

The results of the 1-D Plate problem are shown below. The x-displacement of the steel plate is used for comparison. Figure 101 shows the x-displacement of the steel plate versus the analytical solution for the entire run-time of 0.1sec. (Appendix APPENDIX F). Figure 102 shows a detail plot of the x-displacement of the steel plate versus the analytical solution from time t = 0 sec. to a point in time just after the plane wave impacts the steel plate. From Figure 102 the FEA plate maximum x-displacement is 0.00645m and occurs at 0.00133sec. The analytical solution maximum x-displacement is 0.00644m and occurs at 0.00198sec. Figure 103 shows the pressure-time history at a point 0.5m in front of the steel plate compared to the analytic pressure solution ($P_T(t)$ in Appendix F). Figure 103 shows the peak pressure of the plane wave before it impacts the steel plate and shows the peak pressure of the reflected wave for both cases. The 1-D FE Analysis result shows cavitation region collapse and subsequent reloading of the steel plate. The cavitation region is the section of the curve just after the reflected wave peak and before the reloading pressure peak. This is a region of the curve that has zero pressure. LS-DYNA calculates cavitation pressure by defining a cut-off pressure, -1.0E-20 Pa. in this case, and does not calculate negative pressures smaller than the cut-off pressure. Any cavitation will show up as a negative pressure in the pressure-time history curve.

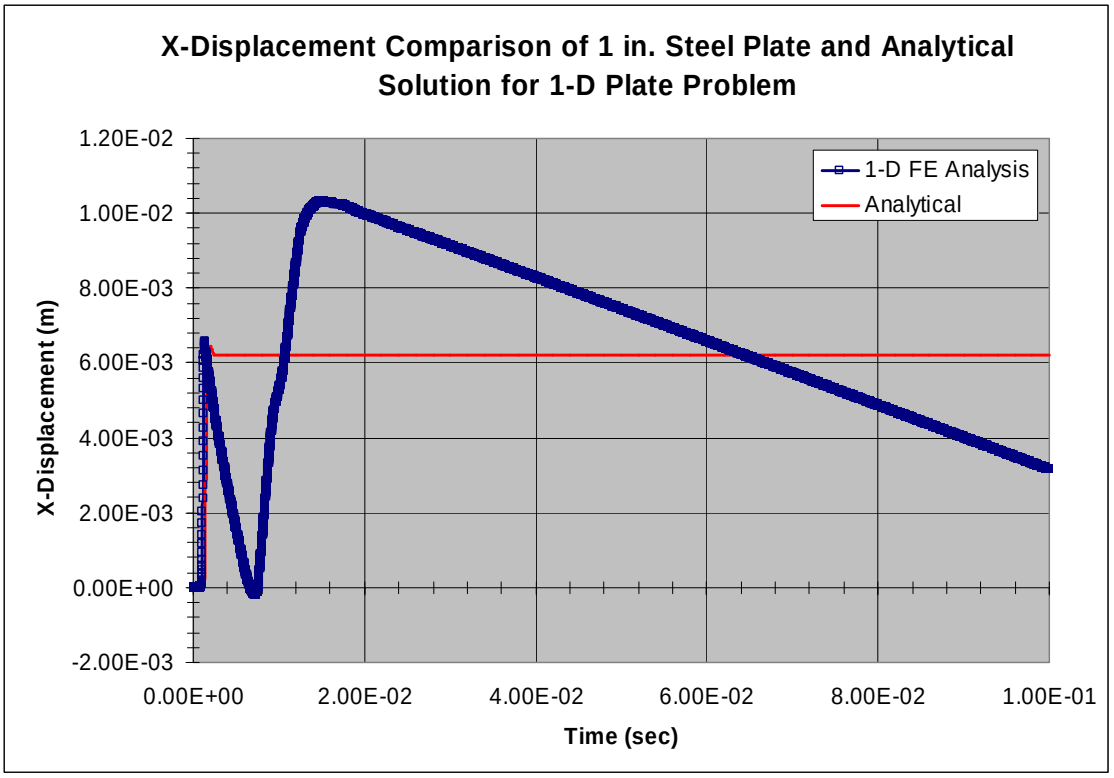

Figure 101 - X-Displacement of 1 in. Steel Plate and Analytical Solution for 1-D Plate Problem

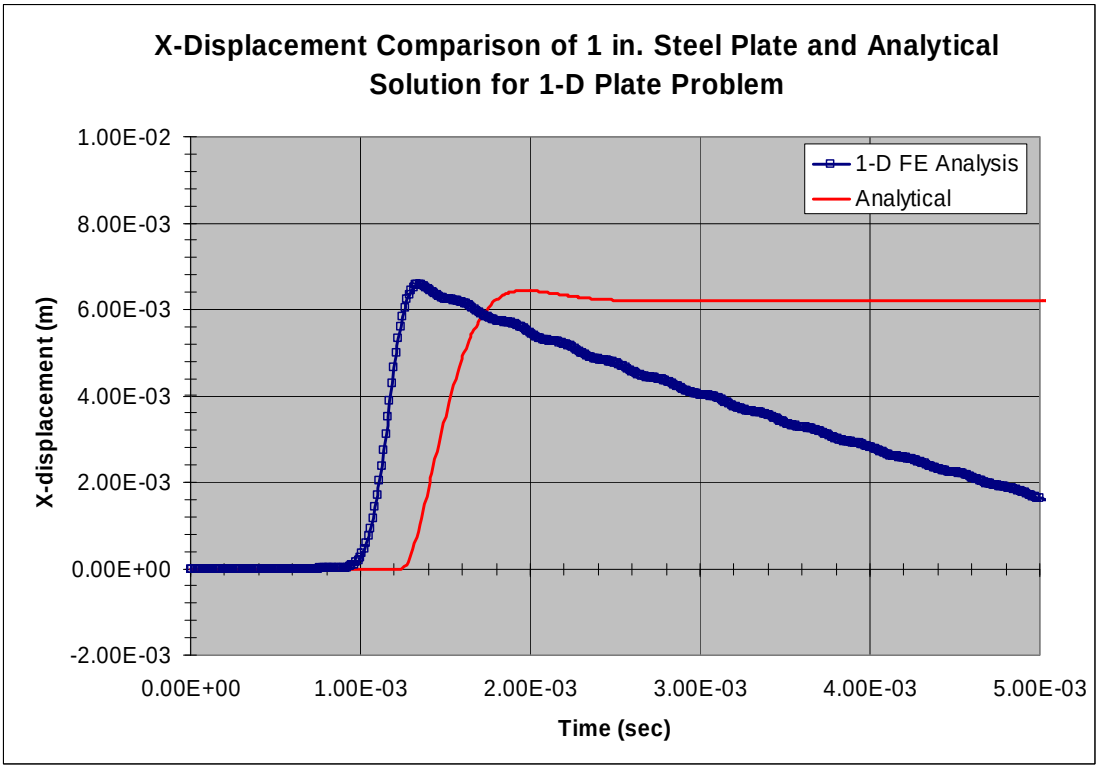

Figure 102 - Close-up of X-Displacement of 1 in. Steel Plate and Analytical Solution for 1-D Plate Problem at Time of Plane Wave Impact

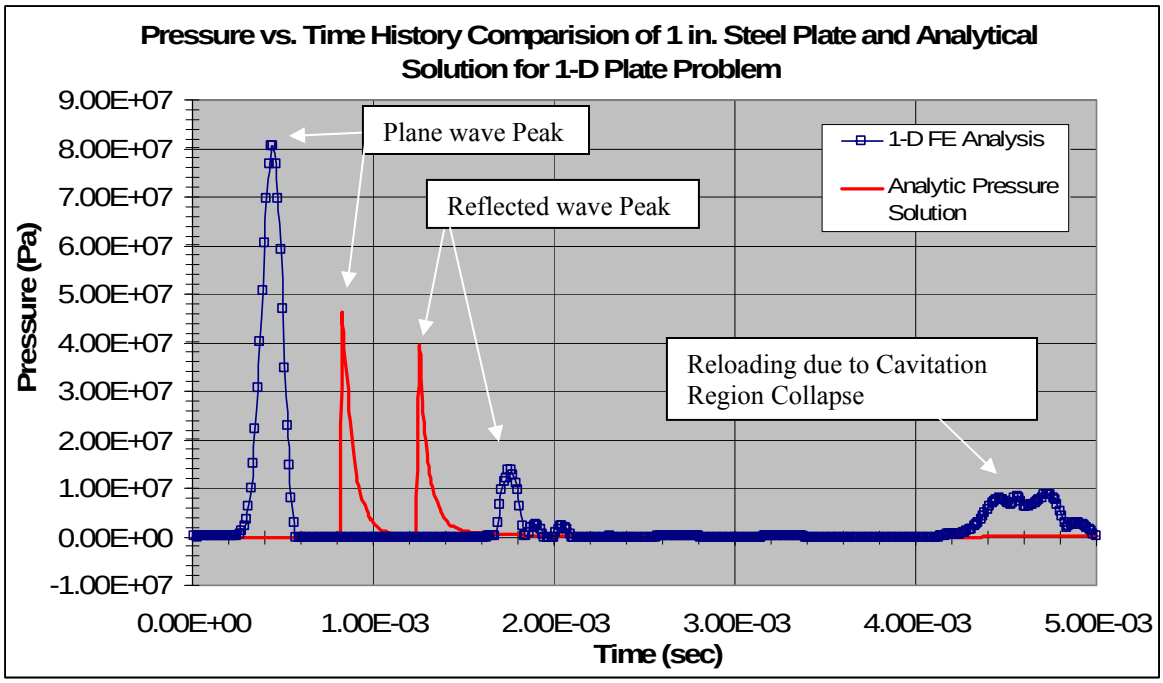

Figure 103 - Pressure Comparison of Analytic Solution and FE Analysis in Front of Steel Plate.

4.1.4 Discussion

The results shown in Section 4.1.3 show there is are differences between the analytical and FEA solution. There is a 0.155% difference between the maximum x-displacement and a 32.8% difference between the time the maximums occur. The percent difference in the time of occurrence seems large however the difference is on the order of 0.1 milliseconds. Figure 102 shows the plate rebounding from the displaced location and oscillating about its initial position. The analytical solution shows the plate rebounding about 1mm and maintaining its displaced location. This is due to the analytical solution not accounting for cavitation in the fluid. In the FE analysis, when the pressure wave reflects off the plate and travels back through the fluid it creates tension in the fluid. A region of cavitation forms near the plate. The overall density of the cavitation region is less than the density of the fluid region on the other side of the plate. This causes a pressure difference around the plate. The pressure is lower in the less dense cavitation region and higher in the fluid region. The plate is "pushed" back in the direction of its initial position until the cavitation region collapses, fluid rushes into the collapsed cavitation region, reloading the plate and essentially "pushing" the plate in the opposite direction. Oscillation about zero displacement continues until pressure equilibrium is restored around the plate. The analytical solution does not account for the effect of the cavitation region in front of the plate. Appendix APPENDIX F shows plots of the plane wave interacting with the plate and

the reflected wave shows there is no cavitation region. The cavitation region would be shown in the plots by the pressure behind the peak dropping below zero. The indicates that capturing the cavitation region and the spatial distribution of cavitation is important in both the numerical and analytical solutions.

4.2 US Navy Blast Test Study – Circular Steel Plate

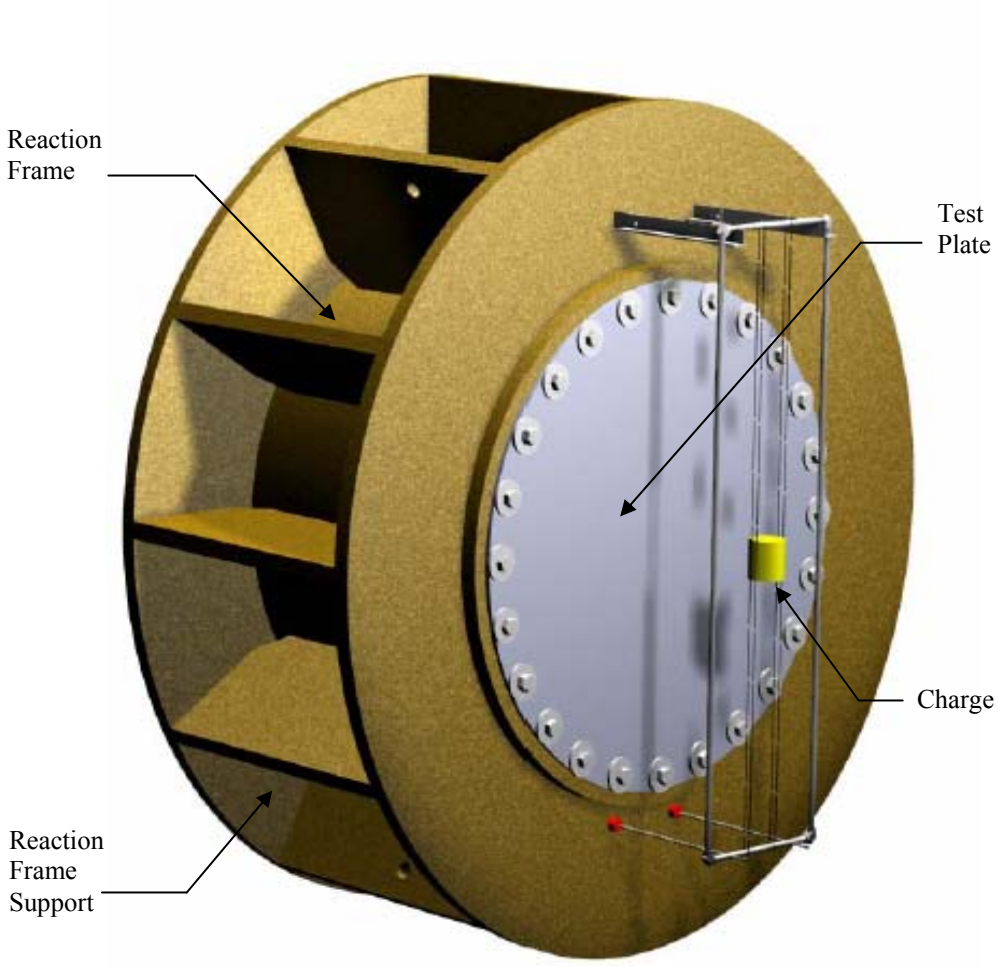

Figure 104 - U.S. Navy Blast Test Configuration [28]

4.2.1 Description

A simulation of a U.S. Navy Blast Test conducted on a ½ in. thick air-backed circular steel plate was performed using LS-DYNA. The Navy test was performed to compare the behavior of an equivalent weight steel plate to Intelligent Engineering's Sandwich Panel System (SPS) plate under similar blast loads. In the Navy blast test the test plate is bolted to a reaction frame and submerged just below the water surface. Figure 104 illustrates the blast test configuration.

4.2.2 Problem Setup in LSDYNA

The U.S. Navy blast test on the air-backed steel plate is modeled in LSDYNA using the same modeling and setup technique discussed in Section 3.2.2.3.5. The fluid model uses the 1pt.

MMALE formulation (Section 2.1.3.6). The seawater properties are simulated using material type 11, null material, with the Gruneisen equation of state and new coefficients discussed in Section 3.2.2.2.1. Table 21 shows data for the seawater. Air properties are simulated using the null material with a linear polynomial equation of state. The steel plate is modeled using Belytschko-Tsay shell elements and the material properties are described with a piecewise linear elasto-plastic material (material type 24) that incorporates an arbitrary stress strain curve and failure based on plastic strain. Table 22 shows the input data for the steel plate and the steel plate measurements are given in Table 19. Sections 4.2.2.1 through 4.2.2.3 describe the charge, steel plate/reaction frame, and fluid setup in more detail. Figure 105 illustrates the FE model setup for the steel plate and reaction frame. Appendix APPENDIX G shows the LS-DYNA keyword file for U.S. Navy Blast Test on a circular steel plate.

4.2.2.1 Cylindrical Shape TNT Charge

A cylindrical shape charge weighing 3 lbs. is placed 9 in. away from the center of the plate. The charge weight and stand-off distance are estimated based on comparing the scale of the the plate, charge, and stand-off distance in Figure 104 to the actual plate size. The cylindrical shape charge of TNT is simulated in LS-DYNA using the *INITIAL_VOLUME_FRACTION_GEOMETRY card (Section 2.1.3.10). Table 20 shows the TNT parameters used.

Table 20 Parameters for US Navy Blast Test Cylindrical Shape TNT Charge

Parameter	*Value*	*Units*
Charge Type	TNT	--
Charge Density	1630	kg/m^3
Charge Weight	3	lbs
Charge Mass	1.36	kg
Charge Depth	2	m
Charge Detonation Velocity	6930	m/s
Chapman-Jouguet Pressure	2.10E+10	N/m^2
Jones-Wilkens-Lee Coefficient A	3.71E+11	N/m^2
Jones-Wilkens-Lee Coefficient B	3.21E+09	N/m^2
Jones-Wilkens-Lee Coefficient R1	4.15	--
Jones-Wilkens-Lee Coefficient R2	0.95	--
Jones-Wilkens-Lee Coefficient Omega	0.3	--
Internal Energy of Explosive per Reference Specific Volume	6.99E+09	J/m^3
Charge Volume	0.000835	m^3
Charge Length	0.0762	m
Charge Radius	0.0596	m
Stand-off Distance	0.2286	m

4.2.2.2 Reaction Frame/Steel Plate Structure

In the model, the reaction frame supports, illustrated in Figure 104, are smeared into the thickness of the front and back face. The smearing is done by calculating the volume of each support and dividing the total support volume evenly between the front and back face plate. The length and width dimensions of the reaction frame face plates is held constant. This method is acceptable since the response of the reaction frame is of no interest in this thesis.

The steel plate and the reaction frame are modeled as two separate parts as shown in Figure 105. Appendix APPENDIX I-I.3 shows the Truegrid modeling commands used to create the steel plate and reaction frame mesh. The steel plate element size used in this analysis is selected so that maximum resolution of stress effects can be captured with minimul computational expense. The reaction frame mesh is developed from the steel plate mesh so there is one to one nodal alignment.

In order to simulate the steel plate model and the reaction frame model interaction, so that it closely represents the real life physical interaction, it is necessary to account for the region where

the steel plate is bolted to the reaction frame. Modeling the detailed bolted region is to complex. A simple way to simulate the bolted region that connects the steel plate and the reaction frame is to make sure that the coincident nodes between the steel plate model and the reaction frame model are not merged together. This merging will not allow the plate and reaction frame to act independantly as it would if the plate and reaction frame nodes were coincident. Coincident nodes transfer the same information as merged nodes, only they allow for structures to act independently of one another. The simulated bolt connections between the nodes on the outer edge of the steel plate model and the coincident nodes in the reaction frame model is established using the *CONSTRAINED_TIE-BREAK card in LS-DYNA. This card defines an interface that ties the outer edge of the steel plate to the reaction frame, where the bolted connection is, and allows for failure based on an input plastic failure strain. The plastic failure strain value is set at 1.0E+20 microstrain to insure that the bolted region behaves properly.

The reaction frame/steel plate structure is coupled to the fluid using the *CONSTRAINED_LAGRANGE_IN_SOLID card, where the fluid is the master contact and the reaction frame/steel plate structure is the slave contact. Figure 106 shows a profile view of the explosive charge/fluid/structure model. The mesh lines have been removed for better viewing.

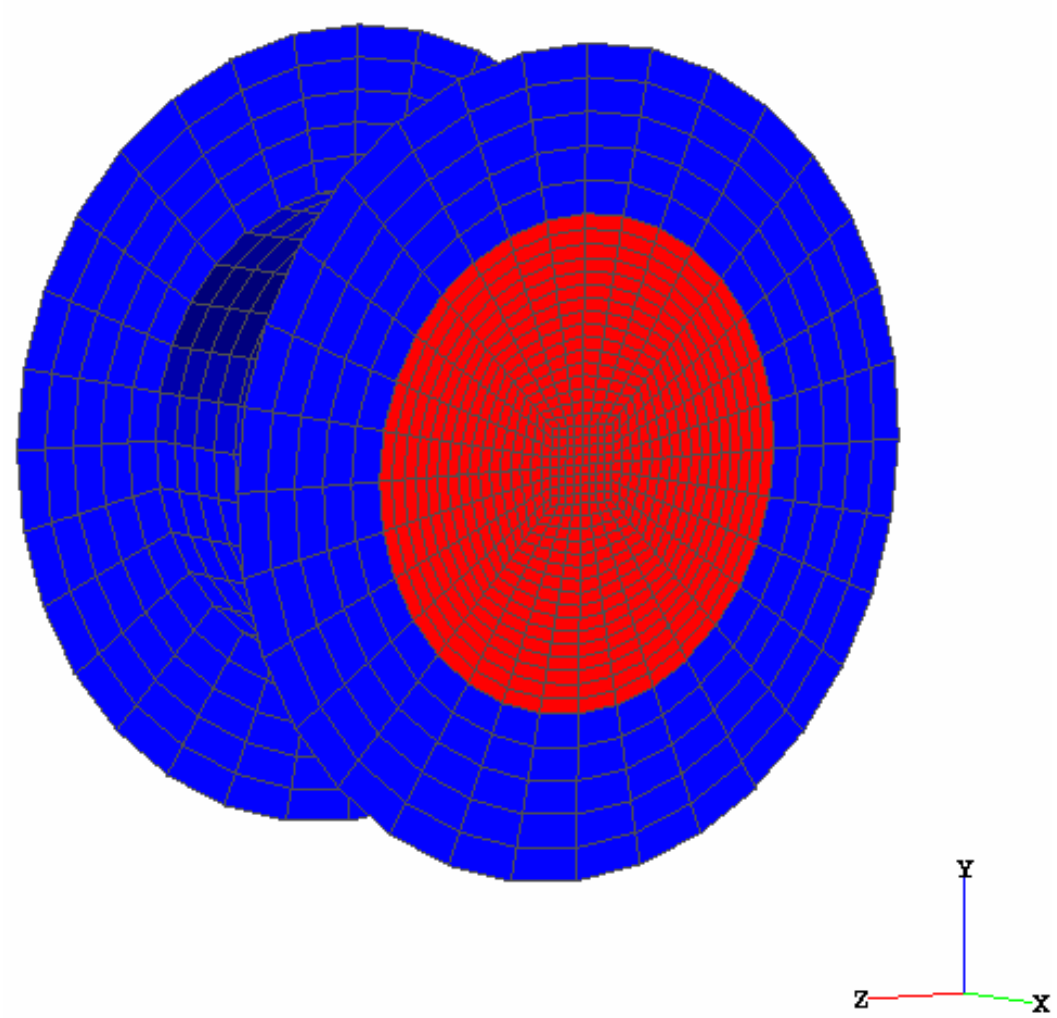

Figure 105 - FEA Model Setup for US Navy Blast Test Reaction Frame and Steel Plate

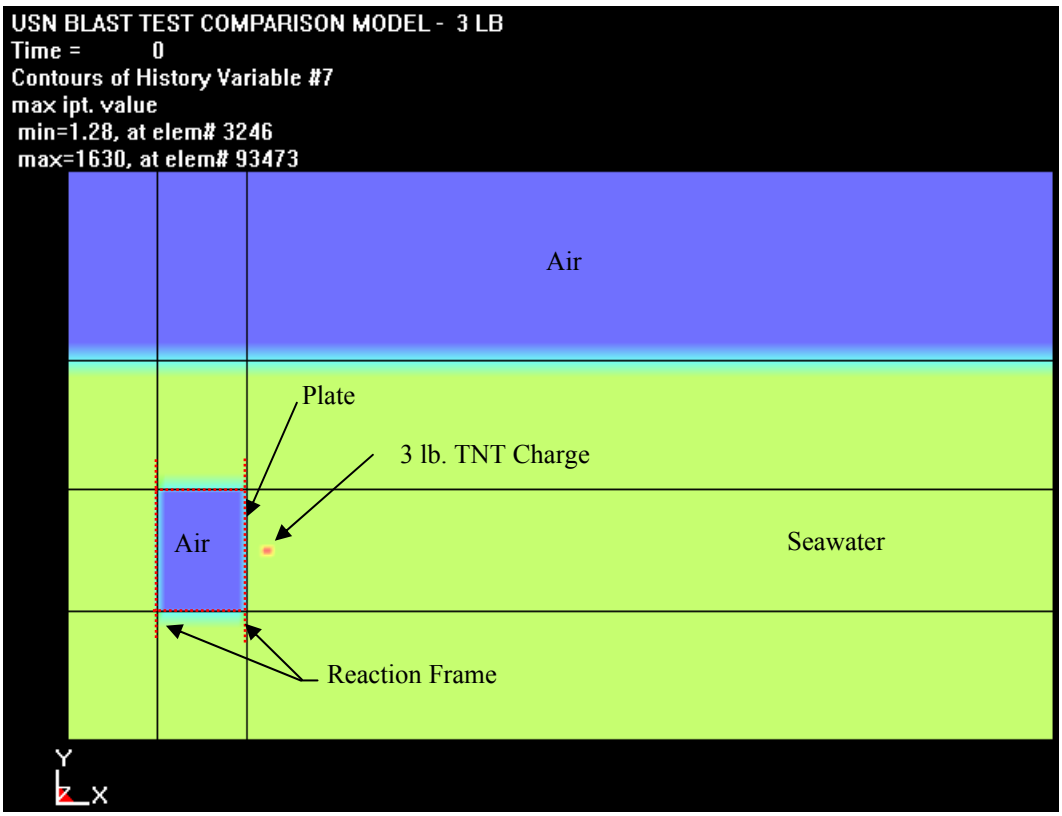

Figure 106 - US Navy Blast Test Study Steel Plate Case FEA Model with Mesh Lines Removed

Table 21 Constant Parameters for Seawater

Parameter	*Value*	*Units*
Water Type	Sea	--
Water Density	1025	kg/m^3
Speed of Sound in Water	1480	m/s
Dynamic Viscosity Coefficient	1.13E-03	Ns/m^2
Intercept of vs-vp Curve	2417	m/s
Gruneisen Coefficient S1	1.41	--
Gruneisen Coefficient S2	0	--
Gruneisen Coefficient S3	0	--
Water Temperature	20	Degrees Celsius
Gruneisen Gamma	1	--
First Order Volume Correction to Gamma	0	--
Internal Energy of Water per Reference Specific Volume	121435.5	J/m^3
Relative Volume at Time 0 to Reference Specific Volume	1	--

Table 22 Constants for US Navy Blast Test Steel Plate [28]

Parameter	*Value*	*Units*
Plate Type	Steel	--
Plate Density	7780	kg/m^3
Young's Modulus	2.06E+11	Pa
Poisson's Ratio	0.281	
Yield Stress	3.55E+08	Pa
Tangent Modulus	0.0	Pa
Hardening parameter	0.0	--
Cowper Symonds strain rate parameter, C	40.4	--
Cowper Symonds strain rate parameter, P	5.0	
Failure Strain	0.1	--
Plate thickness	0.0127	m
Plate Inner Diameter	1.0668	m
Plate Outer Diameter	1.2954	m

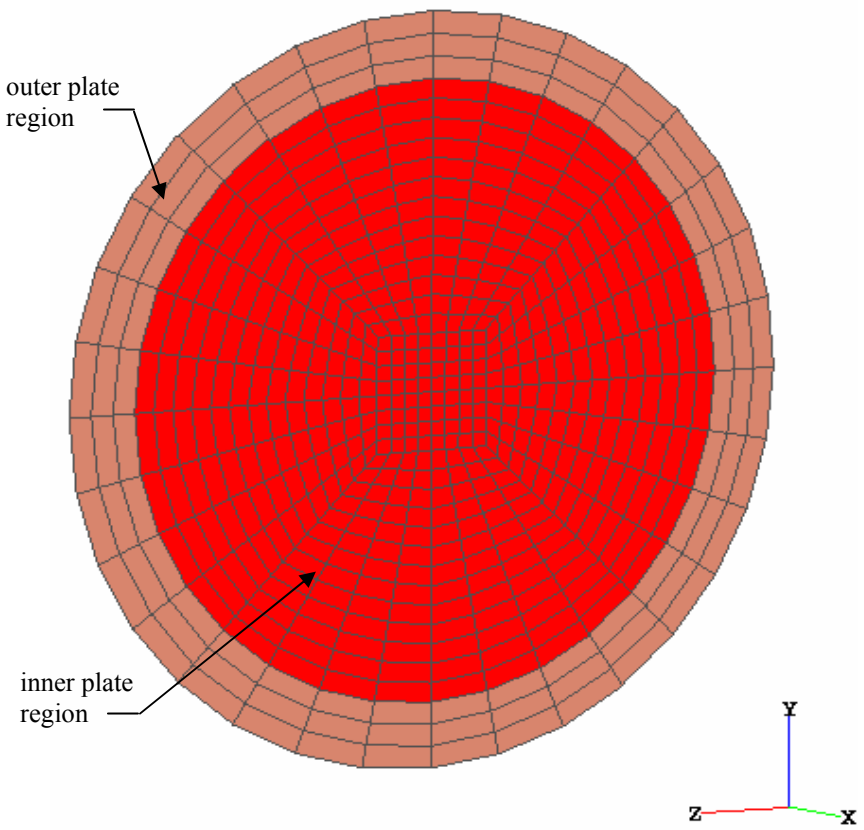

Figure 107 - Inner and Outer Region of US Navy Blast Test Steel Plate FEA Model

The steel plate is modeled in two sections, an inner section and an outer section. Figure 107 shows the two regions. The steel plate is divided into two separate regions to handle the tooling effect that occurs around the bolted region of the plate. The outer region is the portion where the steel plate extends over the reaction frame and is bolted to the reaction frame. The inner region is the air-backed portion of the steel plate.

Tooling is a term used to describe the physical phenomena that occurs when metals are stretched and shaped, "stamped", into a mold. A similar process occurs when the steel plate deforms and the bolted region of the plate stretches. The elongation of the bolted region is a strain. Material type 24 is not able to differentiate between shear strain and axial strains. A single failure strain value is defined, when the strain reaches this value the element is deleted. The value of the strain in the outer region can reach values higher than the defined failure strain value causing the elements in the outer region to be deleted. The connection between the steel plate and the reaction frame is lost and the plate behavior is no longer valid. The plate is modeled in two different region using the same material card for each, only defining a failure strain value for the inner region, and not defining a failure strain for the outer region. The outer bolted region is able to stretch without element deletion and the plate behaves properly. A failure strain value of 0.1 microstrain is used (See section 3.7.2 of Reference [29]). Figure 108 illustrates the strain differences in the inner and outer regions of the steel plate. The Fringe Levels in Figure 108 represent the range of effective plastic strain. Figure 108 shows that the outer region of the steel plate model has an effective plastic strain value higher than 0.1 and that the outer region strain values are on the order of 10 times greater than the rest of the plate.

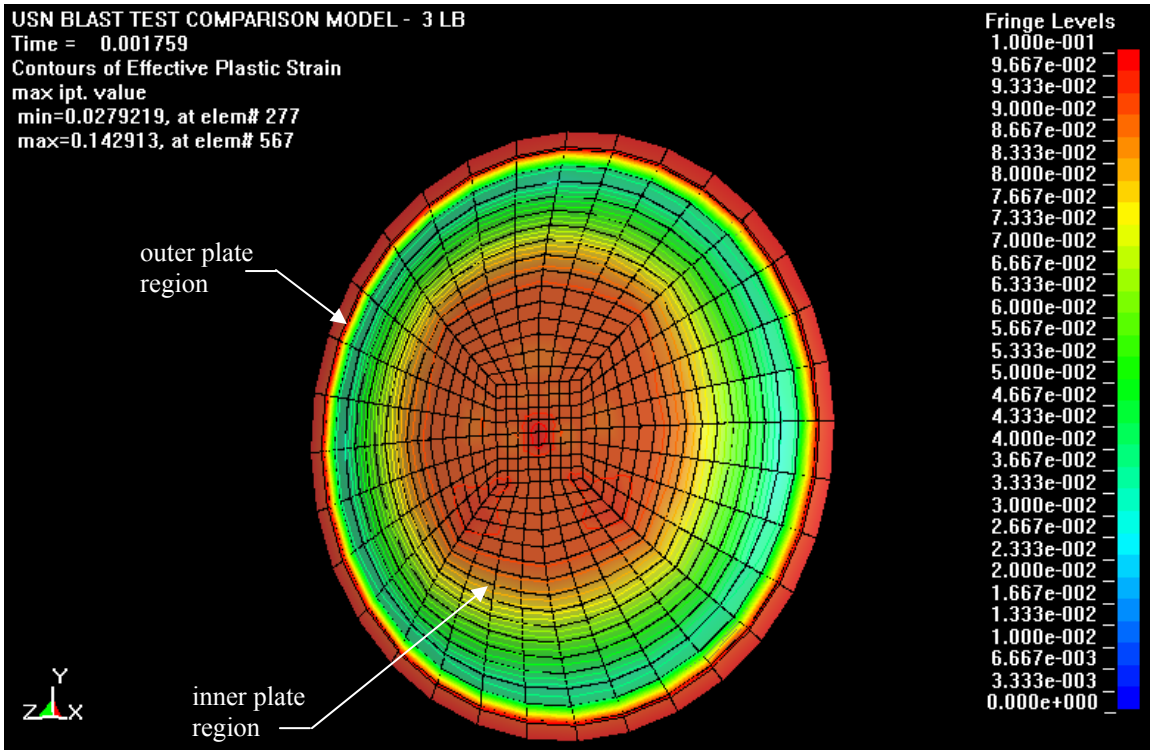

Figure 108 - Line Contours of Effective Failure Strain for Inner and Outer Region of Steel Plate

4.2.2.3 Fluid Model

The fluid model used for this analysis uses the same techniques that are used in Chapter 3. The fluid model is a cylindrical model that is developed so that the reaction frame, steel plate, and fluid meshes all have one to one nodal alignment. The steel plate mesh element size determines what the reaction frame and fluid mesh element sizes will be. The size of fluid mesh modeled is determined by the amount of fluid needed so that shock wave outer boundary reflections do not effect the plate response. This one to one nodal correlation method is used so that nodal force and energy data can be transmitted to the steel plate from the fluid accurately (See Section 3.2.2.3.4). Figure 109 and Figure 110 show an x-y plane slice view of the cylindrical mesh configuration. Figure 110 shows a close-up view of the fluid model around the reaction frame. Figure 111 shows an x-y plane slice view of the fluid mesh and the full reaction frame/steel plate structure model. Figure 111 also shows the reaction frame is not coincident with the fluid nodes, since the response of the reaction frame is of no interest in this paper. All fluid mesh nodes are unconstrained and all outer surfaces have Non-Reflecting Boundary Conditions (Section 2.1.3.9).

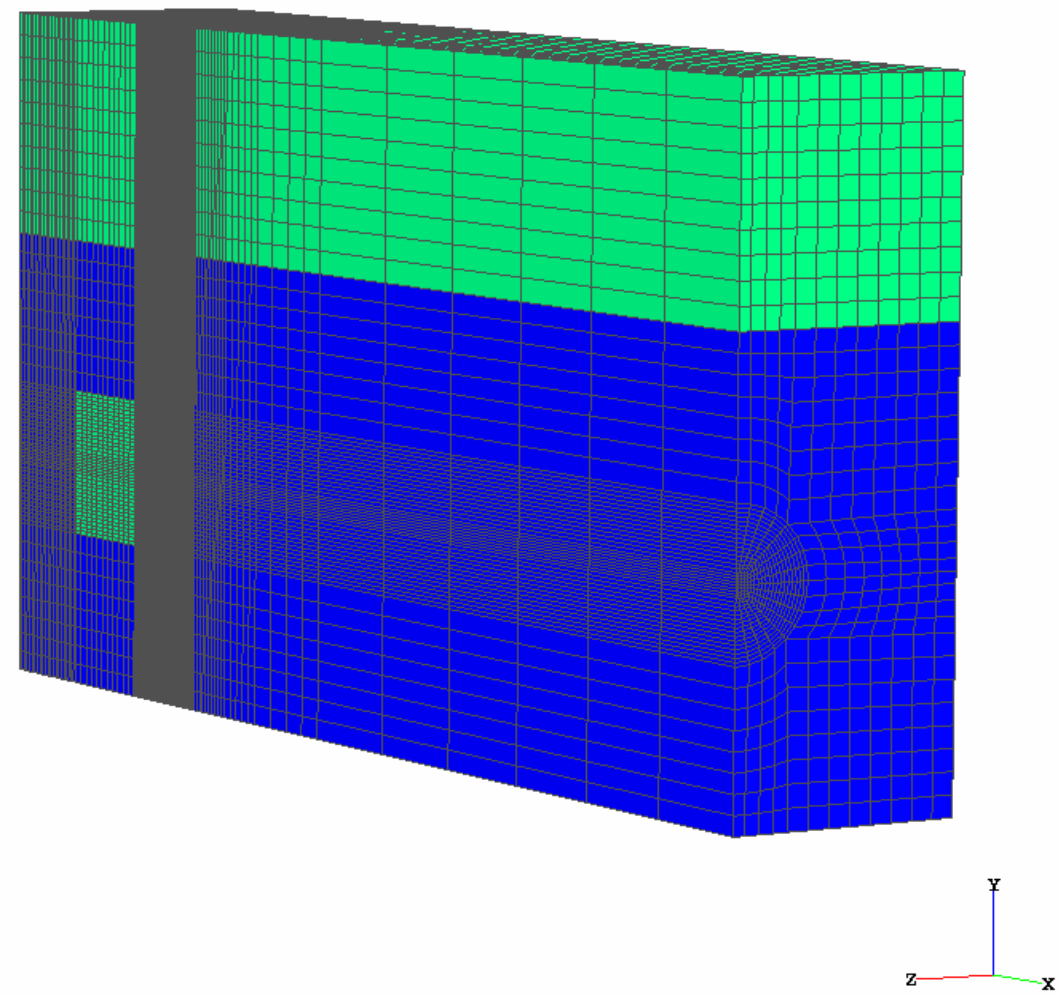

Figure 109 - X-Y Plane Slice View of FEA Cylindrical Fluid Mesh Model for US Navy Blast Test Study

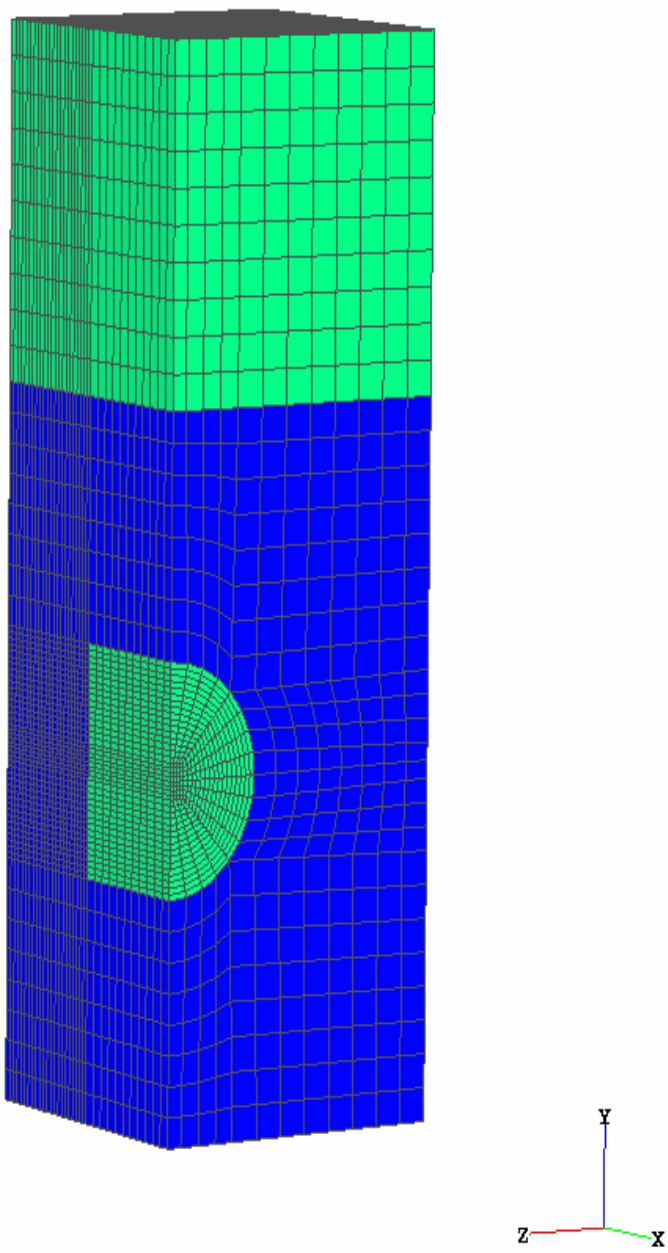

Figure 110 - Close-up View of X-Y Plane Slice of FEA Cylindrical Fluid Mesh Model for US Navy Blast Test Study

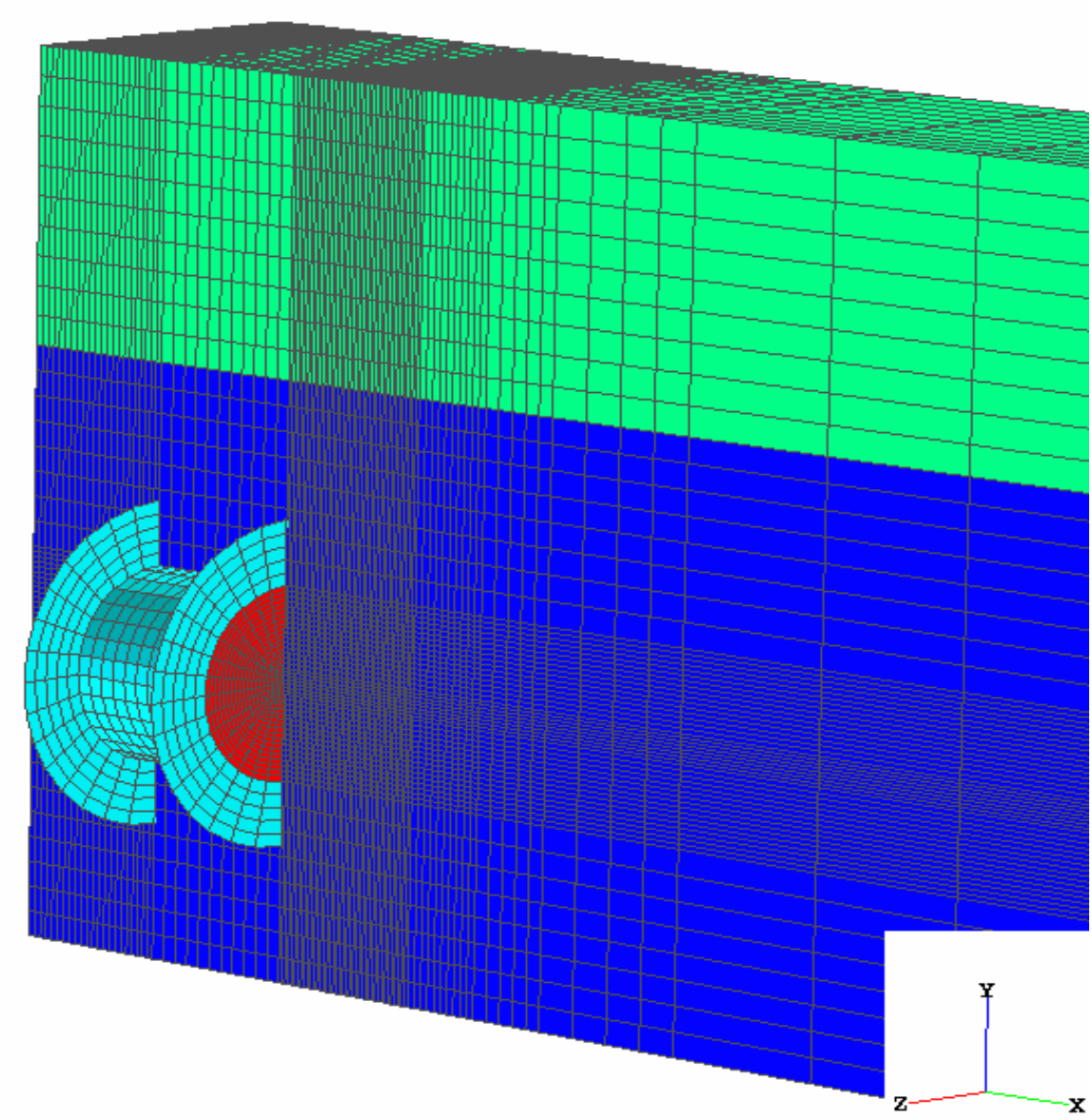

Figure 111 - Close-up View of Cylindrical FEA Model for US Navy Blast Test Steel Plate Case

4.2.3 Results

No test result data from the US Navy Blast Test was available. The termination time for this FEA test is 0.003 seconds. The actual computational time for the SPS plate test is approximately 2 hours 8 minutes on a Pentium III desktop PC, requiring 46.8 Mb. of memory for an explicit solution. The timestep size approximately ranges from 9.0E-07 to 1.0E-06 seconds. Rupture begins with the first shell element failure and subsequent deletion. The first shell element deletion occurs at 1.763E-03 seconds. Visual comparisons are made between the ruptured plate results pictured in Figure 113 and Figure 115. The results from the FEA simulation of the US Navy Blast Test Study are shown in Figure 112. This shows the rupture of the FE steel panel and the ensuing petaling of the plate.

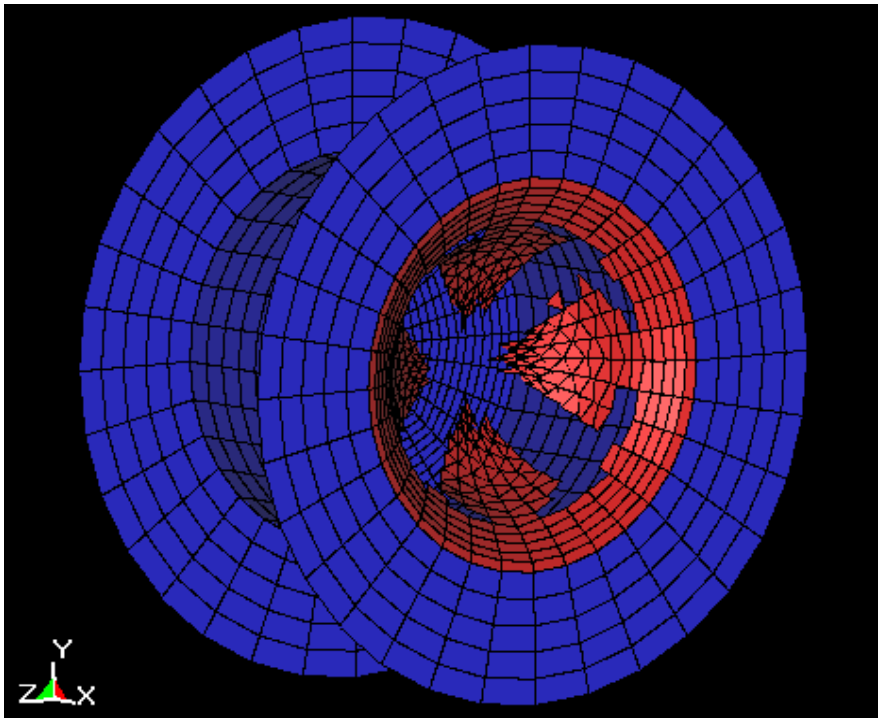

Figure 112 - FE Analysis of US Navy Blast Test Study Steel Plate Result

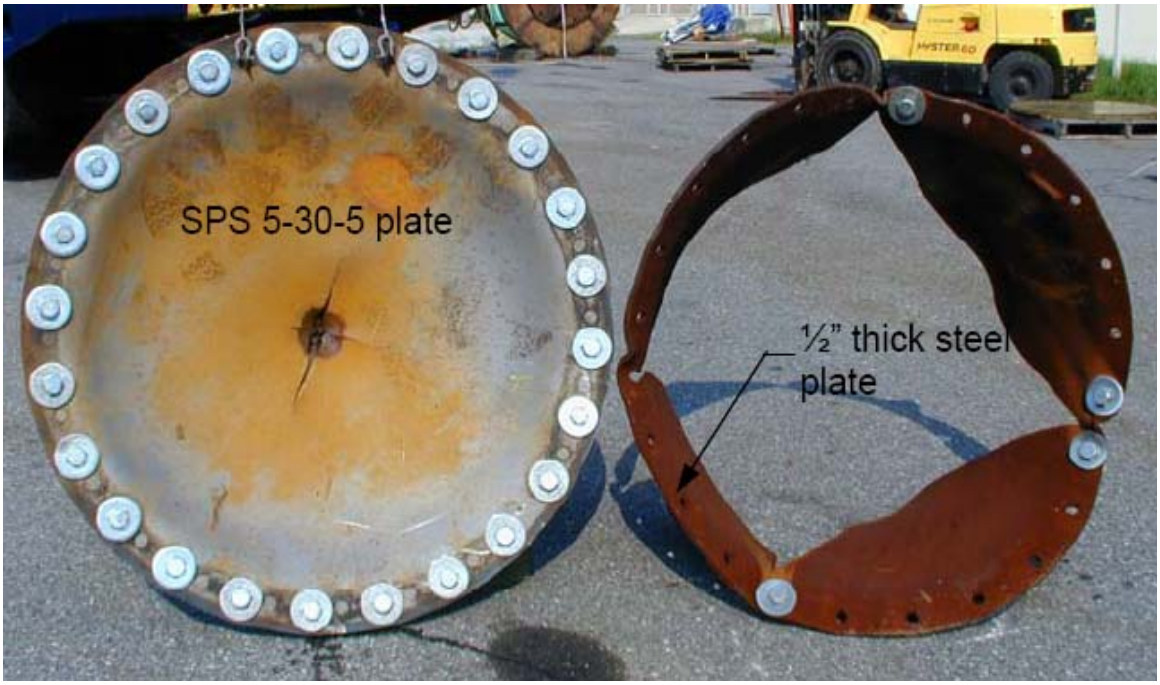

Figure 113 - US Navy Blast Test Results for Steel and SPS Plates [28]

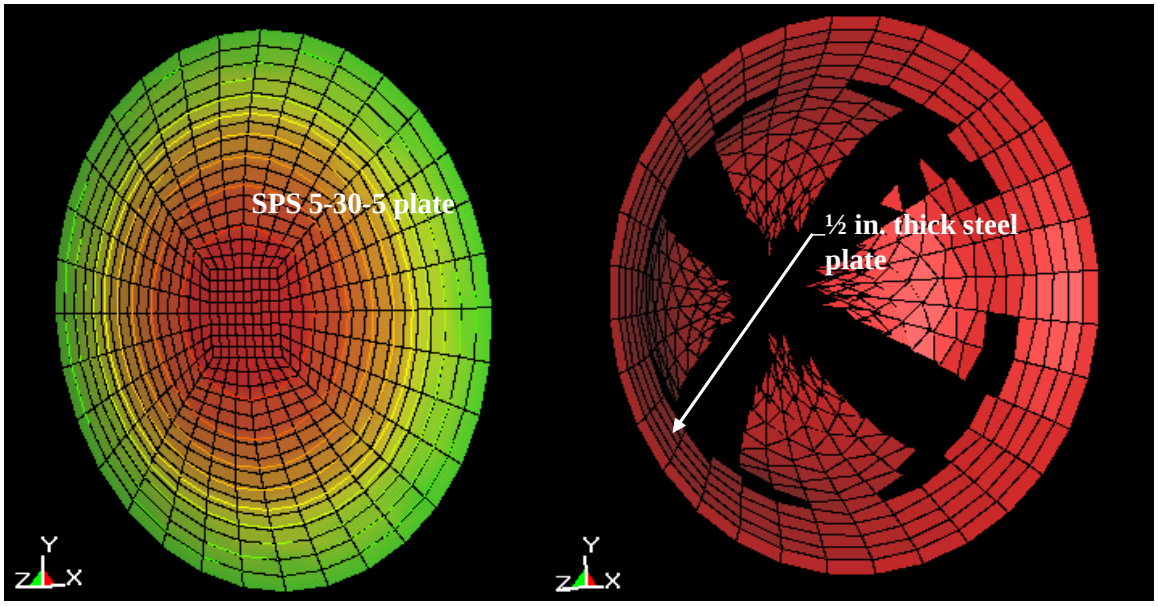

Figure 114 - FE Analysis Results of US Navy Blast Test Steel and SPS Plates

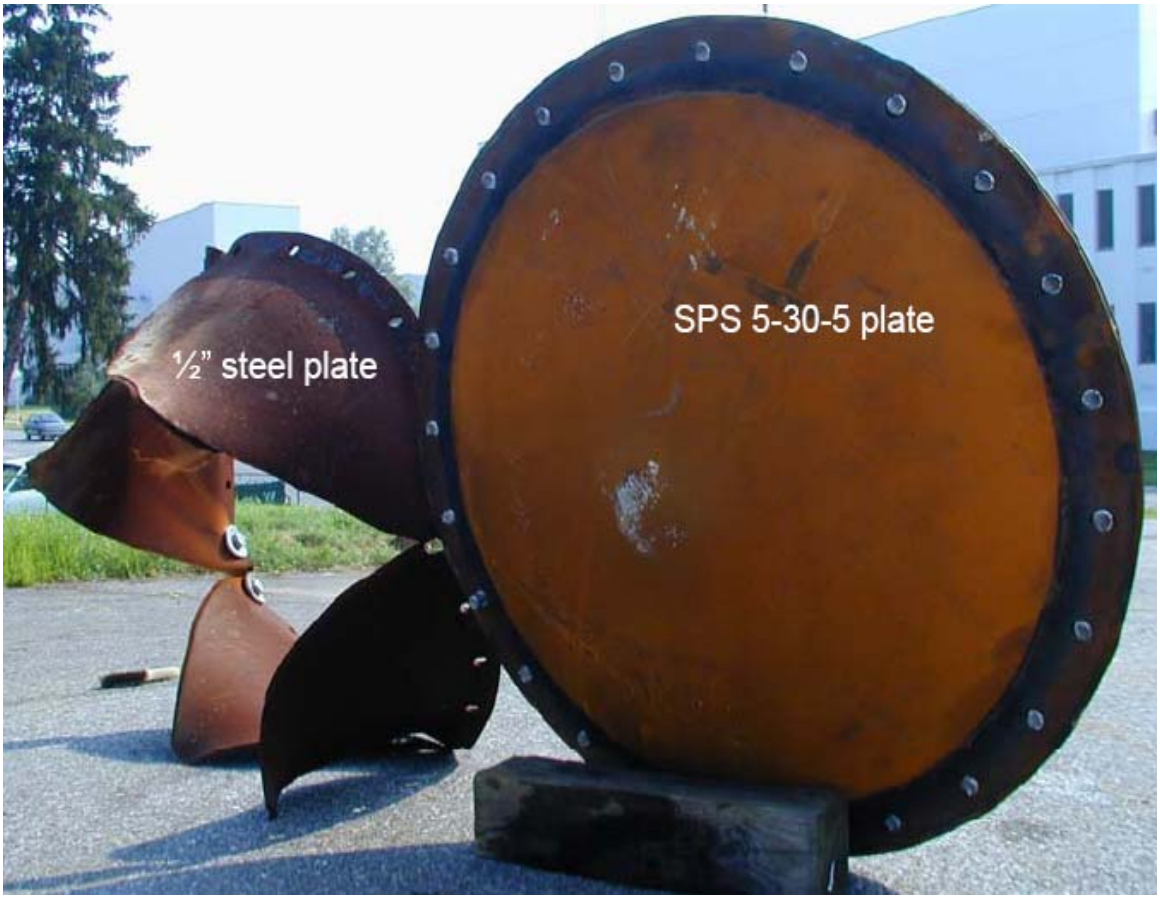

Figure 115 - US Navy Blast Test Results for Steel and SPS Plates [28]

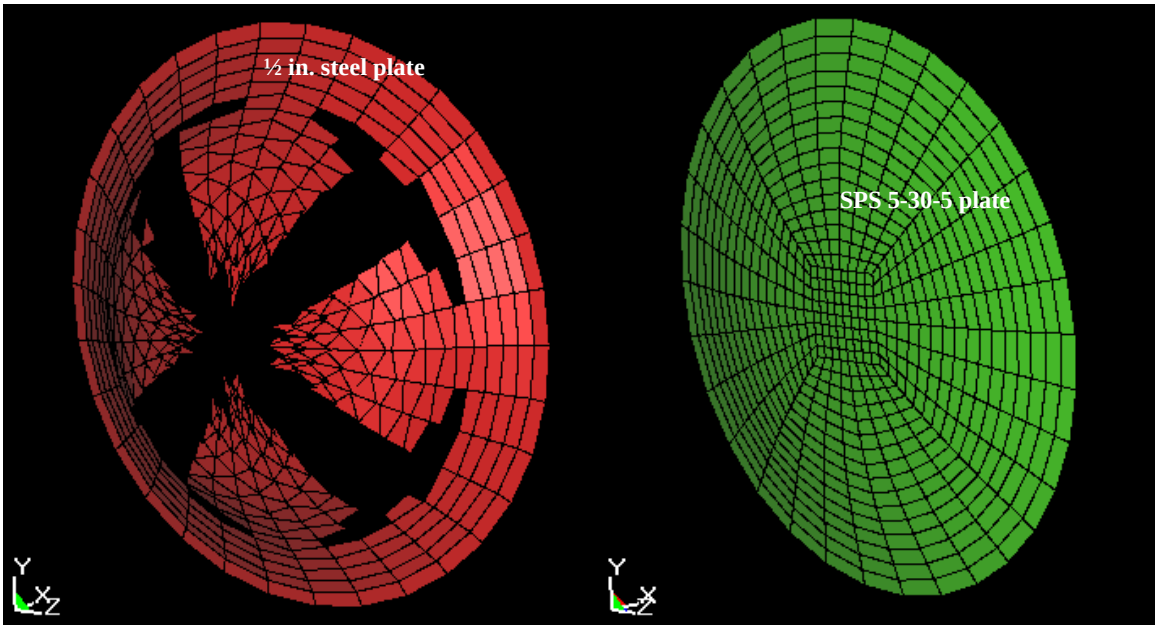

Figure 116 - FE Analysis Results of US Navy Blast Test Steel and SPS Plates

Figure 113 and Figure 114 show the comparison between the side of the plate facing the charge for the US Navy Blast Test Study steel plate result and the FE analysis steel plate result. Figure 115 and Figure 116 show comparison between the side of the plate facing away from the charge for the US Navy Blast Test Study steel plate and the FE analysis steel plate results. Figure 117 through Figure 124 show the complete fluid/structure interaction including the bubble growth and interaction with the steel structure. The fluid/structure interactions in Figure 117 through Figure 124 show density distributions at various times for the complete fluid/structure model.

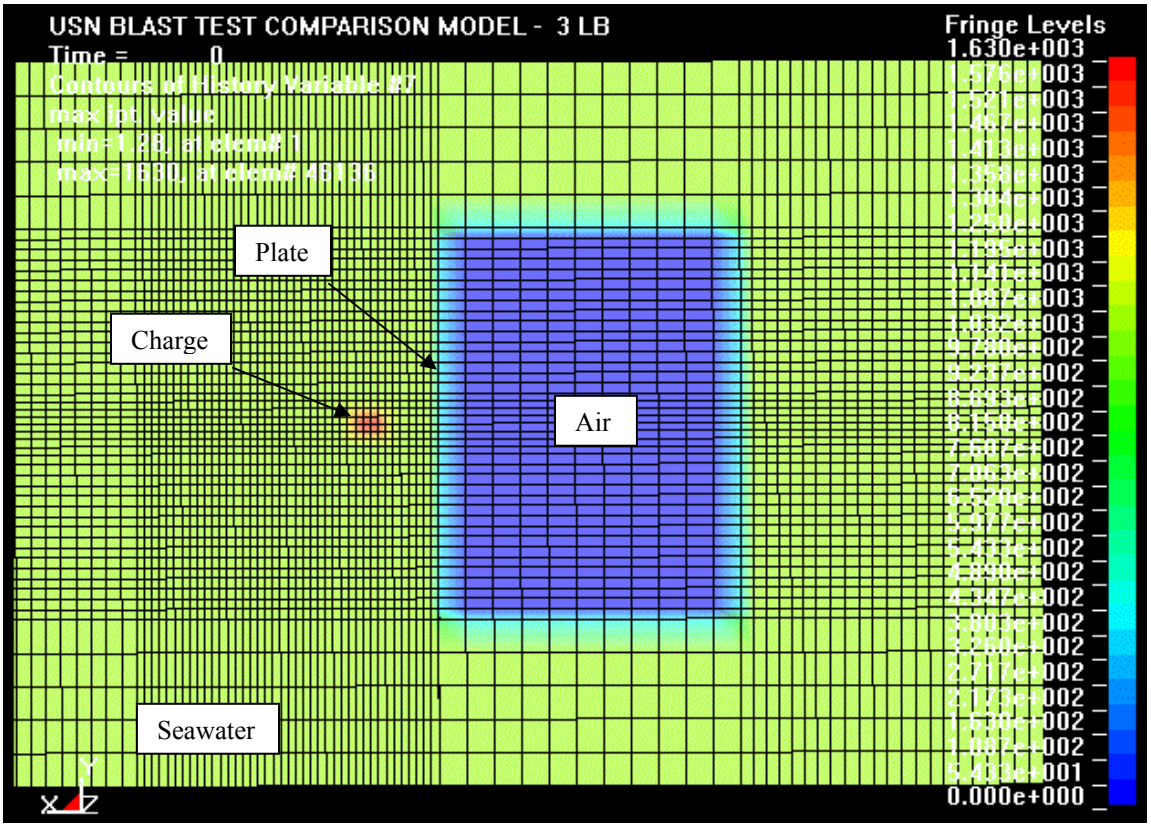

Figure 117 - US Navy Blast Test Study Steel Plate Case FEA Density at Time = 0 seconds.

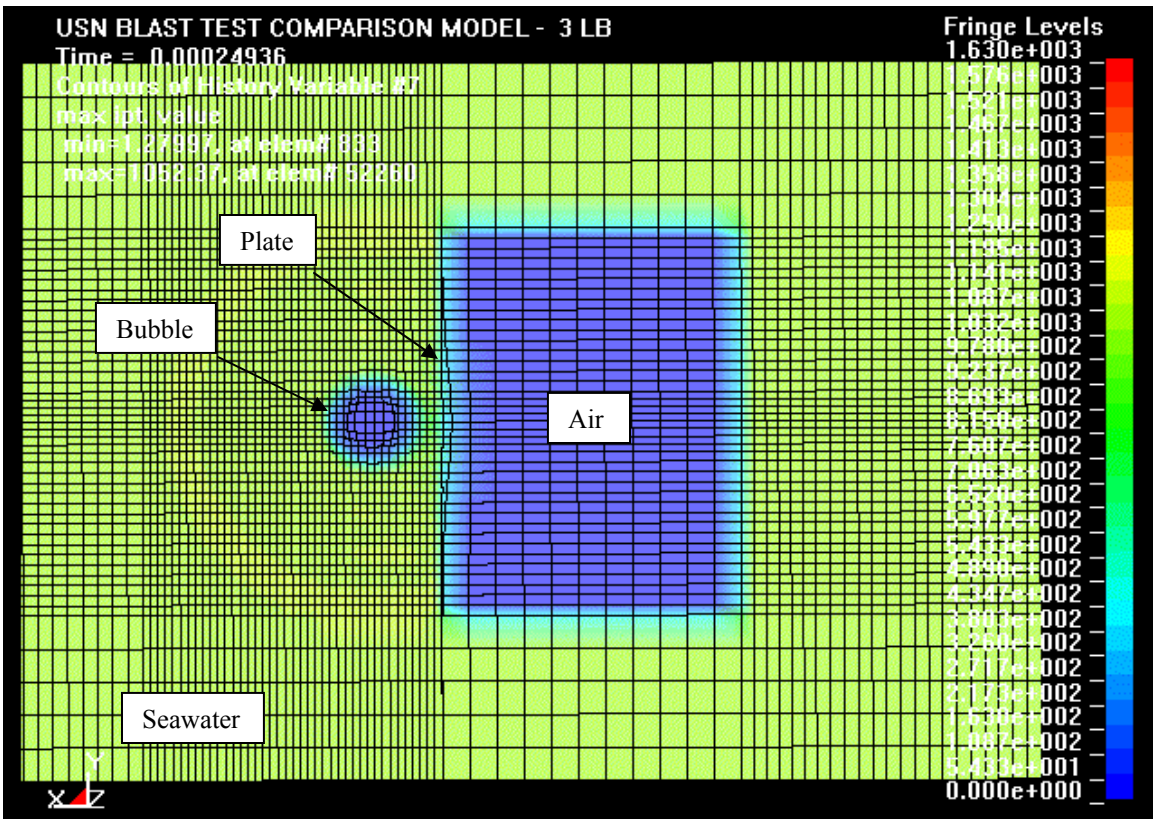

Figure 118 - US Navy Blast Test Study Steel Plate Case FEA Density at Time = 0.00025 seconds.

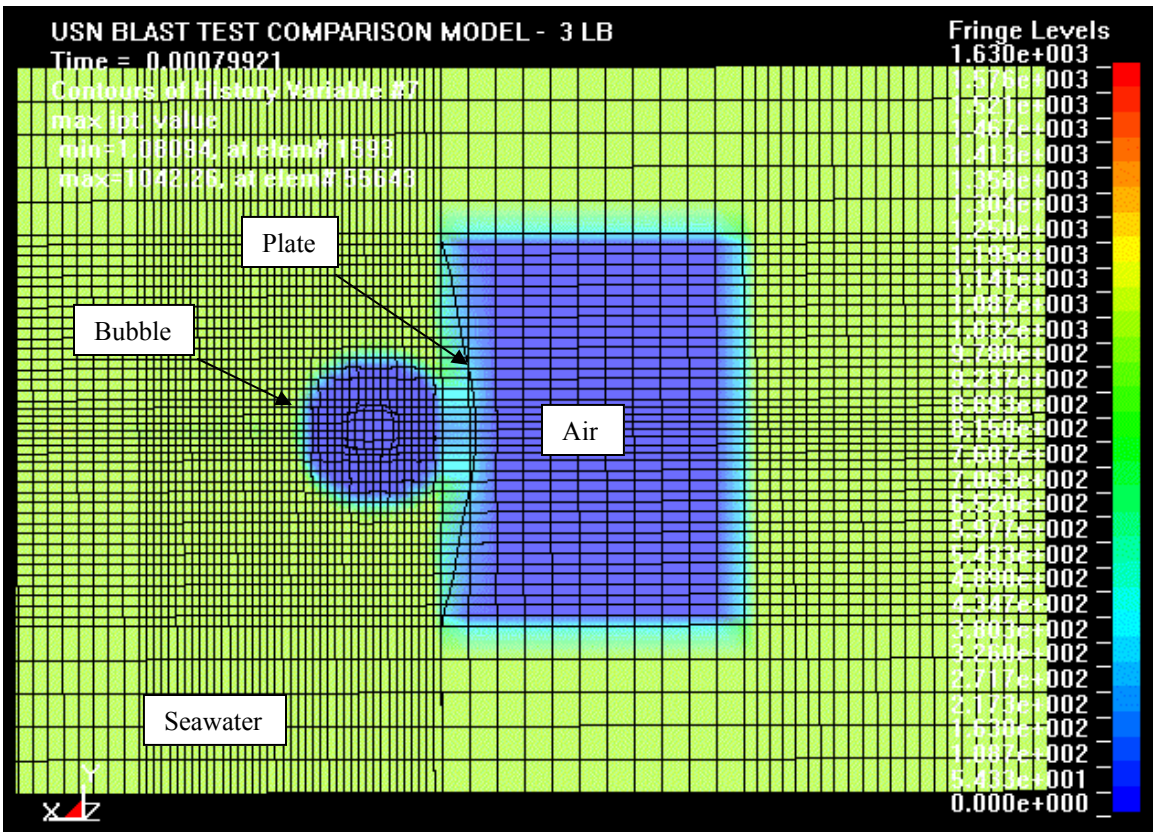

Figure 119 - US Navy Blast Test Study Steel Plate Case FEA Density at Time = 0.00079 seconds.

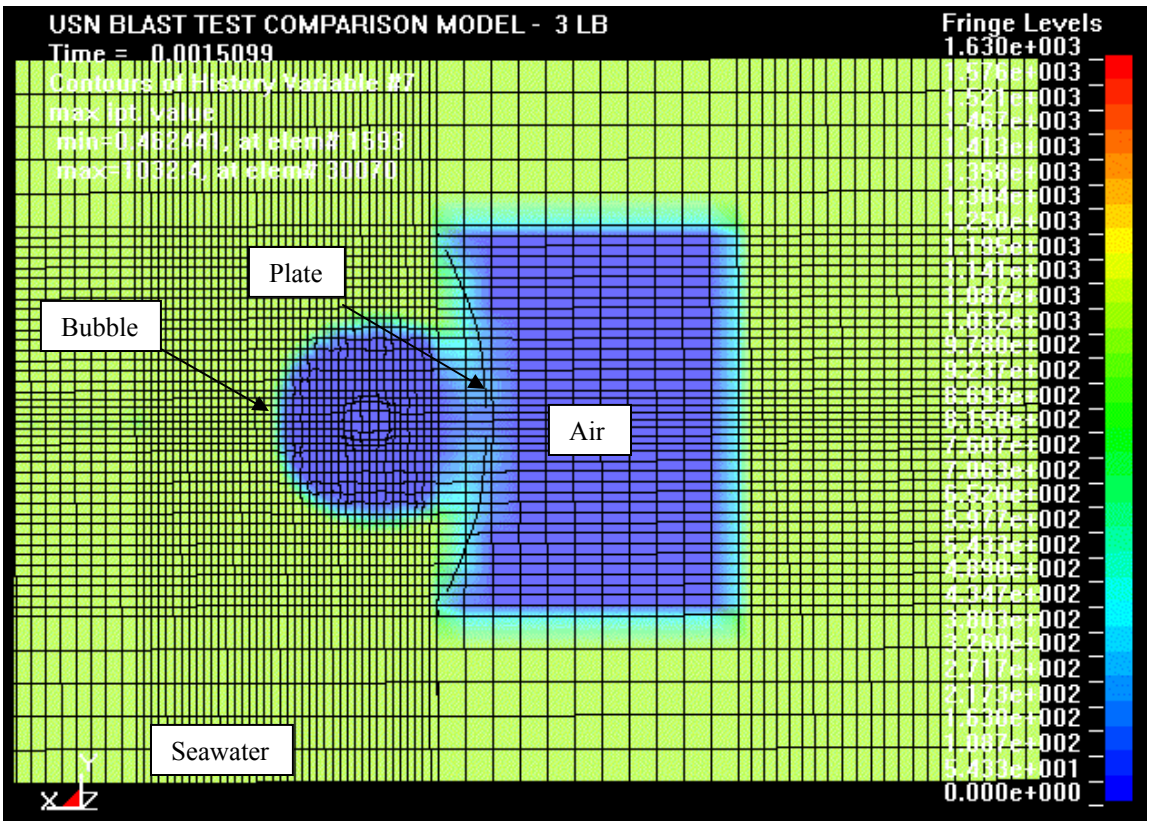

Figure 120 - US Navy Blast Test Study Steel Plate Case FEA Density at Time = 0.0015 seconds.

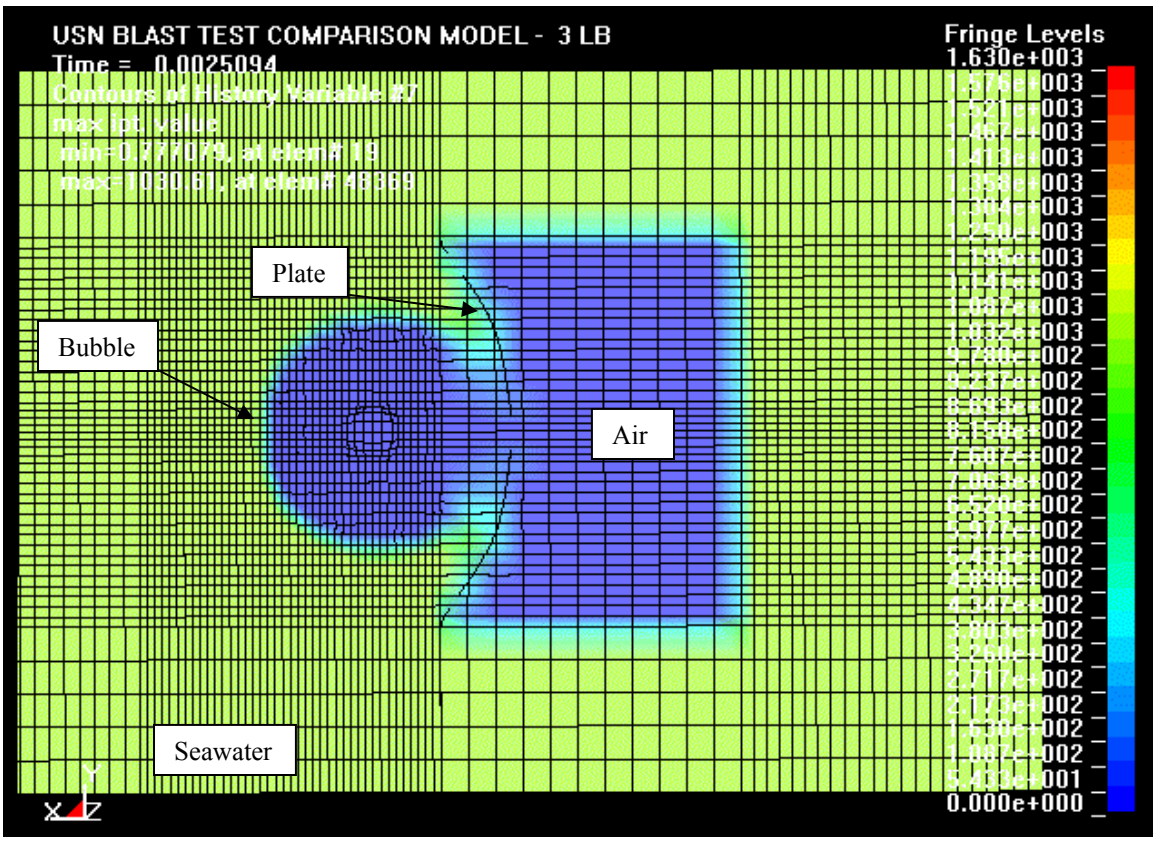

Figure 121 - US Navy Blast Test Study Steel Plate Case FEA Density at Time = 0.0025 seconds.

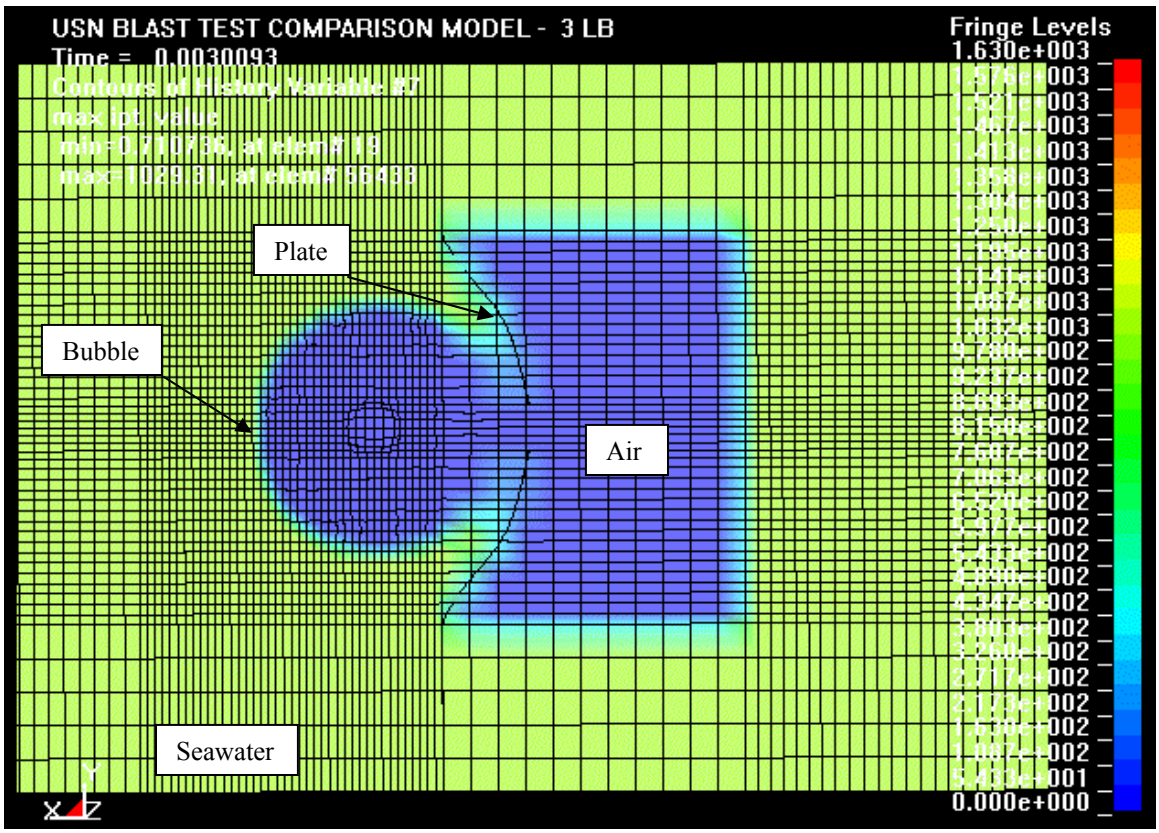

Figure 122 - US Navy Blast Test Study Steel Plate Case FEA Density at Time = 0.003 seconds.

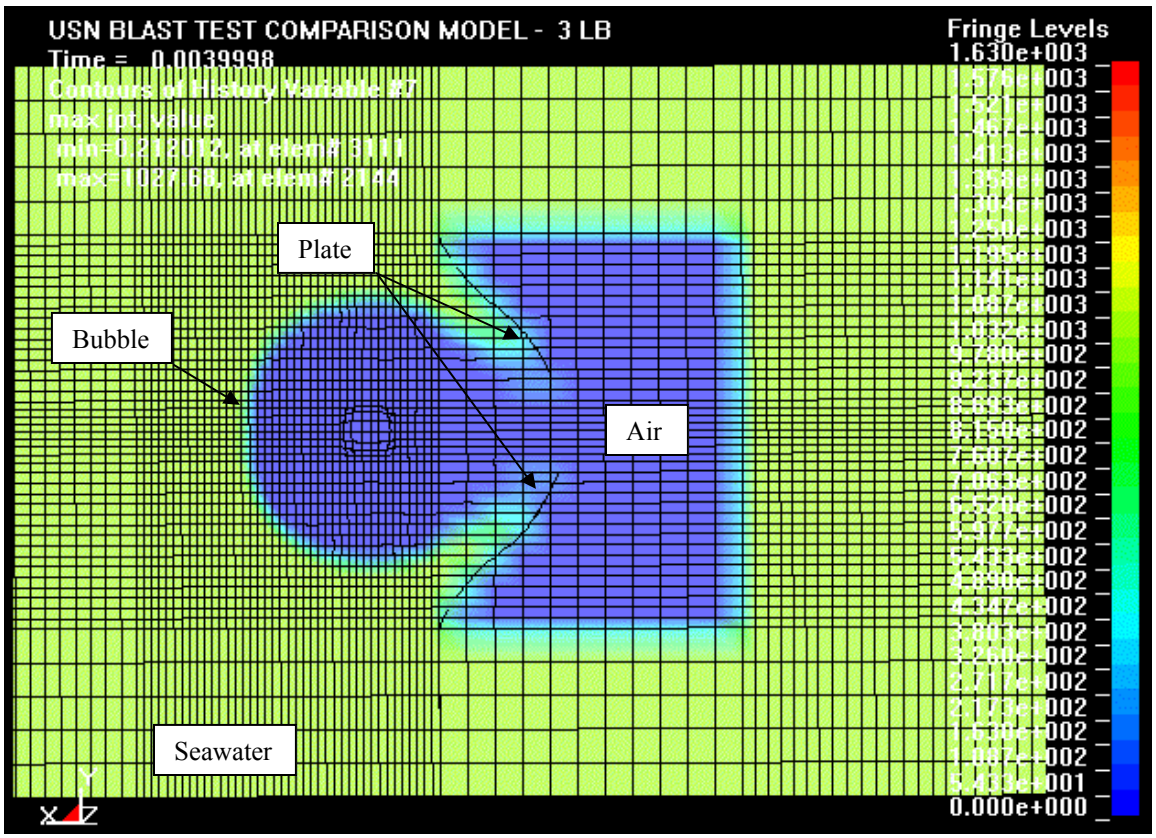

Figure 123 - US Navy Blast Test Study Steel Plate Case FEA Density at Time = 0.004 seconds.

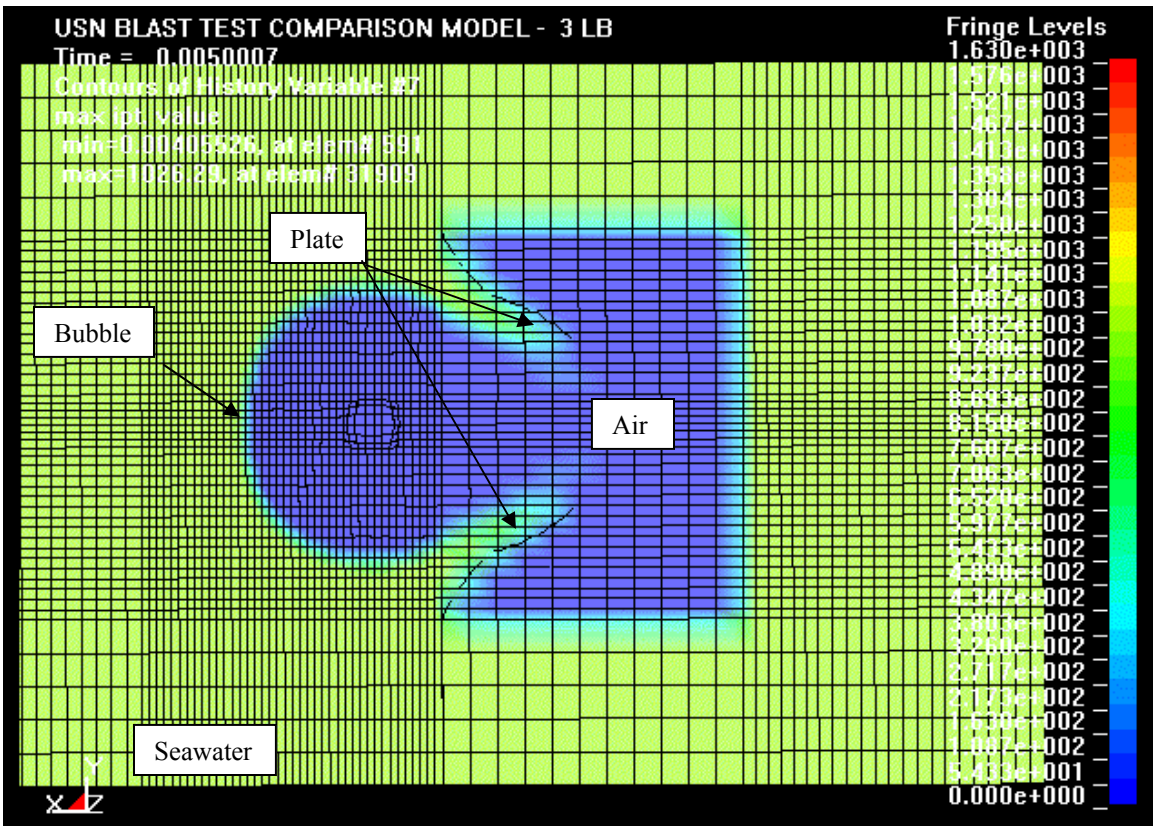

Figure 124 - US Navy Blast Test Study Steel Plate Case FEA Density at Time = 0.005 seconds.

4.2.4 Discussion

Comparison of the steel plate in Figure 113 with Figure 114 and Figure 115 with Figure 116 shows the FE analysis produces similar results. The petaling of the steel plate resembles that of the actual test. The accuracy of the plate response and behavior could be more precisely determined had more data about the test case been available. Figure 117 through Figure 124 shows the explosive bubble effects on the steel plate are being captured by the FE Analysis. Figure 121 shows the classic "mushroom" shape that the bubble forms when the bubble attaches to the plate. This shape occurs prior to plate rupture and is lost after plate rupture.

4.3 US Navy Blast Test Study – SPS Plate

4.3.1 Description

Intelligent Engineering developed and patented the Sandwich Plate System (SPS), which integrates a steel-elastomer-steel composite structural laminate in place of conventional stiffened steel plates. The US Navy conducted a blast test on an SPS 5-30-5 plate to determine the behavior of an SPS plate under blast load. Figure 104 shows the blast test configuration.

4.3.2 Problem Setup in LSDYNA

The U.S. Navy blast test simulation on the SPS plate is modeled in LSDYNA using the 1pt. MMALE formulation for the solid fluid elements. Figure 125 illustrates the FE model setup for the SPS plate and reaction frame. The fluid elements are a material type 11, null material, with the Gruneisen equation of state. Table 21 shows data for the fluid. The fluid setup and the explosive setup are the same as the cylindrical fluid mesh shown in Figure 109, Figure 110, and Figure 111 of the steel plate test. The SPS plate is modeled using shell elements and the *MAT_LAYERED_LINEAR_PLASTICITY card.

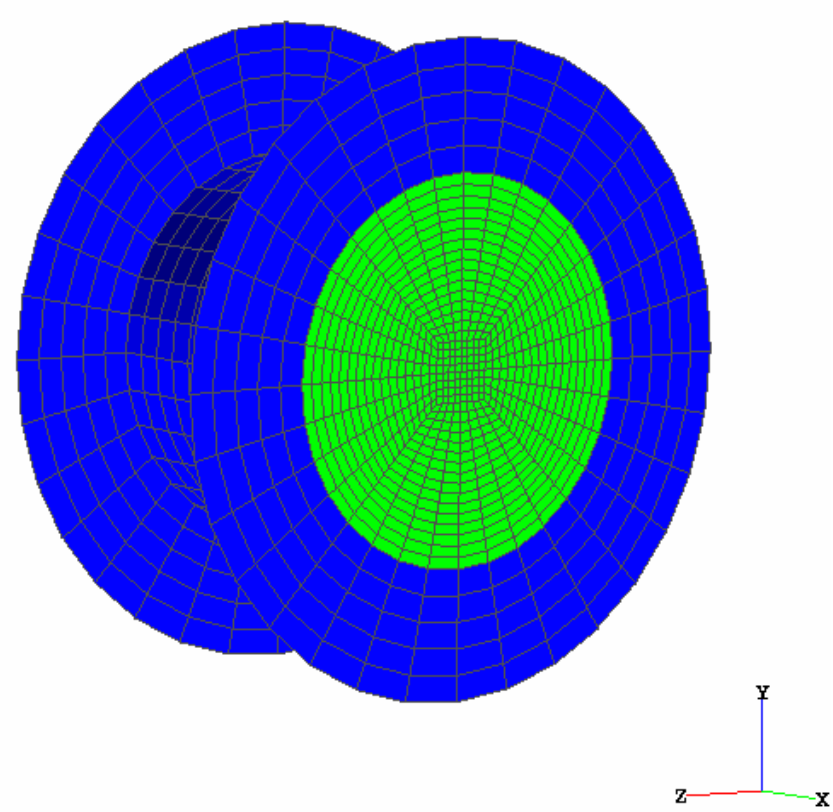

Figure 125 - FEA Model Setup for US Navy Blast Test Reaction Frame and SPS Plate

4.3.2.1 Sandwich Plate System Model

The SPS plate model mesh is constructed the same way as the steel plate from section 4.2.2.2. Appendix APPENDIX I-I.4 shows the Truegrid modeling commands used to construct the SPS plate mesh. The SPS plate material, both steel portions and the elastomer portion, are simulated by using material type 114, *MAT LAYERED LINEAR PLASTICITY. This material model is a layered elastoplastic material for modeling laminated composite and sandwich shells where each layer can be represented by elastoplastic behavior with constitutive constants that vary from layer to layer [21]. The material model also has a defined stress versus strain curve for various strain rates. Table 23 shows the input parameters for the two steel plates and Table 24 shows the input parameters for the elastomer core of the SPS plate. The SPS plate is divided into an outer and inner region to account for the section of the SPS plate that is bolted to the reaction frame (See section 4.2.2.2). Appendix APPENDIX H shows the LS-DYNA keyword file for the U.S. Navy Blast Test SPS Plate Study.

Table 23 Constants for US Navy Blast Test SPS Steel Plates [28]

Parameter	*Value*	*Units*
Plate Type	Steel	--
Plate Density	7780	kg/m^3
Young's Modulus	2.06E+11	Pa
Poisson's Ratio	0.281	
Yield Stress	3.55E+08	Pa
Tangent Modulus	0.0	Pa
Hardening parameter	0.0	--
Cowper Symonds strain rate parameter, C	40.4	--
Cowper Symonds strain rate parameter, P	5.0	
Failure Strain	0.1	--
Plate thickness	0.0047625	m
Plate Inner Diameter	1.0668	m
Plate Outer Diameter	1.2954	m

Table 24 Constants for US Navy Blast Test SPS Elastomer Core [28]

Parameter	*Value*	*Units*
Plate Type	Polyurethane Elastomer	--
Plate Density	1190	kg/m^3
Young's Modulus	6.854E+08	Pa
Poisson's Ratio	0.4	
Yield Stress	5.86E+07	Pa
Tangent Modulus	0.0	Pa
Hardening parameter	0.0	--
Cowper Symonds strain rate parameter, C	0.0	--
Cowper Symonds strain rate parameter, P	0.0	
Failure Strain	0.4	--
Plate thickness	0.0301625	m
Plate Inner Diameter	1.0668	m
Plate Outer Diameter	1.2954	m

The stress versus strain curve data at various strain rates is given for the elastomer core [28]. This data is input into the *MAT_LAYERED_LINEAR_PLASTICITY card as a table of load curves. The shell elements are given a thickness equal to the total thickness of the panel system. The total thickness is 0.0396875 m. In order to give the layers different properties, the *INTEGRATION_SHELL card must be used. This card allows the user to define through thickness integration points and assign material properties to each integration point. A weighting factor must also be defined that is equal to the material thickness associated with the integration point divided by the actual shell thickness. The order of the integration points is arbitrary. Figure 126 and Table 25 shows the integration point setup for the SPS plate. Each layer of the SPS plate has three integration points; 1 on the upper surface, 1 on the lower surface, and 1 at the midsurface.

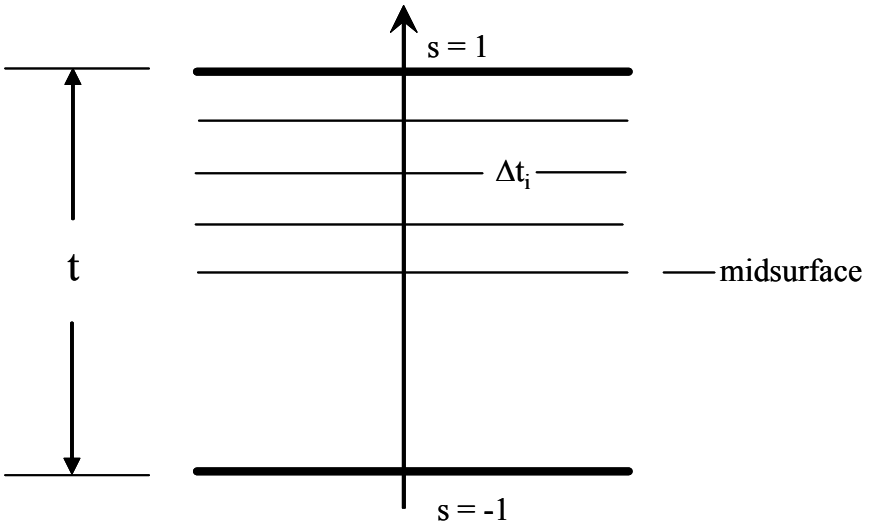

Figure 126 - Illustration of User Defined Shell Integration Rule [21]

Table 25 User Defined Shell Integration Points for SPS Plate Material Model

Material	*Integration Point*	*Coordinate (s)*	*Weight Factor*
Steel	9	1	1.0
Steel	8	0.94	0.94
Steel	7	0.88	0.88
Elastomer	6	0.88	0.88
Elastomer	5	0	0.5
Elastomer	4	-0.88	0.12
Steel	3	-0.88	0.12
Steel	2	-0.94	0.06
Steel	1	-1	0

4.3.3 Results

No test result data from the US Navy Blast Test was available. The termination time for this FEA test is 0.005 seconds. The actual computational time for the SPS plate test is approximately 31 minutes on a Pentium IV desktop PC, requiring 28.5 Mb. of memory for an explicit solution.. The timestep size ranges from 1.0E-07 to 1.0E-06 seconds. Visual comparisons are made between the SPS plate results pictured in Figure 113 and Figure 115. The results from the FEA simulation of the US Navy Blast Test Study are shown in Figure 127. Figure 127 shows the deformation of the SPS plate without rupture.

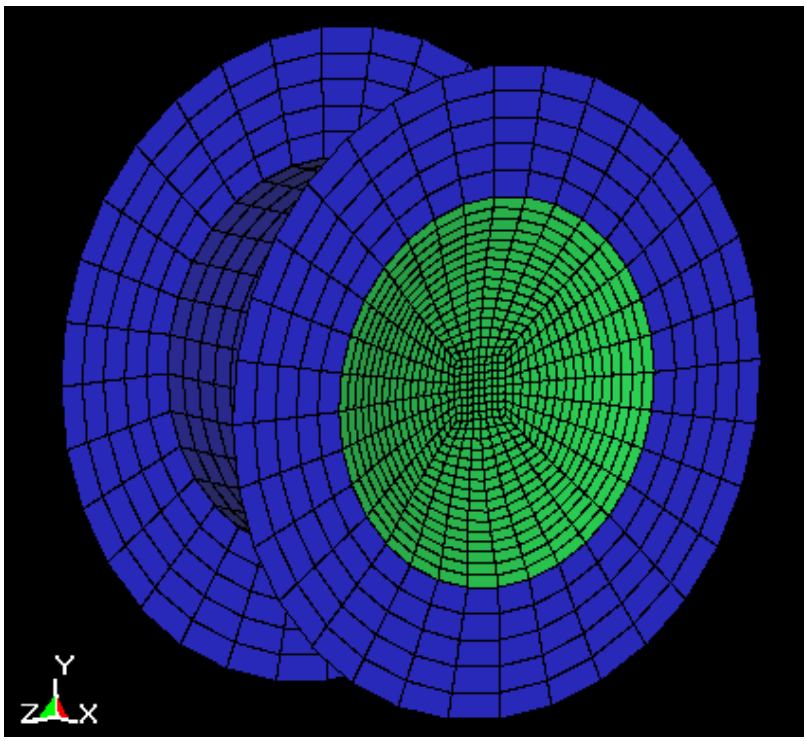

Figure 127 - FE Analysis of US Navy Blast Test Study SPS Plate Result

Figure 113 and Figure 114 show the comparison between the side of the plate facing the charge for the US Navy Blast Test Study SPS plate result and the FE analysis SPS plate result. Figure 115 and Figure 116 show comparison between the side of the plate facing away from the charge for the US Navy Blast Test Study SPS plate and the FE analysis SPS plate results. The FEA SPS plate model is shown with line contours in Figure 114 to aid in the visualization of the deformation.

4.3.4 Discussion

Comparison of the SPS plate in Figure 113 with Figure 114 and Figure 115 with Figure 116 shows the FE analysis produces similar results. The bulge of the SPS plate and the non-rupture resembles that of the actual test. The accuracy of the plate response and behavior could be more precisely determined had more data about the test case been available.

CHAPTER 5 CONCLUSIONS AND FUTURE WORK

In this thesis a 1-D and 3-D underwater explosion (the Deep Spherical Bubble Problem [17,36,37]) and a simulation of a U.S. Navy Blast Test conducted on a ½ in. thick air-backed circular steel plate were used to investigate the ability of the Multi-material Arbitrary Lagrangian/Eulerian method in LS-DYNA to simulate the non-linear dynamic response of a ship-like structure to a near-field underwater explosion. The results obtained from LS-DYNA were analyzed and compared against the general physics of underwater explosions and results from previous work.

The LS-DYNA FE analyses show the ability of the Multi-material Arbitrary Lagrangian/Eulerian method to capture the physical phenomena that occur during a close proximity underwater explosion. However, the ability to produce the correct results is dependant on many other factors such as meshing technique, mesh density, Equation of State Models and their input parameters, Material Models and their input parameters, Boundary Conditions, and Nodal Constraints.

Section 3.2.2.3 shows that the mesh technique and mesh density directly impacts the magnitude of the peak pressure wave that the LS-DYNA MMALE method captures. The mesh technique used to model the explosive, fluid, and structure of an UNDEX event will have a significant impact on the analysis results. Since the fluid mesh needs to have node to node correlation with the explosive and, more importantly, structural meshes, the structural and explosive meshes can at times drive the fluid mesh generation , and density, in a specific direction. This can result in a complex and non-orthogonal fluid mesh that will not be able to translate mass, momentum, or energy data properly. Modeling the explosive using the initial volume fraction model (Section 2.1.3.10) eliminates the complexities of generating an orthogonal mesh that has different coincident node patterns at either end. Another important factor is to model all fluid (air and water) around structure (inside and outside). This is due to the way the ALE method works. Since the ALE method allows the structure to move independently of the fluid mesh via the Constrained Lagrange in Solid constraint (Section 2.1.3.5). It is important in the ALE method that all structure and fluid nodes are coincident, not merged. Only the air and water nodes are merged. This will allow the structure to deform, from its position at the air/water boundary, into the air mesh region, as shown in the US Navy Blast Test (Section 4.2.3). If the air were not modeled, a voided space would exist (a space with no mesh) and a computational error will

occur and the analysis will terminate. Thus, in a full ship model, the air in every compartment needs to be modeled.

Mesh density effects the magnitude of the peak pressure wave. As the mesh density increases, the magnitude of the peak pressure converges. Since the structural and fluid mesh nodes need to be coincident, the structural mesh density now determines the fluid mesh density. Typically large structural meshes, as in full ship models, have large elements to cut down on the total number of elements, thus decreasing the run time of structural analyses while still providing acceptable results. This structural element size would not be adequate for the fluid mesh model to capture the correct peak pressure. Use of a mesh that is not dense enough will underpredict the magnitude of the peak pressure wave. This translates into the improper loading of the structure and consequently improper structural responses. The structural mesh model should be generated taking into account the fluid mesh density needed to capture the correct peak magnitude of the pressure wave.

The Gruneisen Equation of State model in LS-DYNA (Section 2.1.3.7) has been shown to be an acceptable method of describing the fluid properties of water. It has been shown in Section 3.2.2.2 that the Gruneisen Equation of State input parameters have a major impact on the ability of the MMALE method to capture the peak pressure. This inability to capture the correct pressure translates into the improper loading of the structure and consequently false structural responses. Fluid input parameters, specifically water or seawater, that have been proven in far-field analyses are not suitable for close proximity simulations. This is due to the pressure wave traveling faster than the speed of sound in water in the vicinity of the charge. The pressure wave does not decrease to the speed of sound in water until farther away from the charge origin (Section 1.2, p23). When looking at proximity underwater explosion events using the standard value for speed of sound in water as the intercept of the V_S-V_P curve is not valid. The Linear Polynomial Equation of State (Section 2.1.3.7) for use in simulating the properties of air has been shown to work. This linear equation of state is an effective means to model a fluid where the effect of the fluid is needed in the solution calculations, but actual data does not need to be collected from the fluid. The simplicity of the equation of state reduces computational time.

Material models in LS-DYNA (Section 2.1.3.8) also have major effect on the fluid response to an underwater explosion. The Null material has shown to provide accurate results for fluid/structure interaction problems. Elastic material models are not robust enough for use with the ALE method.

Sections 3.2.2.3.2, 3.2.2.3.2.2.1, and 3.2.2.3.2.2.2 show that the Non-Reflecting Boundary Condition (NRBC) in LS-DYNA is not an acceptable boundary condition for a close proximity UNDEX event. The Non-Reflecting Boundary Condition (Section 2.1.3.9) was used to simulate an infinite domain of fluid. This was done so that a small fluid domain could be modeled that effects the explosive charge and subsequent bubble growth in the same way as the full model (Section 3.2.2.3.3). It is shown in Section 3.2.2.3.2 that applying the NRBC to a reduced fluid mesh domain does not produce the late-time bubble effects of an underwater explosion. The NRBC does not account for the added mass effects the fluid has on the explosive gas bubble as it grows. It is simply an impedance matching function that mathematically negates the reflection of the pressure wave at a boundary. The explosive gas bubble grows and reaches equilibrium with the surrounding fluid, but does not collapse (see section 1.2.3.2 on gas bubble dynamics). As of now, in order to capture the correct influence of the fluid domain on the bubble, a complete fluid model is needed.

To improve the accuracy and extend the application of LS-DYNA to larger scale structural models subjected to close proximity underwater explosions and to contact underwater explosions, which will have similar modeling and physics based problems, the following future work is recommended.

1. Increase the computing power and use more elements in the LS-DYNA fluid mesh to assess the improvement in capturing the shock wave and bubble pulse phenomena.
2. Research and develop a more robust set of Gruneisen Equation of State input parameters that will accurately simulate the physical phenomena around the charge and structure of a close proximity UNDEX event, as well as a far-field UNDEX event. Parameters that work well for both events do not currently exist.
3. Develop an infinite boundary condition specifically for the UNDEX problem that models the finite fluid domain as an infinite fluid domain.

REFERENCES

1. OPNAVINST 9070.1
2. GAO-01-493 Navy Acquisitions
3. NavSource Online: Amphibious Photo Archive – USS Tripoli
4. Slade, S., *Princeton's Mine Encounter*, http://www.warships1.com/US/BB61stats/index-BB2-pst17.htm
5. Misovec, A.P., *Explosion Phenomena*. 1976, David W. Taylor Naval Ship Research and Development Center.
6. Cole, R.H., *Underwater Explosions*. 1948, Princeton, New Jersey: Princeton University Press.
7. Reid, W.D., *The Response of Surface Ships to Underwater Explosions*. 1994, Department of Defense.
8. Keil, A.H., *The Response of Ships to Underwater Explosions*. 1961, Department of the Navy.
9. Naval Surface Warfare Center - Carderock Division, http://www.dt.navy.mil/sites/uerd/carrier.html
10. Wood, S.L., *Cavitation Effects on a Ship-Like Box Structure Subjected to an Underwater Explosion*, in *Mechanical Engineering*. 1998, Naval Postgraduate School: Monterey, CA.
11. Makinen, K., *Cavitation Models for Structures Excited by a Plane Shock Wave.* Journal of Fluids and Structures, 1998. 12: p. 85-101.
12. Mair, H.U., et al., *Lagrangian Hydrocode Modeling of Underwater Explosive/Target Interaction.* 61st Shock and Vibration Symposium, 1990. 5: p. 79-89.
13. Schittke, H.J., et al. *The Program DYSMAS/ELC and its Application on Underwater Shock Loading of Vessels*. in *60th Shock and Vibration Symposium*. 1989.
14. Virginia Tech Ship Survivability Research Group, 8/19/04 Meeting
15. Swisdak, M. "Explosion Effects and Properties: Part II – Explosion Effects in Water". NSWC/WOR TR 76-116, 1978.

16. Arons, A.B. “Secondary Pressure Pulses Due to Gas Globe Oscillation in Underwater Explosions. II. Selection of Adiabatic Parameters in the Theory of Oscillation”. *J. Acoust. Soc. Am.* 20, 277 1948.

17. Chisum, J.E., Simulation of the Dynamic Behavior of Explosive Gas Bubbles in a Compressible Fluid Medium, Naval Postgraduate School Dissertation, Monterey, CA, 1996

18. Mair, H. U., Benchmarks for Submerged Structure Response to Underwater Explosions, Shock and Vibration 6 (1999).

19. Mair, H. U., Review: Hydrocodes for the Structural Response to Underwater Explosions, Shock and Vibration 6/2 (1999), pp 81-96.

20. Wardlaw, A. B., 1998, Coupled Hydrocode Prediction of Underwater Explosion Damage, Report OCLC 45320130, Naval Surface Warfare Center Indian Head Division, Indian Head, MD.

21. Olovsson, Lars and Souli, M’hamed, 2000, ALE and Fluid Structure Interaction Capabilities in LS-DYNA, Livermore Software Technology Corporation, Livermore, CA.

22. Trevino, T. and Shin, Y. S., 2000, Applications of Arbitrary Lagrangian Eulerian (ALE) Analysis Approach to Underwater and Air Explosive Problems, Master's Thesis, Naval Postgraduate School, Monterey, CA

23. Hallquist, J.O (2003), “LS-DYNA Keyword Users Manual - Nonlinear Dynamic Structural Analysis of Structures - Version 970”, Livermore Software Technology Corporation (LSTC), April 2003.

24. Hallquist, J.O (1998), “LS-DYNA Theoretical Manual", Livermore Software Technology Corporation (LSTC), May 1998.

25. Souli, M. (2003), "LS-DYNA Advanced Course in ALE and Fluid/Structure Coupling Notes", Livermore Software Technology Corporation (LSTC), February 2003.

26. Marsh, LASL Shock Hugonoit Data, University of California Press, 1980

27. Wardlaw, A. B. and Mair, H. U., Spherical Solutions of an Underwater Explosion Bubble, Shock and Vibration 5 (1998), pp 89-102.]

28. Kennedy, Dr. Stephen J., Input Data for Virginia Tech US Navy Blast Test Study, Proprietary and Confidential US Navy Blast Test Study Report, Intelligent Engineering (Canada) Limited, February 2005.

29. Brown, A.J. and Sajdak, J., Modeling Longitudinal Damage in Ship Collision, Ship Structure Committee, Report SSC-437/SR-1426.

30. Karamcheti, Krishnamurty, 1966, Principles of Ideal-Fluid Aerodynamics, Wiley, New York.

31. Klenow, B., UNDEX Phenomenon Report, Virginia Tech Department of Aerospace and Ocean Engineering, 2005.

32. Brown, A.J. (2004), "AOE 5315 Naval Ship Vulnerability and Underwater Explosion - Introduction to Survivability OnLine Lecture 1", Virginia Tech Department of Aerospace and Ocean Engineering, January 2004.

33. Brown, A.J. (2004), "AOE 5315 Naval Ship Vulnerability and Underwater Explosion - Introduction to Survivability OnLine Lecture 2", Virginia Tech Department of Aerospace and Ocean Engineering, January 2004.

34. Unofficial US Navy Website, http://navysite.de/index.htm

35. Wikipedia, http://en.wikipedia.org/wiki/Naval_mine

36. Chisum, J.E., and Shin, Y.S., Multimaterial Eulerian and Coupled Lagrangian-Eulerian Finite Element Analysis of Underwater Shock Problems, Naval Postgraduate School Technical Report NPS-ME-95-001, Monterey, CA, 1995.

37. Shin, Y. S. and Chisum, J. E., Modeling and Simulation of Underwater Shock Problems Using a Coupled Lagrangian-Eulerian Analysis Approach, Shock and Vibration 4/1 (1997), pp 1-10

38. Huang, H., “An Exact Analysis of the Transient Interaction of Acoustic Plane Waves with a Cylindrical Elastic Shell”, Transactions of the ASME, December, 1970, pp 1091-1099.

39. Hildebrand, F.B., “Advanced Calculus for Applications”, Prentice-Hall, New Jersey, 1960.

40. Taylor,G.I., “The Pressure and Impulse of Submarine Explosion Waves on Plates”, Underwater Explosion Research, Volume 1, Office of Naval Research, 1950, pp 1155-1173.

APPENDIX A PEAK APPROXIMATION CALCULATION FOR TNT IN AVERAGE OCEAN WATER

Unit Definitions:

$gram := \frac{kg}{1000}$ $Bar := 100000Pa$ $Kbar := 1000Bar$

Initial Conditions:

$W := 0.66lbf$ Charge Weight

$R := 0.8m$ $R = 2.625ft$ Radial Distance From Charge

$\rho_{TNT} := 1.59\frac{gram}{cm^3}$ Density of TNT (1.5 to 1.65 gram/cm^3)

$\alpha := 1.16$ Empiracally Fit Power Factor (1.13 to 1.21)

$k := 2.38 \cdot 10^4$ Empiracally Fit Coefficient (2.16 to 2.60 X 10^4)

$k_2 := 0.058$ Empiracally Fit Cefficient (Given by Shin)

$\alpha_2 := -0.185$ Empiracally Fit Power Factor (Given By Shin)

$C := 1415\frac{m}{s}$ Acoustic Speed of Sound in Water

$D := 178m$ Charge Depth

$P_{depth} := 1atm + 1025\frac{kg}{m^3} \cdot g \cdot D$ $P_{depth} = 1.891 \times 10^6 Pa$ Static Pressure at Charge Depth

$\gamma := 1.25$ Ratio of Specific Heats for TNT gas products

Analysis Proceedure:

$$P_{max} := k \cdot \left[\frac{\left(\frac{W}{lbf}\right)^{\frac{1}{3}}}{\frac{R}{ft}} \right]^{\alpha} \frac{lbf}{in^2}$$

$P_{max} = 4.562 \times 10^7 Pa$ Maximum Pressure

$$\theta := k_2 \cdot \left(\frac{W}{lbf}\right)^{\frac{1}{3}} \cdot \left[\frac{\left(\frac{W}{lbf}\right)^{\frac{1}{3}}}{\frac{R}{ft}} \right]^{\alpha_2} \frac{s}{1000}$$

$\theta = 6.193 \times 10^{-5} s$ Decay Constant

$t_1 := \frac{R}{C}$

$t_1 = 5.654 \times 10^{-4} s$ Time to reach Location of interest

$$P(t) := \begin{cases} \left[P_{max} \cdot e^{-\left(\frac{t - \frac{t_1}{s}}{\frac{\theta}{s}} \right)} \right] + P_{depth} & \text{if } t \geq \frac{t_1}{s} \\ P_{depth} & \text{otherwise} \end{cases}$$ Peak Approximation

Bubble Dynamics:

$z_0 := D + 33ft$ $z_0 = 188.058m$ Define initial depth from level of zero pressure

$K_1 := \left(\frac{W}{.66lbf} \right)^{.7}$ $K_1 = 1$ Define Power Coefficient for Jones Constant

$K_2 := \left(.52 - \frac{7 \cdot 10^{-5} \cdot D}{ft} \right)^3$ $K_2 = 0.11$ Define Constant Coefficient for Jones Constant

$K := K_1 \cdot K_2 \cdot 7.8 \cdot \frac{Kbar}{gm} \cdot cm^{3.75}$ $K = 2.713 \times 10^3 \frac{m^{2.75}}{s^2}$ Define Jones Constant

$a_0 := \left(\frac{W}{\rho_{TNT} \cdot g} \right)^{\frac{1}{3}}$ $a_0 = 0.057m$ Calculate initial charge radius at t=0 seconds

$Q_0 := \frac{K}{\gamma - 1} \cdot \left(\frac{4 \cdot \pi}{3} \cdot a_0^3 \right)^{1-\gamma}$ $Q_0 = 6.475 \times 10^4 \frac{m^2}{s^2}$ Calculate initial energy per mass for explosive charge (TNT)

$Y_0 := \frac{W}{g} \cdot Q_0 + \frac{4 \cdot \pi}{3} \cdot 1025 \frac{kg}{m^3} \cdot a_0^3 \cdot g \cdot z_0$ $Y_0 = 2.088 \times 10^4 J$ Calculate remaining energy after release of shock wave

$Q_1 := .34 \cdot Q_0$ $Q_1 = 2.202 \times 10^4 \frac{m^2}{s^2}$ Approximate energy per mass at t=t1 seconds

$Q_2 := .1836 \cdot Q_0$ $Q_2 = 1.189 \times 10^4 \frac{m^2}{s^2}$ Approximate energy per mass at t=t2 seconds

$Y_1 := .34 \cdot Y_0$ $Y_1 = 7.098 \times 10^3 J$ Approximate remaining energy at t=t1 seconds

$Y_2 := .1836 \cdot Y_0$ $Y_2 = 3.833 \times 10^3 J$ Approximate remaining energy at t=t2 seconds

$$A_{M1} := \left[\left(\frac{4 \cdot \pi}{3} \cdot 1025 \frac{kg}{m^3} \cdot g \cdot z_0 \right)^{-1} \cdot Y_0 \right]^{\frac{1}{3}} \qquad A_{M1} = 0.138m$$

Approximate gas sphere maximum bubble radius at t=tm1 seconds

$$A_{M2} := \left[\left(\frac{4 \cdot \pi}{3} \cdot 1025 \frac{kg}{m^3} \cdot g \cdot z_0 \right)^{-1} \cdot Y_1 \right]^{\frac{1}{3}} \qquad A_{M2} = 3.796in$$

Approximate gas sphere radius at t=tm2 seconds

$$t_{b1} := 1.14 \left(1025 \frac{kg}{m^3} \right)^{\frac{1}{2}} \cdot \frac{Y_0^{\frac{1}{3}}}{\left(1025 \frac{kg}{m^3} \cdot g \cdot z_0 \right)^{\frac{5}{6}}} \qquad t_{b1} = 5.912 \times 10^{-3} s$$

Approximate time at which gas sphere is at first minimum

$$t_{b2} := t_{b1} + 1.14 \left(1025 \frac{kg}{m^3} \right)^{\frac{1}{2}} \cdot \frac{Y_1^{\frac{1}{3}}}{\left(1025 \frac{kg}{m^3} \cdot g \cdot z_0 \right)^{\frac{5}{6}}} \qquad t_{b2} = 0.01s$$

Approximate time at which gas sphere is at second minimum

$$t_{bM1} := 0.5 \cdot t_{b1} \qquad t_{bM1} = 2.956 \times 10^{-3} s$$

Approximate time at which gas sphere is at first maximum

$$t_{bM2} := t_{b1} + 0.5 \cdot (t_{b2} - t_{b1}) \qquad t_{bM2} = 7.975 \times 10^{-3} s$$

Approximate time at which gas sphere is at second maximum

Secondary Pressure Pulse:

$$P_{2max} := \left[2590 \frac{\left(\frac{W}{lbf} \right)^{\frac{1}{3}}}{\left(\frac{R}{ft} \right)} \cdot \frac{lbf}{in^2} \right] \qquad P_{2max} = 5.924 \times 10^6 Pa$$

Maximum Pressure of Secondary Pressure Pulse

$$I_2 := 0.21 \cdot 440^{\frac{2}{3}} \cdot \left(\frac{z_0}{ft} \right)^{\frac{-1}{6}} \cdot \left[\frac{\left(\frac{W}{lbf} \right)^{\frac{2}{3}}}{\left(\frac{R}{ft} \right)} \cdot \frac{lbf \cdot s}{in^2} \right] \qquad I_2 = 8.291 \times 10^3 \frac{kg}{ms}$$

Impulse of Secondary Pressure Pulse

$T_2 := \frac{I_2}{P_{2max}}$ $T_2 = 1.4 \times 10^{-3}\,s$ Secondary Pressure Pulse Period

$u := \frac{\pi}{2}\left(\frac{A_{M1} - a_0}{t_{bM1}}\right)$ $u = 42.957\frac{m}{s}$ Estimated Pulse Velocity

$t_{2p} := \frac{R}{u}$ $t_{2p} = 0.019s$ Time of Secondary Pulse maximum Pressure

$S_p := \frac{P_{2max}}{0.5 \cdot T_2}$ $S_p = 8.464 \times 10^{9}\,\frac{kg}{m\,s^3}$ Pressure Time Slope of secondary Pulse

$$P(t) := \begin{cases} \left[P_{max} \cdot e^{-\left(\frac{t - \frac{t_1}{s}}{\frac{\theta}{s}}\right)}\right] + P_{depth} & \text{if } \frac{t_1}{s} \le t < \frac{t_{2p} - 0.5 \cdot T_2}{s} \\ \left[P_{depth} + S_p \cdot s \cdot \left[t - \left(\frac{t_{2p}}{s} - 0.5 \cdot \frac{T_2}{s}\right)\right]\right] & \text{if } \frac{t_{2p} - 0.5 \cdot T_2}{s} \le t < \frac{t_{2p}}{s} \\ \left[P_{depth} + P_{2max} - S_p \cdot s \cdot \left(t - \frac{t_{2p}}{s}\right)\right] & \text{if } \frac{t_{2p}}{s} \le t < \frac{t_{2p} + 0.5 \cdot T_2}{s} \\ P_{depth} & \text{otherwise} \end{cases}$$

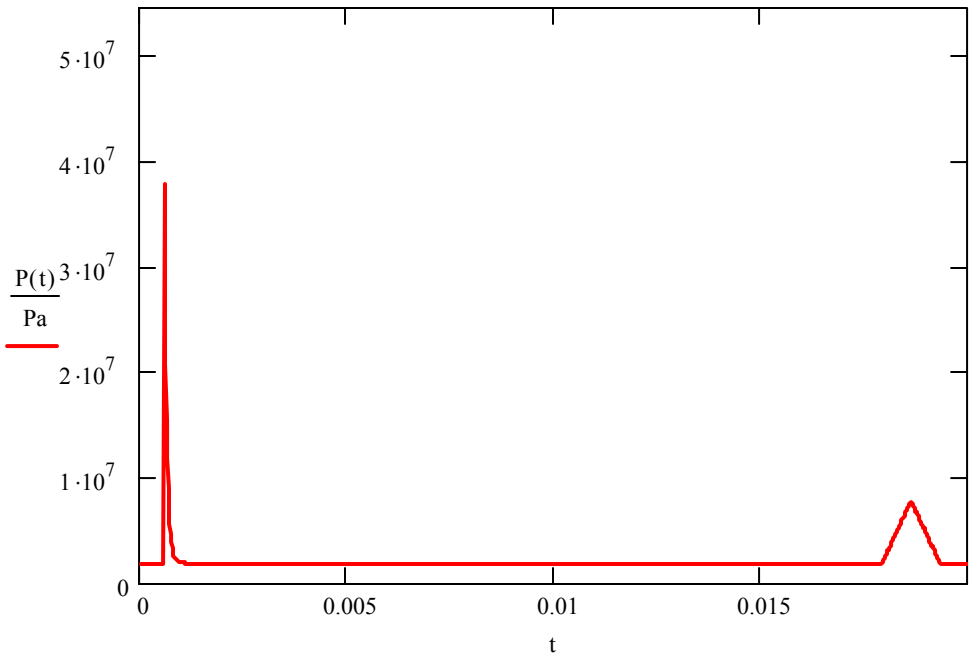

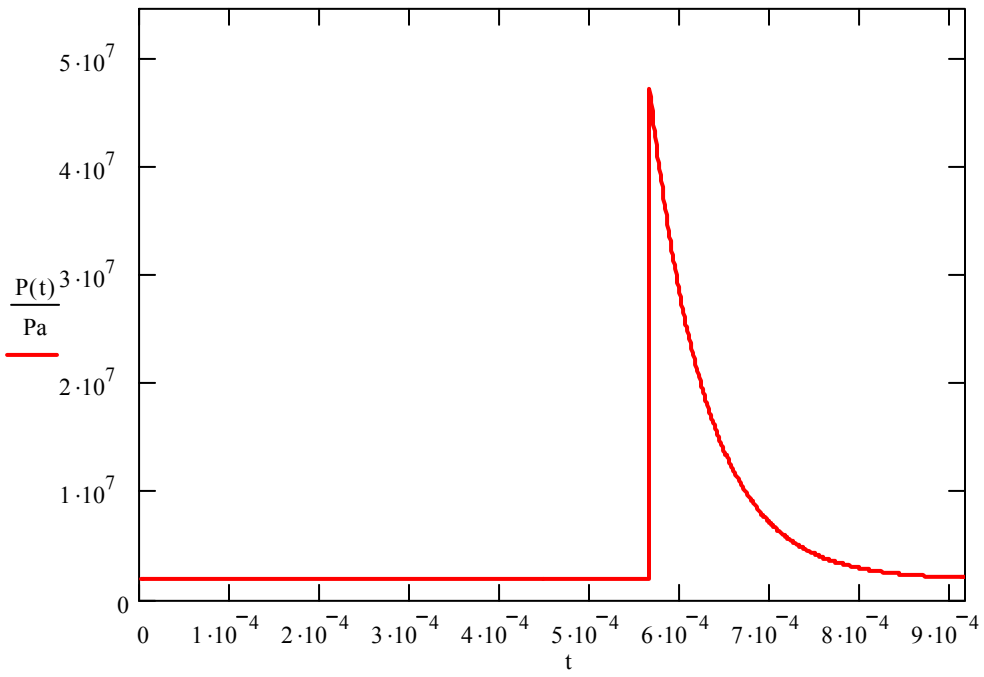

$\alpha = 1.16$ Empiracally Fit Power Factor (1.13 to 1.21)

$k = 2.38 \times 10^{4}$ Empiracally Fit Coefficient (2.16 to 2.60 X 10^4)

$k_2 = 0.058$ Empiracally Fit Cefficient (Given by Shin)

$\alpha_2 = -0.185$ Empiracally Fit Power Factor (Given By Shin)

$\gamma = 1.25$ Ratio of Specific Heats for TNT gas products

Results of Analysis:

$t_1 = 5.654 \times 10^{-4}\,s$ Time of Shock Wave Peak Pressure

$P\left(\frac{t_1}{s}\right) = 4.751 \times 10^{7}\,Pa$ Peak Pressure of Shock Wave

$t_{2p} = 0.019s$ Time of Secondary Pressure Pulse

$P\left(\frac{t_{2p}}{s}\right) = 7.814 \times 10^{6}\,Pa$ Maximum Pressure of Secondary Pressure Pulse

$t_{bM1} = 2.956 \times 10^{-3}\,s$ Time of First Bubble Maximum

$A_{M1} = 0.138m$ Maximum Bubble Radius

APPENDIX B LS-DYNA VOLUME INTEGRATION CALCULATION

Approximate Volume Calculation

Define Nodal Coordinates for 8 Node Solid Hexahedron Element

$$N := \begin{pmatrix} .1 & 0 & 0 \\ 1 & 0 & 0 \\ 1 & 1 & 0 \\ 0 & 1 & 0 \\ 0 & 0 & 1 \\ 1 & 0 & 1 \\ 1 & 1 & 1 \\ 0 & 1 & 1 \end{pmatrix} \qquad N := \begin{pmatrix} 0 & 0 & 0 \\ 1 & 0 & 0 \\ 1 & 1 & 0 \\ 0 & 1 & 0 \\ 0 & 0 & 1 \\ 1 & 0 & 1 \\ 1 & 1 & 1 \\ 0 & 1 & 1 \end{pmatrix}$$

Cube, Volume = 1

Define Shape Functions

$$h_1(\varepsilon, \eta, \zeta) := \frac{1}{8} \cdot (1 - \varepsilon) \cdot (1 - \eta) \cdot (1 - \zeta)$$

$$h_2(\varepsilon, \eta, \zeta) := \frac{1}{8} \cdot (1 + \varepsilon) \cdot (1 - \eta) \cdot (1 - \zeta)$$

$$h_3(\varepsilon, \eta, \zeta) := \frac{1}{8} \cdot (1 + \varepsilon) \cdot (1 + \eta) \cdot (1 - \zeta)$$

$$h_4(\varepsilon, \eta, \zeta) := \frac{1}{8} \cdot (1 - \varepsilon) \cdot (1 + \eta) \cdot (1 - \zeta)$$

$$h_5(\varepsilon, \eta, \zeta) := \frac{1}{8} \cdot (1 - \varepsilon) \cdot (1 - \eta) \cdot (1 + \zeta)$$

$$h_6(\varepsilon, \eta, \zeta) := \frac{1}{8} \cdot (1 + \varepsilon) \cdot (1 - \eta) \cdot (1 + \zeta)$$

$$h_7(\varepsilon, \eta, \zeta) := \frac{1}{8} \cdot (1 + \varepsilon) \cdot (1 + \eta) \cdot (1 + \zeta)$$

$$h_8(\varepsilon, \eta, \zeta) := \frac{1}{8} \cdot (1 - \varepsilon) \cdot (1 + \eta) \cdot (1 + \zeta)$$

Define Interpolation Functions

$$x(\varepsilon,\eta,\zeta) := N_{0,0}\cdot h_1(\varepsilon,\eta,\zeta) + N_{1,0}\cdot h_2(\varepsilon,\eta,\zeta) + N_{2,0}\cdot h_3(\varepsilon,\eta,\zeta) + N_{3,0}\cdot h_4(\varepsilon,\eta,\zeta) + N_{4,0}\cdot h_5(\varepsilon,\eta,\zeta) + N_{5,0}\cdot h_6(\varepsilon,\eta,\zeta) + N_{6,0}\cdot h_7(\varepsilon,\eta,\zeta) + N_{7,0}\cdot h_8(\varepsilon,\eta,\zeta)$$

$$y(\varepsilon,\eta,\zeta) := N_{0,1}\cdot h_1(\varepsilon,\eta,\zeta) + N_{1,1}\cdot h_2(\varepsilon,\eta,\zeta) + N_{2,1}\cdot h_3(\varepsilon,\eta,\zeta) + N_{3,1}\cdot h_4(\varepsilon,\eta,\zeta) + N_{4,1}\cdot h_5(\varepsilon,\eta,\zeta) + N_{5,1}\cdot h_6(\varepsilon,\eta,\zeta) + N_{6,1}\cdot h_7(\varepsilon,\eta,\zeta) + N_{7,1}\cdot h_8(\varepsilon,\eta,\zeta)$$

$$z(\varepsilon,\eta,\zeta) := N_{0,2}\cdot h_1(\varepsilon,\eta,\zeta) + N_{1,2}\cdot h_2(\varepsilon,\eta,\zeta) + N_{2,2}\cdot h_3(\varepsilon,\eta,\zeta) + N_{3,2}\cdot h_4(\varepsilon,\eta,\zeta) + N_{4,2}\cdot h_5(\varepsilon,\eta,\zeta) + N_{5,2}\cdot h_6(\varepsilon,\eta,\zeta) + N_{6,2}\cdot h_7(\varepsilon,\eta,\zeta) + N_{7,2}\cdot h_8(\varepsilon,\eta,\zeta)$$

Define The Components of the Jacobian Matrix

$$J_{11}(\varepsilon,\eta,\zeta) := \frac{d}{d\varepsilon}x(\varepsilon,\eta,\zeta) \qquad J_{12}(\varepsilon,\eta,\zeta) := \frac{d}{d\varepsilon}y(\varepsilon,\eta,\zeta) \qquad J_{13}(\varepsilon,\eta,\zeta) := \frac{d}{d\varepsilon}z(\varepsilon,\eta,\zeta)$$

$$J_{21}(\varepsilon,\eta,\zeta) := \frac{d}{d\eta}x(\varepsilon,\eta,\zeta) \qquad J_{22}(\varepsilon,\eta,\zeta) := \frac{d}{d\eta}y(\varepsilon,\eta,\zeta) \qquad J_{23}(\varepsilon,\eta,\zeta) := \frac{d}{d\eta}z(\varepsilon,\eta,\zeta)$$

$$J_{31}(\varepsilon,\eta,\zeta) := \frac{d}{d\zeta}x(\varepsilon,\eta,\zeta) \qquad J_{32}(\varepsilon,\eta,\zeta) := \frac{d}{d\zeta}y(\varepsilon,\eta,\zeta) \qquad J_{33}(\varepsilon,\eta,\zeta) := \frac{d}{d\zeta}z(\varepsilon,\eta,\zeta)$$

Define the Jacobian Determinant

$$J_{D1}(\varepsilon,\eta,\zeta) := J_{11}(\varepsilon,\eta,\zeta)\left[\left(J_{22}(\varepsilon,\eta,\zeta)\cdot J_{33}(\varepsilon,\eta,\zeta)\right) - \left(J_{23}(\varepsilon,\eta,\zeta)\cdot J_{32}(\varepsilon,\eta,\zeta)\right)\right]$$

$$J_{D2}(\varepsilon,\eta,\zeta) := J_{12}(\varepsilon,\eta,\zeta)\left[\left(J_{21}(\varepsilon,\eta,\zeta)\cdot J_{33}(\varepsilon,\eta,\zeta)\right) - \left(J_{23}(\varepsilon,\eta,\zeta)\cdot J_{31}(\varepsilon,\eta,\zeta)\right)\right]$$

$$J_{D3}(\varepsilon,\eta,\zeta) := J_{13}(\varepsilon,\eta,\zeta)\left[\left(J_{21}(\varepsilon,\eta,\zeta)\cdot J_{32}(\varepsilon,\eta,\zeta)\right) - \left(J_{22}(\varepsilon,\eta,\zeta)\cdot J_{31}(\varepsilon,\eta,\zeta)\right)\right]$$

$$J_{DET}(\varepsilon,\eta,\zeta) := J_{D1}(\varepsilon,\eta,\zeta) - J_{D2}(\varepsilon,\eta,\zeta) + J_{D3}(\varepsilon,\eta,\zeta)$$

Determine the Approximate Element Volume

$$V_{approx} := 8\cdot J_{DET}(0,0,0) \qquad V_{approx} = 0.975$$

Actual Volume Calculation

Determine Element Center

$$x_c := \frac{1}{8}\cdot\left(N_{0,0} + N_{1,0} + N_{2,0} + N_{3,0} + N_{4,0} + N_{5,0} + N_{6,0} + N_{7,0}\right) \qquad x_c = 0.513$$

$$y_c := \frac{1}{8}\cdot\left(N_{0,1} + N_{1,1} + N_{2,1} + N_{3,1} + N_{4,1} + N_{5,1} + N_{6,1} + N_{7,1}\right) \qquad y_c = 0.5$$

$$z_c := \frac{1}{8}\cdot\left(N_{0,2} + N_{1,2} + N_{2,2} + N_{3,2} + N_{4,2} + N_{5,2} + N_{6,2} + N_{7,2}\right) \qquad z_c = 0.5$$

Determine Vectors

$$C1 := \begin{pmatrix} N_{0,0} - x_c \\ N_{0,1} - y_c \\ N_{0,2} - z_c \end{pmatrix} \quad C2 := \begin{pmatrix} N_{1,0} - x_c \\ N_{1,1} - y_c \\ N_{1,2} - z_c \end{pmatrix} \quad C3 := \begin{pmatrix} N_{2,0} - x_c \\ N_{2,1} - y_c \\ N_{2,2} - z_c \end{pmatrix} \quad C4 := \begin{pmatrix} N_{3,0} - x_c \\ N_{3,1} - y_c \\ N_{3,2} - z_c \end{pmatrix}$$

$$C5 := \begin{pmatrix} N_{4,0} - x_c \\ N_{4,1} - y_c \\ N_{4,2} - z_c \end{pmatrix} \quad C6 := \begin{pmatrix} N_{5,0} - x_c \\ N_{5,1} - y_c \\ N_{5,2} - z_c \end{pmatrix} \quad C7 := \begin{pmatrix} N_{6,0} - x_c \\ N_{6,1} - y_c \\ N_{6,2} - z_c \end{pmatrix} \quad C8 := \begin{pmatrix} N_{7,0} - x_c \\ N_{7,1} - y_c \\ N_{7,2} - z_c \end{pmatrix}$$

Determine the Actual Element Volume

$$V_1 := \frac{1}{6}(C2 \times C1)\cdot C3 \qquad V_7 := \frac{1}{6}(C5 \times C6)\cdot C7 \qquad V_4 := \frac{1}{6}(C1 \times C2)\cdot C6 \qquad V_{10} := \frac{1}{6}(C4 \times C8)\cdot C7$$

$$V_2 := \frac{1}{6}(C1 \times C4)\cdot C3 \qquad V_8 := \frac{1}{6}(C8 \times C5)\cdot C7 \qquad V_5 := \frac{1}{6}(C6 \times C2)\cdot C7 \qquad V_{11} := \frac{1}{6}(C1 \times C5)\cdot C8$$

$$V_3 := \frac{1}{6}(C5 \times C1)\cdot C6 \qquad V_9 := \frac{1}{6}(C3 \times C4)\cdot C7 \qquad V_6 := \frac{1}{6}(C2 \times C3)\cdot C7 \qquad V_{12} := \frac{1}{6}(C4 \times C1)\cdot C8$$

$$V_{actual} := V_1 + V_2 + V_3 + V_4 + V_5 + V_6 + V_7 + V_8 + V_9 + V_{10} + V_{11} + V_{12} \qquad \boxed{V_{actual} = 0.967}$$

Determine Volume Ratio, Approximate over Actual

$$V_{approx} = 0.975 \qquad V_{actual} = 0.967 \qquad V_R := \frac{V_{approx}}{V_{actual}} \qquad \boxed{V_R = 1.009}$$

APPENDIX C LS-DYNA FILE FOR 1-D DEEP SPHERICAL BUBBLE MODEL

The LS-DYNA input file is given for the test case from Section 3.1. Input files for all other test cases are the same except input cards containing node and element information. To decrease space, not all elements and nodes are listed.

```
*KEYWORD
*INCLUDE
pyramid20_1.inc
*TITLE
1-D FLUID BLOCK MODEL(178.6m)
$
$-----------------------------------------------------
$ ANALYSIS OF DEEP SPHERICAL BUBBLE PROBLEM
$
$ SET ID:   #       DESCRIPTION
$
$          601     X-Y-Z CONSTRAINED NODE SET
$          602     Y-Z CONSTRAINED NODE SET
$          603     NR SET
$--------------------------
$ ANALYSIS CONTROL CARDS
$--------------------------
*CONTROL_TERMINATION
0.05,0,0.000E+00,0.000E+00,0.000E+00
*DATABASE_BINARY_D3PLOT
1.000E-04,0
*DATABASE_GLSTAT
1.0E-04,1
$---------------------------------------
$ charge DEFINITION CARDS
$---------------------------------------
*PART
```

```
CHARGE
100,101,102,103,104,0,0,0
*INITIAL_DETONATION
0,0.0,0.0,0.0,0.
*SECTION_SOLID
101,11
*MAT_HIGH_EXPLOSIVE_BURN
102,1630.,6930.,2.1E+10,0.0
*EOS_JWL
103,3.712E+11,3.231E+09,4.15,0.95,0.3,6.99E+09,1.0
*HOURGLASS
104,1,1.0E-04,1,1.5,0.06
$---------------------------------------
$ FLUID DEFINITION CARDS
$---------------------------------------
*PART
FLUID
200,201,202,203,204,0,0,0
*PART
FLUID
300,201,202,203,204,0,0,0
*PART
FLUID
400,201,202,203,204,0,0,0
*PART
FLUID
500,201,202,203,204,0,0,0
*PART
FLUID
600,201,202,203,204,0,0,0
*SECTION_SOLID
201,11
*MAT_NULL
202,1025.,-1.000E-20,1.13E-03,0.,0.,0.,0.
```

```
*EOS_GRUNEISEN
$203,1480,2.56,1.986,1.2268,1.0,0.0,3.85E+06
203,1480,2.56,1.986,1.2268,1.0,0.0,3.85E+06
1.
*HOURGLASS
204,1,1.000E-04,1,4.0,0.2
*SET_PART_LIST
2000
200,300,400,500,600
$----------------------------------------
$ ALE DEFINITION CARDS
$----------------------------------------
*ALE_MULTI-MATERIAL_GROUP
100,1
2000,0
*CONTROL_ALE
3,3,2,-1
$----------------------------------------
$ BOUNDARY CONDITION CARDS
$----------------------------------------
*BOUNDARY_SPC_SET
601,0,1,1,1,1,1,1
*BOUNDARY_SPC_SET
602,0,0,1,1,1,1,1
*BOUNDARY_SPC_SET
603,1,1,1,0,1,1,1
*BOUNDARY_SPC_SET
604,2,1,1,0,1,1,1
*BOUNDARY_SPC_SET
605,3,1,1,0,1,1,1
*BOUNDARY_SPC_SET
606,4,1,1,0,1,1,1
*BOUNDARY_NON_REFLECTING
607,0,0
```

```
*END
------------------------------------------------------------------------------------------
$---+----1----+----2----+----3----+----4----+----5----+----6----+----7----+----8
$                                                   $
$                    SOLID ELEMENT SET CARDS                    $
$                                                   $
$---+----1----+----2----+----3----+----4----+----5----+----6----+----7----+----8
*SET_SOLID_TITLE
Database_History
$     SID
      700
$      K1       K2       K3       K4       K5       K6       K7       K8
       808      809      810      811      812      813      814      815
       816      817      818      819      820      821      822      823
       824      825      826      827      828      829      830      831
       832      833      834      835      836      837      838      839
       840      841      842      843      844      845      846      847
       848      849      850      851      852      853      854      855
       856      857      858      859      860      861      862      863
       864      865      866      867      868      869      870      871
       872      873      874      875      876      877      878      879
       880      881      882      883      884      885      886      887
       888      889      890      891      892      893      894      895
       896      897      898      899      900      901      902      903
       904      905      906      907      908      909      910      911
       912      913      914      915      916      917      918      919
       920      921      922      923      924      925      926      927
       928      929      930      931      932      933      934      935
       936      937      938      939      940      941      942      943
       944      945      946      947      948      949      950      951
       952      953      954      955      956      957      958      959
       960      961      962      963      964      965      966      967
       968      969      970      971      972      973      974      975
       976      977      978      979      980      981      982      983
```

```
     984      985      986      987      988      989      990      991
     992      993      994      995      996      997      998      999
    1000     1001     1002     1003     1004     1005     1006
$---+----1----+----2----+----3----+----4----+----5----+----6----+----7----+----8
$                                                   $
$                    SEGMENT SET CARDS                          $
$                                                   $
$---+----1----+----2----+----3----+----4----+----5----+----6----+----7----+----8
*SET_SEGMENT_TITLE
Segment_set 1
$     SID      DA1      DA2      DA3      DA4
      607      0.0      0.0      0.0      0.0
$      N1       N2       N3       N4       A1       A2       A3       A4
    3597     3598     3599     3600      0.0      0.0      0.0      0.0
$---+----1----+----2----+----3----+----4----+----5----+----6----+----7----+----8
$                                                   $
$                      NODE SET CARDS                           $
$                                                   $
$---+----1----+----2----+----3----+----4----+----5----+----6----+----7----+----8
*SET_NODE_LIST_TITLE
Node_set 1
$     SID      DA1      DA2      DA3      DA4
      602      0.0      0.0      0.0      0.0
$    NID1     NID2     NID3     NID4     NID5     NID6     NID7     NID8
       8        7        6        9       12       11       10        5
*SET_NODE_LIST_TITLE
601
$     SID      DA1      DA2      DA3      DA4
      601      0.0      0.0      0.0      0.0
$    NID1     NID2     NID3     NID4     NID5     NID6     NID7     NID8
       2        3        4        1
*SET_NODE_LIST_TITLE
Node_set 603
$     SID      DA1      DA2      DA3      DA4
```

```
    603     0.0     0.0     0.0     0.0
$   NID1    NID2    NID3    NID4    NID5    NID6    NID7    NID8
     13     101      97      93      89      85      81      77
     73      69      65      61      57      53      49      45
     41      37      33      29      25      21      17    3597
   3593    3589    3585    3581    3577    3573    3569    3565
   3561    3557    3553    3549    3545    3541    3537    3533
   3529    3525    3521    3517    3513    3509    3505    3501
   3497    3493    3489    3485    3481    3477    3473    3469
   3465    3461    3457    3453    3449    3445    3441    3437
   3433    3429    3425    3421    3417    3413    3409    3405
   3401    3397    3393    3389    3385    3381    3377    3373
   3369    3365    3361    3357    3353    3349    3345    3341
   3337    3333    3329    3325    3321    3317    3313    3309
   3305    3301    3297    3293    3289    3285    3281    3277
   3273    3269    3265    3261    3257    3253    3249    3245
   3241    3237    3233    3229    3225    3221    3217    3213
   3209    3205    3201    3197    3193    3189    3185    3181
   3177    3173    3169    3165    3161    3157    3153    3149
   3145    3141    3137    3133    3129    3125    3121    3117
   3113    3109    3105    3101    3097    3093    3089    3085
   3081    3077    3073    3069    3065    3061    3057    3053
   3049    3045    3041    3037    3033    3029    3025    3021
   3017    3013    3009    3005    3001    2997    2993    2989
   2985    2981    2977    2973    2969    2965    2961    2957
   2953    2949    2945    2941    2937    2933    2929    2925
   2921    2917    2913    2909    2905    2901    2897    2893
   2889    2885    2881    2877    2873    2869    2865    2861
   2857    2853    2849    2845    2841    2837    2833    2829
   2825    2821    2817    2813    2809    2805    2801    2797
   2793    2789    2785    2781    2777    2773    2769    2765
   2761    2757    2753    2749    2745    2741    2737    2733
   2729    2725    2721    2717    2713    2709    2705    2701
   2697    2693    2689    2685    2681    2677    2673    2669
```

2665 2661 2657 2653 2649 2645 2641 2637
2633 2629 2625 2621 2617 2613 2609 2605
2601 2597 2593 2589 2585 2581 2577 2573
2569 2565 2561 2557 2553 2549 2545 2541
2537 2533 2529 2525 2521 2517 2513 2509
2505 2501 2497 2493 2489 2485 2481 2477
2473 2469 2465 2461 2457 2453 2449 2445
2441 2437 2433 2429 2425 2421 2417 2413
2409 2405 2401 2397 2393 2389 2385 2381
2377 2373 2369 2365 2361 2357 2353 2349
2345 2341 2337 2333 2329 2325 2321 2317
2313 2309 2305 2301 2297 2293 2289 2285
2281 2277 2273 2269 2265 2261 2257 2253
2249 2245 2241 2237 2233 2229 2225 2221
2217 2213 2209 2205 2201 2197 2193 2189
2185 2181 2177 2173 2169 2165 2161 2157
2153 2149 2145 2141 2137 2133 2129 2125
2121 2117 2113 2109 2105 2101 2097 2093
2089 2085 2081 2077 2073 2069 2065 2061
2057 2053 2049 2045 2041 2037 2033 2029
2025 2021 2017 2013 2009 2005 2001 1997
1993 1989 1985 1981 1977 1973 1969 1965
1961 1957 1953 1949 1945 1941 1937 1933
1929 1925 1921 1917 1913 1909 1905 1901
1897 1893 1889 1885 1881 1877 1873 1869
1865 1861 1857 1853 1849 1845 1841 1837
1833 1829 1825 1821 1817 1813 1809 1805
1801 1797 1793 1789 1785 1781 1777 1773
1769 1765 1761 1757 1753 1749 1745 1741
1737 1733 1729 1725 1721 1717 1713 1709
1705 1701 1697 1693 1689 1685 1681 1677
1673 1669 1665 1661 1657 1653 1649 1645
1641 1637 1633 1629 1625 1621 1617 1613
1609 1605 1601 1597 1593 1589 1585 1581

1577 1573 1569 1565 1561 1557 1553 1549
1545 1541 1537 1533 1529 1525 1521 1517
1513 1509 1505 1501 1497 1493 1489 1485
1481 1477 1473 1469 1465 1461 1457 1453
1449 1445 1441 1437 1433 1429 1425 1421
1417 1413 1409 1405 1401 1397 1393 1389
1385 1381 1377 1373 1369 1365 1361 1357
1353 1349 1345 1341 1337 1333 1329 1325
1321 1317 1313 1309 1305 1301 1297 1293
1289 1285 1281 1277 1273 1269 1265 1261
1257 1253 1249 1245 1241 1237 1233 1229
1225 1221 1217 1213 1209 1205 1201 1197
1193 1189 1185 1181 1177 1173 1169 1165
1161 1157 1153 1149 1145 1141 1137 1133
1129 1125 1121 1117 1113 1109 1105 1101
1097 1093 1089 1085 1081 1077 1073 1069
1065 1061 1057 1053 1049 1045 1041 1037
1033 1029 1025 1021 1017 1013 1009 1005
1001 997 993 989 985 981 977 973
969 965 961 957 953 949 945 941
937 933 929 925 921 917 913 909
905 901 897 893 889 885 881 877
873 869 865 861 857 853 849 845
841 837 833 829 825 821 817 813
809 805 801 797 793 789 785 781
777 773 769 765 761 757 753 749
745 741 737 733 729 725 721 717
713 709 705 701 697 693 689 685
681 677 673 669 665 661 657 653
649 645 641 637 633 629 625 621
617 613 609 605 601 597 593 589
585 581 577 573 569 565 561 557
553 549 545 541 537 533 529 525
521 517 513 509 505 501 497 493

489 485 481 477 473 469 465 461
457 453 449 445 441 437 433 429
425 421 417 413 409 405 401 397
393 389 385 381 377 373 369 365
361 357 353 349 345 341 337 333
329 325 321 317 313 309 305 301
297 293 289 285 281 277 273 269
265 261 257 253 249 245 241 237
233 229 225 221 217 213 209 205
201 197 193 189 185 181 177 173
169 165 161 157 153 149 145 141
137 133 129 125 121 117 113 109
105

*SET_NODE_LIST_TITLE
Node_set 604
$ SID DA1 DA2 DA3 DA4
604 0.0 0.0 0.0 0.0
$ NID1 NID2 NID3 NID4 NID5 NID6 NID7 NID8
14 54 50 46 42 38 34 30
26 22 18 3598 3594 3590 3586 3582
3578 3574 3570 3566 3562 3558 3554 3550
3546 3542 3538 3534 3530 3526 3522 3518
3514 3510 3506 3502 3498 3494 3490 3486
3482 3478 3474 3470 3466 3462 3458 3454
3450 3446 3442 3438 3434 3430 3426 3422
3418 3414 3410 3406 3402 3398 3394 3390
3386 3382 3378 3374 3370 3366 3362 3358
3354 3350 3346 3342 3338 3334 3330 3326
3322 3318 3314 3310 3306 3302 3298 3294
3290 3286 3282 3278 3274 3270 3266 3262
3258 3254 3250 3246 3242 3238 3234 3230
3226 3222 3218 3214 3210 3206 3202 3198
3194 3190 3186 3182 3178 3174 3170 3166
3162 3158 3154 3150 3146 3142 3138 3134

3130 3126 3122 3118 3114 3110 3106 3102
3098 3094 3090 3086 3082 3078 3074 3070
3066 3062 3058 3054 3050 3046 3042 3038
3034 3030 3026 3022 3018 3014 3010 3006
3002 2998 2994 2990 2986 2982 2978 2974
2970 2966 2962 2958 2954 2950 2946 2942
2938 2934 2930 2926 2922 2918 2914 2910
2906 2902 2898 2894 2890 2886 2882 2878
2874 2870 2866 2862 2858 2854 2850 2846
2842 2838 2834 2830 2826 2822 2818 2814
2810 2806 2802 2798 2794 2790 2786 2782
2778 2774 2770 2766 2762 2758 2754 2750
2746 2742 2738 2734 2730 2726 2722 2718
2714 2710 2706 2702 2698 2694 2690 2686
2682 2678 2674 2670 2666 2662 2658 2654
2650 2646 2642 2638 2634 2630 2626 2622
2618 2614 2610 2606 2602 2598 2594 2590
2586 2582 2578 2574 2570 2566 2562 2558
2554 2550 2546 2542 2538 2534 2530 2526
2522 2518 2514 2510 2506 2502 2498 2494
2490 2486 2482 2478 2474 2470 2466 2462
2458 2454 2450 2446 2442 2438 2434 2430
2426 2422 2418 2414 2410 2406 2402 2398
2394 2390 2386 2382 2378 2374 2370 2366
2362 2358 2354 2350 2346 2342 2338 2334
2330 2326 2322 2318 2314 2310 2306 2302
2298 2294 2290 2286 2282 2278 2274 2270
2266 2262 2258 2254 2250 2246 2242 2238
2234 2230 2226 2222 2218 2214 2210 2206
2202 2198 2194 2190 2186 2182 2178 2174
2170 2166 2162 2158 2154 2150 2146 2142
2138 2134 2130 2126 2122 2118 2114 2110
2106 2102 2098 2094 2090 2086 2082 2078
2074 2070 2066 2062 2058 2054 2050 2046

2042 2038 2034 2030 2026 2022 2018 2014
2010 2006 2002 1998 1994 1990 1986 1982
1978 1974 1970 1966 1962 1958 1954 1950
1946 1942 1938 1934 1930 1926 1922 1918
1914 1910 1906 1902 1898 1894 1890 1886
1882 1878 1874 1870 1866 1862 1858 1854
1850 1846 1842 1838 1834 1830 1826 1822
1818 1814 1810 1806 1802 1798 1794 1790
1786 1782 1778 1774 1770 1766 1762 1758
1754 1750 1746 1742 1738 1734 1730 1726
1722 1718 1714 1710 1706 1702 1698 1694
1690 1686 1682 1678 1674 1670 1666 1662
1658 1654 1650 1646 1642 1638 1634 1630
1626 1622 1618 1614 1610 1606 1602 1598
1594 1590 1586 1582 1578 1574 1570 1566
1562 1558 1554 1550 1546 1542 1538 1534
1530 1526 1522 1518 1514 1510 1506 1502
1498 1494 1490 1486 1482 1478 1474 1470
1466 1462 1458 1454 1450 1446 1442 1438
1434 1430 1426 1422 1418 1414 1410 1406
1402 1398 1394 1390 1386 1382 1378 1374
1370 1366 1362 1358 1354 1350 1346 1342
1338 1334 1330 1326 1322 1318 1314 1310
1306 1302 1298 1294 1290 1286 1282 1278
1274 1270 1266 1262 1258 1254 1250 1246
1242 1238 1234 1230 1226 1222 1218 1214
1210 1206 1202 1198 1194 1190 1186 1182
1178 1174 1170 1166 1162 1158 1154 1150
1146 1142 1138 1134 1130 1126 1122 1118
1114 1110 1106 1102 1098 1094 1090 1086
1082 1078 1074 1070 1066 1062 1058 1054
1050 1046 1042 1038 1034 1030 1026 1022
1018 1014 1010 1006 1002 998 994 990
986 982 978 974 970 966 962 958

954 950 946 942 938 934 930 926
922 918 914 910 906 902 898 894
890 886 882 878 874 870 866 862
858 854 850 846 842 838 834 830
826 822 818 814 810 806 802 798
794 790 786 782 778 774 770 766
762 758 754 750 746 742 738 734
730 726 722 718 714 710 706 702
698 694 690 686 682 678 674 670
666 662 658 654 650 646 642 638
634 630 626 622 618 614 610 606
602 598 594 590 586 582 578 574
570 566 562 558 554 550 546 542
538 534 530 526 522 518 514 510
506 502 498 494 490 486 482 478
474 470 466 462 458 454 450 446
442 438 434 430 426 422 418 414
410 406 402 398 394 390 386 382
378 374 370 366 362 358 354 350
346 342 338 334 330 326 322 318
314 310 306 302 298 294 290 286
282 278 274 270 266 262 258 254
250 246 242 238 234 230 226 222
218 214 210 206 202 198 194 190
186 182 178 174 170 166 162 158
154 150 146 142 138 134 130 126
122 118 114 110 106 102 98 94
90 86 82 78 74 70 66 62
58

*SET_NODE_LIST_TITLE

Node_set 605

$ SID DA1 DA2 DA3 DA4

605 0.0 0.0 0.0 0.0

$ NID1 NID2 NID3 NID4 NID5 NID6 NID7 NID8

15 99 95 91 87 83 79 75
71 67 63 59 55 51 47 43
39 35 31 27 23 19 359 355
351 347 343 339 335 331 327 323
319 315 311 307 303 299 295 291
287 283 279 275 271 267 263 259
255 251 247 243 239 235 231 227
223 219 215 211 207 203 199 195
191 187 183 179 175 171 167 163
159 155 151 147 143 139 135 131
127 123 119 115 111 107 103 3599
3595 3591 3587 3583 3579 3575 3571 3567
3563 3559 3555 3551 3547 3543 3539 3535
3531 3527 3523 3519 3515 3511 3507 3503
3499 3495 3491 3487 3483 3479 3475 3471
3467 3463 3459 3455 3451 3447 3443 3439
3435 3431 3427 3423 3419 3415 3411 3407
3403 3399 3395 3391 3387 3383 3379 3375
3371 3367 3363 3359 3355 3351 3347 3343
3339 3335 3331 3327 3323 3319 3315 3311
3307 3303 3299 3295 3291 3287 3283 3279
3275 3271 3267 3263 3259 3255 3251 3247
3243 3239 3235 3231 3227 3223 3219 3215
3211 3207 3203 3199 3195 3191 3187 3183
3179 3175 3171 3167 3163 3159 3155 3151
3147 3143 3139 3135 3131 3127 3123 3119
3115 3111 3107 3103 3099 3095 3091 3087
3083 3079 3075 3071 3067 3063 3059 3055
3051 3047 3043 3039 3035 3031 3027 3023
3019 3015 3011 3007 3003 2999 2995 2991
2987 2983 2979 2975 2971 2967 2963 2959
2955 2951 2947 2943 2939 2935 2931 2927
2923 2919 2915 2911 2907 2903 2899 2895
2891 2887 2883 2879 2875 2871 2867 2863

2859 2855 2851 2847 2843 2839 2835 2831
2827 2823 2819 2815 2811 2807 2803 2799
2795 2791 2787 2783 2779 2775 2771 2767
2763 2759 2755 2751 2747 2743 2739 2735
2731 2727 2723 2719 2715 2711 2707 2703
2699 2695 2691 2687 2683 2679 2675 2671
2667 2663 2659 2655 2651 2647 2643 2639
2635 2631 2627 2623 2619 2615 2611 2607
2603 2599 2595 2591 2587 2583 2579 2575
2571 2567 2563 2559 2555 2551 2547 2543
2539 2535 2531 2527 2523 2519 2515 2511
2507 2503 2499 2495 2491 2487 2483 2479
2475 2471 2467 2463 2459 2455 2451 2447
2443 2439 2435 2431 2427 2423 2419 2415
2411 2407 2403 2399 2395 2391 2387 2383
2379 2375 2371 2367 2363 2359 2355 2351
2347 2343 2339 2335 2331 2327 2323 2319
2315 2311 2307 2303 2299 2295 2291 2287
2283 2279 2275 2271 2267 2263 2259 2255
2251 2247 2243 2239 2235 2231 2227 2223
2219 2215 2211 2207 2203 2199 2195 2191
2187 2183 2179 2175 2171 2167 2163 2159
2155 2151 2147 2143 2139 2135 2131 2127
2123 2119 2115 2111 2107 2103 2099 2095
2091 2087 2083 2079 2075 2071 2067 2063
2059 2055 2051 2047 2043 2039 2035 2031
2027 2023 2019 2015 2011 2007 2003 1999
1995 1991 1987 1983 1979 1975 1971 1967
1963 1959 1955 1951 1947 1943 1939 1935
1931 1927 1923 1919 1915 1911 1907 1903
1899 1895 1891 1887 1883 1879 1875 1871
1867 1863 1859 1855 1851 1847 1843 1839
1835 1831 1827 1823 1819 1815 1811 1807
1803 1799 1795 1791 1787 1783 1779 1775

1771 1767 1763 1759 1755 1751 1747 1743
1739 1735 1731 1727 1723 1719 1715 1711
1707 1703 1699 1695 1691 1687 1683 1679
1675 1671 1667 1663 1659 1655 1651 1647
1643 1639 1635 1631 1627 1623 1619 1615
1611 1607 1603 1599 1595 1591 1587 1583
1579 1575 1571 1567 1563 1559 1555 1551
1547 1543 1539 1535 1531 1527 1523 1519
1515 1511 1507 1503 1499 1495 1491 1487
1483 1479 1475 1471 1467 1463 1459 1455
1451 1447 1443 1439 1435 1431 1427 1423
1419 1415 1411 1407 1403 1399 1395 1391
1387 1383 1379 1375 1371 1367 1363 1359
1355 1351 1347 1343 1339 1335 1331 1327
1323 1319 1315 1311 1307 1303 1299 1295
1291 1287 1283 1279 1275 1271 1267 1263
1259 1255 1251 1247 1243 1239 1235 1231
1227 1223 1219 1215 1211 1207 1203 1199
1195 1191 1187 1183 1179 1175 1171 1167
1163 1159 1155 1151 1147 1143 1139 1135
1131 1127 1123 1119 1115 1111 1107 1103
1099 1095 1091 1087 1083 1079 1075 1071
1067 1063 1059 1055 1051 1047 1043 1039
1035 1031 1027 1023 1019 1015 1011 1007
1003 999 995 991 987 983 979 975
971 967 963 959 955 951 947 943
939 935 931 927 923 919 915 911
907 903 899 895 891 887 883 879
875 871 867 863 859 855 851 847
843 839 835 831 827 823 819 815
811 807 803 799 795 791 787 783
779 775 771 767 763 759 755 751
747 743 739 735 731 727 723 719
715 711 707 703 699 695 691 687

683 679 675 671 667 663 659 655
651 647 643 639 635 631 627 623
619 615 611 607 603 599 595 591
587 583 579 575 571 567 563 559
555 551 547 543 539 535 531 527
523 519 515 511 507 503 499 495
491 487 483 479 475 471 467 463
459 455 451 447 443 439 435 431
427 423 419 415 411 407 403 399
395 391 387 383 379 375 371 367
363

*SET_NODE_LIST_TITLE
Node_set 606
$ SID DA1 DA2 DA3 DA4
606 0.0 0.0 0.0 0.0
$ NID1 NID2 NID3 NID4 NID5 NID6 NID7 NID8
16 68 64 60 56 52 48 44
40 36 32 28 24 20 3600 3596
3592 3588 3584 3580 3576 3572 3568 3564
3560 3556 3552 3548 3544 3540 3536 3532
3528 3524 3520 3516 3512 3508 3504 3500
3496 3492 3488 3484 3480 3476 3472 3468
3464 3460 3456 3452 3448 3444 3440 3436
3432 3428 3424 3420 3416 3412 3408 3404
3400 3396 3392 3388 3384 3380 3376 3372
3368 3364 3360 3356 3352 3348 3344 3340
3336 3332 3328 3324 3320 3316 3312 3308
3304 3300 3296 3292 3288 3284 3280 3276
3272 3268 3264 3260 3256 3252 3248 3244
3240 3236 3232 3228 3224 3220 3216 3212
3208 3204 3200 3196 3192 3188 3184 3180
3176 3172 3168 3164 3160 3156 3152 3148
3144 3140 3136 3132 3128 3124 3120 3116
3112 3108 3104 3100 3096 3092 3088 3084

3080 3076 3072 3068 3064 3060 3056 3052
3048 3044 3040 3036 3032 3028 3024 3020
3016 3012 3008 3004 3000 2996 2992 2988
2984 2980 2976 2972 2968 2964 2960 2956
2952 2948 2944 2940 2936 2932 2928 2924
2920 2916 2912 2908 2904 2900 2896 2892
2888 2884 2880 2876 2872 2868 2864 2860
2856 2852 2848 2844 2840 2836 2832 2828
2824 2820 2816 2812 2808 2804 2800 2796
2792 2788 2784 2780 2776 2772 2768 2764
2760 2756 2752 2748 2744 2740 2736 2732
2728 2724 2720 2716 2712 2708 2704 2700
2696 2692 2688 2684 2680 2676 2672 2668
2664 2660 2656 2652 2648 2644 2640 2636
2632 2628 2624 2620 2616 2612 2608 2604
2600 2596 2592 2588 2584 2580 2576 2572
2568 2564 2560 2556 2552 2548 2544 2540
2536 2532 2528 2524 2520 2516 2512 2508
2504 2500 2496 2492 2488 2484 2480 2476
2472 2468 2464 2460 2456 2452 2448 2444
2440 2436 2432 2428 2424 2420 2416 2412
2408 2404 2400 2396 2392 2388 2384 2380
2376 2372 2368 2364 2360 2356 2352 2348
2344 2340 2336 2332 2328 2324 2320 2316
2312 2308 2304 2300 2296 2292 2288 2284
2280 2276 2272 2268 2264 2260 2256 2252
2248 2244 2240 2236 2232 2228 2224 2220
2216 2212 2208 2204 2200 2196 2192 2188
2184 2180 2176 2172 2168 2164 2160 2156
2152 2148 2144 2140 2136 2132 2128 2124
2120 2116 2112 2108 2104 2100 2096 2092
2088 2084 2080 2076 2072 2068 2064 2060
2056 2052 2048 2044 2040 2036 2032 2028
2024 2020 2016 2012 2008 2004 2000 1996

1992 1988 1984 1980 1976 1972 1968 1964
1960 1956 1952 1948 1944 1940 1936 1932
1928 1924 1920 1916 1912 1908 1904 1900
1896 1892 1888 1884 1880 1876 1872 1868
1864 1860 1856 1852 1848 1844 1840 1836
1832 1828 1824 1820 1816 1812 1808 1804
1800 1796 1792 1788 1784 1780 1776 1772
1768 1764 1760 1756 1752 1748 1744 1740
1736 1732 1728 1724 1720 1716 1712 1708
1704 1700 1696 1692 1688 1684 1680 1676
1672 1668 1664 1660 1656 1652 1648 1644
1640 1636 1632 1628 1624 1620 1616 1612
1608 1604 1600 1596 1592 1588 1584 1580
1576 1572 1568 1564 1560 1556 1552 1548
1544 1540 1536 1532 1528 1524 1520 1516
1512 1508 1504 1500 1496 1492 1488 1484
1480 1476 1472 1468 1464 1460 1456 1452
1448 1444 1440 1436 1432 1428 1424 1420
1416 1412 1408 1404 1400 1396 1392 1388
1384 1380 1376 1372 1368 1364 1360 1356
1352 1348 1344 1340 1336 1332 1328 1324
1320 1316 1312 1308 1304 1300 1296 1292
1288 1284 1280 1276 1272 1268 1264 1260
1256 1252 1248 1244 1240 1236 1232 1228
1224 1220 1216 1212 1208 1204 1200 1196
1192 1188 1184 1180 1176 1172 1168 1164
1160 1156 1152 1148 1144 1140 1136 1132
1128 1124 1120 1116 1112 1108 1104 1100
1096 1092 1088 1084 1080 1076 1072 1068
1064 1060 1056 1052 1048 1044 1040 1036
1032 1028 1024 1020 1016 1012 1008 1004
1000 996 992 988 984 980 976 972
968 964 960 956 952 948 944 940
936 932 928 924 920 916 912 908

```
      904     900     896     892     888     884     880     876
      872     868     864     860     856     852     848     844
      840     836     832     828     824     820     816     812
      808     804     800     796     792     788     784     780
      776     772     768     764     760     756     752     748
      744     740     736     732     728     724     720     716
      712     708     704     700     696     692     688     684
      680     676     672     668     664     660     656     652
      648     644     640     636     632     628     624     620
      616     612     608     604     600     596     592     588
      584     580     576     572     568     564     560     556
      552     548     544     540     536     532     528     524
      520     516     512     508     504     500     496     492
      488     484     480     476     472     468     464     460
      456     452     448     444     440     436     432     428
      424     420     416     412     408     404     400     396
      392     388     384     380     376     372     368     364
      360     356     352     348     344     340     336     332
      328     324     320     316     312     308     304     300
      296     292     288     284     280     276     272     268
      264     260     256     252     248     244     240     236
      232     228     224     220     216     212     208     204
      200     196     192     188     184     180     176     172
      168     164     160     156     152     148     144     140
      136     132     128     124     120     116     112     108
      104     100      96      92      88      84      80      76
       72
$---+----1----+----2----+----3----+----4----+----5----+----6----+----7----+----8
$                                                   $
$                   COORDINATE SYSTEM CARDS                     $
$                                                   $
$---+----1----+----2----+----3----+----4----+----5----+----6----+----7----+----8
*DEFINE_COORDINATE_SYSTEM_TITLE
SYSTEM
```

```
$     CID       XO       YO       ZO       XL       YL       ZL
       1   0.03526 0.0058765-0.0058765-0.0642629 0.0058765 -1.000912
$      XP       YP       ZP
-0.0632820  1.0009610.00397963
*DEFINE_COORDINATE_SYSTEM_TITLE
SYSTEM
$     CID       XO       YO       ZO       XL       YL       ZL
       2   0.03526 0.0058765 0.0058765 0.1347829 0.0058765-0.9891587
$      XP       YP       ZP
 -0.063282  1.000961-0.0039796
*DEFINE_COORDINATE_SYSTEM_TITLE
SYSTEM
$     CID       XO       YO       ZO       XL       YL       ZL
       3   0.03526-0.0058765 0.0058765 0.1347829-0.0058765-0.9891587
$      XP       YP       ZP
  0.133802 0.98920760.01573262
*DEFINE_COORDINATE_SYSTEM_TITLE
SYSTEM
$     CID       XO       YO       ZO       XL       YL       ZL
       4   0.03526-0.0058765-0.0058765-0.0642629-0.0058765 -1.000912
$      XP       YP       ZP
  0.133802 0.9892076-0.0157326
$---+----1----+----2----+----3----+----4----+----5----+----6----+----7----+----8
$                                                     $
$                        NODE INFORMATION                         $
$                                                     $
$---+----1----+----2----+----3----+----4----+----5----+----6----+----7----+----8
*NODE
$   NID              X              Y              Z      TC      RC
      1            0.0       0.0058765      -0.0058765     0.0     0.0
      4            0.0      -0.0058765      -0.0058765     0.0     0.0
      2            0.0       0.0058765       0.0058765     0.0     0.0
      3            0.0      -0.0058765       0.0058765     0.0     0.0
      5     0.01175333     0.005876501    -0.005876501     0.0     0.0
```

```
       8      0.01175333    -0.005876501    -0.005876501      0.0      0.0
       6      0.01175333     0.005876501     0.005876501      0.0      0.0
       7      0.01175333    -0.005876501     0.005876501      0.0      0.0
       9      0.02350667       0.0058765      -0.0058765      0.0      0.0
      12      0.02350667      -0.0058765      -0.0058765      0.0      0.0
      10      0.02350666       0.0058765       0.0058765      0.0      0.0
***  Nodes 11 – 3597 not included to conserve space
    3598       178.6353        17.8659        17.8659      0.0      0.0
    3599       178.6353       -17.8659        17.8659      0.0      0.0
$---+----1----+----2----+----3----+----4----+----5----+----6----+----7----+----8
$                                                                             $
$                        ELEMENTS INFORMATION                                 $
$                                                                             $
$---+----1----+----2----+----3----+----4----+----5----+----6----+----7----+----8
$---+----1----+----2----+----3----+----4----+----5----+----6----+----7----+----8
$                                                                             $
$                          SOLID ELEMENTS                                     $
$                                                                             $
$---+----1----+----2----+----3----+----4----+----5----+----6----+----7----+----8
*ELEMENT_SOLID
$   EID     PID    NID1    NID2    NID3    NID4    NID5    NID6    NID7    NID8
     805     100       1       2       3       4       5       6       7       8
     806     100       5       6       7       8       9      10      11      12
     807     100       9      10      11      12      13      14      15      16
     808     200      13      14      15      16      17      18      19      20
     809     200      17      18      19      20      21      22      23      24
     810     200      21      22      23      24      25      26      27      28
***   Elements 811 – 1702 not included to conserve space
    1703     600    3593    3594    3595    3596    3597    3598    3599    3600
$---+----1----+----2----+----3----+----4----+----5----+----6----+----7----+----8
*END
```

APPENDIX D LS-DYNA FILE FOR 3-D DEEP SPHERICAL BUBBLE MODEL

The LS-DYNA input file is given for the test case from Section 3.2.2.2.2.1. Input files for all other test cases are the same except input cards containing node and element information. To decrease space, not all elements and nodes are listed.

```
*KEYWORD
*TITLE
LARGE ELEMENT DEEP SPHERICAL BUBBLE EIGHTH SPHERE MODEL
$
$-----------------------------------------------------
$
$ ANALYSIS OF DEEP SPHERICAL BUBBLE PROBLEM
$ WRITTEN BY KEITH G. WEBSTER
$
$
$ SET ID:  #       DESCRIPTION
$
$         1      X-Y FACE SEGMENT SET
$         2      Y-Z FACE SEGMENT SET
$         3      X-Z FACE SEGMENT SET
$         4      ROUND FACE NRBC SEGMENT SET
$         5      ROUND FACE NRBC SEGMENT SET
$         6      ROUND FACE NRBC SEGMENT SET
$         7      DET. PT. NODE SET
$         8      X-AXIS NODE SET
$         9      Y-AXIS NODE SET
$         10     Z-AXIS NODE SET
$         11     X-Y FACE NODE SET MINUS SET 7,8,9
$         12     Y-Z FACE NODE SET MINUS SET 7,9,10
$         13     X-Z FACE NODE SET MINUS SET 7,8,10
$         14     X-Y FACE RIGIDWALL NODE SET
```

```
$          15      Y-Z FACE RIGIDWALL NODE SET
$          16      X-Z FACE RIGIDWALL NODE SET
$          17      ROUND FACE NODE SET FOR NSIDEBC
$
$------------------------------------------------------
$
$ ANALYSIS CONTROL CARDS
$
*CONTROL_TERMINATION
1.00E-03,0,0.000E+00,0.000E+00,0.000E+00
*CONTROL_TIMESTEP
0,0.67,0,0.000E+00,0.000E+00,0,0,0
*CONTROL_HOURGLASS
1,1.0E-04
*CONTROL_ACCURACY
0,3,0
*CONTROL_ENERGY
2,2,2,2
*CONTROL_DAMPING
250,0.001,0.995
*CONTROL_OUTPUT
0,0,0,0,0.000E+00,0,100,5000
0
*CONTROL_ALE
3,10,2,0.0,0.0,0,1.0,0
0.000E+00,1.000E+20,1.,1.000E-06,0,2,1.891e+06,17
$
$ ANALYSIS OUTPUT CARDS
$
*DATABASE_BINARY_D3PLOT
1.000E-05,0
*DATABASE_BINARY_D3THDT
1.000E-05,0
*DATABASE_EXTENT_BINARY
```

```
0,0,3,1,1,1,1,1
0,0,0,0,0,0,2
1
*DATABASE_GLSTAT
1.0E-05,1
*DATABASE_MATSUM
1.0E-05,1
*DATABASE_TRACER
0,1,0.4618,0.4618,0.4618
*DATABASE_TRHIST
1.0E-05,1
$
$ FLUID DEFINITION CARDS
$
*PART
FLUID
200,201,202,203,204,0,0,0
*SECTION_SOLID_ALE
201,11
0.0,0.0,0,1.0,0,1.00E+20,0.5
*MAT_NULL
202,1025.,-1.000E-20,1.13E-03,0.,0.,0.,0.
*EOS_GRUNEISEN
203,2417.52,1.41,0.0,0.0,1.0,0.0,1.891E+06
1.
*HOURGLASS
204,1,1.000E-04,1,1.5,0.06
$
$ EXPLOSIVE DEFINITION CARDS
$
*PART
EXPLOSIVE
100,101,102,103,104,0,0,0
*SECTION_SOLID_ALE
```

```
101,11
0.25,0.25,0,0.5,0,1.00E+20,1
*MAT_HIGH_EXPLOSIVE_BURN
102,1630.,6930.,2.1E+10,0.5
*EOS_JWL
103,3.71E+11,3.23E+09,4.15,0.95,0.3,7.00E+09,1.
*HOURGLASS
104,1,1.0E-04,1,1.5,0.06
$
$ ALE DEFINITION CARDS
$
*SET_PART_LIST
300
100,200
*ALE_MULTI-MATERIAL_GROUP
100,1
200,1
*ALE_REFERENCE_SYSTEM_GROUP
300,0,8,0,0,0,0,1
0.,0.,0.,0,0.5
$
$ ANALYSIS DETONATION CARDS
$
*INITIAL_DETONATION
0,0.,0.,0.,0.0
$
$ ANALYSIS BOUNDARY CONDITION CARDS
$
*BOUNDARY_SPC_SET
7,0,1,1,1,1,1,1
*BOUNDARY_SPC_SET
8,0,0,1,1,1,1,1
*BOUNDARY_SPC_SET
9,0,1,0,1,1,1,1
```

```
*BOUNDARY_SPC_SET
10,0,1,1,0,1,1,1
*BOUNDARY_SPC_SET
11,0,0,0,1,1,1,1
*BOUNDARY_SPC_SET
12,0,1,0,0,1,1,1
*BOUNDARY_SPC_SET
13,0,0,1,0,1,1,1
$
$ ANALYSIS MODEL GEOMETRY CARDS
$
$ NODES
$
*NODE
1,0.000000000E+00,0.000000000E+00,0.000000000E+00,0,0
2,0.000000000E+00,0.000000000E+00,2.666666987E-04,0,0
3,0.000000000E+00,0.000000000E+00,5.333333975E-04,0,0
4,0.000000000E+00,0.000000000E+00,8.000000962E-04,0,0
5,0.000000000E+00,0.000000000E+00,1.066666795E-03,0,0
6,0.000000000E+00,0.000000000E+00,1.333333435E-03,0,0
7,0.000000000E+00,0.000000000E+00,1.600000076E-03,0,0
8,0.000000000E+00,0.000000000E+00,1.866666717E-03,0,0
9,0.000000000E+00,0.000000000E+00,2.133333590E-03,0,0
10,0.000000000E+00,0.000000000E+00,2.400000114E-03,0,0
***
74030,0.990744114,0.901596904,0.674943805,0,0
74031,0.968136549,0.882208109,0.731040597,0,0
74032,0.943835080,0.861285985,0.785723686,0,0
74033,0.917904973,0.838883340,0.838883340,0,0
$
$ ELEMENT CARDS FOR SOLID ELEMENTS
$
*ELEMENT_SOLID
1,100,1,257,273,17,2,258,274,18
```

2,100,257,513,529,273,258,514,530,274
3,100,513,769,785,529,514,770,786,530
4,100,769,1025,1041,785,770,1026,1042,786
5,100,1025,1281,1297,1041,1026,1282,1298,1042
6,100,1281,1537,1553,1297,1282,1538,1554,1298
7,100,1537,1793,1809,1553,1538,1794,1810,1554
8,100,1793,2049,2065,1809,1794,2050,2066,1810
9,100,2049,2305,2321,2065,2050,2306,2322,2066
10,100,2305,2561,2577,2321,2306,2562,2578,2322
***
68845,200,72683,72908,52133,52118,28915,28916,28923,28922
68846,200,72908,73133,52148,52133,28916,28917,28924,28923
68847,200,73133,73358,52163,52148,28917,28918,28925,28924
68848,200,73358,73583,52178,52163,28918,28919,28926,28925
68849,200,73583,73808,52193,52178,28919,28920,28927,28926
68850,200,73808,74033,52208,52193,28920,28921,28928,28927
$
$ Node set 7
$
*SET_NODE_LIST
7,0.,0.,0.,0.
1
$
$ Node set 8
$
*SET_NODE_LIST
8,0.,0.,0.,0.
1,257,513,769,1025,1281,1537,1793
2049,2305,2561,2817,3073,3329,3585,3841
52209,52434,52659,52884,53109,53334,53559,53784
54009,54234,54459,54684,54909,55134,55359,55584
55809,56034,56259,56484,56709,56934,57159,57384
57609,57834,58059,58284,58509,58734,58959,59184
59409,59634,59859,60084,60309,60534,60759,60984

61209,61434,61659,61884,62109,62334,62559,62784
63009,63234,63459,63684,63909,64134,64359,64584
64809,65034,65259,65484,65709,65934,66159,66384
66609,66834,67059,67284,67509,67734,67959,68184
68409,68634,68859,69084,69309,69534,69759,69984
70209,70434,70659,70884,71109,71334,71559,71784
72009,72234,72459,72684,72909,73134,73359,73584
73809
$
$ Node set 9
$
*SET_NODE_LIST
9,0.,0.,0.,0.
1,17,33,49,65,81,97,113
129,145,161,177,193,209,225,241
28929,28944,28959,28974,28989,29004,29019,29034
29049,29064,29079,29094,29109,29124,29139,29154
29169,29184,29199,29214,29229,29244,29259,29274
29289,34929,34944,34959,34974,34989,35004,35019
35034,35049,35064,35079,35094,35109,38049,38064
38079,38094,38109,38124,38139,38154,38169,38184
38199,38214,38229,41169,41184,41199,41214,41229
41244,41259,41274,41289,41304,41319,41334,41349
44289,44304,44319,44334,44349,44364,44379,44394
44409,44424,44439,44454,44469,47409,47424,47439
47454,47469,47484,47499,47514,47529,47544,47559
47574,47589,50529,50544,50559,50574,50589,50604
50619
$
$ Node set 10
$
*SET_NODE_LIST
10,0.,0.,0.,0.
1,2,3,4,5,6,7,8

9,10,11,12,13,14,15,16
4097,4098,4099,4100,4101,4102,4103,4104
4105,4106,4107,4108,4109,4110,4111,4112
4113,4114,4115,4116,4117,4118,4119,4120
4121,10497,10498,10499,10500,10501,10502,10503
10504,10505,10506,10507,10508,10509,13825,13826
13827,13828,13829,13830,13831,13832,13833,13834
13835,13836,13837,17153,17154,17155,17156,17157
17158,17159,17160,17161,17162,17163,17164,17165
20481,20482,20483,20484,20485,20486,20487,20488
20489,20490,20491,20492,20493,23809,23810,23811
23812,23813,23814,23815,23816,23817,23818,23819
23820,23821,27137,27138,27139,27140,27141,27142
27143
$
$ Node set 11
$
*SET_NODE_LIST
11,0.,0.,0.,0.
18,34,50,66,82,98,114,130
146,162,178,194,210,226,242,28930
28945,28960,28975,28990,29005,29020,29035,29050
29065,29080,29095,29110,29125,29140,29155,29170
29185,29200,29215,29230,29245,29260,29275,29290
34930,34945,34960,34975,34990,35005,35020,35035
35050,35065,35080,35095,35110,38050,38065,38080
38095,38110,38125,38140,38155,38170,38185,38200
***
27232,27239,27149,27156,27163,27170,27177,27184
27191,27198,27205,27212,27219,27226,27233,27240
27150,27157,27164,27171,27178,27185,27192,27199
27206,27213,27220,27227,27234,27241
$
$ Node set 12

```
$
*SET_NODE_LIST
12,0.,0.,0.,0.
273,529,785,1041,1297,1553,1809,2065
2321,2577,2833,3089,3345,3601,3857,52224
52449,52674,52899,53124,53349,53574,53799,54024
54249,54474,54699,54924,55149,55374,55599,55824
56049,56274,56499,56724,56949,57174,57399,57624
57849,58074,58299,58524,58749,58974,59199,59424
59649,59874,60099,60324,60549,60774,60999,61224
***
51339,51444,51549,51654,51759,51864,51969,52074
50724,50829,50934,51039,51144,51249,51354,51459
51564,51669,51774,51879,51984,52089
$
$ Node set 13
$
*SET_NODE_LIST
13,0.,0.,0.,0.
258,514,770,1026,1282,1538,1794,2050
2306,2562,2818,3074,3330,3586,3842,52210
52435,52660,52885,53110,53335,53560,53785,54010
54235,54460,54685,54910,55135,55360,55585,55810
56035,56260,56485,56710,56935,57160,57385,57610
***
27926,28038,28150,28262,28374,28486,28598,28710
27255,27367,27479,27591,27703,27815,27927,28039
28151,28263,28375,28487,28599,28711
$
$ Node set 14
$
*SET_NODE_LIST
14,0.,0.,0.,0.
1,17,33,49,65,81,97,113
```

```
129,145,161,177,193,209,225,241
28929,28944,28959,28974,28989,29004,29019,29034
29049,29064,29079,29094,29109,29124,29139,29154
***
27191,27198,27205,27212,27219,27226,27233,27240
27143,27150,27157,27164,27171,27178,27185,27192
27199,27206,27213,27220,27227,27234,27241
$
$ Node set 15
$
*SET_NODE_LIST
15,0.,0.,0.,0.
1,257,513,769,1025,1281,1537,1793
2049,2305,2561,2817,3073,3329,3585,3841
52209,52434,52659,52884,53109,53334,53559,53784
54009,54234,54459,54684,54909,55134,55359,55584
***
51339,51444,51549,51654,51759,51864,51969,52074
50619,50724,50829,50934,51039,51144,51249,51354
51459,51564,51669,51774,51879,51984,52089
$
$ Node set 16
$
*SET_NODE_LIST
16,0.,0.,0.,0.
1,257,513,769,1025,1281,1537,1793
2049,2305,2561,2817,3073,3329,3585,3841
52209,52434,52659,52884,53109,53334,53559,53784
54009,54234,54459,54684,54909,55134,55359,55584
***
27926,28038,28150,28262,28374,28486,28598,28710
27143,27255,27367,27479,27591,27703,27815,27927
28039,28151,28263,28375,28487,28599,28711
$
```

```
$ Node set 17
$
*SET_NODE_LIST
17,0.,0.,0.,0.
27143,27255,27367,27479,27591,27703,27815,27927
28039,28151,28263,28375,28487,28599,28711,28823
27150,27262,27374,27486,27598,27710,27822,27934
28046,28158,28270,28382,28494,28606,28718,28830
***
51997,52102,50633,50738,50843,50948,51053,51158
51263,51368,51473,51578,51683,51788,51893,51998
52103
$
$ Face set 1
$
*SET_SEGMENT
1,0.000E+00,0.000E+00,0.000E+00,0.000E+00
1,17,18,2,0.000E+00,0.000E+00,0.000E+00,0.000E+00
17,33,34,18,0.000E+00,0.000E+00,0.000E+00,0.000E+00
28929,28944,28945,28930,0.000E+00,0.000E+00,0.000E+00,0.000E+00
***
    4267,4292,4293,4268,0.000E+00,0.000E+00,0.000E+00,0.000E+00
    17288,17301,17302,17289,0.000E+00,0.000E+00,0.000E+00,0.000E+00
    27237,27244,27245,27238,0.000E+00,0.000E+00,0.000E+00,0.000E+00
$
$ Face set 2
$
*SET_SEGMENT
2,0.000E+00,0.000E+00,0.000E+00,0.000E+00
1,257,273,17,0.000E+00,0.000E+00,0.000E+00,0.000E+00
257,513,529,273,0.000E+00,0.000E+00,0.000E+00,0.000E+00
769,1025,1041,785,0.000E+00,0.000E+00,0.000E+00,0.000E+00
***
```

71919,72144,72159,71934,0.000E+00,0.000E+00,0.000E+00,0.000E+00
70389,70614,70629,70404,0.000E+00,0.000E+00,0.000E+00,0.000E+00
71769,71994,50484,50469,0.000E+00,0.000E+00,0.000E+00,0.000E+00
$
$ Face set 3
$
*SET_SEGMENT
3,0.000E+00,0.000E+00,0.000E+00,0.000E+00
1,2,258,257,0.000E+00,0.000E+00,0.000E+00,0.000E+00
257,258,514,513,0.000E+00,0.000E+00,0.000E+00,0.000E+00
***
55813,55814,56039,56038,0.000E+00,0.000E+00,0.000E+00,0.000E+00
63243,63244,63469,63468,0.000E+00,0.000E+00,0.000E+00,0.000E+00
$
$ Face set 4
$
*SET_SEGMENT
4,0.000E+00,0.000E+00,0.000E+00,0.000E+00
27143,27255,27262,27150,0.000E+00,0.000E+00,0.000E+00,0.000E+00
27262,27374,27381,27269,0.000E+00,0.000E+00,0.000E+00,0.000E+00
***
28340,28452,28459,28347,0.000E+00,0.000E+00,0.000E+00,0.000E+00
28578,28690,28697,28585,0.000E+00,0.000E+00,0.000E+00,0.000E+00
$
$ Face set 5
$
*SET_SEGMENT
5,0.000E+00,0.000E+00,0.000E+00,0.000E+00
73809,73824,73825,73810,0.000E+00,0.000E+00,0.000E+00,0.000E+00
73839,73854,73855,73840,0.000E+00,0.000E+00,0.000E+00,0.000E+00
***
73878,73893,73894,73879,0.000E+00,0.000E+00,0.000E+00,0.000E+00
73910,73925,73926,73911,0.000E+00,0.000E+00,0.000E+00,0.000E+00
73942,73957,73958,73943,0.000E+00,0.000E+00,0.000E+00,0.000E+00

```
$
$ Face set 6
$
*SET_SEGMENT
6,0.000E+00,0.000E+00,0.000E+00,0.000E+00
50619,50620,50725,50724,0.000E+00,0.000E+00,0.000E+00,0.000E+00
50724,50725,50830,50829,0.000E+00,0.000E+00,0.000E+00,0.000E+00
***
50629,50630,50735,50734,0.000E+00,0.000E+00,0.000E+00,0.000E+00
52101,52102,52207,52206,0.000E+00,0.000E+00,0.000E+00,0.000E+00
51157,51158,51263,51262,0.000E+00,0.000E+00,0.000E+00,0.000E+00
*END
```

APPENDIX E LS-DYNA FILE FOR 1-D PLATE MODEL

The LS-DYNA input file is given. To decrease space, not all elements and nodes are listed.

```
*KEYWORD
*TITLE
1-D FLUID BLOCK MODEL
$-----------------------------------------------------
$
$ ANALYSIS OF 1-D PLANE WAVE - PLATE PROBLEM
$ WRITTEN BY KEITH G. WEBSTER
$
$
$ SET ID:   #       DESCRIPTION
$
$         1      Y-Z CONSTRAINED NODE SET
$         2      X-Y-Z CONSTRAINED NODE SET
$         3      EBC EXCLUDED NODE SET
$         4      PLATE EDGES NODE SET
$         5      PLATE INTERNAL NODE SET
$         6      PRESSURE LOAD SEGMENT SET
$         7      NRBC SEGMENT SET
$
$-----------------------------------------------------
$
$ ANALYSIS CONTROL CARDS
$
*CONTROL_TERMINATION
0.50E-02,0,0.000E+00,0.000E+00,0.000E+00
*CONTROL_TIMESTEP
0,0.67,0,0.000E+00,0.000E+00,0,0,0
*CONTROL_HOURGLASS
1,1.0E-04
```

```
*CONTROL_ACCURACY
0,3,0
*CONTROL_ENERGY
2,2,2,2
*CONTROL_DYNAMIC_RELAXATION
250,0.001,0.995
*CONTROL_OUTPUT
0,0,0,0,0.000E+00,0,100,5000
0
*CONTROL_ALE
3,1,2,0.0,0.0,0,1.0,0
0.000E+00,1.000E+20,1.,1.000E-06,0,2,0.0,3
$
$ ANALYSIS OUTPUT CARDS
$
*DATABASE_BINARY_D3PLOT
1.000E-06,0
*DATABASE_BINARY_D3THDT
1.000E-06,0
*DATABASE_EXTENT_BINARY
0,0,3,1,1,1,1,1
0,0,0,0,0,0,2
1
*DATABASE_GLSTAT
1.0E-06,1
*DATABASE_MATSUM
1.0E-06,1
*DATABASE_TRACER
0,1,1.0,0.25,0.25
0,2,2.0,0.25,0.25
0,3,2.49,0.25,0.25
*DATABASE_TRHIST
1.0E-06,1
$$$
```

```
*SET_NODE_LIST
300,0.0,0.0,0.0,0.0
1858
$
*DATABASE_NODAL_FORCE_GROUP
300
*DATABASE_NODFOR
1.0E-06,1
$
$ FLUID DEFINITION CARDS
$
*PART
FLUID
200,201,202,203,204,0,0,0
*SECTION_SOLID_ALE
201,5
0.0,0.0,0,1.0,0,1.00E+20,0.5
*MAT_NULL
202,1025.,-1.000E-20,0.0E-00,0.,0.,0.,0.
*EOS_GRUNEISEN
203,2417,1.41,0.0,0.0,1.0,0.0,0.0
1.
*HOURGLASS
204,1,1.000E-04,1,1.5,0.06
$
$ STRUCTURE DEFINITION CARDS
$
*PART
PLATE
100,101,102,,104,0,0,0
*SECTION_SHELL
101,2,0.000E+00,3.00,0.000E+00,0.000E+00,0
0.0254,0.0254,0.0254,0.0254,0.000E+00
*MAT_PLASTIC_KINEMATIC
```

```
102,7780.0,2.06E+11,0.281,3.55E+08,0.0,0.0
0.000E+00,0.000E+00,0.000E+00
*HOURGLASS
104,1,1.000E-04,1,1.5,0.06
$
*CONSTRAINED_LAGRANGE_IN_SOLID
100,200,1,1,0,4,1,0
0,1.0E+10,0.1
$
$ ALE DEFINITION CARDS
$
*SET_PART_LIST
500
100,200
*ALE_REFERENCE_SYSTEM_GROUP
500,0,8,0,0,0,0,1
0.,0.,0.,0,0.5
$
$ NODAL CONSTRAINT CARDS
$
*BOUNDARY_SPC_SET
1,0,0,1,1,1,1,1
*BOUNDARY_SPC_SET
2,0,0,1,1,1,1,1
$ Plate
*BOUNDARY_SPC_SET
5,0,0,1,1,1,1,1
$
$ PRESSURE LOAD CARD
$
*LOAD_SEGMENT_SET
6,2,1.0,0.000E+00
$
$ BOUNDARY CONDITION CARD
```

```
$
*BOUNDARY_NON_REFLECTING
7,0.0,0.0
$
$ ANALYSIS MODEL GEOMETRY CARDS
$
$ NODES
$
*NODE
1,0.000000000E+00,0.000000000E+00,0.000000000E+00,0,0
2,0.000000000E+00,0.000000000E+00,0.100000001,0,0
3,0.000000000E+00,0.000000000E+00,0.200000003,0,0
4,0.000000000E+00,0.000000000E+00,0.300000012,0,0
***
1870,2.50000000,0.500000000,0.300000012,0,0
1871,2.50000000,0.500000000,0.400000006,0,0
1872,2.50000000,0.500000000,0.500000000,0,0
$
$ ELEMENT CARDS FOR SOLID ELEMENTS
$
*ELEMENT_SOLID
1,200,1,37,43,7,2,38,44,8
2,200,37,73,79,43,38,74,80,44
3,200,73,109,115,79,74,110,116,80
4,200,109,145,151,115,110,146,152,116
5,200,145,181,187,151,146,182,188,152
***
1249,200,1757,1793,1799,1763,1758,1794,1800,1764
1250,200,1793,1829,1835,1799,1794,1830,1836,1800
$
$ ELEMENT CARDS FOR SHELL ELEMENTS
$
*ELEMENT_SHELL_THICKNESS
1,100,1837,1843,1844,1838
```

0.000000E+00,0.000000E+00,0.000000E+00,0.000000E+00
2,100,1843,1849,1850,1844
0.000000E+00,0.000000E+00,0.000000E+00,0.000000E+00
***
24,100,1859,1865,1866,1860
0.000000E+00,0.000000E+00,0.000000E+00,0.000000E+00
25,100,1865,1871,1872,1866
0.000000E+00,0.000000E+00,0.000000E+00,0.000000E+00
$
$ Node set yz
$
*SET_NODE_LIST
1,0.,0.,0.,0.
37,73,109,145,181,217,253,289
325,361,397,433,469,505,541,577
613,649,685,721,757,793,829,865
901,937,973,1009,1045,1081,1117,1153
***
1296,1332,1368,1404,1440,1476,1512,1548
1584,1620,1656,1692,1728,1764,1800,1836
$
$ Node set xyz
$
*SET_NODE_LIST
2,0.,0.,0.,0.
1,7,13,19,25,31,2,8
14,20,26,32,3,9,15,21
27,33,4,10,16,22,28,34
5,11,17,23,29,35,6,12
18,24,30,36
$
$ Node set ebc
$
*SET_NODE_LIST

```
3,0.,0.,0.,0.
1801,1807,1813,1819,1825,1831,1802,1808
1814,1820,1826,1832,1803,1809,1815,1821
1827,1833,1804,1810,1816,1822,1828,1834
1805,1811,1817,1823,1829,1835,1806,1812
1818,1824,1830,1836
$
$ Node set pyz
$
*SET_NODE_LIST
5,0.,0.,0.,0.
1837,1843,1849,1855,1861,1867,1838,1844
1850,1856,1862,1868,1839,1845,1851,1857
1863,1869,1840,1846,1852,1858,1864,1870
1841,1847,1853,1859,1865,1871,1842,1848
1854,1860,1866,1872
$
$ Face set pload
$
*SET_SEGMENT
6,0.000E+00,0.000E+00,0.000E+00,0.000E+00
1,7,8,2,0.000E+00,0.000E+00,0.000E+00,0.000E+00
7,13,14,8,0.000E+00,0.000E+00,0.000E+00,0.000E+00
13,19,20,14,0.000E+00,0.000E+00,0.000E+00,0.000E+00
25,31,32,26,0.000E+00,0.000E+00,0.000E+00,0.000E+00
20,26,27,21,0.000E+00,0.000E+00,0.000E+00,0.000E+00
10,16,17,11,0.000E+00,0.000E+00,0.000E+00,0.000E+00
29,35,36,30,0.000E+00,0.000E+00,0.000E+00,0.000E+00
15,21,22,16,0.000E+00,0.000E+00,0.000E+00,0.000E+00
5,11,12,6,0.000E+00,0.000E+00,0.000E+00,0.000E+00
8,14,15,9,0.000E+00,0.000E+00,0.000E+00,0.000E+00
3,9,10,4,0.000E+00,0.000E+00,0.000E+00,0.000E+00
22,28,29,23,0.000E+00,0.000E+00,0.000E+00,0.000E+00
26,32,33,27,0.000E+00,0.000E+00,0.000E+00,0.000E+00
```

27,33,34,28,0.000E+00,0.000E+00,0.000E+00,0.000E+00
17,23,24,18,0.000E+00,0.000E+00,0.000E+00,0.000E+00
19,25,26,20,0.000E+00,0.000E+00,0.000E+00,0.000E+00
2,8,9,3,0.000E+00,0.000E+00,0.000E+00,0.000E+00
21,27,28,22,0.000E+00,0.000E+00,0.000E+00,0.000E+00
16,22,23,17,0.000E+00,0.000E+00,0.000E+00,0.000E+00
9,15,16,10,0.000E+00,0.000E+00,0.000E+00,0.000E+00
11,17,18,12,0.000E+00,0.000E+00,0.000E+00,0.000E+00
14,20,21,15,0.000E+00,0.000E+00,0.000E+00,0.000E+00
4,10,11,5,0.000E+00,0.000E+00,0.000E+00,0.000E+00
28,34,35,29,0.000E+00,0.000E+00,0.000E+00,0.000E+00
23,29,30,24,0.000E+00,0.000E+00,0.000E+00,0.000E+00
$
$ Face set nrbc
$
*SET_SEGMENT
7,0.000E+00,0.000E+00,0.000E+00,0.000E+00
1801,1807,1808,1802,0.000E+00,0.000E+00,0.000E+00,0.000E+00
1807,1813,1814,1808,0.000E+00,0.000E+00,0.000E+00,0.000E+00
1819,1825,1826,1820,0.000E+00,0.000E+00,0.000E+00,0.000E+00
1814,1820,1821,1815,0.000E+00,0.000E+00,0.000E+00,0.000E+00
1804,1810,1811,1805,0.000E+00,0.000E+00,0.000E+00,0.000E+00
***
1827,1833,1834,1828,0.000E+00,0.000E+00,0.000E+00,0.000E+00
1822,1828,1829,1823,0.000E+00,0.000E+00,0.000E+00,0.000E+00
1817,1823,1824,1818,0.000E+00,0.000E+00,0.000E+00,0.000E+00
$
$ 1-D PRESSURE WAVE
$
*DEFINE_CURVE
2,2,1.0,-1.0,0.0,0.0,0
0.00E+00,4.75E+07
9.17E-07,4.68E+07
2.75E-06,4.55E+07

3.67E-06,4.49E+07
5.50E-06,4.36E+07
7.34E-06,4.24E+07
9.17E-06,4.12E+07
1.19E-05,3.95E+07
1.47E-05,3.79E+07
1.65E-05,3.68E+07
1.83E-05,3.58E+07
2.02E-05,3.48E+07
2.29E-05,3.34E+07
2.57E-05,3.20E+07
2.93E-05,3.03E+07
3.30E-05,2.86E+07
3.58E-05,2.75E+07
3.85E-05,2.64E+07
4.31E-05,2.46E+07
4.59E-05,2.36E+07
5.04E-05,2.21E+07
5.50E-05,2.06E+07
5.96E-05,1.93E+07
6.33E-05,1.83E+07
6.79E-05,1.71E+07
7.24E-05,1.60E+07
7.79E-05,1.48E+07
8.34E-05,1.37E+07
8.99E-05,1.26E+07
9.63E-05,1.15E+07
1.03E-04,1.06E+07
1.14E-04,9.16E+06
1.26E-04,7.89E+06
1.28E-04,7.63E+06
1.38E-04,6.76E+06
1.47E-04,6.16E+06
1.61E-04,5.26E+06

1.73E-04,4.67E+06
1.91E-04,3.99E+06
2.07E-04,3.50E+06
2.19E-04,3.22E+06
2.38E-04,2.86E+06
2.60E-04,2.58E+06
2.75E-04,2.43E+06
2.94E-04,2.28E+06
3.14E-04,2.18E+06
3.33E-04,2.10E+06
3.55E-04,2.04E+06
3.79E-04,1.99E+06
3.98E-04,1.96E+06
4.25E-04,1.94E+06
4.45E-04,1.93E+06
4.71E-04,1.91E+06
5.21E-04,1.90E+06
5.49E-04,1.90E+06
5.84E-04,1.89E+06
7.14E-04,1.89E+06
1.18E-03,1.89E+06
1.68E-03,1.89E+06
2.19E-03,1.89E+06
2.72E-03,1.89E+06
3.23E-03,1.89E+06
3.77E-03,1.89E+06
4.28E-03,1.89E+06
4.79E-03,1.89E+06
5.24E-03,1.89E+06
5.84E-03,1.89E+06
6.33E-03,1.89E+06
6.86E-03,1.89E+06
7.35E-03,1.89E+06
7.88E-03,1.89E+06

8.35E-03,1.89E+06
8.85E-03,1.89E+06
9.42E-03,1.89E+06
9.89E-03,1.89E+06
1.00E-02,1.89E+06
*END

APPENDIX F 1-D PLATE ANALYTICAL SOLUTION

Reference [38], [39], and [40] are used to derive the 1-D Plate Analytical solution.

Interactions of an Acoustic Peak Approximation Shock Wave with an Infinite Plate Supported by a Spring-damper System

(Shock Wave is treated as a Plane Propagating Wave from an Initial Disturbanc
where the Initial Disturbance is the Peak Approximation Shock Wave Calculatec
and Determined at the Specified Standoff Distance)

calculations prepared by: Dr. J.A.W. Sajdak

last modified: 03/30/05

revised by: Keith Webster

revised for comparison to LS-DYNA test run 1D_5x5_0.5_Plate_a.dyn

last revision: 04/04/05

Define Fluid Properties :

$\rho := 1025$ Density (kg/m^3)

$c := 2417$ Acoustic Speed of Sound in Fluid (m/s)

$P_{fs} := 101325.93$ $P_{fs} := 0$ Free Surface Pressure (Pa)

$a := 9.81$ Acceleration due to gravity (m/s^2)

Define Plate Properties :

$\rho_{plate} := 7780$ Plate Density (kg/m^3)

$A_{plate} := 0.5 \cdot 0.5$ $A_{plate} = 0.25$ Frontal Area of plate (m^2)

$t_{plate} := 0.0254$ $0.0254\,m = 1\,in$ Plate thickness (m)

$M_{plate} := \rho_{plate} \cdot (A_{plate} \cdot t_{plate})$ $M_{plate} = 49.403$ Plate Mass (kg)

$\mu := \frac{M_{plate}}{A_{plate}}$ $\mu = 197.612$ Plate mass per unit area (kg/m^2)

$\beta := 1.7 \cdot \rho \cdot c$ $\beta = 4.261171 \times 10^{6}$ Damping coefficient per unit area of plate

$\kappa := 1.9 \cdot \left[\frac{(\beta - \rho \cdot c)^2}{4 \cdot \mu} \right]$ $\kappa = 7.64797255 \times 10^{9}$ Spring (Restoring) coefficient per unit area of plate

$x_0 := 3$ Initial spacial location of plate measured along x-axis (m)

Define Explosive Charge (TNT) Parameters :

$Z := 0$	Explosive Depth (Surface to Charge Center, Positive toward center of earth) (m)
$W := 0.299$	Explosive Charge Weight (assumed spherical charge) (kg)
$R_{standoff} := 0.01$	Standoff Distance from center of charge to plate (assumed plate orthogonal to blast wave) (m)
$K_P := 36.27 \cdot 10^4$	Peak Shock Pressure Coefficient
$\alpha_P := 1.16$	Peak Shock Pressure Power Constant
$K_\tau := 0.24349$	Pressure Decay Time Coefficient
$\alpha_\tau := -0.23$	Pressure Decay Power Constant

Define Static Pressure at Depth Z :

$P_{static} := P_{fs} + \rho \cdot a \cdot Z$ $\quad P_{static} = 1.0132593 \times 10^5$ (Pa)

Define Spacial Peak Pressure Decay Constant for "Right" (positive x-dir.) traveling wave :

$$b := \frac{1}{c \cdot \tau} \qquad b = 6.6806689 \qquad \text{(1/m)}$$

Define "Feasibility" Condition Variable :

$$Q := (\beta - \rho \cdot c)^2 - 4 \cdot \mu \cdot \kappa \qquad Q = -2.86357481 \times 10^{12}$$

Define Plate Displacement Function :

$$x_b(t) := \begin{cases} \left[\frac{-4 \cdot \mu \cdot P_{peak}}{(\rho \cdot c - \beta)^2 - Q} \cdot \left[\left[\frac{\sqrt{-Q}}{Q} \cdot e^{-\left(\frac{\beta - \rho \cdot c}{2 \cdot \mu}\right) \cdot \left(t - \frac{x_0}{c}\right)} \cdot \left[(\rho \cdot c - \beta) \cdot \sin\left[\frac{\sqrt{-Q}}{2 \cdot \mu} \cdot \left(t - \frac{x_0}{c} \right) \right] - \sqrt{-Q} \cdot \cos\left[\frac{\sqrt{-Q}}{2 \cdot \mu} \cdot \left(t - \frac{x_0}{c} \right) \right] \right] \right] - 1 \right] + x_0 & \text{if } t \geq \frac{x_0}{c} \\ x_0 & \text{otherwise} \end{cases}$$

Define "Right" (positive x-dir.) traveling Pressure Wave Velocity Potential :

$$\phi_T(x,t) := \frac{P_{peak}}{\rho \cdot c \cdot b} \cdot \left[\begin{cases} \left[\left[e^{b \cdot (x - c \cdot t)} - 1 \right] \right] & \text{if } \left(\frac{x}{c} \leq t < \frac{x_0 + x_b(t) - x}{c} \right) \\ \left[e^{b \cdot (x - c \cdot t)} - e^{-b \cdot \left(x + c \cdot t - x_0 - x_b(t) \right)} - \frac{b \cdot \rho \cdot c^2}{\kappa} \cdot e^{-\left(\frac{\beta - \rho \cdot c}{2 \cdot \mu \cdot c}\right) \cdot \left(x + c \cdot t - x_0 - x_b(t) \right)} \cdot \left[\cos\left[\frac{\sqrt{-Q}}{2 \cdot \mu \cdot c} \cdot \left(x + c \cdot t - x_0 - x_b(t) \right) \right] + (\beta - \rho \cdot c) \cdot \sin\left[\frac{\sqrt{-Q}}{2 \cdot \mu \cdot c} \cdot \left(x + c \cdot t - x_0 - x_b(t) \right) \right] \right] + \frac{b \cdot \rho \cdot c^2}{\kappa} \right] & \text{if } t \geq \frac{x_0 + x_b(t) - x}{c} \\ 0 & \text{otherwise} \end{cases} \right]$$

Define Peak Pressure from Explosive Charge at Standoff Distance :

$$P_{peak} := K_P \cdot \left(\frac{W^{\frac{1}{3}}}{R_{standoff}} \right)^{\alpha P}$$

$P_{peak} = 4.75124124 \times 10^{7}$ (Pa) $4.75 \cdot 10^{7}$

Define Time Constant of Peak Pressure Decay :

$$\tau := W^{\frac{1}{3}} \cdot \frac{K_\tau}{1000} \cdot \left(\frac{W^{\frac{1}{3}}}{R_{standoff}} \right)^{\alpha_\tau}$$

$\tau = 6.19303311 \times 10^{-5}$ (sec) $6.193 \cdot 10^{-5}$

Define Time (post detonation) that Pressure Wave reaches Standoff Distance :

$$t_{peak} := \frac{R_{standoff}}{c}$$

$t_{peak} = 4.13736036 \times 10^{-6}$ (sec)

Define Unobstructed Pressure Time History at Standoff Location :

$$P_U(t) := \begin{cases} \left[\left[P_{peak} \cdot e^{-\left(\frac{t - t_{peak}}{\tau} \right)} \right] + P_{static} \right] & \text{if } t \geq t_{peak} \\ P_{static} & \text{otherwise} \end{cases}$$

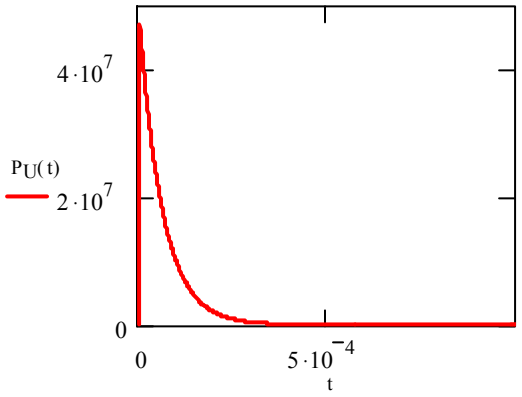

Unobstructed Pressure time History by Peak Approximation at Standoff Distance with Given Explosive Charge Mass

Pressure in Pa
Time in sec

Define Pressure Wave Equation for inclusion of Taylor Plate :

$$\text{Input}(x,t) := \left[e^{b\cdot(x-c\cdot t)} + e^{-b\cdot\left(x+c\cdot t-x_0-x_b(t)\right)} + \frac{\rho\cdot c}{2\cdot\kappa\cdot\mu}\cdot\left[e^{-\left(\frac{\beta-\rho\cdot c}{2\cdot\mu\cdot c}\right)\cdot\left(x+c\cdot t-x_0-x_b(t)\right)} \right]\cdot\left[\left[\left(\sqrt{-Q}-1\right)-(\beta-\rho\cdot c)\right]\cdot\cos\left[\frac{\sqrt{-Q}}{2\cdot\mu\cdot c}\cdot\left(x+c\cdot t-x_0-x_b(t)\right)\right] + \left[(\beta-\rho\cdot c)-\sqrt{-Q}\right]\cdot\sin\left[\frac{\sqrt{-Q}}{2\cdot\mu\cdot c}\cdot\left(x+c\cdot t-x_0-x_b(t)\right)\right] \right] \right]$$

$$P_T(x,t) := \begin{cases} 0 & \text{if } x > x_b(t) \\ \left[P_{peak}\cdot \left[\begin{cases} e^{b\cdot(x-c\cdot t)} & \text{if } \left(\frac{x}{c} < t < \frac{x_0+x_b(t)-x}{c}\right) \\ \text{Input}(x,t) & \text{if } t \geq \frac{x_0+x_b(t)-x}{c} \\ 0 & \text{otherwise} \end{cases} \right] \right] & \text{otherwise} \end{cases} \quad \text{(Pa)}$$

Define Plate "Wall" Location for Showing With Pressure :

$$\text{wall}(x,t) := \begin{cases} \left(-0.5\right) & \text{if } x < x_b(t) \\ 4\cdot P_{peak} & \text{otherwise} \end{cases}$$

Provide Pressure (Pa) vs. Position along x-axis (m) Plots at Various Times :

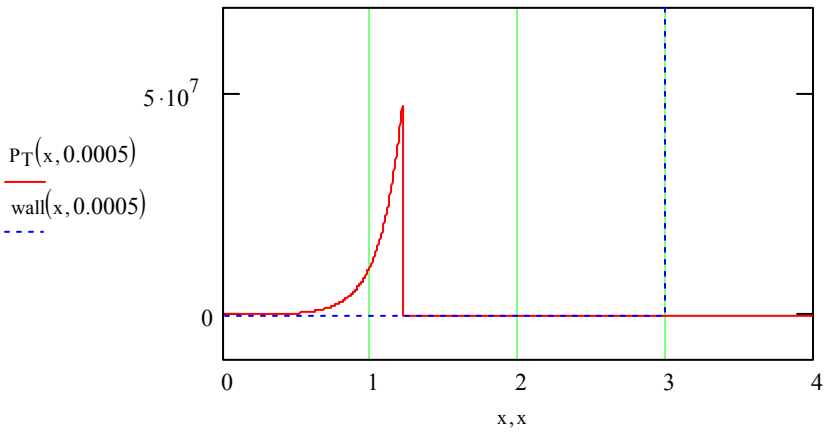

At time = 0.0005 sec.

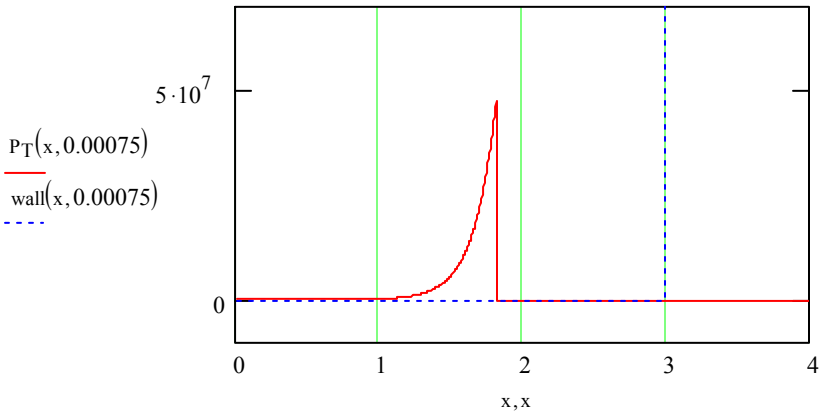

At time = 0.00075 sec.

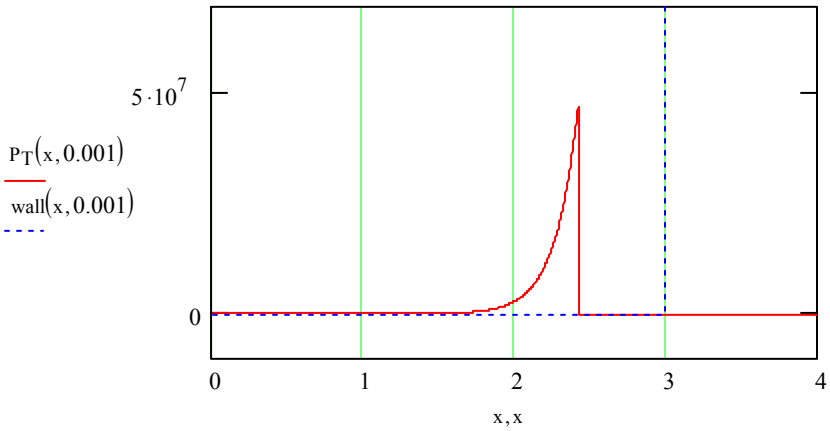

At time = 0.001 sec.

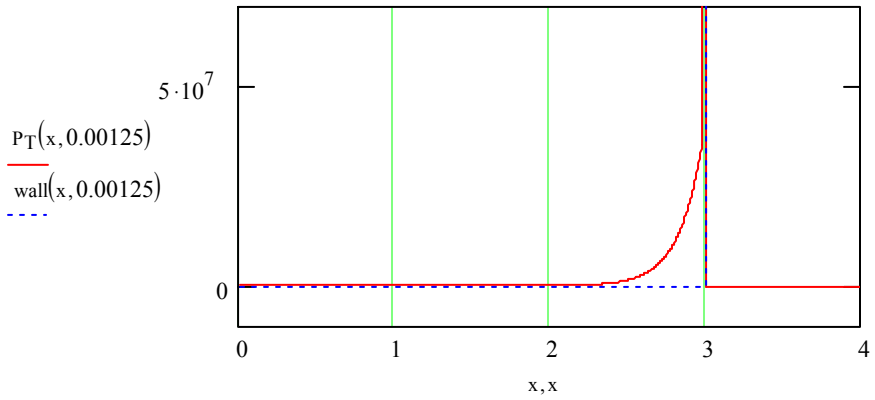

At time = 0.00125 sec.

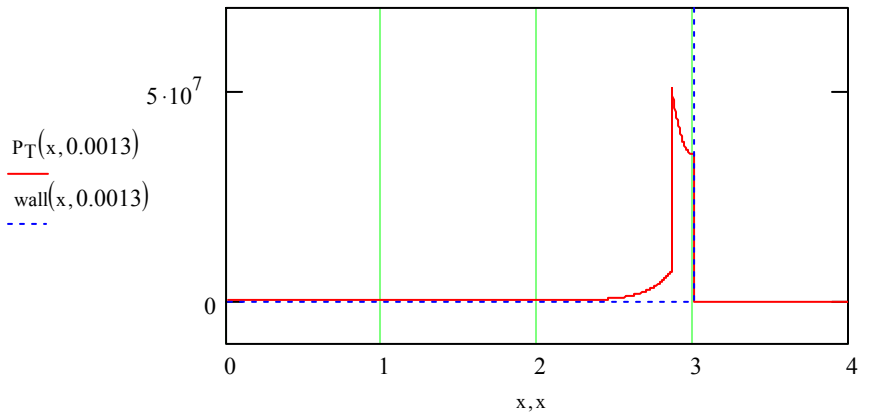

At time = 0.0013 sec.

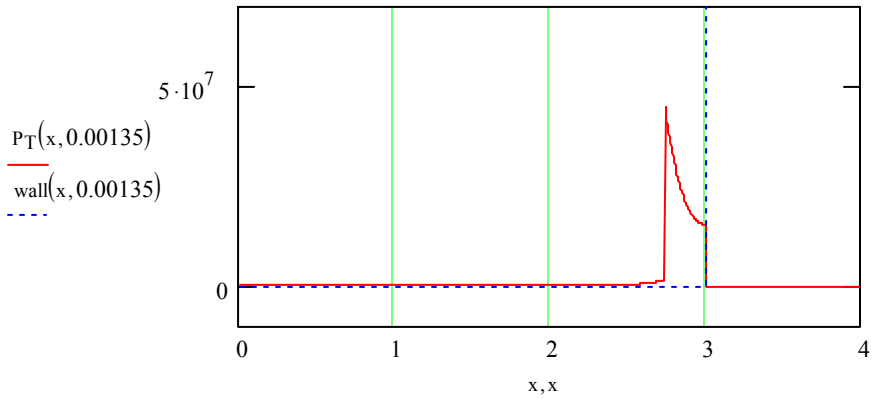

At time = 0.00135 sec.

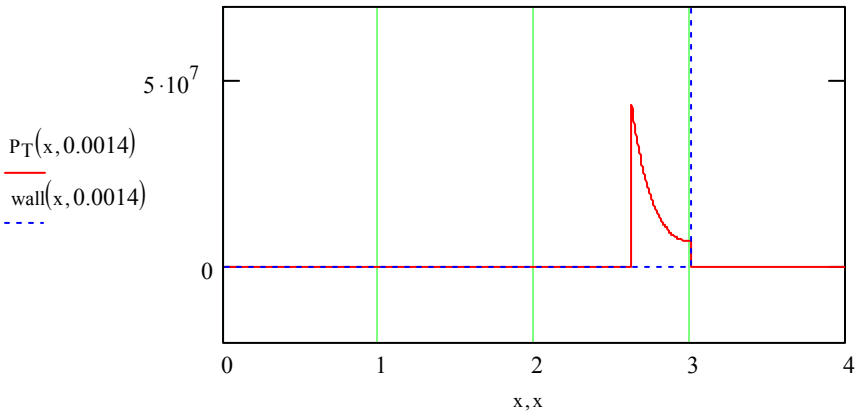

At time = 0.0014 sec.

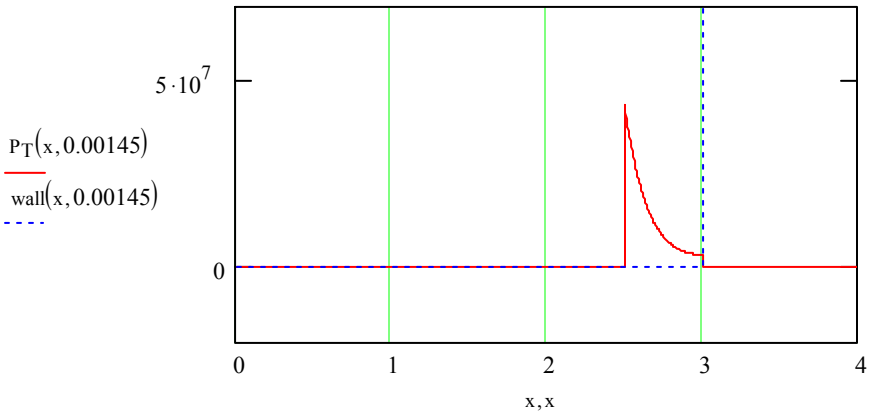

At time = 0.00145 sec.

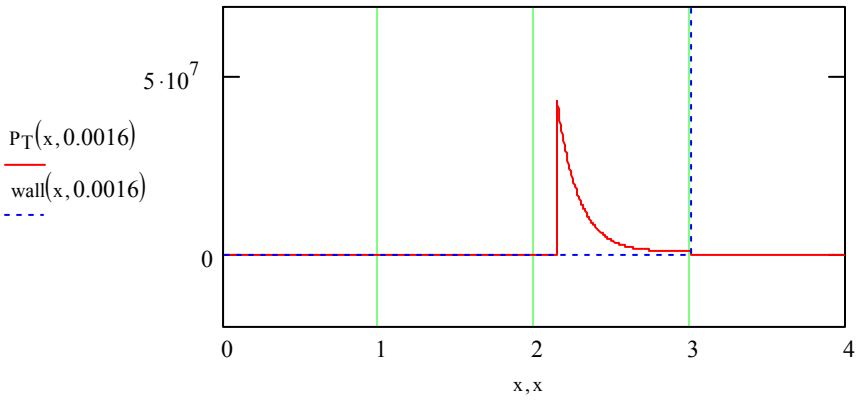

At time = 0.0016 sec.

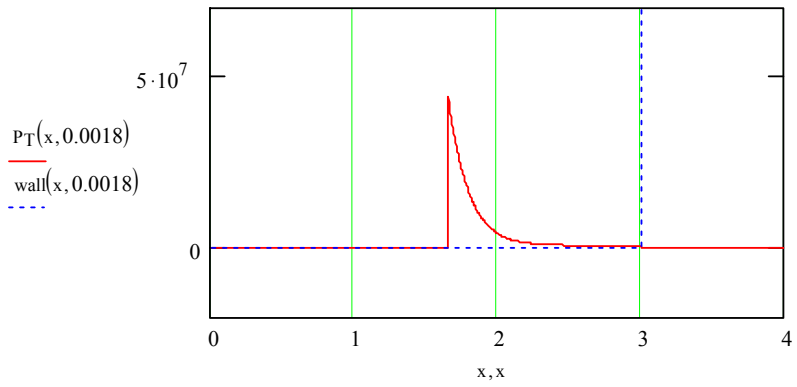

At time = 0.0018 sec.

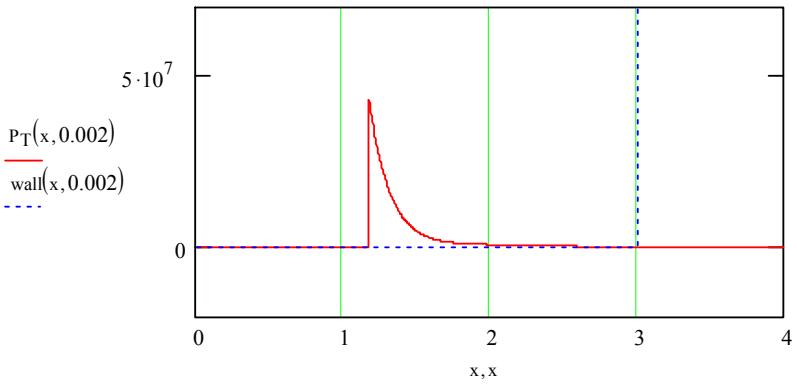

At time = 0.002 sec.

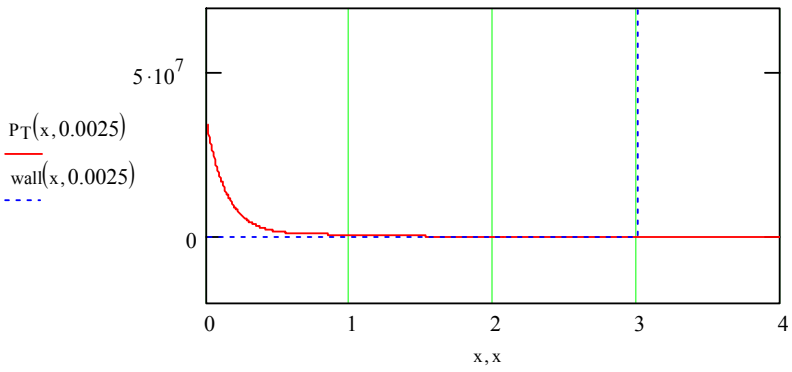

At time = 0.0025 sec.

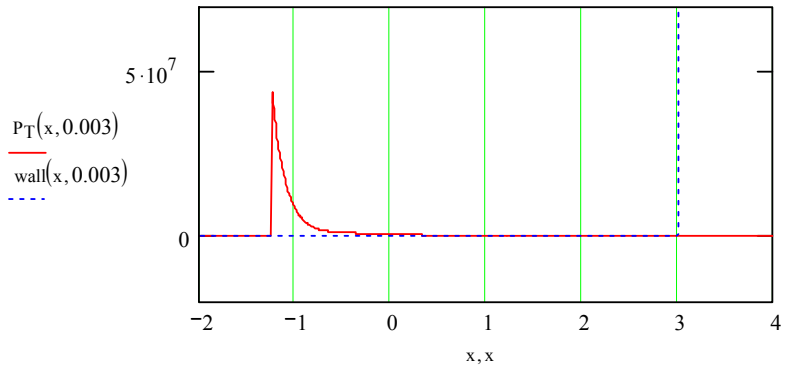

At time = 0.003 sec.

Provide Plate Position (m) vs. time (sec) Plot :

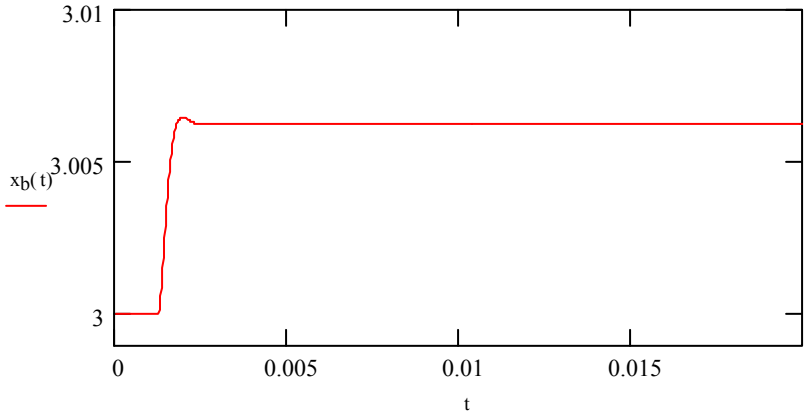

Provide Plate Displacement (m) vs. time (sec) Plot :

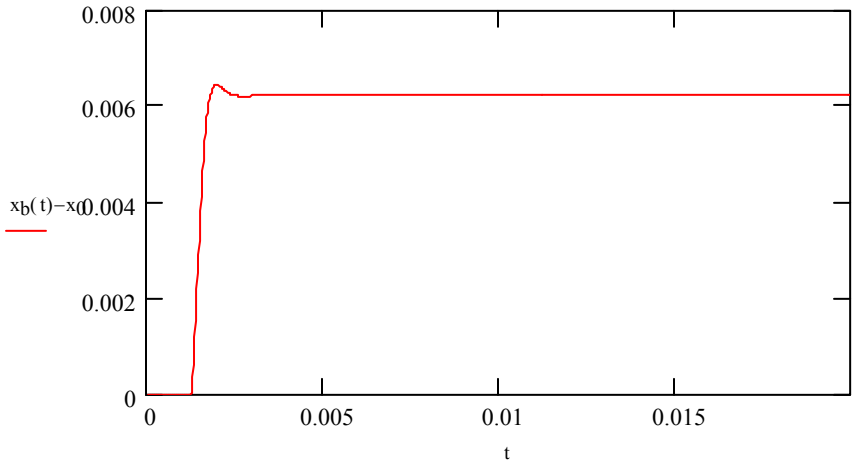

APPENDIX G LS-DYNA FILE FOR US NAVY BLAST TEST STUDY – CIRCULAR STEEL PLATE MODEL

The LS-DYNA input file is given. To decrease space, not all elements and nodes are listed.

```
*KEYWORD
*TITLE
USN BLAST TEST COMPARISON MODEL -  3 lb. charge TNT
$-------------------------------------------------------
$
$ ANALYSIS OF US NAVY BLAST TEST STUDY – STEEL PLATE
$ WRITTEN BY KEITH G. WEBSTER
$
$
$ SET ID:   #       DESCRIPTION
$
$          1       SLAVE PLATE EDGE NODE SET
$          2       MASTER FRAME EDGE NODE SET
$          3       REACTION FRAME NODE SET
$          4       NRBC SEGMENT SET
$
$-------------------------------------------------------
$
$ ANALYSIS CONTROL CARDS
$
*CONTROL_TERMINATION
3.0E-03,0,0.000E+00,0.000E+00,0.000E+00
*CONTROL_TIMESTEP
0,0.67,0,0.000E+00,0.000E+00,0,0,0
*CONTROL_HOURGLASS
1,1.0E-04
*CONTROL_ACCURACY
0,3,0
```

```
*CONTROL_ENERGY
2,2,2,2
*CONTROL_DAMPING
250,0.001,0.995
*CONTROL_OUTPUT
0,0,0,0,0.000E+00,0,100,5000
0
*CONTROL_ALE
3,10,2,0.0,0.0,0,1.0,0
0.000E+00,1.000E+20,1.,1.000E-06,0,0,101325.0
$
*CONTROL_SHELL
20.0,0,-1,0,2,2,1,0
$
$ ANALYSIS OUTPUT CARDS
$
*DATABASE_BINARY_D3PLOT
1.000E-05,0
*DATABASE_BINARY_D3THDT
1.000E-05,0
*DATABASE_EXTENT_BINARY
0,0,3,1,1,1,1,1
0,0,0,0,0,0,2
1
*DATABASE_GLSTAT
1.0E-05,1
*DATABASE_MATSUM
1.0E-05,1
$ STANDOFF DISTANCE 0.2286m = 9"
*DATABASE_TRACER
0,1,1.1143,-1.25,0
0,2,1.0001,-1.25,0
0,3,3.0,-1.25,0
*DATABASE_TRHIST
```

```
1.0E-06,1
$$$
$
$ FLUID DEFINITION CARDS
$
*PART
FLUID - WATER
100,201,202,203,204,0,0,0
*SECTION_SOLID_ALE
201,11
0.0,0.0,0,1.0,0,1.00E+20,0.5
*MAT_NULL
202,1025.,-1.000E-20,1.13E-03,0.,0.,0.,0.
$ Patm = 101325.0 Pa , P(2.0m) = 20110.5 Pa
*EOS_GRUNEISEN
203,2417,1.41,0.0,0.0,1.0,0.0,121435.5
1.
*HOURGLASS
204,1,1.000E-04,1,1.5,0.06
$
*PART
FLUID - AIR
500,501,502,503,504,0,0,0
*SECTION_SOLID_ALE
501,11
0.0,0.0,0,1.0,0,1.00E+20,0.5
*MAT_NULL
502,1.280,0.000E+00,0.000E+00,0.,0.,0.,0.
*EOS_LINEAR_POLYNOMIAL
503,0.000E+00,0.000E+00,0.000E+00,0.000E+00,0.400,0.400,0.000E+00
253312.5,1.0
*HOURGLASS
504,1,1.000E-04,1,1.5,0.06
$
```

```
*PART
FLUID - AIR
501,501,502,503,504,0,0,0
*PART
FLUID - AIR
502,501,502,503,504,0,0,0
*PART
FLUID - AIR
503,501,502,503,504,0,0,0
*PART
FLUID - AIR
504,501,502,503,504,0,0,0
*PART
FLUID - AIR
505,501,502,503,504,0,0,0
*PART
FLUID - AIR
506,501,502,503,504,0,0,0
*PART
FLUID - AIR
507,501,502,503,504,0,0,0
$
$
$
$ STRUCTURE DEFINITION CARDS
$
$ INNER PLATE REGION, FAILURE t=0.5"
$
*PART
STEEL TEST PLATE
400,404,405,,406,0,0,0
*SECTION_SHELL_ALE
404,2,1.0,3.00,0.0,0.0,0
0.0127,0.0127,0.0127,0.0127,0.0
```

```
-1.0,0.0,0.0,0.0,0.0,0.00E+00,1.00E+20,0.5
*MAT_PIECEWISE_LINEAR_PLASTICITY
405,7780.0,2.06E+11,0.281,3.55E+08,0,0.1,0
40.4,5.0,0,0,1.0
0,0,0,0,0,0,0,0
0,0,0,0,0,0,0,0
*HOURGLASS
406,1,1.000E-06,1,1.5,0.06
$
*PART
STEEL TEST PLATE
402,404,405,,406,0,0,0
$
$ OUTER PLATE REGION, NO FAILURE t=0.5"
$
*PART
STEEL TEST PLATE
401,404,407,,406,0,0,0
*MAT_PLASTIC_KINEMATIC
407,7780.0,2.06E+11,0.281,3.55E+08,0.0,0.0
40.4,5.0
$
*PART
STEEL TEST PLATE
403,404,407,,406,0,0,0
$
$
*PART
STEEL TUBE -x
300,301,302,,304,0,0,0
*SECTION_SHELL
301,2,0.000E+00,3.00,0.000E+00,0.000E+00,0
0.0365,0.0365,0.0365,0.0365,0.000E+00
*MAT_PLASTIC_KINEMATIC
```

```
302,7800.0,2.0E+09,0.300,5.00E+06,0.000E+00,0.000E+00
0.000E+00,0.000E+00,0.000E+00
*HOURGLASS
304,1,1.000E-04,1,1.5,0.06
$
*PART
STEEL TUBE +x
301,301,302,,304,0,0,0
$
$
*PART
STEEL TUBE PLATE 1 -x
302,305,302,,304,0,0,0
*SECTION_SHELL
305,2,0.000E+00,3.00,0.000E+00,0.000E+00,0
0.077,0.077,0.077,0.077,0.000E+00
$
*PART
STEEL TUBE PLATE 1 +x
303,305,302,,304,0,0,0
$
*PART
STEEL TUBE PLATE 2 -x
304,305,302,,304,0,0,0
$
*PART
STEEL TUBE PLATE 2 +x
305,305,302,,304,0,0,0
$
*PART
STEEL TUBE PLATE 3 -x
306,305,302,,304,0,0,0
$
*PART
```

STEEL TUBE PLATE 3 +x
307,305,302,,304,0,0,0
$
$
$
$ EXPLOSIVE DEFINITION CARDS
$
*PART
EXPLOSIVE
200,101,102,103,104,0,0,0
*SECTION_SOLID_ALE
101,11
0.0,0.0,0,1.0,0,1.00E+20,0.5
*MAT_HIGH_EXPLOSIVE_BURN
102,1630.,6930.,2.1E+10,2.0,0.5
*EOS_JWL
103,3.71E+11,3.23E+09,4.15,0.95,0.3,7.00E+09,1.
*HOURGLASS
104,1,1.0E-04,1,1.5,0.06
$
*PART
EXPLOSIVE
201,101,102,103,104,0,0,0
*PART
EXPLOSIVE
202,101,102,103,104,0,0,0
*PART
EXPLOSIVE
203,101,102,103,104,0,0,0
*PART
EXPLOSIVE
204,101,102,103,104,0,0,0
*PART
EXPLOSIVE

```
205,101,102,103,104,0,0,0
*PART
EXPLOSIVE
206,101,102,103,104,0,0,0
*PART
EXPLOSIVE
207,101,102,103,104,0,0,0
*PART
EXPLOSIVE
208,101,102,103,104,0,0,0
*PART
EXPLOSIVE
209,101,102,103,104,0,0,0
$
$ DETONATION CARD
$
*INITIAL_DETONATION
0,1.2286,-1.25,0,1.00E-20
$
$ ALE DEFINITION CARDS
$
*SET_PART_LIST
600
300,301,302,303,304,305,306,307
400,401,402,403
*SET_PART_LIST
700
200,201,202,203,204,205,206,207
208,209,500,501,502,503,504,505
506,507
*SET_PART_LIST
800
200,201,202,203,204,205,206,207
208,209
```

```
*SET_PART_LIST
900
500,501,502,503,504,505,506,507
*ALE_MULTI-MATERIAL_GROUP
800,0
100,1
900,0
$
*ALE_REFERENCE_SYSTEM_GROUP
700,0,8,0,0,0,0,1
0.,0.,0.,0,0.5
$
$ INITIAL VOLUME FRACTION CARD
$
*INITIAL_VOLUME_FRACTION_GEOMETRY
800,0,1
4,1,2
1.2286,-2.0381,0.0,1.2286,-1.9619,0.0,0.05969,0.05969
$
$ BOUNDARY CONDITION CARDS
$
*BOUNDARY_NON_REFLECTING
4,0.0,0.0
$
$ CONSTRAINT CARDS
$
*CONSTRAINED_LAGRANGE_IN_SOLID
600,700,0,0,0,4,1,0
0,1.0E+10,0.1
$
*CONSTRAINED_TIE-BREAK
1,2,1.0E+20
$
*BOUNDARY_SPC_SET
```

```
1,0,1,1,1,1,1,1
*BOUNDARY_SPC_SET
3,0,1,1,1,1,1,1
$
$ ANALYSIS MODEL GEOMETRY CARDS
$
$ NODES
$
*NODE
1,1.00000000,-2.53340006,0.000000000E+00,0,0
2,1.00000000,-2.52315092,0.104061112,0,0
3,1.00000000,-2.49279737,0.204123452,0,0
4,1.00000000,-2.44350576,0.296341389,0,0
5,1.00000000,-2.37717056,0.377170950,0,0
***

139170,10.0000000,2.00000000,-0.233333319,0,0
139171,10.0000000,2.00000000,-0.100000001,0,0
$
$ ELEMENT CARDS FOR SOLID ELEMENTS
$
*ELEMENT_SOLID
1,500,1859,1944,1949,1864,1860,1945,1950,1865
2,500,1944,2029,2034,1949,1945,2030,2035,1950
3,500,2029,2114,2119,2034,2030,2115,2120,2035
4,500,2114,2199,2204,2119,2115,2200,2205,2120
5,500,2199,2284,2289,2204,2200,2285,2290,2205
***
130143,507,139108,139138,139141,139111,130668,130688,130690,130670
130144,507,139138,139168,139171,139141,130688,130708,130710,130690
$
$ ELEMENT CARDS FOR SHELL ELEMENTS
$
*ELEMENT_SHELL_THICKNESS
1,400,1,6,7,2
```

0.000000E+00,0.000000E+00,0.000000E+00,0.000000E+00
2,400,6,11,12,7
0.000000E+00,0.000000E+00,0.000000E+00,0.000000E+00
***
1823,307,1858,1855,1590,1594
0.000000E+00,0.000000E+00,0.000000E+00,0.000000E+00
1824,307,944,1858,1594,750
0.000000E+00,0.000000E+00,0.000000E+00,0.000000E+00
$
$ Node set p-edge
$
*SET_NODE_LIST
1,0.,0.,0.,0.
267,268,269,270,271,284,287,290
293,296,299,302,305,314,315,316
317,549,550,551,552,561,564,567
570,573,576,579,582,591,592,593
$
$ Node set m-edge
$
*SET_NODE_LIST
2,0.,0.,0.,0.
616,617,651,652,653,687,688,689
701,713,747,748,749,772,773,796
797,842,843,844,845,879,880,881
893,905,939,940,941,975,976,977
$
$ Node set frame
$
*SET_NODE_LIST
3,0.,0.,0.,0.
594,595,596,597,598,599,600,601
602,603,604,605,606,607,608,609
610,611,612,613,614,615,616,617

618,619,620,621,622,623,624,625
626,627,628,629,630,631,632,633
634,635,636,637,638,639,640,641
642,643,644,645,646,647,648,649
***
1842,1843,1844,1845,1846,1847,1848,1849
1850,1851,1852,1853,1854,1855,1856,1857
1858
$
$ Face set nrbc
$
*SET_SEGMENT
4,0.000E+00,0.000E+00,0.000E+00,0.000E+00
8975,8991,8992,8976,0.000E+00,0.000E+00,0.000E+00,0.000E+00
8991,9007,9008,8992,0.000E+00,0.000E+00,0.000E+00,0.000E+00
9023,9039,9040,9024,0.000E+00,0.000E+00,0.000E+00,0.000E+00
9087,9103,9104,9088,0.000E+00,0.000E+00,0.000E+00,0.000E+00
9088,9104,9359,9335,0.000E+00,0.000E+00,0.000E+00,0.000E+00
***
114075,114074,114389,114386,0.000E+00,0.000E+00,0.000E+00,0.000E+00
114386,114389,114390,114387,0.000E+00,0.000E+00,0.000E+00,0.000E+00
*END

APPENDIX H LS-DYNA FILE FOR US NAVY BLAST TEST STUDY – CIRCULAR SPS PLATE MODEL

The LS-DYNA input file is given. To decrease space, not all elements and nodes are listed. The stress vs. strain curve data for the elastomer core is proprietary and confidential and is not included.

```
*KEYWORD
*TITLE
USN BLAST TEST SPS COMPARISON MODEL -  3 lb. charge TNT
$-----------------------------------------------------
$
$ ANALYSIS OF US NAVY BLAST TEST STUDY – SPS PLATE
$ WRITTEN BY KEITH G. WEBSTER
$
$
$ SET ID:   #       DESCRIPTION
$
$          1      SLAVE PLATE EDGE NODE SET
$          2      MASTER FRAME EDGE NODE SET
$          3      REACTION FRAME NODE SET
$          4      NRBC SEGMENT SET
$
$-----------------------------------------------------
$
$ ANALYSIS CONTROL CARDS
$
*CONTROL_TERMINATION
5.0E-03,0,0.000E+00,0.000E+00,0.000E+00
*CONTROL_TIMESTEP
0,0.67,0,0.000E+00,0.000E+00,0,0,0
*CONTROL_HOURGLASS
1,1.0E-04
```

```
*CONTROL_ACCURACY
0,3,0
*CONTROL_ENERGY
2,2,2,2
*CONTROL_DAMPING
250,0.001,0.995
*CONTROL_OUTPUT
0,0,0,0,0.000E+00,0,100,5000
0
*CONTROL_ALE
3,10,2,0.0,0.0,0,1.0,0
0.000E+00,1.000E+20,1.,1.000E-06,0,0,0.0
$
*CONTROL_SHELL
20.0,0,-1,0,2,2,1,0
$
$ ANALYSIS OUTPUT CARDS
$
*DATABASE_BINARY_D3PLOT
1.000E-05,0
*DATABASE_BINARY_D3THDT
1.000E-05,0
*DATABASE_EXTENT_BINARY
0,0,3,1,1,1,1,1
0,0,0,0,0,0,2
1
*DATABASE_GLSTAT
1.0E-05,1
*DATABASE_MATSUM
1.0E-05,1
$ STANDOFF DISTANCE 0.2286m = 9"
*DATABASE_TRACER
0,1,1.1143,0,0
0,2,1.0001,0,0
```

```
*DATABASE_TRHIST
1.0E-06,1
$$$
$
$ FLUID DEFINITION CARDS
$
*PART
FLUID - WATER
100,201,202,203,204,0,0,0
*SECTION_SOLID_ALE
201,11
0.0,0.0,0,1.0,0,1.00E+20,0.5
*MAT_NULL
202,1025.,-1.000E-20,1.13E-03,0.,0.,0.,0.
*EOS_GRUNEISEN
203,2417,1.41,0.0,0.0,1.0,0.0,0.0
1.
*HOURGLASS
204,1,1.000E-04,1,1.5,0.06
$
*PART
FLUID - AIR
500,501,502,503,504,0,0,0
*SECTION_SOLID_ALE
501,11
0.0,0.0,0,1.0,0,1.00E+20,0.5
*MAT_NULL
502,1.280,0.000E+00,0.000E+00,0.,0.,0.,0.
*EOS_LINEAR_POLYNOMIAL
503,0.000E+00,1.000E-02,0.000E+00,0.000E+00,0.400,0.400,0.000E+00
0.000E+00,0.000E+00
*HOURGLASS
504,1,1.000E-04,1,1.5,0.06
$
```

```
*PART
FLUID - AIR
501,501,502,503,504,0,0,0
$
$ STRUCTURE DEFINITION CARDS
$
$ LAYER INTEGRATION POINTS
$
*INTEGRATION_SHELL
1,9,0
-1,0.0
-0.94,0.06
-0.88,0.12
-0.88,0.12,600
0,0.5,600
0.88,0.88,600
0.88,0.88
0.94,0.94
1.0,1.0
$
*INTEGRATION_SHELL
2,9,0
-1,0.0
-0.94,0.06
-0.88,0.12
-0.88,0.12,600
0,0.5,600
0.88,0.88,600
0.88,0.88
0.94,0.94
1.0,1.0
$
$ ELASTOMER CORE
$
```

```
*PART
ELASTOMER
600,404,605,,406,0,0,0
$ 600,,605,,406,0,0,0
*MAT_LAYERED_LINEAR_PLASTICITY
605,1190.0,685.4E+06,0.4,58.6E+06,0,0.4
0.0,0.0,50,0
0,0,0,0,0,0,0,0
0,0,0,0,0,0,0,0
$
$ INNER PLATE REGION, FAILURE
$
*PART
STEEL TEST PLATE
400,404,405,,406,0,0,0
*SECTION_SHELL
404,2,1.0,3.00,0.0,-1,0
0.0396875,0.0396875,0.0396875,0.0396875,0.0
*MAT_LAYERED_LINEAR_PLASTICITY
405,7780.0,2.06E+11,0.281,3.55E+08,0,0.1
40.4,5.0,0,0
0,0,0,0,0,0,0,0
0,0,0,0,0,0,0,0
*HOURGLASS
406,1,1.000E-06,1,1.5,0.06
$
*PART
STEEL TEST PLATE
402,404,405,,406,0,0,0
$
$ OUTER PLATE REGION, NO FAILURE
$
*PART
STEEL TEST PLATE
```

401,408,407,,406,0,0,0
*SECTION_SHELL
408,2,1.0,3.00,0.0,-2,0
0.0396875,0.0396875,0.0396875,0.0396875,0.0
*MAT_LAYERED_LINEAR_PLASTICITY
407,7780.0,2.06E+11,0.281,3.55E+08,0
40.4,5.0,0,0
0,0,0,0,0,0,0,0
0,0,0,0,0,0,0,0
$
*PART
STEEL TEST PLATE
403,408,407,,406,0,0,0
$
$ REACTION FRAME
$
*PART
STEEL TUBE -x
300,301,302,,304,0,0,0
*SECTION_SHELL
301,2,0.000E+00,3.00,0.000E+00,0.000E+00,0
0.0365,0.0365,0.0365,0.0365,0.000E+00
*MAT_PLASTIC_KINEMATIC
302,7800.0,2.0E+09,0.300,5.00E+06,0.000E+00,0.000E+00
0.000E+00,0.000E+00,0.000E+00
*HOURGLASS
304,1,1.000E-04,1,1.5,0.06
$
*PART
STEEL TUBE +x
301,301,302,,304,0,0,0
$
$
*PART

STEEL TUBE PLATE 1 -x
302,305,302,,304,0,0,0
*SECTION_SHELL
305,2,0.000E+00,3.00,0.000E+00,0.000E+00,0
0.077,0.077,0.077,0.077,0.000E+00
$
*PART
STEEL TUBE PLATE 1 +x
303,305,302,,304,0,0,0
$
*PART
STEEL TUBE PLATE 2 -x
304,305,302,,304,0,0,0
$
*PART
STEEL TUBE PLATE 2 +x
305,305,302,,304,0,0,0
$
*PART
STEEL TUBE PLATE 3 -x
306,305,302,,304,0,0,0
$
*PART
STEEL TUBE PLATE 3 +x
307,305,302,,304,0,0,0
$
$
$
$ EXPLOSIVE DEFINITION CARDS
$
*PART
EXPLOSIVE
200,101,102,103,104,0,0,0
*SECTION_SOLID_ALE

101,11
0.0,0.0,0,1.0,0,1.00E+20,0.5
*MAT_HIGH_EXPLOSIVE_BURN
102,1630.,6930.,2.1E+10,2.0,0.5
*EOS_JWL
103,3.71E+11,3.23E+09,4.15,0.95,0.3,7.00E+09,1.
*HOURGLASS
104,1,1.0E-04,1,1.5,0.06
$
*PART
EXPLOSIVE
201,101,102,103,104,0,0,0
*PART
EXPLOSIVE
202,101,102,103,104,0,0,0
*PART
EXPLOSIVE
203,101,102,103,104,0,0,0
*PART
EXPLOSIVE
204,101,102,103,104,0,0,0
*PART
EXPLOSIVE
205,101,102,103,104,0,0,0
*PART
EXPLOSIVE
206,101,102,103,104,0,0,0
*PART
EXPLOSIVE
207,101,102,103,104,0,0,0
*PART
EXPLOSIVE
208,101,102,103,104,0,0,0
*PART

EXPLOSIVE
209,101,102,103,104,0,0,0
$
$ DETONATION CARD
$
*INITIAL_DETONATION
0,1.2286,0,0,1.00E-20
$
$ CONSTRAINT CARDS
$
*SET_PART_LIST
600
300,301,302,303,304,305,306,307
400,401,402,403
$
*SET_PART_LIST
700
200,201,202,203,204,205,206,207
208,209,500,501
$
*CONSTRAINED_LAGRANGE_IN_SOLID
600,700,0,0,0,4,1,0
0,1.0E+10,0.1
$
*CONSTRAINED_TIE-BREAK
1,2,1.0E+20
$
*BOUNDARY_SPC_SET
1,0,1,1,1,1,1,1
*BOUNDARY_SPC_SET
3,0,1,1,1,1,1,1
$
$ ALE DEFINITION CARDS
$

```
*SET_PART_LIST
800
200,201,202,203,204,205,206,207
208,209
*SET_PART_LIST
900
500,501
*ALE_MULTI-MATERIAL_GROUP
800,0
100,1
900,0
$
*ALE_REFERENCE_SYSTEM_GROUP
700,0,8,0,0,0,0,1
0.,0.,0.,0,0.5
$
$ INITIAL VOLUME FRACTION CARD
$
*INITIAL_VOLUME_FRACTION_GEOMETRY
800,0,1
4,1,2
1.2286,-0.0381,0.0,1.2286,0.0381,0.0,0.05969,0.05969
$
$ BOUNDARY CONDITION CARDS
$
*BOUNDARY_NON_REFLECTING
4,0.0,0.0
$
$ Strain Stress Curves for Elastomer
$
*DEFINE_TABLE
50
1
2
```

```
3
4
5
$ 0.01 (mm/mm)/S
*DEFINE_CURVE
1,0,1.0,1.0,0.0,0.0,0
***
$
$ 0.1 (mm/mm)/S
*DEFINE_CURVE
2,0,1.0,1.0,0.0,0.0,0
***
$
$ 1 (mm/mm)/S
*DEFINE_CURVE
3,0,1.0,1.0,0.0,0.0,0
***
$
$ 10 (mm/mm)/S
*DEFINE_CURVE
4,0,1.0,1.0,0.0,0.0,0
***
$
$ 100 (mm/mm)/S
*DEFINE_CURVE
5,0,1.0,1.0,0.0,0.0,0
***
$
$ ANALYSIS MODEL GEOMETRY CARDS
$
$ NODES
$
*NODE
1,1.00000000,-0.533399999,0.000000000E+00,0,0
```

```
2,1.00000000,-0.523150921,0.104061060,0,0
***
84792,5.00000000,0.565075934,-0.234598294,0,0
84793,5.00000000,0.600134015,-0.119459510,0,0
$
$ ELEMENT CARDS FOR SOLID ELEMENTS
$
*ELEMENT_SOLID
1,500,1859,1944,1949,1864,1860,1945,1950,1865
2,500,1944,2029,2034,1949,1945,2030,2035,1950
3,500,2029,2114,2119,2034,2030,2115,2120,2035
4,500,2114,2199,2204,2119,2115,2200,2205,2120
***
78583,209,84271,84748,50539,50257,68269,68809,41315,40919
78584,209,84748,84793,50557,50539,68809,68869,41327,41315
$
$ ELEMENT CARDS FOR SHELL ELEMENTS
$
*ELEMENT_SHELL_THICKNESS
1,400,1,6,7,2
0.000000E+00,0.000000E+00,0.000000E+00,0.000000E+00
2,400,6,11,12,7
0.000000E+00,0.000000E+00,0.000000E+00,0.000000E+00
***
1823,307,1858,1855,1590,1594
0.000000E+00,0.000000E+00,0.000000E+00,0.000000E+00
1824,307,944,1858,1594,750
0.000000E+00,0.000000E+00,0.000000E+00,0.000000E+00
$
$ Node set pedge
$
*SET_NODE_LIST
1,0.,0.,0.,0.
267,268,269,270,271,284,287,290
```

293,296,299,302,305,314,315,316
317,549,550,551,552,561,564,567
570,573,576,579,582,591,592,593
$
$ Node set medge
$
*SET_NODE_LIST
2,0.,0.,0.,0.
616,617,651,652,653,687,688,689
701,713,747,748,749,772,773,796
797,842,843,844,845,879,880,881
893,905,939,940,941,975,976,977
$
$ Node set frame
$
*SET_NODE_LIST
3,0.,0.,0.,0.
594,595,596,597,598,599,600,601
602,603,604,605,606,607,608,609
610,611,612,613,614,615,616,617
618,619,620,621,622,623,624,625
626,627,628,629,630,631,632,633
***
1842,1843,1844,1845,1846,1847,1848,1849
1850,1851,1852,1853,1854,1855,1856,1857
1858
$
$ Face set nrbc
$
*SET_SEGMENT
4,0.000E+00,0.000E+00,0.000E+00,0.000E+00
8975,8985,8986,8976,0.000E+00,0.000E+00,0.000E+00,0.000E+00
8985,8995,8996,8986,0.000E+00,0.000E+00,0.000E+00,0.000E+00
9005,9015,9016,9006,0.000E+00,0.000E+00,0.000E+00,0.000E+00

9045,9055,9056,9046,0.000E+00,0.000E+00,0.000E+00,0.000E+00
***
84752,84755,84756,84753,0.000E+00,0.000E+00,0.000E+00,0.000E+00
84753,84756,84757,84754,0.000E+00,0.000E+00,0.000E+00,0.000E+00
84754,84757,68821,68817,0.000E+00,0.000E+00,0.000E+00,0.000E+00
*END

APPENDIX I TRUEGRID MODELING COMMANDS

I.1 3-D DSB Mesh Model

The Truegrid mesh modeler file for the ES15_25 cases is given. The mesh is modeled out to 1.5 meters. It is important to note in this type of eighth sphere model where the explosive charge is located in the center of the sphere that a completely spherical model cannot be used. The radial lines all converge into a single point at the center of the sphere and the angles between the radial lines becomes very small. LS-DYNA cannot handle angles this small between the elements. A rectangular mesh that transitions into a spherical mesh is needed. It is also important that the region where the mesh transitions from rectilinear to spherical coordinates be located inside the portion of the mesh where the explosive charge is modeled. If the transition region is modeled in the fluid domain the shock wave will reflect off the boundary between the two coordinate systems. This is more of a numerical reflection rather than a physical reflection. The numerical reflection occurs due to the angle change of the element in the rectilinear region and its adjacent element in the spherical region. This reflection can interfere with the bubble growth and dynamics and cause improper behavior.

```
lsdyna keyword
block
1 2 3 4 5 6 7 8 9;
1 2 3 4 5 6 7 8 9;
1 2 3 4 5 6 7 8 9;
0 0.004 0.03525 0.0705 0.141 0.282 0.564 1.128 1.5;
0 0.004 0.03525 0.0705 0.141 0.282 0.564 1.128 1.5;
0 0.004 0.03525 0.0705 0.141 0.282 0.564 1.128 1.5;
dei 3 9; 2 9; 3 9;
dei 2 3; 2 9; 2 9;
dei 3 9; 2 9; 2 3;
dei 2 9; 1 2; 2 9;
dei 1 2; 2 9; 2 9;
dei 2 9; 2 9; 1 2;
pb 1 2 3 1 2 3 xyz 0.000000e+00 4.000000e-03 4.000000e-03
pb 1 3 2 1 3 2 xyz 0.000000e+00 4.000000e-03 4.000000e-03
```

pb 2 3 1 2 3 1 xyz 4.000000e-03 4.000000e-03 0.000000e+00
pb 3 2 1 3 2 1 xyz 4.000000e-03 4.000000e-03 0.000000e+00
pb 2 2 3 2 2 3 xyz 4.000000e-03 4.000000e-03 4.000000e-03
pb 3 2 2 3 2 2 xyz 4.000000e-03 4.000000e-03 4.000000e-03
pb 3 1 2 3 1 2 xyz 4.000000e-03 0.000000e+00 4.000000e-03
pb 2 1 3 2 1 3 xyz 4.000000e-03 0.000000e+00 4.000000e-03
pb 2 3 2 2 3 2 xyz 4.000000e-03 4.000000e-03 4.000000e-03
pb 1 2 4 1 2 4 xyz 0.000000e+00 4.000000e-03 4.000000e-03
pb 1 2 5 1 2 5 xyz 0.000000e+00 4.000000e-03 4.000000e-03
pb 1 2 6 1 2 6 xyz 0.000000e+00 4.000000e-03 4.000000e-03
pb 1 2 7 1 2 7 xyz 0.000000e+00 4.000000e-03 4.000000e-03
pb 1 2 8 1 2 8 xyz 0.000000e+00 4.000000e-03 4.000000e-03
pb 1 2 9 1 2 9 xyz 0.000000e+00 4.000000e-03 4.000000e-03
pb 2 2 4 2 2 4 xyz 4.000000e-03 4.000000e-03 4.000000e-03
pb 2 2 5 2 2 5 xyz 4.000000e-03 4.000000e-03 4.000000e-03
pb 2 2 6 2 2 6 xyz 4.000000e-03 4.000000e-03 4.000000e-03
pb 2 2 7 2 2 7 xyz 4.000000e-03 4.000000e-03 4.000000e-03
pb 2 2 8 2 2 8 xyz 4.000000e-03 4.000000e-03 4.000000e-03
pb 2 2 9 2 2 9 xyz 4.000000e-03 4.000000e-03 4.000000e-03
pb 2 1 4 2 1 4 xyz 4.000000e-03 0.000000e+00 4.000000e-03
pb 2 1 5 2 1 5 xyz 4.000000e-03 0.000000e+00 4.000000e-03
pb 2 1 6 2 1 6 xyz 4.000000e-03 0.000000e+00 4.000000e-03
pb 2 1 7 2 1 7 xyz 4.000000e-03 0.000000e+00 4.000000e-03
pb 2 1 8 2 1 8 xyz 4.000000e-03 0.000000e+00 4.000000e-03
pb 2 1 9 2 1 9 xyz 4.000000e-03 0.000000e+00 4.000000e-03
pb 4 2 1 4 2 1 xyz 4.000000e-03 4.000000e-03 0.000000e+00
pb 5 2 1 5 2 1 xyz 4.000000e-03 4.000000e-03 0.000000e+00
pb 6 2 1 6 2 1 xyz 4.000000e-03 4.000000e-03 0.000000e+00
pb 7 2 1 7 2 1 xyz 4.000000e-03 4.000000e-03 0.000000e+00
pb 8 2 1 8 2 1 xyz 4.000000e-03 4.000000e-03 0.000000e+00
pb 9 2 1 9 2 1 xyz 4.000000e-03 4.000000e-03 0.000000e+00
pb 4 2 2 4 2 2 xyz 4.000000e-03 4.000000e-03 4.000000e-03
pb 5 2 2 5 2 2 xyz 4.000000e-03 4.000000e-03 4.000000e-03
pb 6 2 2 6 2 2 xyz 4.000000e-03 4.000000e-03 4.000000e-03

pb 7 2 2 7 2 2 xyz 4.000000e-03 4.000000e-03 4.000000e-03
pb 8 2 2 8 2 2 xyz 4.000000e-03 4.000000e-03 4.000000e-03
pb 9 2 2 9 2 2 xyz 4.000000e-03 4.000000e-03 4.000000e-03
pb 4 1 2 4 1 2 xyz 4.000000e-03 0.000000e+00 4.000000e-03
pb 5 1 2 5 1 2 xyz 4.000000e-03 0.000000e+00 4.000000e-03
pb 6 1 2 6 1 2 xyz 4.000000e-03 0.000000e+00 4.000000e-03
pb 7 1 2 7 1 2 xyz 4.000000e-03 0.000000e+00 4.000000e-03
pb 8 1 2 8 1 2 xyz 4.000000e-03 0.000000e+00 4.000000e-03
pb 9 1 2 9 1 2 xyz 4.000000e-03 0.000000e+00 4.000000e-03
pb 1 4 2 1 4 2 xyz 0.000000e+00 4.000000e-03 4.000000e-03
pb 1 5 2 1 5 2 xyz 0.000000e+00 4.000000e-03 4.000000e-03
pb 1 6 2 1 6 2 xyz 0.000000e+00 4.000000e-03 4.000000e-03
pb 1 7 2 1 7 2 xyz 0.000000e+00 4.000000e-03 4.000000e-03
pb 1 8 2 1 8 2 xyz 0.000000e+00 4.000000e-03 4.000000e-03
pb 1 9 2 1 9 2 xyz 0.000000e+00 4.000000e-03 4.000000e-03
pb 2 4 1 2 4 1 xyz 4.000000e-03 4.000000e-03 0.000000e+00
pb 2 5 1 2 5 1 xyz 4.000000e-03 4.000000e-03 0.000000e+00
pb 2 6 1 2 6 1 xyz 4.000000e-03 4.000000e-03 0.000000e+00
pb 2 7 1 2 7 1 xyz 4.000000e-03 4.000000e-03 0.000000e+00
pb 2 8 1 2 8 1 xyz 4.000000e-03 4.000000e-03 0.000000e+00
pb 2 9 1 2 9 1 xyz 4.000000e-03 4.000000e-03 0.000000e+00
pb 2 4 2 2 4 2 xyz 4.000000e-03 4.000000e-03 4.000000e-03
pb 2 5 2 2 5 2 xyz 4.000000e-03 4.000000e-03 4.000000e-03
pb 2 6 2 2 6 2 xyz 4.000000e-03 4.000000e-03 4.000000e-03
pb 2 7 2 2 7 2 xyz 4.000000e-03 4.000000e-03 4.000000e-03
pb 2 8 2 2 8 2 xyz 4.000000e-03 4.000000e-03 4.000000e-03
pb 2 9 2 2 9 2 xyz 4.000000e-03 4.000000e-03 4.000000e-03
sd 1 sp 0 0 0 0.03525 ;
sd 2 sp 0 0 0 0.0705 ;
sd 3 sp 0 0 0 0.141 ;
sd 4 sp 0 0 0 0.282 ;
sd 5 sp 0 0 0 0.564 ;
sd 6 sp 0 0 0 1.128 ;
sd 7 sp 0 0 0 1.5 ;

```
sfi 1 2; 1 2; -3;sd 1
sfi -3; 1 2; 1 2;sd 1
sfi 1 2; -3; 1 2;sd 1
sfi 1 2; 1 2; -4;sd 2
sfi -4; 1 2; 1 2;sd 2
sfi 1 2; -4; 1 2;sd 2
sfi 1 2; -5; 1 2;sd 3
sfi 1 2; 1 2; -5;sd 3
sfi -5; 1 2; 1 2;sd 3
sfi 1 2; -6; 1 2;sd 4
sfi 1 2; 1 2; -6;sd 4
sfi -6; 1 2; 1 2;sd 4
sfi 1 2; -7; 1 2;sd 5
sfi 1 2; 1 2; -7;sd 5
sfi -7; 1 2; 1 2;sd 5
sfi 1 2; -8; 1 2;sd 6
sfi 1 2; 1 2; -8;sd 6
sfi -8; 1 2; 1 2;sd 6
sfi 1 2; -9; 1 2;sd 7
sfi 1 2; 1 2; -9;sd 7
sfi -9; 1 2; 1 2;sd 7
mseq i 14 24 12 12 12 12 12 6;
mseq j 14 24 12 12 12 12 12 6;
mseq k 14 24 12 12 12 12 12 6;
mate 200
mti 1 3;1 3;1 3;100
fseti -1;1 9;1 9;= 1
fseti 1 9;1 9;-1;= 2
fseti 1 9;-1;1 9;= 3
fseti 1 2;1 2;-9;= 4
fseti -9;1 2;1 2;= 5
fseti 1 2;-9;1 2;= 6

nseti -1;-1;-1;= 7
```

```
nseti 1 9;-1;-1;= 8
nseti -1;1 9;-1;= 9
nseti -1;-1;1 9;= 10
nseti -1;1 9;1 9;= 11
nseti -1;1 9;-1;- 11
nseti -1;-1;1 9;- 11
nseti -1;-1;-1;- 11
nseti 1 9;1 9;-1;= 12
nseti -1;1 9;-1;- 12
nseti 1 9;-1;-1;- 12
nseti -1;-1;-1;- 12
nseti 1 9;-1;1 9;= 13
nseti -1;-1;1 9;- 13
nseti 1 9;-1;-1;- 13
nseti -1;-1;-1;- 13
nseti -1;1 9;1 9;= 14
nseti 1 9;1 9;-1;= 15
nseti 1 9;-1;1 9;= 16
nset 1 1 9 2 2 9 = 17
nseti -9;1 2;1 2;or 17
nseti 1 2;-9;1 2;or 17
endpart merge
stp 0.0001
set mcolor 200 0 0 1
set mcolor 100 1 0 0
set bgcolr on
```

I.2 1-D Plate Mesh Model

The Truegrid mesh modeler file for the 1-D Plate case is given.

```
lsdyna keyword
c 1-d fluid column
block
1 2;
1 2;
1 2;
0 5;
0 0.5;
0 0.5;
mseq i 49;
mseq j 4;
mseq k 4;
nseti 1 2;1 2;1 2;= YZ
nseti -1 2;1 2;1 2;- YZ
nseti -1;1 2;1 2;= XYZ
fseti -1 2;1 2;1 2;= PLOAD
nseti 1 -2;1 2;1 2;= EBC
fseti 1 -2;-1 -2;-1 -2;= NRBC
mate 200
endpart
c shell plate
block
-1;
1 2;
1 2;
2.5;
0 0.5;
0 0.5;

mseq j 4;
```

```
mseq k 4;
mate 400
c plate node set
nseti -1;1 2;1 2;= PYZ
bptol 1 2 -1
stp 0.001
endpart
merge
set mcolor 100 1 0 0
set mcolor 200 0 0 1
```

I.3 US Navy Blast Test Study Steel Plate Mesh Model

```
lsdyna keyword
c units n/m/sec
c mate 100      h.e.
c mate 200-209  water
c mate 300-307  steel reaction frame
c mate 400-401  steel plate
c mate 500-507  air
c $$$$$$$$$$$$$$$$$$$$$$$$$$$$$$$$$$$$$$
sd 1 cy 0 -2 0 1 0 0 0.6477
sd 2 cy 0 -2 0 1 0 0 1.085
c $$$$$$$$$$$$$$$ steel plate $$$$$$$$$$$$$$$$
c part 1a
c   2.5cm elem size = 0.025m
block
-1;
1 2 3 4 5;
1 2 3 4 5;
1;
-0.5 -0.1 0 0.1 0.5;
-0.5 -0.1 0 0.1 0.5;
mseq j 15 3 3 15;
mseq k 15 3 3 15;
dei -1; 1 5; 1 3;
dei -1; 4 5; 4 5;
dei -1; 1 2; 4 5;
pb 1 5 4 1 5 4 xyz 1.000000e+00 1.000000e-01 1.000000e-01
pb 1 4 5 1 4 5 xyz 1.000000e+00 1.000000e-01 1.000000e-01
pb 1 5 3 1 5 3 xyz 1.000000e+00 1.000000e-01 0.000000e+00
pb 1 3 5 1 3 5 xyz 1.000000e+00 0.000000e+00 1.000000e-01
pb 1 2 5 1 2 5 xyz 1.000000e+00 -1.000000e-01 1.000000e-01
pb 1 1 4 1 1 4 xyz 1.000000e+00 -1.000000e-01 1.000000e-01
pb 1 1 3 1 1 3 xyz 1.000000e+00 -1.000000e-01 0.000000e+00
mb 1 1 1 1 5 5 y -2
```

```
sfi -1; -5; 3 4;sd 1
sfi -1; 3 4; -5;sd 1
sfi -1; 2 3; -5;sd 1
sfi -1; -1; 3 4;sd 1
orpt - 0.5 -2 0
n 1 1 3 1 5 5
mate 400
insprt -1 4 4 13
insprt -1 6 4 13
insprt -1 3 2 13
sd 3 cy 0 -2 0 1 0 0 0.5334 ;
sfi -1; -6; 3 4;sd 3
sfi -1; 3 5; -5;sd 3
sfi -1; -2; 3 4;sd 3
dei -1; 6 7; 3 4;
dei -1; 3 5; 5 6;
dei -1; 1 2; 3 4;
ptol 1 0.001
endpart
c part 2a
c   2.5cm elem size = 0.025m
block
-1;
1 2 3 4 5;
1 2 3 4 5;
1;
-0.5 -0.1 0 0.1 0.5;
-0.5 -0.1 0 0.1 0.5;
mseq j 15 3 3 15;
mseq k 15 3 3 15;
dei -1; 1 5; 1 3;
dei -1; 4 5; 4 5;
dei -1; 1 2; 4 5;
pb 1 5 4 1 5 4 xyz 1.000000e+00 1.000000e-01 1.000000e-01
```

```
pb 1 4 5 1 4 5 xyz 1.000000e+00 1.000000e-01 1.000000e-01
pb 1 5 3 1 5 3 xyz 1.000000e+00 1.000000e-01 0.000000e+00
pb 1 3 5 1 3 5 xyz 1.000000e+00 0.000000e+00 1.000000e-01
pb 1 2 5 1 2 5 xyz 1.000000e+00 -1.000000e-01 1.000000e-01
pb 1 1 4 1 1 4 xyz 1.000000e+00 -1.000000e-01 1.000000e-01
pb 1 1 3 1 1 3 xyz 1.000000e+00 -1.000000e-01 0.000000e+00
mb 1 1 1 1 5 5 y -2
sfi -1; -5; 3 4;sd 1
sfi -1; 3 4; -5;sd 1
sfi -1; 2 3; -5;sd 1
sfi -1; -1; 3 4;sd 1
orpt - 0.5 -2 0
n 1 1 3 1 5 5
mate 401
insprt -1 4 4 13
insprt -1 6 4 13
insprt -1 3 2 13
sfi -1; -6; 3 4;sd 3
sfi -1; 3 5; -5;sd 3
sfi -1; -2; 3 4;sd 3
dei -1; 2 6; 3 4;
dei -1; 3 5; 4 5;
ptol 2 0.001
endpart
c $$$$$$$$
c part 3a
block
-1;
1 2 3 4 5;
1 2 3 4 5;
1;
-0.5 -0.1 0 0.1 0.5;
-0.5 -0.1 0 0.1 0.5;
mseq j 15 3 3 15;
```

```
mseq k 15 3 3 15;
dei -1; 1 5; 3 5;
dei -1; 4 5; 1 2;
dei -1; 1 2; 1 2;
pb 1 5 3 1 5 3 xyz 1.000000e+00 1.000000e-01 0.000000e+00
pb 1 5 2 1 5 2 xyz 1.000000e+00 1.000000e-01 -1.000000e-01
pb 1 4 1 1 4 1 xyz 1.000000e+00 1.000000e-01 -1.000000e-01
pb 1 3 1 1 3 1 xyz 1.000000e+00 0.000000e+00 -1.000000e-01
pb 1 2 1 1 2 1 xyz 1.000000e+00 -1.000000e-01 -1.000000e-01
pb 1 1 2 1 1 2 xyz 1.000000e+00 -1.000000e-01 -1.000000e-01
pb 1 1 3 1 1 3 xyz 1.000000e+00 -1.000000e-01 0.000000e+00
mb 1 1 1 1 5 5 y -2
sfi -1; -5; 2 3;sd 1
sfi -1; 3 4; -1;sd 1
sfi -1; 2 3; -1;sd 1
sfi -1; -1; 2 3;sd 1
n 1 1 1 1 5 3
mate 402
insprt -1 4 4 13
insprt -1 3 2 13
insprt -1 5 2 13
sfi -1; -6; 3 4;sd 3
sfi -1; 3 5; -2;sd 3
sfi -1; -2; 3 4;sd 3
dei -1; 6 7; 3 4;
dei -1; 3 5; 1 2;
dei -1; 1 2; 3 4;
ptol 3 0.001
endpart
c $$$$$$$$
c part 4a
block
-1;
1 2 3 4 5;
```

```
1 2 3 4 5;
1;
-0.5 -0.1 0 0.1 0.5;
-0.5 -0.1 0 0.1 0.5;
mseq j 15 3 3 15;
mseq k 15 3 3 15;
dei -1; 1 5; 3 5;
dei -1; 4 5; 1 2;
dei -1; 1 2; 1 2;
pb 1 5 3 1 5 3 xyz 1.000000e+00 1.000000e-01 0.000000e+00
pb 1 5 2 1 5 2 xyz 1.000000e+00 1.000000e-01 -1.000000e-01
pb 1 4 1 1 4 1 xyz 1.000000e+00 1.000000e-01 -1.000000e-01
pb 1 3 1 1 3 1 xyz 1.000000e+00 0.000000e+00 -1.000000e-01
pb 1 2 1 1 2 1 xyz 1.000000e+00 -1.000000e-01 -1.000000e-01
pb 1 1 2 1 1 2 xyz 1.000000e+00 -1.000000e-01 -1.000000e-01
pb 1 1 3 1 1 3 xyz 1.000000e+00 -1.000000e-01 0.000000e+00
mb 1 1 1 1 5 5 y -2
sfi -1; -5; 2 3;sd 1
sfi -1; 3 4; -1;sd 1
sfi -1; 2 3; -1;sd 1
sfi -1; -1; 2 3;sd 1
n 1 1 1 1 5 3
mate 403
insprt -1 4 4 13
insprt -1 3 2 13
insprt -1 5 2 13
sfi -1; -6; 3 4;sd 3
sfi -1; 3 5; -2;sd 3
sfi -1; -2; 3 4;sd 3
dei -1; 3 5; 2 4;
dei -1; 2 6; 3 4;
ptol 4 0.001
st 0.001
c       143 nodes were deleted by tolerancing
```

```
c        143 nodes were deleted by tolerancing
endpart merge
c $$$$$$$$$$$$$$$ reaction frame $$$$$$$$$$$$$$$$$$$
c   5cm elem size = 0.05m
c part 5b
block
-1 -2;
-1 -2 -3 -4 -5;
-1 -2 -3 -4 -5;
0 1;
-0.5 -0.1 0 0.1 0.5;
-0.5 -0.1 0 0.1 0.5;
mseq i 10;
mseq j 2 0 0 2;
mseq k 2 0 0 2;
dei ;; -2 0 -3 0 -4;
dei ; -2 0 -3 0 -4;;
dei -1 0 -2;;;
dei -1 -2; -1 -5;-1 -3;
mb 1 1 3 2 5 5 y -2
sfi 1 2; -5; 3 5;sd 1
sfi 1 2; 1 5; -3;sd 1
sfi 1 2; -1; 3 5;sd 1
sfi 1 2; 1 5; -5;sd 1
res 1 1 3 1 5 5 j 1
res 1 1 3 1 5 5 k 1
n 1 5 3 2 5 5
n 1 1 5 2 5 5
n 1 1 3 2 1 5
ptol 5 0.001
mate 300
endpart
c $$$$$$
c part 6b
```

```
block
-1 -2;
-1 -2 -3 -4 -5;
-1 -2 -3 -4 -5;
0 1;
-0.5 -0.1 0 0.1 0.5;
-0.5 -0.1 0 0.1 0.5;
mseq i 10;
mseq j 2 0 0 2;
mseq k 2 0 0 2;
dei 1 2; 1 5; 3 5;
dei ; -2 0 -3 0 -4;;
dei -1 0 -2;;;
dei ;; -2;
mb 1 1 1 2 5 3 y -2
sfi 1 2; -5; 1 3;sd 1
sfi 1 2; 1 5; -1;sd 1
sfi 1 2; -1; 1 3;sd 1
sfi 1 2; 1 5; -3;sd 1
res 1 1 1 1 5 3 j 1
res 1 1 1 1 5 3 k 1
n 1 5 1 2 5 3
n 1 1 1 2 5 1
n 1 1 1 2 1 3
mate 301
ptol 6 0.001
bptol 5 6 0.001
endpart
c $$$$$$
c part 7c
block
-1;
1 2 3 4 5 6 7;
1 2 3 4 5 6 7;
```

1;
-1.0 -0.5 -0.1 0 0.1 0.5 1.0;
-1.0 -0.5 -0.1 0 0.1 0.5 1.0;
dei -1; 1 7; 1 4;
dei -1; 6 7; 6 7;
dei -1; 1 2; 6 7;
pb 1 7 4 1 7 4 xyz 1.000000e+00 5.000000e-01 0.000000e+00
pb 1 7 5 1 7 5 xyz 1.000000e+00 5.000000e-01 1.000000e-01
pb 1 7 6 1 7 6 xyz 1.000000e+00 5.000000e-01 5.000000e-01
pb 1 6 7 1 6 7 xyz 1.000000e+00 5.000000e-01 5.000000e-01
pb 1 5 7 1 5 7 xyz 1.000000e+00 1.000000e-01 5.000000e-01
pb 1 4 7 1 4 7 xyz 1.000000e+00 0.000000e+00 5.000000e-01
pb 1 3 7 1 3 7 xyz 1.000000e+00 -1.000000e-01 5.000000e-01
pb 1 2 7 1 2 7 xyz 1.000000e+00 -5.000000e-01 5.000000e-01
pb 1 1 6 1 1 6 xyz 1.000000e+00 -5.000000e-01 5.000000e-01
pb 1 1 5 1 1 5 xyz 1.000000e+00 -5.000000e-01 1.000000e-01
pb 1 1 4 1 1 4 xyz 1.000000e+00 -5.000000e-01 0.000000e+00
n 1 1 5 1 7 7
mseq j 4 2 0 0 2 4;
mseq k 4 2 0 0 2 4;
mb 1 1 1 1 7 7 y -2
sfi -1; -7; 4 5;sd 2
sfi -1; -7; 5 6;sd 2
sfi -1; 5 6; -7;sd 2
sfi -1; 4 5; -7;sd 2
sfi -1; 3 4; -7;sd 2
sfi -1; 2 3; -7;sd 2
sfi -1; -1; 5 6;sd 2
sfi -1; -1; 4 5;sd 2
dei -1; 2 6; 4 6;
sfi -1; -6; 4 5;sd 1
sfi -1; -6; 5 6;sd 1
sfi -1; 5 6; -6;sd 1
sfi -1; 4 5; -6;sd 1

sfi -1; 3 4; -6;sd 1
sfi -1; 2 3; -6;sd 1
sfi -1; -2; 5 6;sd 1
sfi -1; -2; 4 5;sd 1
mate 302
ptol 7 0.001
endpart
c part 8c
block
-1;
1 2 3 4 5 6 7;
1 2 3 4 5 6 7;
1;
-1.0 -0.5 -0.1 0 0.1 0.5 1.0;
-1.0 -0.5 -0.1 0 0.1 0.5 1.0;
dei -1; 1 7; 4 7;
dei -1; 6 7; 1 2;
dei -1; 1 2; 1 2;
n 1 1 1 1 7 3
pb 1 7 4 1 7 4 xyz 1.000000e+00 5.000000e-01 0.000000e+00
pb 1 7 3 1 7 3 xyz 1.000000e+00 5.000000e-01 -1.000000e-01
pb 1 7 2 1 7 2 xyz 1.000000e+00 5.000000e-01 -5.000000e-01
pb 1 6 1 1 6 1 xyz 1.000000e+00 5.000000e-01 -5.000000e-01
pb 1 5 1 1 5 1 xyz 1.000000e+00 1.000000e-01 -5.000000e-01
pb 1 4 1 1 4 1 xyz 1.000000e+00 0.000000e+00 -5.000000e-01
pb 1 3 1 1 3 1 xyz 1.000000e+00 -1.000000e-01 -5.000000e-01
pb 1 2 1 1 2 1 xyz 1.000000e+00 -5.000000e-01 -5.000000e-01
pb 1 1 2 1 1 2 xyz 1.000000e+00 -5.000000e-01 -5.000000e-01
pb 1 1 3 1 1 3 xyz 1.000000e+00 -5.000000e-01 -1.000000e-01
pb 1 1 4 1 1 4 xyz 1.000000e+00 -5.000000e-01 0.000000e+00
mseq j 4 2 0 0 2 4;
mseq k 4 2 0 0 2 4;
mb 1 1 1 1 7 7 y -2
sfi -1; -7; 3 4;sd 2

sfi -1; -7; 2 3;sd 2
sfi -1; 5 6; -1;sd 2
sfi -1; 4 5; -1;sd 2
sfi -1; 3 4; -1;sd 2
sfi -1; 2 3; -1;sd 2
sfi -1; -1; 2 3;sd 2
sfi -1; -1; 3 4;sd 2
dei -1; 2 6; 2 4;
sfi -1; -6; 3 4;sd 1
sfi -1; -6; 2 3;sd 1
sfi -1; 5 6; -2;sd 1
sfi -1; 4 5; -2;sd 1
sfi -1; 3 4; -2;sd 1
sfi -1; 2 3; -2;sd 1
sfi -1; -2; 2 3;sd 1
sfi -1; -2; 3 4;sd 1
mate 303
ptol 8 0.001
endpart
c part 9d
block
-1;
1 2 3 4 5 6 7;
1 2 3 4 5 6 7;
0;
-1.0 -0.5 -0.1 0 0.1 0.5 1.0;
-1.0 -0.5 -0.1 0 0.1 0.5 1.0;
dei -1; 1 7; 1 4;
dei -1; 6 7; 6 7;
dei -1; 1 2; 6 7;
pb 1 7 4 1 7 4 xyz 0.000000e+00 5.000000e-01 0.000000e+00
pb 1 7 5 1 7 5 xyz 0.000000e+00 5.000000e-01 1.000000e-01
pb 1 7 6 1 7 6 xyz 0.000000e+00 5.000000e-01 5.000000e-01
pb 1 6 7 1 6 7 xyz 0.000000e+00 5.000000e-01 5.000000e-01

pb 1 5 7 1 5 7 xyz 0.000000e+00 1.000000e-01 5.000000e-01
pb 1 4 7 1 4 7 xyz 0.000000e+00 0.000000e+00 5.000000e-01
pb 1 3 7 1 3 7 xyz 0.000000e+00 -1.000000e-01 5.000000e-01
pb 1 2 7 1 2 7 xyz 0.000000e+00 -5.000000e-01 5.000000e-01
pb 1 1 6 1 1 6 xyz 0.000000e+00 -5.000000e-01 5.000000e-01
pb 1 1 5 1 1 5 xyz 0.000000e+00 -5.000000e-01 1.000000e-01
pb 1 1 4 1 1 4 xyz 0.000000e+00 -5.000000e-01 0.000000e+00
mseq j 4 2 0 0 2 4;
mseq k 4 2 0 0 2 4;
mb 1 1 1 1 7 7 y -2
sfi -1; -7; 4 5;sd 2
sfi -1; -7; 5 6;sd 2
sfi -1; 5 6; -7;sd 2
sfi -1; 4 5; -7;sd 2
sfi -1; 3 4; -7;sd 2
sfi -1; 2 3; -7;sd 2
sfi -1; -1; 5 6;sd 2
sfi -1; -1; 4 5;sd 2
dei -1; 2 6; 4 6;
sfi -1; -6; 4 5;sd 1
sfi -1; -6; 5 6;sd 1
sfi -1; 5 6; -6;sd 1
sfi -1; 4 5; -6;sd 1
sfi -1; 3 4; -6;sd 1
sfi -1; 2 3; -6;sd 1
sfi -1; -2; 5 6;sd 1
sfi -1; -2; 4 5;sd 1
mate 304
ptol 9 0.001
endpart
c part 10d
block
-1;
1 2 3 4 5 6 7;

1 2 3 4 5 6 7;
0;
-1.0 -0.5 -0.1 0 0.1 0.5 1.0;
-1.0 -0.5 -0.1 0 0.1 0.5 1.0;
dei -1; 1 7; 4 7;
dei -1; 6 7; 1 2;
dei -1; 1 2; 1 2;
pb 1 7 4 1 7 4 xyz 0.000000e+00 5.000000e-01 0.000000e+00
pb 1 7 3 1 7 3 xyz 0.000000e+00 5.000000e-01 -1.000000e-01
pb 1 7 2 1 7 2 xyz 0.000000e+00 5.000000e-01 -5.000000e-01
pb 1 6 1 1 6 1 xyz 0.000000e+00 5.000000e-01 -5.000000e-01
pb 1 5 1 1 5 1 xyz 0.000000e+00 1.000000e-01 -5.000000e-01
pb 1 4 1 1 4 1 xyz 0.000000e+00 0.000000e+00 -5.000000e-01
pb 1 3 1 1 3 1 xyz 0.000000e+00 -1.000000e-01 -5.000000e-01
pb 1 2 1 1 2 1 xyz 0.000000e+00 -5.000000e-01 -5.000000e-01
pb 1 1 2 1 1 2 xyz 0.000000e+00 -5.000000e-01 -5.000000e-01
pb 1 1 3 1 1 3 xyz 0.000000e+00 -5.000000e-01 -1.000000e-01
pb 1 1 4 1 1 4 xyz 0.000000e+00 -5.000000e-01 0.000000e+00
mseq j 4 2 0 0 2 4;
mseq k 4 2 0 0 2 4;
mb 1 1 1 1 7 7 y -2
sfi -1; -7; 3 4;sd 2
sfi -1; -7; 2 3;sd 2
sfi -1; 5 6; -1;sd 2
sfi -1; 4 5; -1;sd 2
sfi -1; 3 4; -1;sd 2
sfi -1; 2 3; -1;sd 2
sfi -1; -1; 2 3;sd 2
sfi -1; -1; 3 4;sd 2
dei -1; 2 6; 2 4;
sfi -1; -6; 3 4;sd 1
sfi -1; -6; 2 3;sd 1
sfi -1; 5 6; -2;sd 1
sfi -1; 4 5; -2;sd 1

```
sfi -1; 3 4; -2;sd 1
sfi -1; 2 3; -2;sd 1
sfi -1; -2; 2 3;sd 1
sfi -1; -2; 3 4;sd 1
mate 305
ptol 10 0.001
endpart
c $$$$
c part 11d
block
-1;
1 2 3 4 5;
1 2 3 4 5;
0;
-0.5 -0.1 0 0.1 0.5;
-0.5 -0.1 0 0.1 0.5;
mseq j 15 3 3 15;
mseq k 15 3 3 15;
dei -1; 1 5; 1 3;
dei -1; 4 5; 4 5;
dei -1; 1 2; 4 5;
pb 1 5 4 1 5 4 xyz 0.000000e+00 1.000000e-01 1.000000e-01
pb 1 4 5 1 4 5 xyz 0.000000e+00 1.000000e-01 1.000000e-01
pb 1 5 3 1 5 3 xyz 0.000000e+00 1.000000e-01 0.000000e+00
pb 1 3 5 1 3 5 xyz 0.000000e+00 0.000000e+00 1.000000e-01
pb 1 2 5 1 2 5 xyz 0.000000e+00 -1.000000e-01 1.000000e-01
pb 1 1 4 1 1 4 xyz 0.000000e+00 -1.000000e-01 1.000000e-01
pb 1 1 3 1 1 3 xyz 0.000000e+00 -1.000000e-01 0.000000e+00
n 1 1 3 1 5 5
mb 1 1 1 1 5 5 y -2
sfi -1; -5; 3 4;sd 1
sfi -1; 3 4; -5;sd 1
sfi -1; 2 3; -5;sd 1
sfi -1; -1; 3 4;sd 1
```

```
mate 306
ptol 11 0.001
endpart
c part 12d
block
-1;
1 2 3 4 5;
1 2 3 4 5;
0;
-0.5 -0.1 0 0.1 0.5;
-0.5 -0.1 0 0.1 0.5;
mseq j 15 3 3 15;
mseq k 15 3 3 15;
dei -1; 1 5; 3 5;
dei -1; 4 5; 1 2;
dei -1; 1 2; 1 2;
pb 1 5 3 1 5 3 xyz 0.000000e+00 1.000000e-01 0.000000e+00
pb 1 5 2 1 5 2 xyz 0.000000e+00 1.000000e-01 -1.000000e-01
pb 1 4 1 1 4 1 xyz 0.000000e+00 1.000000e-01 -1.000000e-01
pb 1 3 1 1 3 1 xyz 0.000000e+00 0.000000e+00 -1.000000e-01
pb 1 2 1 1 2 1 xyz 0.000000e+00 -1.000000e-01 -1.000000e-01
pb 1 1 2 1 1 2 xyz 0.000000e+00 -1.000000e-01 -1.000000e-01
pb 1 1 3 1 1 3 xyz 0.000000e+00 -1.000000e-01 0.000000e+00
mb 1 1 1 1 5 5 y -2
n 1 1 1 1 5 3
sfi -1; -5; 2 3;sd 1
sfi -1; 3 4; -1;sd 1
sfi -1; 2 3; -1;sd 1
sfi -1; -1; 2 3;sd 1
mate 307
ptol 12 0.001
c ##nodal merging between plate and reaction frame##
bptol 1 5 -1
bptol 1 6 -1
```

```
bptol 1 7 -1
bptol 1 8 -1
bptol 1 9 -1
bptol 1 10 -1
bptol 1 11 -1
bptol 1 12 -1
bptol 2 5 -1
bptol 2 6 -1
bptol 2 7 -1
bptol 2 8 -1
bptol 2 9 -1
bptol 2 10 -1
bptol 2 11 -1
bptol 2 12 -1
bptol 3 5 -1
bptol 3 6 -1
bptol 3 7 -1
bptol 3 8 -1
bptol 3 9 -1
bptol 3 10 -1
bptol 3 11 -1
bptol 3 12 -1
bptol 4 5 -1
bptol 4 6 -1
bptol 4 7 -1
bptol 4 8 -1
bptol 4 9 -1
bptol 4 10 -1
bptol 4 11 -1
bptol 4 12 -1
c ##
st 0.001
c       432 nodes were deleted by tolerancing
c       432 nodes were deleted by tolerancing
```

endpart merge
c $$$$$$$$$$$$$$$ air $$$$$$$$$$$$$$$$$
c part 13e
block
1 2;
1 2 3 4 5;
1 2 3 4 5;
0 1;
-0.5 -0.1 0 0.1 0.5;
-0.5 -0.1 0 0.1 0.5;
dei 1 2; 1 5; 1 3;
dei 1 2; 4 5; 4 5;
dei 1 2; 1 2; 4 5;
mseq i 10;
mseq j 15 3 3 15;
mseq k 15 3 3 15;
pb 1 5 4 1 5 4 xyz 0.000000e+00 1.000000e-01 1.000000e-01
pb 2 5 4 2 5 4 xyz 1.000000e+00 1.000000e-01 1.000000e-01
pb 1 4 5 1 4 5 xyz 0.000000e+00 1.000000e-01 1.000000e-01
pb 2 4 5 2 4 5 xyz 1.000000e+00 1.000000e-01 1.000000e-01
pb 2 2 5 2 2 5 xyz 1.000000e+00 -1.000000e-01 1.000000e-01
pb 2 1 4 2 1 4 xyz 1.000000e+00 -1.000000e-01 1.000000e-01
pb 1 1 4 1 1 4 xyz 0.000000e+00 -1.000000e-01 1.000000e-01
pb 1 2 5 1 2 5 xyz 0.000000e+00 -1.000000e-01 1.000000e-01
mb 1 1 3 2 5 5 y -2
sfi 1 2; -5; 3 4;sd 1
sfi 1 2; 3 4; -5;sd 1
sfi 1 2; 2 3; -5;sd 1
sfi 1 2; -1; 3 4;sd 1
mate 500
ptol 13 0.001
c part 14e
block
1 2;

```
1 2 3 4 5;
1 2 3 4 5;
0 1;
-0.5 -0.1 0 0.1 0.5;
-0.5 -0.1 0 0.1 0.5;
dei 1 2; 1 5; 3 5;
dei 1 2; 4 5; 1 2;
dei 1 2; 1 2; 1 2;
mseq i 10;
mseq j 15 3 3 15;
mseq k 15 3 3 15;
pb 2 5 2 2 5 2 xyz 1.000000e+00 1.000000e-01 -1.000000e-01
pb 1 5 2 1 5 2 xyz 0.000000e+00 1.000000e-01 -1.000000e-01
pb 1 4 1 1 4 1 xyz 0.000000e+00 1.000000e-01 -1.000000e-01
pb 2 4 1 2 4 1 xyz 1.000000e+00 1.000000e-01 -1.000000e-01
pb 2 2 1 2 2 1 xyz 1.000000e+00 -1.000000e-01 -1.000000e-01
pb 1 2 1 1 2 1 xyz 0.000000e+00 -1.000000e-01 -1.000000e-01
pb 2 1 2 2 1 2 xyz 1.000000e+00 -1.000000e-01 -1.000000e-01
pb 1 1 2 1 1 2 xyz 0.000000e+00 -1.000000e-01 -1.000000e-01
mb 1 1 1 2 5 3 y -2
sfi 1 2; -5; 2 3;sd 1
sfi 1 2; 3 4; -1;sd 1
sfi 1 2; 2 3; -1;sd 1
sfi 1 2; -1; 2 3;sd 1
mate 501
ptol 14 0.001
c ##nodal merging between plate, reaction frame and air##
bptol 13 1 -1
bptol 13 2 -1
bptol 13 3 -1
bptol 13 4 -1
bptol 13 5 -1
bptol 13 6 -1
bptol 13 7 -1
```

```
bptol 13 8 -1
bptol 11 9 -1
bptol 13 10 -1
bptol 13 11 -1
bptol 13 12 -1
bptol 14 1 -1
bptol 14 2 -1
bptol 14 3 -1
bptol 14 4 -1
bptol 14 5 -1
bptol 14 6 -1
bptol 14 7 -1
bptol 14 8 -1
bptol 14 9 -1
bptol 14 10 -1
bptol 14 11 -1
bptol 14 12 -1
st 0.001
c       1692 nodes were deleted by tolerancing
c       1692 nodes were deleted by tolerancing
endpart merge
c $$$$$$$$$$$$$$$ water $$$$$$$$$$$$$$$$$
c part 15f middle fluid
block
1 2;
1 2 3 4 5 6 7;
1 2 3 4 5 6 7;
0 1;
-2 -0.5 -0.1 0 0.1 0.5 2;
-2 -0.5 -0.1 0 0.1 0.5 2;
mseq i 10;
mseq j 7 2 0 0 2 7;
mseq k 7 2 0 0 2 7;
dei 1 2; 2 6; 2 6;
```

dei 1 2; 1 7; 1 4;
mb 1 1 4 2 7 7 y -2
sfi 1 2; -6; 4 6;sd 1
sfi 1 2; 2 6; -6;sd 1
sfi 1 2; -2; 4 6;sd 1
res 1 6 4 2 6 6 k 1
res 1 2 4 2 2 6 k 1
res 1 2 6 2 6 6 j 1
ptol 15 0.001
mate 200
bb 1 7 4 2 7 7 1 ;
endpart
c part 16f middle fluid
block
1 2;
1 2 3 4 5 6 7;
1 2 3 4 5 6 7;
0 1;
-2 -0.5 -0.1 0 0.1 0.5 2;
-2 -0.5 -0.1 0 0.1 0.5 2;
mseq i 10;
mseq j 7 2 0 0 2 7;
mseq k 7 2 0 0 2 7;
dei 1 2; 1 7; 4 7;
dei 1 2; 2 6; 2 4;
mb 1 1 1 2 7 4 y -2
sfi 1 2; -6; 2 4;sd 1
sfi 1 2; 2 6; -2;sd 1
sfi 1 2; -2; 2 4;sd 1
res 1 2 2 2 2 4 k 1
res 1 6 2 2 6 4 k 1
res 1 2 2 2 6 2 j 1
ptol 16 0.001
mate 201

```
bb 1 7 1 2 7 4 2 ;
endpart
c part 17g fluid -x+z
block
1 2 3;
1 2 3 4 5 6 7;
1 2 3 4 5 6 7;
-1 -0.25 0;
-2 -0.5 -0.1 0 0.1 0.5 2;
-2 -0.5 -0.1 0 0.1 0.5 2;
mseq i 15 5;
mseq j 7 2 0 0 2 7;
mseq k 7 2 0 0 2 7;
dei 1 3; 1 7; 1 4;
dei 1 3; 2 6; 4 6;
mb 1 1 4 3 7 7 y -2
sfi 1 3; -6; 4 6;sd 1
sfi 1 3; 2 6; -6;sd 1
sfi 1 3; -2; 4 6;sd 1
res 1 2 4 3 2 6 k 1
res 1 6 4 3 6 6 k 1
res 1 2 6 3 6 6 j 1
ptol 17 0.001
mate 202
bb 1 7 4 3 7 7 3 ;
endpart
c part 18g fluid -x-z
block
1 2 3;
1 2 3 4 5 6 7;
1 2 3 4 5 6 7;
-1 -0.25 0;
-2 -0.5 -0.1 0 0.1 0.5 2;
-2 -0.5 -0.1 0 0.1 0.5 2;
```

mseq i 15 5;
mseq j 7 2 0 0 2 7;
mseq k 7 2 0 0 2 7;
dei 1 3; 1 7; 4 7;
dei 1 3; 2 6; 2 4;
mb 1 1 1 3 7 4 y -2
sfi 1 3; -2 -6; -2 4;sd 1
res 1 2 2 3 2 4 k 1
res 1 6 2 3 6 4 k 1
res 1 2 2 3 6 2 j 1
ptol 18 0.001
mate 203
bb 1 7 1 3 7 4 4 ;
endpart
c part 19g fluid -x+z inner
block
1 2 3;
1 2 3 4 5;
1 2 3 4 5;
-1 -0.25 0;
-0.5 -0.1 0 0.1 0.5;
-0.5 -0.1 0 0.1 0.5;
dei 1 3; 1 5; 1 3;
dei 1 3; 4 5; 4 5;
dei 1 3; 1 2; 4 5;
mseq i 15 5;
mseq j 15 3 3 15;
mseq k 15 3 3 15;
pb 1 5 4 1 5 4 xyz -1.000000e+00 2.500000e-01 2.500000e-01
pb 1 4 5 1 4 5 xyz -1.000000e+00 2.500000e-01 2.500000e-01
pb 2 5 4 2 5 4 xyz -2.500000e-01 2.500000e-01 2.500000e-01
pb 2 4 5 2 4 5 xyz -2.500000e-01 2.500000e-01 2.500000e-01
pb 3 5 4 3 5 4 xyz 0.000000e+00 2.500000e-01 2.500000e-01
pb 3 4 5 3 4 5 xyz 0.000000e+00 2.500000e-01 2.500000e-01

pb 3 1 4 3 1 4 xyz 0.000000e+00 -2.500000e-01 2.500000e-01
pb 3 2 5 3 2 5 xyz 0.000000e+00 -2.500000e-01 2.500000e-01
pb 2 2 5 2 2 5 xyz -2.500000e-01 -2.500000e-01 2.500000e-01
pb 2 1 4 2 1 4 xyz -2.500000e-01 -2.500000e-01 2.500000e-01
pb 1 1 4 1 1 4 xyz -1.000000e+00 -2.500000e-01 2.500000e-01
pb 1 2 5 1 2 5 xyz -1.000000e+00 -2.500000e-01 2.500000e-01
mb 1 1 3 3 5 5 y -2
sfi 1 3; -5; 3 4;sd 1
sfi 1 3; 2 4; -5;sd 1
sfi 1 3; -1; 3 4;sd 1
ptol 19 0.001
mate 204
endpart
c part 20g fluid -x-z inner
block
1 2 3;
1 2 3 4 5;
1 2 3 4 5;
-1 -0.25 0;
-0.5 -0.1 0 0.1 0.5;
-0.5 -0.1 0 0.1 0.5;
mseq i 15 5;
mseq j 15 3 3 15;
mseq k 15 3 3 15;
dei 1 3; 1 5; 3 5;
dei 1 3; 4 5; 1 2;
dei 1 3; 1 2; 1 2;
pb 3 5 2 3 5 2 xyz 0.000000e+00 2.500000e-01 -2.500000e-01
pb 3 4 1 3 4 1 xyz 0.000000e+00 2.500000e-01 -2.500000e-01
pb 2 5 2 2 5 2 xyz -2.500000e-01 2.500000e-01 -2.500000e-01
pb 2 4 1 2 4 1 xyz -2.500000e-01 2.500000e-01 -2.500000e-01
pb 1 5 2 1 5 2 xyz -1.000000e+00 2.500000e-01 -2.500000e-01
pb 1 4 1 1 4 1 xyz -1.000000e+00 2.500000e-01 -2.500000e-01
pb 3 1 2 3 1 2 xyz 0.000000e+00 -2.500000e-01 -2.500000e-01

```
pb 3 2 1 3 2 1 xyz 0.000000e+00 -2.500000e-01 -2.500000e-01
pb 2 2 1 2 2 1 xyz -2.500000e-01 -2.500000e-01 -2.500000e-01
pb 2 1 2 2 1 2 xyz -2.500000e-01 -2.500000e-01 -2.500000e-01
pb 1 1 2 1 1 2 xyz -1.000000e+00 -2.500000e-01 -2.500000e-01
pb 1 2 1 1 2 1 xyz -1.000000e+00 -2.500000e-01 -2.500000e-01
mb 1 1 1 3 5 3 y -2
sfi 1 3; -5; 2 3;sd 1
sfi 1 3; 2 4; -1;sd 1
sfi 1 3; -1; 2 3;sd 1
ptol 20 0.001
mate 205
endpart
c part 21g fluid +x+z
block
1 41 51 56 60 66;
1 2 3 4 5 6 7;
1 2 3 4 5 6 7;
1 2 2.5 3 4 10;
-2 -0.5 -0.1 0 0.1 0.5 2;
-2 -0.5 -0.1 0 0.1 0.5 2;
dei 1 6; 1 7; 1 4;
dei 1 6; 2 6; 4 6;
mseq j 7 2 0 0 2 7;
mseq k 7 2 0 0 2 7;
mb 1 1 4 6 7 7 y -2
sfi 1 6; -2 -6; 4 6;sd 1
sfi 1 6; 2 6; 4 -6;sd 1
res 1 2 6 6 6 6 j 1
res 1 6 4 6 6 6 k 1
res 1 2 4 6 2 6 k 1
ptol 21 0.001
mate 206
bb 1 7 4 6 7 7 5 ;
endpart
```

```
c part 22g fluid +x-z
block
1 41 51 56 60 66;
1 2 3 4 5 6 7;
1 2 3 4 5 6 7;
1 2 2.5 3 4 10;
-2 -0.5 -0.1 0 0.1 0.5 2;
-2 -0.5 -0.1 0 0.1 0.5 2;
mseq j 7 2 0 0 2 7;
mseq k 7 2 0 0 2 7;
dei 1 6; 1 7; 4 7;
dei 1 6; 2 6; 2 4;
mb 1 1 1 6 7 4 y -2
sfi 1 6; -6; 2 4;sd 1
sfi 1 6; 2 6; -2;sd 1
sfi 1 6; -2; 2 4;sd 1
res 1 2 2 6 2 4 k 1
res 1 6 2 6 6 4 k 1
res 1 2 2 6 6 2 j 1
ptol 22 0.001
mate 207
bb 1 7 1 6 7 4 6 ;
endpart
c part 23g fluid +x+z inner
block
1 41 51 56 60 66;
1 2 3 4 5;
1 2 3 4 5;
1 2 2.5 3 4 10;
-0.5 -0.1 0 0.1 0.5;
-0.5 -0.1 0 0.1 0.5;
mseq j 15 3 3 15;
mseq k 15 3 3 15;
dei 1 6; 1 5; 1 3;
```

dei 1 6; 4 5; 4 5;
dei 1 6; 1 2; 4 5;
pb 1 5 4 1 5 4 xyz 1.000000e+00 2.500000e-01 2.500000e-01
pb 1 4 5 1 4 5 xyz 1.000000e+00 2.500000e-01 2.500000e-01
pb 2 5 4 2 5 4 xyz 2.000000e+00 2.500000e-01 2.500000e-01
pb 2 4 5 2 4 5 xyz 2.000000e+00 2.500000e-01 2.500000e-01
pb 3 5 4 3 5 4 xyz 2.500000e+00 2.500000e-01 2.500000e-01
pb 3 4 5 3 4 5 xyz 2.500000e+00 2.500000e-01 2.500000e-01
pb 4 5 4 4 5 4 xyz 3.000000e+00 2.500000e-01 2.500000e-01
pb 4 4 5 4 4 5 xyz 3.000000e+00 2.500000e-01 2.500000e-01
pb 5 5 4 5 5 4 xyz 4.000000e+00 2.500000e-01 2.500000e-01
pb 5 4 5 5 4 5 xyz 4.000000e+00 2.500000e-01 2.500000e-01
pb 6 5 4 6 5 4 xyz 10.000000e+00 2.500000e-01 2.500000e-01
pb 6 4 5 6 4 5 xyz 10.000000e+00 2.500000e-01 2.500000e-01
pb 1 2 5 1 2 5 xyz 1.000000e+00 -2.500000e-01 2.500000e-01
pb 1 1 4 1 1 4 xyz 1.000000e+00 -2.500000e-01 2.500000e-01
pb 2 2 5 2 2 5 xyz 2.000000e+00 -2.500000e-01 2.500000e-01
pb 2 1 4 2 1 4 xyz 2.000000e+00 -2.500000e-01 2.500000e-01
pb 3 1 4 3 1 4 xyz 2.500000e+00 -2.500000e-01 2.500000e-01
pb 3 2 5 3 2 5 xyz 2.500000e+00 -2.500000e-01 2.500000e-01
pb 4 2 5 4 2 5 xyz 3.000000e+00 -2.500000e-01 2.500000e-01
pb 4 1 4 4 1 4 xyz 3.000000e+00 -2.500000e-01 2.500000e-01
pb 5 2 5 5 2 5 xyz 4.000000e+00 -2.500000e-01 2.500000e-01
pb 5 1 4 5 1 4 xyz 4.000000e+00 -2.500000e-01 2.500000e-01
pb 6 2 5 6 2 5 xyz 10.000000e+00 -2.500000e-01 2.500000e-01
pb 6 1 4 6 1 4 xyz 10.000000e+00 -2.500000e-01 2.500000e-01
mb 1 1 3 6 5 5 y -2
sfi 1 6; -5; 3 4;sd 1
sfi 1 6; 2 4; -5;sd 1
sfi 1 6; -1; 3 4;sd 1
ptol 23 0.001
mate 208
endpart
c part 24g fluid +x-z inner

block
1 41 51 56 60 66;
1 2 3 4 5;
1 2 3 4 5;
1 2 2.5 3 4 10;
-0.5 -0.1 0 0.1 0.5;
-0.5 -0.1 0 0.1 0.5;
mseq j 15 3 3 15;
mseq k 15 3 3 15;
dei 1 6; 1 5; 3 5;
dei 1 6; 4 5; 1 2;
dei 1 6; 1 2; 1 2;
pb 1 5 2 1 5 2 xyz 1.000000e+00 2.500000e-01 -2.500000e-01
pb 1 4 1 1 4 1 xyz 1.000000e+00 2.500000e-01 -2.500000e-01
pb 2 5 2 2 5 2 xyz 2.000000e+00 2.500000e-01 -2.500000e-01
pb 2 4 1 2 4 1 xyz 2.000000e+00 2.500000e-01 -2.500000e-01
pb 3 5 2 3 5 2 xyz 2.500000e+00 2.500000e-01 -2.500000e-01
pb 3 4 1 3 4 1 xyz 2.500000e+00 2.500000e-01 -2.500000e-01
pb 4 5 2 4 5 2 xyz 3.000000e+00 2.500000e-01 -2.500000e-01
pb 4 4 1 4 4 1 xyz 3.000000e+00 2.500000e-01 -2.500000e-01
pb 5 5 2 5 5 2 xyz 4.000000e+00 2.500000e-01 -2.500000e-01
pb 5 4 1 5 4 1 xyz 4.000000e+00 2.500000e-01 -2.500000e-01
pb 6 5 2 6 5 2 xyz 10.000000e+00 2.500000e-01 -2.500000e-01
pb 6 4 1 6 4 1 xyz 10.000000e+00 2.500000e-01 -2.500000e-01
pb 1 2 1 1 2 1 xyz 1.000000e+00 -2.500000e-01 -2.500000e-01
pb 1 1 2 1 1 2 xyz 1.000000e+00 -2.500000e-01 -2.500000e-01
pb 2 2 1 2 2 1 xyz 2.000000e+00 -2.500000e-01 -2.500000e-01
pb 2 1 2 2 1 2 xyz 2.000000e+00 -2.500000e-01 -2.500000e-01
pb 3 2 1 3 2 1 xyz 2.500000e+00 -2.500000e-01 -2.500000e-01
pb 3 1 2 3 1 2 xyz 2.500000e+00 -2.500000e-01 -2.500000e-01
pb 4 2 1 4 2 1 xyz 3.000000e+00 -2.500000e-01 -2.500000e-01
pb 4 1 2 4 1 2 xyz 3.000000e+00 -2.500000e-01 -2.500000e-01
pb 5 1 2 5 1 2 xyz 4.000000e+00 -2.500000e-01 -2.500000e-01
pb 5 2 1 5 2 1 xyz 4.000000e+00 -2.500000e-01 -2.500000e-01

pb 6 2 1 6 2 1 xyz 10.000000e+00 -2.500000e-01 -2.500000e-01

pb 6 1 2 6 1 2 xyz 10.000000e+00 -2.500000e-01 -2.500000e-01

mb 1 1 1 6 5 3 y -2

sfi 1 6; -5; 2 3;sd 1

sfi 1 6; 2 4; -1;sd 1

sfi 1 6; -1; 2 3;sd 1

ptol 24 0.001

mate 209

c ##nodal merging between plate, reaction frame and water##

bptol 1 15 -1

bptol 1 16 -1

bptol 1 17 -1

bptol 1 18 -1

bptol 1 19 -1

bptol 1 20 -1

bptol 1 21 -1

bptol 1 22 -1

bptol 1 23 -1

bptol 1 24 -1

bptol 2 15 -1

bptol 2 16 -1

bptol 2 17 -1

bptol 2 18 -1

bptol 2 19 -1

bptol 2 20 -1

bptol 2 21 -1

bptol 2 22 -1

bptol 2 23 -1

bptol 2 24 -1

bptol 3 15 -1

bptol 3 16 -1

bptol 3 17 -1

bptol 3 18 -1

bptol 3 19 -1

bptol 3 20 -1
bptol 3 21 -1
bptol 3 22 -1
bptol 3 23 -1
bptol 3 24 -1
bptol 4 15 -1
bptol 4 16 -1
bptol 4 17 -1
bptol 4 18 -1
bptol 4 19 -1
bptol 4 20 -1
bptol 4 21 -1
bptol 4 22 -1
bptol 4 23 -1
bptol 4 24 -1
bptol 5 15 -1
bptol 5 16 -1
bptol 5 17 -1
bptol 5 18 -1
bptol 5 19 -1
bptol 5 20 -1
bptol 5 21 -1
bptol 5 22 -1
bptol 5 23 -1
bptol 5 24 -1
bptol 6 15 -1
bptol 6 16 -1
bptol 6 17 -1
bptol 6 18 -1
bptol 6 19 -1
bptol 6 20 -1
bptol 6 21 -1
bptol 6 22 -1
bptol 6 23 -1

bptol 6 24 -1
bptol 7 15 -1
bptol 7 16 -1
bptol 7 17 -1
bptol 7 18 -1
bptol 7 19 -1
bptol 7 20 -1
bptol 7 21 -1
bptol 7 22 -1
bptol 7 23 -1
bptol 7 24 -1
bptol 8 15 -1
bptol 8 16 -1
bptol 8 17 -1
bptol 8 18 -1
bptol 8 19 -1
bptol 8 20 -1
bptol 8 21 -1
bptol 8 22 -1
bptol 8 23 -1
bptol 8 24 -1
bptol 9 15 -1
bptol 9 16 -1
bptol 9 17 -1
bptol 9 18 -1
bptol 9 19 -1
bptol 9 20 -1
bptol 9 21 -1
bptol 9 22 -1
bptol 9 23 -1
bptol 9 24 -1
bptol 10 15 -1
bptol 10 16 -1
bptol 10 17 -1

bptol 10 18 -1
bptol 10 19 -1
bptol 10 20 -1
bptol 10 21 -1
bptol 10 22 -1
bptol 10 23 -1
bptol 10 24 -1
bptol 11 15 -1
bptol 11 16 -1
bptol 11 17 -1
bptol 11 18 -1
bptol 11 19 -1
bptol 11 20 -1
bptol 11 21 -1
bptol 11 22 -1
bptol 11 23 -1
bptol 11 24 -1
bptol 12 15 -1
bptol 12 16 -1
bptol 12 17 -1
bptol 12 18 -1
bptol 12 19 -1
bptol 12 20 -1
bptol 12 21 -1
bptol 12 22 -1
bptol 12 23 -1
bptol 12 24 -1
c ##nodal merging between plate and reaction frame##
bptol 1 5 -1
bptol 1 6 -1
bptol 1 7 -1
bptol 1 8 -1
bptol 1 9 -1
bptol 1 10 -1

bptol 1 11 -1
bptol 1 12 -1
bptol 2 5 -1
bptol 2 6 -1
bptol 2 7 -1
bptol 2 8 -1
bptol 2 9 -1
bptol 2 10 -1
bptol 2 11 -1
bptol 2 12 -1
bptol 3 5 -1
bptol 3 6 -1
bptol 3 7 -1
bptol 3 8 -1
bptol 3 9 -1
bptol 3 10 -1
bptol 3 11 -1
bptol 3 12 -1
bptol 4 5 -1
bptol 4 6 -1
bptol 4 7 -1
bptol 4 8 -1
bptol 4 9 -1
bptol 4 10 -1
bptol 4 11 -1
bptol 4 12 -1
c ##nodal merging between plate, reaction frame and air##
bptol 13 1 -1
bptol 13 2 -1
bptol 13 3 -1
bptol 13 4 -1
bptol 13 5 -1
bptol 13 6 -1
bptol 13 7 -1

```
bptol 13 8 -1
bptol 11 9 -1
bptol 13 10 -1
bptol 13 11 -1
bptol 13 12 -1
bptol 14 1 -1
bptol 14 2 -1
bptol 14 3 -1
bptol 14 4 -1
bptol 14 5 -1
bptol 14 6 -1
bptol 14 7 -1
bptol 14 8 -1
bptol 14 9 -1
bptol 14 10 -1
bptol 14 11 -1
bptol 14 12 -1
st 0.001
endpart merge
c $$$$$$$$$$$$$$$$$$$$$$$$$$$$$$$$$$$$$$$$$$$$4
c
c surface air
c part 25
block
1 2;
1 2;
1 2 3 4 5 6 7;
0 1;
-2 0;
-2 -0.5 -0.1 0 0.1 0.5 2;
mseq i 10;
mseq j 9;
mseq k 7 2 0 0 2 7;
dei 1 2; 1 2; 1 4;
```

```
bb 1 1 4 2 1 7 1 ;
mb 1 1 4 2 2 7 y +2
mate 502
endpart
c part 26
block
1 2;
1 2;
1 2 3 4 5 6 7;
0 1;
-2 0;
-2 -0.5 -0.1 0 0.1 0.5 2;
mseq i 10;
mseq j 9;
mseq k 7 2 0 0 2 7;
dei 1 2; 1 2; 4 7;
bb 1 1 1 2 1 4 2 ;
mb 1 1 1 2 2 4 y +2
mate 503
endpart
c part 27
block
1 2 3;
1 2;
1 2 3 4 5 6 7;
-1 -0.25 0;
-2 0;
-2 -0.5 -0.1 0 0.1 0.5 2;
mseq i 15 5;
mseq j 9;
mseq k 7 2 0 0 2 7;
dei 1 3; 1 2; 1 4;
mb 1 1 4 3 2 7 y +2
bb 1 1 4 3 1 7 3 ;
```

mate 504
endpart
c part 28
block
1 2 3;
1 2;
1 2 3 4 5 6 7;
-1 -0.25 0;
-2 0;
-2 -0.5 -0.1 0 0.1 0.5 2;
mseq i 15 5;
mseq j 9;
mseq k 7 2 0 0 2 7;
dei 1 3; 1 2; 4 7;
mb 1 1 1 3 2 4 y +2
bb 1 1 1 3 1 4 4 ;
mate 505
endpart
c part 29
block
1 41 51 56 60 66;
1 2;
1 2 3 4 5 6 7;
1 2 2.5 3 4 10;
-2 0;
-2 -0.5 -0.1 0 0.1 0.5 2;
dei 1 6; 1 2; 1 4;
mseq j 9;
mseq k 7 2 0 0 2 7;
mb 1 1 4 6 2 7 y +2
bb 1 1 4 6 1 7 5 ;
mate 506
endpart
c part 30

```
block
1 41 51 56 60 66;
1 2;
1 2 3 4 5 6 7;
1 2 2.5 3 4 10;
-2 0;
-2 -0.5 -0.1 0 0.1 0.5 2;
dei 1 6; 1 2; 4 7;
mseq j 9;
mseq k 7 2 0 0 2 7;
mb 1 1 1 6 2 4 y +2
bb 1 1 1 6 1 4 6 ;
mate 507
c merging between air
bptol 25 26 0.001
bptol 25 27 0.001
bptol 25 28 0.001
bptol 25 29 0.001
bptol 25 30 0.001
bptol 26 27 0.001
bptol 26 28 0.001
bptol 26 29 0.001
bptol 26 30 0.001
bptol 27 28 0.001
bptol 27 29 0.001
bptol 27 30 0.001
bptol 28 29 0.001
bptol 28 30 0.001
bptol 29 30 0.001
c merging between air and water
stp 0.001
endpart merge
```

I.4 US Navy Blast Test Study SPS Plate Mesh Model

```
lsdyna keyword
c units n/m/sec
c mate 100      h.e.
c mate 200-209  water
c mate 300-307  steel reaction frame
c mate 400-401  steel plate
c mate 500-507  air
c $$$$$$$$$$$$$$$$$$$$$$$$$$$$$$$$$$$$$$
sd 1 cy 0 -2 0 1 0 0 0.6477
sd 2 cy 0 -2 0 1 0 0 1.085
c $$$$$$$$$$$$$$$ steel plate $$$$$$$$$$$$$$$$
c part 1a
c   2.5cm elem size = 0.025m
block
-1;
1 2 3 4 5;
1 2 3 4 5;
1;
-0.5 -0.1 0 0.1 0.5;
-0.5 -0.1 0 0.1 0.5;
mseq j 15 3 3 15;
mseq k 15 3 3 15;
dei -1; 1 5; 1 3;
dei -1; 4 5; 4 5;
dei -1; 1 2; 4 5;
pb 1 5 4 1 5 4 xyz 1.000000e+00 1.000000e-01 1.000000e-01
pb 1 4 5 1 4 5 xyz 1.000000e+00 1.000000e-01 1.000000e-01
pb 1 5 3 1 5 3 xyz 1.000000e+00 1.000000e-01 0.000000e+00
pb 1 3 5 1 3 5 xyz 1.000000e+00 0.000000e+00 1.000000e-01
pb 1 2 5 1 2 5 xyz 1.000000e+00 -1.000000e-01 1.000000e-01
pb 1 1 4 1 1 4 xyz 1.000000e+00 -1.000000e-01 1.000000e-01
pb 1 1 3 1 1 3 xyz 1.000000e+00 -1.000000e-01 0.000000e+00
mb 1 1 1 1 5 5 y -2
```

```
sfi -1; -5; 3 4;sd 1
sfi -1; 3 4; -5;sd 1
sfi -1; 2 3; -5;sd 1
sfi -1; -1; 3 4;sd 1
orpt - 0.5 -2 0
n 1 1 3 1 5 5
mate 400
insprt -1 4 4 13
insprt -1 6 4 13
insprt -1 3 2 13
sd 3 cy 0 -2 0 1 0 0 0.5334 ;
sfi -1; -6; 3 4;sd 3
sfi -1; 3 5; -5;sd 3
sfi -1; -2; 3 4;sd 3
dei -1; 6 7; 3 4;
dei -1; 3 5; 5 6;
dei -1; 1 2; 3 4;
ptol 1 0.001
endpart
c part 2a
c   2.5cm elem size = 0.025m
block
-1;
1 2 3 4 5;
1 2 3 4 5;
1;
-0.5 -0.1 0 0.1 0.5;
-0.5 -0.1 0 0.1 0.5;
mseq j 15 3 3 15;
mseq k 15 3 3 15;
dei -1; 1 5; 1 3;
dei -1; 4 5; 4 5;
dei -1; 1 2; 4 5;
pb 1 5 4 1 5 4 xyz 1.000000e+00 1.000000e-01 1.000000e-01
```

```
pb 1 4 5 1 4 5 xyz 1.000000e+00 1.000000e-01 1.000000e-01
pb 1 5 3 1 5 3 xyz 1.000000e+00 1.000000e-01 0.000000e+00
pb 1 3 5 1 3 5 xyz 1.000000e+00 0.000000e+00 1.000000e-01
pb 1 2 5 1 2 5 xyz 1.000000e+00 -1.000000e-01 1.000000e-01
pb 1 1 4 1 1 4 xyz 1.000000e+00 -1.000000e-01 1.000000e-01
pb 1 1 3 1 1 3 xyz 1.000000e+00 -1.000000e-01 0.000000e+00
mb 1 1 1 1 5 5 y -2
sfi -1; -5; 3 4;sd 1
sfi -1; 3 4; -5;sd 1
sfi -1; 2 3; -5;sd 1
sfi -1; -1; 3 4;sd 1
orpt - 0.5 -2 0
n 1 1 3 1 5 5
mate 401
insprt -1 4 4 13
insprt -1 6 4 13
insprt -1 3 2 13
sfi -1; -6; 3 4;sd 3
sfi -1; 3 5; -5;sd 3
sfi -1; -2; 3 4;sd 3
dei -1; 2 6; 3 4;
dei -1; 3 5; 4 5;
ptol 2 0.001
endpart
c $$$$$$$$
c part 3a
block
-1;
1 2 3 4 5;
1 2 3 4 5;
1;
-0.5 -0.1 0 0.1 0.5;
-0.5 -0.1 0 0.1 0.5;
mseq j 15 3 3 15;
```

```
mseq k 15 3 3 15;
dei -1; 1 5; 3 5;
dei -1; 4 5; 1 2;
dei -1; 1 2; 1 2;
pb 1 5 3 1 5 3 xyz 1.000000e+00 1.000000e-01 0.000000e+00
pb 1 5 2 1 5 2 xyz 1.000000e+00 1.000000e-01 -1.000000e-01
pb 1 4 1 1 4 1 xyz 1.000000e+00 1.000000e-01 -1.000000e-01
pb 1 3 1 1 3 1 xyz 1.000000e+00 0.000000e+00 -1.000000e-01
pb 1 2 1 1 2 1 xyz 1.000000e+00 -1.000000e-01 -1.000000e-01
pb 1 1 2 1 1 2 xyz 1.000000e+00 -1.000000e-01 -1.000000e-01
pb 1 1 3 1 1 3 xyz 1.000000e+00 -1.000000e-01 0.000000e+00
mb 1 1 1 1 5 5 y -2
sfi -1; -5; 2 3;sd 1
sfi -1; 3 4; -1;sd 1
sfi -1; 2 3; -1;sd 1
sfi -1; -1; 2 3;sd 1
n 1 1 1 1 5 3
mate 402
insprt -1 4 4 13
insprt -1 3 2 13
insprt -1 5 2 13
sfi -1; -6; 3 4;sd 3
sfi -1; 3 5; -2;sd 3
sfi -1; -2; 3 4;sd 3
dei -1; 6 7; 3 4;
dei -1; 3 5; 1 2;
dei -1; 1 2; 3 4;
ptol 3 0.001
endpart
c $$$$$$$$
c part 4a
block
-1;
1 2 3 4 5;
```

```
1 2 3 4 5;
1;
-0.5 -0.1 0 0.1 0.5;
-0.5 -0.1 0 0.1 0.5;
mseq j 15 3 3 15;
mseq k 15 3 3 15;
dei -1; 1 5; 3 5;
dei -1; 4 5; 1 2;
dei -1; 1 2; 1 2;
pb 1 5 3 1 5 3 xyz 1.000000e+00 1.000000e-01 0.000000e+00
pb 1 5 2 1 5 2 xyz 1.000000e+00 1.000000e-01 -1.000000e-01
pb 1 4 1 1 4 1 xyz 1.000000e+00 1.000000e-01 -1.000000e-01
pb 1 3 1 1 3 1 xyz 1.000000e+00 0.000000e+00 -1.000000e-01
pb 1 2 1 1 2 1 xyz 1.000000e+00 -1.000000e-01 -1.000000e-01
pb 1 1 2 1 1 2 xyz 1.000000e+00 -1.000000e-01 -1.000000e-01
pb 1 1 3 1 1 3 xyz 1.000000e+00 -1.000000e-01 0.000000e+00
mb 1 1 1 1 5 5 y -2
sfi -1; -5; 2 3;sd 1
sfi -1; 3 4; -1;sd 1
sfi -1; 2 3; -1;sd 1
sfi -1; -1; 2 3;sd 1
n 1 1 1 1 5 3
mate 403
insprt -1 4 4 13
insprt -1 3 2 13
insprt -1 5 2 13
sfi -1; -6; 3 4;sd 3
sfi -1; 3 5; -2;sd 3
sfi -1; -2; 3 4;sd 3
dei -1; 3 5; 2 4;
dei -1; 2 6; 3 4;
ptol 4 0.001
st 0.001
c       143 nodes were deleted by tolerancing
```

```
c        143 nodes were deleted by tolerancing
endpart merge
c $$$$$$$$$$$$$$$ reaction frame $$$$$$$$$$$$$$$$$$$
c   5cm elem size = 0.05m
c part 5b
block
-1 -2;
-1 -2 -3 -4 -5;
-1 -2 -3 -4 -5;
0 1;
-0.5 -0.1 0 0.1 0.5;
-0.5 -0.1 0 0.1 0.5;
mseq i 10;
mseq j 2 0 0 2;
mseq k 2 0 0 2;
dei ;; -2 0 -3 0 -4;
dei ; -2 0 -3 0 -4;;
dei -1 0 -2;;;
dei -1 -2; -1 -5;-1 -3;
mb 1 1 3 2 5 5 y -2
sfi 1 2; -5; 3 5;sd 1
sfi 1 2; 1 5; -3;sd 1
sfi 1 2; -1; 3 5;sd 1
sfi 1 2; 1 5; -5;sd 1
res 1 1 3 1 5 5 j 1
res 1 1 3 1 5 5 k 1
n 1 5 3 2 5 5
n 1 1 5 2 5 5
n 1 1 3 2 1 5
ptol 5 0.001
mate 300
endpart
c $$$$$$
c part 6b
```

```
block
-1 -2;
-1 -2 -3 -4 -5;
-1 -2 -3 -4 -5;
0 1;
-0.5 -0.1 0 0.1 0.5;
-0.5 -0.1 0 0.1 0.5;
mseq i 10;
mseq j 2 0 0 2;
mseq k 2 0 0 2;
dei 1 2; 1 5; 3 5;
dei ; -2 0 -3 0 -4;;
dei -1 0 -2;;;
dei ;; -2;
mb 1 1 1 2 5 3 y -2
sfi 1 2; -5; 1 3;sd 1
sfi 1 2; 1 5; -1;sd 1
sfi 1 2; -1; 1 3;sd 1
sfi 1 2; 1 5; -3;sd 1
res 1 1 1 1 5 3 j 1
res 1 1 1 1 5 3 k 1
n 1 5 1 2 5 3
n 1 1 1 2 5 1
n 1 1 1 2 1 3
mate 301
ptol 6 0.001
bptol 5 6 0.001
endpart
c $$$$$$
c part 7c
block
-1;
1 2 3 4 5 6 7;
1 2 3 4 5 6 7;
```

1;
-1.0 -0.5 -0.1 0 0.1 0.5 1.0;
-1.0 -0.5 -0.1 0 0.1 0.5 1.0;
dei -1; 1 7; 1 4;
dei -1; 6 7; 6 7;
dei -1; 1 2; 6 7;
pb 1 7 4 1 7 4 xyz 1.000000e+00 5.000000e-01 0.000000e+00
pb 1 7 5 1 7 5 xyz 1.000000e+00 5.000000e-01 1.000000e-01
pb 1 7 6 1 7 6 xyz 1.000000e+00 5.000000e-01 5.000000e-01
pb 1 6 7 1 6 7 xyz 1.000000e+00 5.000000e-01 5.000000e-01
pb 1 5 7 1 5 7 xyz 1.000000e+00 1.000000e-01 5.000000e-01
pb 1 4 7 1 4 7 xyz 1.000000e+00 0.000000e+00 5.000000e-01
pb 1 3 7 1 3 7 xyz 1.000000e+00 -1.000000e-01 5.000000e-01
pb 1 2 7 1 2 7 xyz 1.000000e+00 -5.000000e-01 5.000000e-01
pb 1 1 6 1 1 6 xyz 1.000000e+00 -5.000000e-01 5.000000e-01
pb 1 1 5 1 1 5 xyz 1.000000e+00 -5.000000e-01 1.000000e-01
pb 1 1 4 1 1 4 xyz 1.000000e+00 -5.000000e-01 0.000000e+00
n 1 1 5 1 7 7
mseq j 4 2 0 0 2 4;
mseq k 4 2 0 0 2 4;
mb 1 1 1 1 7 7 y -2
sfi -1; -7; 4 5;sd 2
sfi -1; -7; 5 6;sd 2
sfi -1; 5 6; -7;sd 2
sfi -1; 4 5; -7;sd 2
sfi -1; 3 4; -7;sd 2
sfi -1; 2 3; -7;sd 2
sfi -1; -1; 5 6;sd 2
sfi -1; -1; 4 5;sd 2
dei -1; 2 6; 4 6;
sfi -1; -6; 4 5;sd 1
sfi -1; -6; 5 6;sd 1
sfi -1; 5 6; -6;sd 1
sfi -1; 4 5; -6;sd 1

sfi -1; 3 4; -6;sd 1
sfi -1; 2 3; -6;sd 1
sfi -1; -2; 5 6;sd 1
sfi -1; -2; 4 5;sd 1
mate 302
ptol 7 0.001
endpart
c part 8c
block
-1;
1 2 3 4 5 6 7;
1 2 3 4 5 6 7;
1;
-1.0 -0.5 -0.1 0 0.1 0.5 1.0;
-1.0 -0.5 -0.1 0 0.1 0.5 1.0;
dei -1; 1 7; 4 7;
dei -1; 6 7; 1 2;
dei -1; 1 2; 1 2;
n 1 1 1 1 7 3
pb 1 7 4 1 7 4 xyz 1.000000e+00 5.000000e-01 0.000000e+00
pb 1 7 3 1 7 3 xyz 1.000000e+00 5.000000e-01 -1.000000e-01
pb 1 7 2 1 7 2 xyz 1.000000e+00 5.000000e-01 -5.000000e-01
pb 1 6 1 1 6 1 xyz 1.000000e+00 5.000000e-01 -5.000000e-01
pb 1 5 1 1 5 1 xyz 1.000000e+00 1.000000e-01 -5.000000e-01
pb 1 4 1 1 4 1 xyz 1.000000e+00 0.000000e+00 -5.000000e-01
pb 1 3 1 1 3 1 xyz 1.000000e+00 -1.000000e-01 -5.000000e-01
pb 1 2 1 1 2 1 xyz 1.000000e+00 -5.000000e-01 -5.000000e-01
pb 1 1 2 1 1 2 xyz 1.000000e+00 -5.000000e-01 -5.000000e-01
pb 1 1 3 1 1 3 xyz 1.000000e+00 -5.000000e-01 -1.000000e-01
pb 1 1 4 1 1 4 xyz 1.000000e+00 -5.000000e-01 0.000000e+00
mseq j 4 2 0 0 2 4;
mseq k 4 2 0 0 2 4;
mb 1 1 1 1 7 7 y -2
sfi -1; -7; 3 4;sd 2

sfi -1; -7; 2 3;sd 2
sfi -1; 5 6; -1;sd 2
sfi -1; 4 5; -1;sd 2
sfi -1; 3 4; -1;sd 2
sfi -1; 2 3; -1;sd 2
sfi -1; -1; 2 3;sd 2
sfi -1; -1; 3 4;sd 2
dei -1; 2 6; 2 4;
sfi -1; -6; 3 4;sd 1
sfi -1; -6; 2 3;sd 1
sfi -1; 5 6; -2;sd 1
sfi -1; 4 5; -2;sd 1
sfi -1; 3 4; -2;sd 1
sfi -1; 2 3; -2;sd 1
sfi -1; -2; 2 3;sd 1
sfi -1; -2; 3 4;sd 1
mate 303
ptol 8 0.001
endpart
c part 9d
block
-1;
1 2 3 4 5 6 7;
1 2 3 4 5 6 7;
0;
-1.0 -0.5 -0.1 0 0.1 0.5 1.0;
-1.0 -0.5 -0.1 0 0.1 0.5 1.0;
dei -1; 1 7; 1 4;
dei -1; 6 7; 6 7;
dei -1; 1 2; 6 7;
pb 1 7 4 1 7 4 xyz 0.000000e+00 5.000000e-01 0.000000e+00
pb 1 7 5 1 7 5 xyz 0.000000e+00 5.000000e-01 1.000000e-01
pb 1 7 6 1 7 6 xyz 0.000000e+00 5.000000e-01 5.000000e-01
pb 1 6 7 1 6 7 xyz 0.000000e+00 5.000000e-01 5.000000e-01

pb 1 5 7 1 5 7 xyz 0.000000e+00 1.000000e-01 5.000000e-01
pb 1 4 7 1 4 7 xyz 0.000000e+00 0.000000e+00 5.000000e-01
pb 1 3 7 1 3 7 xyz 0.000000e+00 -1.000000e-01 5.000000e-01
pb 1 2 7 1 2 7 xyz 0.000000e+00 -5.000000e-01 5.000000e-01
pb 1 1 6 1 1 6 xyz 0.000000e+00 -5.000000e-01 5.000000e-01
pb 1 1 5 1 1 5 xyz 0.000000e+00 -5.000000e-01 1.000000e-01
pb 1 1 4 1 1 4 xyz 0.000000e+00 -5.000000e-01 0.000000e+00
mseq j 4 2 0 0 2 4;
mseq k 4 2 0 0 2 4;
mb 1 1 1 1 7 7 y -2
sfi -1; -7; 4 5;sd 2
sfi -1; -7; 5 6;sd 2
sfi -1; 5 6; -7;sd 2
sfi -1; 4 5; -7;sd 2
sfi -1; 3 4; -7;sd 2
sfi -1; 2 3; -7;sd 2
sfi -1; -1; 5 6;sd 2
sfi -1; -1; 4 5;sd 2
dei -1; 2 6; 4 6;
sfi -1; -6; 4 5;sd 1
sfi -1; -6; 5 6;sd 1
sfi -1; 5 6; -6;sd 1
sfi -1; 4 5; -6;sd 1
sfi -1; 3 4; -6;sd 1
sfi -1; 2 3; -6;sd 1
sfi -1; -2; 5 6;sd 1
sfi -1; -2; 4 5;sd 1
mate 304
ptol 9 0.001
endpart
c part 10d
block
-1;
1 2 3 4 5 6 7;

1 2 3 4 5 6 7;
0;
-1.0 -0.5 -0.1 0 0.1 0.5 1.0;
-1.0 -0.5 -0.1 0 0.1 0.5 1.0;
dei -1; 1 7; 4 7;
dei -1; 6 7; 1 2;
dei -1; 1 2; 1 2;
pb 1 7 4 1 7 4 xyz 0.000000e+00 5.000000e-01 0.000000e+00
pb 1 7 3 1 7 3 xyz 0.000000e+00 5.000000e-01 -1.000000e-01
pb 1 7 2 1 7 2 xyz 0.000000e+00 5.000000e-01 -5.000000e-01
pb 1 6 1 1 6 1 xyz 0.000000e+00 5.000000e-01 -5.000000e-01
pb 1 5 1 1 5 1 xyz 0.000000e+00 1.000000e-01 -5.000000e-01
pb 1 4 1 1 4 1 xyz 0.000000e+00 0.000000e+00 -5.000000e-01
pb 1 3 1 1 3 1 xyz 0.000000e+00 -1.000000e-01 -5.000000e-01
pb 1 2 1 1 2 1 xyz 0.000000e+00 -5.000000e-01 -5.000000e-01
pb 1 1 2 1 1 2 xyz 0.000000e+00 -5.000000e-01 -5.000000e-01
pb 1 1 3 1 1 3 xyz 0.000000e+00 -5.000000e-01 -1.000000e-01
pb 1 1 4 1 1 4 xyz 0.000000e+00 -5.000000e-01 0.000000e+00
mseq j 4 2 0 0 2 4;
mseq k 4 2 0 0 2 4;
mb 1 1 1 1 7 7 y -2
sfi -1; -7; 3 4;sd 2
sfi -1; -7; 2 3;sd 2
sfi -1; 5 6; -1;sd 2
sfi -1; 4 5; -1;sd 2
sfi -1; 3 4; -1;sd 2
sfi -1; 2 3; -1;sd 2
sfi -1; -1; 2 3;sd 2
sfi -1; -1; 3 4;sd 2
dei -1; 2 6; 2 4;
sfi -1; -6; 3 4;sd 1
sfi -1; -6; 2 3;sd 1
sfi -1; 5 6; -2;sd 1
sfi -1; 4 5; -2;sd 1

```
sfi -1; 3 4; -2;sd 1
sfi -1; 2 3; -2;sd 1
sfi -1; -2; 2 3;sd 1
sfi -1; -2; 3 4;sd 1
mate 305
ptol 10 0.001
endpart
c $$$$
c part 11d
block
-1;
1 2 3 4 5;
1 2 3 4 5;
0;
-0.5 -0.1 0 0.1 0.5;
-0.5 -0.1 0 0.1 0.5;
mseq j 15 3 3 15;
mseq k 15 3 3 15;
dei -1; 1 5; 1 3;
dei -1; 4 5; 4 5;
dei -1; 1 2; 4 5;
pb 1 5 4 1 5 4 xyz 0.000000e+00 1.000000e-01 1.000000e-01
pb 1 4 5 1 4 5 xyz 0.000000e+00 1.000000e-01 1.000000e-01
pb 1 5 3 1 5 3 xyz 0.000000e+00 1.000000e-01 0.000000e+00
pb 1 3 5 1 3 5 xyz 0.000000e+00 0.000000e+00 1.000000e-01
pb 1 2 5 1 2 5 xyz 0.000000e+00 -1.000000e-01 1.000000e-01
pb 1 1 4 1 1 4 xyz 0.000000e+00 -1.000000e-01 1.000000e-01
pb 1 1 3 1 1 3 xyz 0.000000e+00 -1.000000e-01 0.000000e+00
n 1 1 3 1 5 5
mb 1 1 1 1 5 5 y -2
sfi -1; -5; 3 4;sd 1
sfi -1; 3 4; -5;sd 1
sfi -1; 2 3; -5;sd 1
sfi -1; -1; 3 4;sd 1
```

```
mate 306
ptol 11 0.001
endpart
c part 12d
block
-1;
1 2 3 4 5;
1 2 3 4 5;
0;
-0.5 -0.1 0 0.1 0.5;
-0.5 -0.1 0 0.1 0.5;
mseq j 15 3 3 15;
mseq k 15 3 3 15;
dei -1; 1 5; 3 5;
dei -1; 4 5; 1 2;
dei -1; 1 2; 1 2;
pb 1 5 3 1 5 3 xyz 0.000000e+00 1.000000e-01 0.000000e+00
pb 1 5 2 1 5 2 xyz 0.000000e+00 1.000000e-01 -1.000000e-01
pb 1 4 1 1 4 1 xyz 0.000000e+00 1.000000e-01 -1.000000e-01
pb 1 3 1 1 3 1 xyz 0.000000e+00 0.000000e+00 -1.000000e-01
pb 1 2 1 1 2 1 xyz 0.000000e+00 -1.000000e-01 -1.000000e-01
pb 1 1 2 1 1 2 xyz 0.000000e+00 -1.000000e-01 -1.000000e-01
pb 1 1 3 1 1 3 xyz 0.000000e+00 -1.000000e-01 0.000000e+00
mb 1 1 1 1 5 5 y -2
n 1 1 1 1 5 3
sfi -1; -5; 2 3;sd 1
sfi -1; 3 4; -1;sd 1
sfi -1; 2 3; -1;sd 1
sfi -1; -1; 2 3;sd 1
mate 307
ptol 12 0.001
c ##nodal merging between plate and reaction frame##
bptol 1 5 -1
bptol 1 6 -1
```

bptol 1 7 -1
bptol 1 8 -1
bptol 1 9 -1
bptol 1 10 -1
bptol 1 11 -1
bptol 1 12 -1
bptol 2 5 -1
bptol 2 6 -1
bptol 2 7 -1
bptol 2 8 -1
bptol 2 9 -1
bptol 2 10 -1
bptol 2 11 -1
bptol 2 12 -1
bptol 3 5 -1
bptol 3 6 -1
bptol 3 7 -1
bptol 3 8 -1
bptol 3 9 -1
bptol 3 10 -1
bptol 3 11 -1
bptol 3 12 -1
bptol 4 5 -1
bptol 4 6 -1
bptol 4 7 -1
bptol 4 8 -1
bptol 4 9 -1
bptol 4 10 -1
bptol 4 11 -1
bptol 4 12 -1
c ##
st 0.001
c 432 nodes were deleted by tolerancing
c 432 nodes were deleted by tolerancing

```
endpart merge
c $$$$$$$$$$$$$$$ air $$$$$$$$$$$$$$$$$
c part 13e
block
1 2;
1 2 3 4 5;
1 2 3 4 5;
0 1;
-0.5 -0.1 0 0.1 0.5;
-0.5 -0.1 0 0.1 0.5;
dei 1 2; 1 5; 1 3;
dei 1 2; 4 5; 4 5;
dei 1 2; 1 2; 4 5;
mseq i 10;
mseq j 15 3 3 15;
mseq k 15 3 3 15;
pb 1 5 4 1 5 4 xyz 0.000000e+00 1.000000e-01 1.000000e-01
pb 2 5 4 2 5 4 xyz 1.000000e+00 1.000000e-01 1.000000e-01
pb 1 4 5 1 4 5 xyz 0.000000e+00 1.000000e-01 1.000000e-01
pb 2 4 5 2 4 5 xyz 1.000000e+00 1.000000e-01 1.000000e-01
pb 2 2 5 2 2 5 xyz 1.000000e+00 -1.000000e-01 1.000000e-01
pb 2 1 4 2 1 4 xyz 1.000000e+00 -1.000000e-01 1.000000e-01
pb 1 1 4 1 1 4 xyz 0.000000e+00 -1.000000e-01 1.000000e-01
pb 1 2 5 1 2 5 xyz 0.000000e+00 -1.000000e-01 1.000000e-01
mb 1 1 3 2 5 5 y -2
sfi 1 2; -5; 3 4;sd 1
sfi 1 2; 3 4; -5;sd 1
sfi 1 2; 2 3; -5;sd 1
sfi 1 2; -1; 3 4;sd 1
mate 500
ptol 13 0.001
c part 14e
block
1 2;
```

```
1 2 3 4 5;
1 2 3 4 5;
0 1;
-0.5 -0.1 0 0.1 0.5;
-0.5 -0.1 0 0.1 0.5;
dei 1 2; 1 5; 3 5;
dei 1 2; 4 5; 1 2;
dei 1 2; 1 2; 1 2;
mseq i 10;
mseq j 15 3 3 15;
mseq k 15 3 3 15;
pb 2 5 2 2 5 2 xyz 1.000000e+00 1.000000e-01 -1.000000e-01
pb 1 5 2 1 5 2 xyz 0.000000e+00 1.000000e-01 -1.000000e-01
pb 1 4 1 1 4 1 xyz 0.000000e+00 1.000000e-01 -1.000000e-01
pb 2 4 1 2 4 1 xyz 1.000000e+00 1.000000e-01 -1.000000e-01
pb 2 2 1 2 2 1 xyz 1.000000e+00 -1.000000e-01 -1.000000e-01
pb 1 2 1 1 2 1 xyz 0.000000e+00 -1.000000e-01 -1.000000e-01
pb 2 1 2 2 1 2 xyz 1.000000e+00 -1.000000e-01 -1.000000e-01
pb 1 1 2 1 1 2 xyz 0.000000e+00 -1.000000e-01 -1.000000e-01
mb 1 1 1 2 5 3 y -2
sfi 1 2; -5; 2 3;sd 1
sfi 1 2; 3 4; -1;sd 1
sfi 1 2; 2 3; -1;sd 1
sfi 1 2; -1; 2 3;sd 1
mate 501
ptol 14 0.001
c ##nodal merging between plate, reaction frame and air##
bptol 13 1 -1
bptol 13 2 -1
bptol 13 3 -1
bptol 13 4 -1
bptol 13 5 -1
bptol 13 6 -1
bptol 13 7 -1
```

```
bptol 13 8 -1
bptol 11 9 -1
bptol 13 10 -1
bptol 13 11 -1
bptol 13 12 -1
bptol 14 1 -1
bptol 14 2 -1
bptol 14 3 -1
bptol 14 4 -1
bptol 14 5 -1
bptol 14 6 -1
bptol 14 7 -1
bptol 14 8 -1
bptol 14 9 -1
bptol 14 10 -1
bptol 14 11 -1
bptol 14 12 -1
st 0.001
endpart merge
c $$$$$$$$$$$$$$$ water $$$$$$$$$$$$$$$$$
c part 15f middle fluid
block
1 2;
1 2 3 4 5 6 7;
1 2 3 4 5 6 7;
0 1;
-2 -0.5 -0.1 0 0.1 0.5 2;
-2 -0.5 -0.1 0 0.1 0.5 2;
mseq i 10;
mseq j 7 2 0 0 2 7;
mseq k 7 2 0 0 2 7;
dei 1 2; 2 6; 2 6;
dei 1 2; 1 7; 1 4;
mb 1 1 4 2 7 7 y -2
```

```
sfi 1 2; -6; 4 6;sd 1
sfi 1 2; 2 6; -6;sd 1
sfi 1 2; -2; 4 6;sd 1
res 1 6 4 2 6 6 k 1
res 1 2 4 2 2 6 k 1
res 1 2 6 2 6 6 j 1
ptol 15 0.001
mate 200
bb 1 7 4 2 7 7 1 ;
endpart
c part 16f middle fluid
block
1 2;
1 2 3 4 5 6 7;
1 2 3 4 5 6 7;
0 1;
-2 -0.5 -0.1 0 0.1 0.5 2;
-2 -0.5 -0.1 0 0.1 0.5 2;
mseq i 10;
mseq j 7 2 0 0 2 7;
mseq k 7 2 0 0 2 7;
dei 1 2; 1 7; 4 7;
dei 1 2; 2 6; 2 4;
mb 1 1 1 2 7 4 y -2
sfi 1 2; -6; 2 4;sd 1
sfi 1 2; 2 6; -2;sd 1
sfi 1 2; -2; 2 4;sd 1
res 1 2 2 2 2 4 k 1
res 1 6 2 2 6 4 k 1
res 1 2 2 2 6 2 j 1
ptol 16 0.001
mate 201
bb 1 7 1 2 7 4 2 ;
endpart
```

```
c part 17g fluid -x+z
block
1 2 3;
1 2 3 4 5 6 7;
1 2 3 4 5 6 7;
-1 -0.25 0;
-2 -0.5 -0.1 0 0.1 0.5 2;
-2 -0.5 -0.1 0 0.1 0.5 2;
mseq i 15 5;
mseq j 7 2 0 0 2 7;
mseq k 7 2 0 0 2 7;
dei 1 3; 1 7; 1 4;
dei 1 3; 2 6; 4 6;
mb 1 1 4 3 7 7 y -2
sfi 1 3; -6; 4 6;sd 1
sfi 1 3; 2 6; -6;sd 1
sfi 1 3; -2; 4 6;sd 1
res 1 2 4 3 2 6 k 1
res 1 6 4 3 6 6 k 1
res 1 2 6 3 6 6 j 1
ptol 17 0.001
mate 202
bb 1 7 4 3 7 7 3 ;
endpart
c part 18g fluid -x-z
block
1 2 3;
1 2 3 4 5 6 7;
1 2 3 4 5 6 7;
-1 -0.25 0;
-2 -0.5 -0.1 0 0.1 0.5 2;
-2 -0.5 -0.1 0 0.1 0.5 2;
mseq i 15 5;
mseq j 7 2 0 0 2 7;
```

mseq k 7 2 0 0 2 7;
dei 1 3; 1 7; 4 7;
dei 1 3; 2 6; 2 4;
mb 1 1 1 3 7 4 y -2
sfi 1 3; -2 -6; -2 4;sd 1
res 1 2 2 3 2 4 k 1
res 1 6 2 3 6 4 k 1
res 1 2 2 3 6 2 j 1
ptol 18 0.001
mate 203
bb 1 7 1 3 7 4 4 ;
endpart
c part 19g fluid -x+z inner
block
1 2 3;
1 2 3 4 5;
1 2 3 4 5;
-1 -0.25 0;
-0.5 -0.1 0 0.1 0.5;
-0.5 -0.1 0 0.1 0.5;
dei 1 3; 1 5; 1 3;
dei 1 3; 4 5; 4 5;
dei 1 3; 1 2; 4 5;
mseq i 15 5;
mseq j 15 3 3 15;
mseq k 15 3 3 15;
pb 1 5 4 1 5 4 xyz -1.000000e+00 2.500000e-01 2.500000e-01
pb 1 4 5 1 4 5 xyz -1.000000e+00 2.500000e-01 2.500000e-01
pb 2 5 4 2 5 4 xyz -2.500000e-01 2.500000e-01 2.500000e-01
pb 2 4 5 2 4 5 xyz -2.500000e-01 2.500000e-01 2.500000e-01
pb 3 5 4 3 5 4 xyz 0.000000e+00 2.500000e-01 2.500000e-01
pb 3 4 5 3 4 5 xyz 0.000000e+00 2.500000e-01 2.500000e-01
pb 3 1 4 3 1 4 xyz 0.000000e+00 -2.500000e-01 2.500000e-01
pb 3 2 5 3 2 5 xyz 0.000000e+00 -2.500000e-01 2.500000e-01

pb 2 2 5 2 2 5 xyz -2.500000e-01 -2.500000e-01 2.500000e-01
pb 2 1 4 2 1 4 xyz -2.500000e-01 -2.500000e-01 2.500000e-01
pb 1 1 4 1 1 4 xyz -1.000000e+00 -2.500000e-01 2.500000e-01
pb 1 2 5 1 2 5 xyz -1.000000e+00 -2.500000e-01 2.500000e-01
mb 1 1 3 3 5 5 y -2
sfi 1 3; -5; 3 4;sd 1
sfi 1 3; 2 4; -5;sd 1
sfi 1 3; -1; 3 4;sd 1
ptol 19 0.001
mate 204
endpart
c part 20g fluid -x-z inner
block
1 2 3;
1 2 3 4 5;
1 2 3 4 5;
-1 -0.25 0;
-0.5 -0.1 0 0.1 0.5;
-0.5 -0.1 0 0.1 0.5;
mseq i 15 5;
mseq j 15 3 3 15;
mseq k 15 3 3 15;
dei 1 3; 1 5; 3 5;
dei 1 3; 4 5; 1 2;
dei 1 3; 1 2; 1 2;
pb 3 5 2 3 5 2 xyz 0.000000e+00 2.500000e-01 -2.500000e-01
pb 3 4 1 3 4 1 xyz 0.000000e+00 2.500000e-01 -2.500000e-01
pb 2 5 2 2 5 2 xyz -2.500000e-01 2.500000e-01 -2.500000e-01
pb 2 4 1 2 4 1 xyz -2.500000e-01 2.500000e-01 -2.500000e-01
pb 1 5 2 1 5 2 xyz -1.000000e+00 2.500000e-01 -2.500000e-01
pb 1 4 1 1 4 1 xyz -1.000000e+00 2.500000e-01 -2.500000e-01
pb 3 1 2 3 1 2 xyz 0.000000e+00 -2.500000e-01 -2.500000e-01
pb 3 2 1 3 2 1 xyz 0.000000e+00 -2.500000e-01 -2.500000e-01
pb 2 2 1 2 2 1 xyz -2.500000e-01 -2.500000e-01 -2.500000e-01

pb 2 1 2 2 1 2 xyz -2.500000e-01 -2.500000e-01 -2.500000e-01
pb 1 1 2 1 1 2 xyz -1.000000e+00 -2.500000e-01 -2.500000e-01
pb 1 2 1 1 2 1 xyz -1.000000e+00 -2.500000e-01 -2.500000e-01
mb 1 1 1 3 5 3 y -2
sfi 1 3; -5; 2 3;sd 1
sfi 1 3; 2 4; -1;sd 1
sfi 1 3; -1; 2 3;sd 1
ptol 20 0.001
mate 205
endpart
c part 21g fluid +x+z
block
1 41 51 56 60 66;
1 2 3 4 5 6 7;
1 2 3 4 5 6 7;
1 2 2.5 3 4 10;
-2 -0.5 -0.1 0 0.1 0.5 2;
-2 -0.5 -0.1 0 0.1 0.5 2;
dei 1 6; 1 7; 1 4;
dei 1 6; 2 6; 4 6;
mseq j 7 2 0 0 2 7;
mseq k 7 2 0 0 2 7;
mb 1 1 4 6 7 7 y -2
sfi 1 6; -2 -6; 4 6;sd 1
sfi 1 6; 2 6; 4 -6;sd 1
res 1 2 6 6 6 6 j 1
res 1 6 4 6 6 6 k 1
res 1 2 4 6 2 6 k 1
ptol 21 0.001
mate 206
bb 1 7 4 6 7 7 5 ;
endpart
c part 22g fluid +x-z
block

1 41 51 56 60 66;
1 2 3 4 5 6 7;
1 2 3 4 5 6 7;
1 2 2.5 3 4 10;
-2 -0.5 -0.1 0 0.1 0.5 2;
-2 -0.5 -0.1 0 0.1 0.5 2;
mseq j 7 2 0 0 2 7;
mseq k 7 2 0 0 2 7;
dei 1 6; 1 7; 4 7;
dei 1 6; 2 6; 2 4;
mb 1 1 1 6 7 4 y -2
sfi 1 6; -6; 2 4;sd 1
sfi 1 6; 2 6; -2;sd 1
sfi 1 6; -2; 2 4;sd 1
res 1 2 2 6 2 4 k 1
res 1 6 2 6 6 4 k 1
res 1 2 2 6 6 2 j 1
ptol 22 0.001
mate 207
bb 1 7 1 6 7 4 6 ;
endpart
c part 23g fluid +x+z inner
block
1 41 51 56 60 66;
1 2 3 4 5;
1 2 3 4 5;
1 2 2.5 3 4 10;
-0.5 -0.1 0 0.1 0.5;
-0.5 -0.1 0 0.1 0.5;
mseq j 15 3 3 15;
mseq k 15 3 3 15;
dei 1 6; 1 5; 1 3;
dei 1 6; 4 5; 4 5;
dei 1 6; 1 2; 4 5;

pb 1 5 4 1 5 4 xyz 1.000000e+00 2.500000e-01 2.500000e-01
pb 1 4 5 1 4 5 xyz 1.000000e+00 2.500000e-01 2.500000e-01
pb 2 5 4 2 5 4 xyz 2.000000e+00 2.500000e-01 2.500000e-01
pb 2 4 5 2 4 5 xyz 2.000000e+00 2.500000e-01 2.500000e-01
pb 3 5 4 3 5 4 xyz 2.500000e+00 2.500000e-01 2.500000e-01
pb 3 4 5 3 4 5 xyz 2.500000e+00 2.500000e-01 2.500000e-01
pb 4 5 4 4 5 4 xyz 3.000000e+00 2.500000e-01 2.500000e-01
pb 4 4 5 4 4 5 xyz 3.000000e+00 2.500000e-01 2.500000e-01
pb 5 5 4 5 5 4 xyz 4.000000e+00 2.500000e-01 2.500000e-01
pb 5 4 5 5 4 5 xyz 4.000000e+00 2.500000e-01 2.500000e-01
pb 6 5 4 6 5 4 xyz 10.000000e+00 2.500000e-01 2.500000e-01
pb 6 4 5 6 4 5 xyz 10.000000e+00 2.500000e-01 2.500000e-01
pb 1 2 5 1 2 5 xyz 1.000000e+00 -2.500000e-01 2.500000e-01
pb 1 1 4 1 1 4 xyz 1.000000e+00 -2.500000e-01 2.500000e-01
pb 2 2 5 2 2 5 xyz 2.000000e+00 -2.500000e-01 2.500000e-01
pb 2 1 4 2 1 4 xyz 2.000000e+00 -2.500000e-01 2.500000e-01
pb 3 1 4 3 1 4 xyz 2.500000e+00 -2.500000e-01 2.500000e-01
pb 3 2 5 3 2 5 xyz 2.500000e+00 -2.500000e-01 2.500000e-01
pb 4 2 5 4 2 5 xyz 3.000000e+00 -2.500000e-01 2.500000e-01
pb 4 1 4 4 1 4 xyz 3.000000e+00 -2.500000e-01 2.500000e-01
pb 5 2 5 5 2 5 xyz 4.000000e+00 -2.500000e-01 2.500000e-01
pb 5 1 4 5 1 4 xyz 4.000000e+00 -2.500000e-01 2.500000e-01
pb 6 2 5 6 2 5 xyz 10.000000e+00 -2.500000e-01 2.500000e-01
pb 6 1 4 6 1 4 xyz 10.000000e+00 -2.500000e-01 2.500000e-01
mb 1 1 3 6 5 5 y -2
sfi 1 6; -5; 3 4;sd 1
sfi 1 6; 2 4; -5;sd 1
sfi 1 6; -1; 3 4;sd 1
ptol 23 0.001
mate 208
endpart
c part 24g fluid +x-z inner
block
1 41 51 56 60 66;

1 2 3 4 5;
1 2 3 4 5;
1 2 2.5 3 4 10;
-0.5 -0.1 0 0.1 0.5;
-0.5 -0.1 0 0.1 0.5;
mseq j 15 3 3 15;
mseq k 15 3 3 15;
dei 1 6; 1 5; 3 5;
dei 1 6; 4 5; 1 2;
dei 1 6; 1 2; 1 2;
pb 1 5 2 1 5 2 xyz 1.000000e+00 2.500000e-01 -2.500000e-01
pb 1 4 1 1 4 1 xyz 1.000000e+00 2.500000e-01 -2.500000e-01
pb 2 5 2 2 5 2 xyz 2.000000e+00 2.500000e-01 -2.500000e-01
pb 2 4 1 2 4 1 xyz 2.000000e+00 2.500000e-01 -2.500000e-01
pb 3 5 2 3 5 2 xyz 2.500000e+00 2.500000e-01 -2.500000e-01
pb 3 4 1 3 4 1 xyz 2.500000e+00 2.500000e-01 -2.500000e-01
pb 4 5 2 4 5 2 xyz 3.000000e+00 2.500000e-01 -2.500000e-01
pb 4 4 1 4 4 1 xyz 3.000000e+00 2.500000e-01 -2.500000e-01
pb 5 5 2 5 5 2 xyz 4.000000e+00 2.500000e-01 -2.500000e-01
pb 5 4 1 5 4 1 xyz 4.000000e+00 2.500000e-01 -2.500000e-01
pb 6 5 2 6 5 2 xyz 10.000000e+00 2.500000e-01 -2.500000e-01
pb 6 4 1 6 4 1 xyz 10.000000e+00 2.500000e-01 -2.500000e-01
pb 1 2 1 1 2 1 xyz 1.000000e+00 -2.500000e-01 -2.500000e-01
pb 1 1 2 1 1 2 xyz 1.000000e+00 -2.500000e-01 -2.500000e-01
pb 2 2 1 2 2 1 xyz 2.000000e+00 -2.500000e-01 -2.500000e-01
pb 2 1 2 2 1 2 xyz 2.000000e+00 -2.500000e-01 -2.500000e-01
pb 3 2 1 3 2 1 xyz 2.500000e+00 -2.500000e-01 -2.500000e-01
pb 3 1 2 3 1 2 xyz 2.500000e+00 -2.500000e-01 -2.500000e-01
pb 4 2 1 4 2 1 xyz 3.000000e+00 -2.500000e-01 -2.500000e-01
pb 4 1 2 4 1 2 xyz 3.000000e+00 -2.500000e-01 -2.500000e-01
pb 5 1 2 5 1 2 xyz 4.000000e+00 -2.500000e-01 -2.500000e-01
pb 5 2 1 5 2 1 xyz 4.000000e+00 -2.500000e-01 -2.500000e-01
pb 6 2 1 6 2 1 xyz 10.000000e+00 -2.500000e-01 -2.500000e-01
pb 6 1 2 6 1 2 xyz 10.000000e+00 -2.500000e-01 -2.500000e-01

```
mb 1 1 1 6 5 3 y -2
sfi 1 6; -5; 2 3;sd 1
sfi 1 6; 2 4; -1;sd 1
sfi 1 6; -1; 2 3;sd 1
ptol 24 0.001
mate 209
c ##nodal merging between plate, reaction frame and water##
bptol 1 15 -1
bptol 1 16 -1
bptol 1 17 -1
bptol 1 18 -1
bptol 1 19 -1
bptol 1 20 -1
bptol 1 21 -1
bptol 1 22 -1
bptol 1 23 -1
bptol 1 24 -1
bptol 2 15 -1
bptol 2 16 -1
bptol 2 17 -1
bptol 2 18 -1
bptol 2 19 -1
bptol 2 20 -1
bptol 2 21 -1
bptol 2 22 -1
bptol 2 23 -1
bptol 2 24 -1
bptol 3 15 -1
bptol 3 16 -1
bptol 3 17 -1
bptol 3 18 -1
bptol 3 19 -1
bptol 3 20 -1
bptol 3 21 -1
```

bptol 3 22 -1
bptol 3 23 -1
bptol 3 24 -1
bptol 4 15 -1
bptol 4 16 -1
bptol 4 17 -1
bptol 4 18 -1
bptol 4 19 -1
bptol 4 20 -1
bptol 4 21 -1
bptol 4 22 -1
bptol 4 23 -1
bptol 4 24 -1
bptol 5 15 -1
bptol 5 16 -1
bptol 5 17 -1
bptol 5 18 -1
bptol 5 19 -1
bptol 5 20 -1
bptol 5 21 -1
bptol 5 22 -1
bptol 5 23 -1
bptol 5 24 -1
bptol 6 15 -1
bptol 6 16 -1
bptol 6 17 -1
bptol 6 18 -1
bptol 6 19 -1
bptol 6 20 -1
bptol 6 21 -1
bptol 6 22 -1
bptol 6 23 -1
bptol 6 24 -1
bptol 7 15 -1

bptol 7 16 -1
bptol 7 17 -1
bptol 7 18 -1
bptol 7 19 -1
bptol 7 20 -1
bptol 7 21 -1
bptol 7 22 -1
bptol 7 23 -1
bptol 7 24 -1
bptol 8 15 -1
bptol 8 16 -1
bptol 8 17 -1
bptol 8 18 -1
bptol 8 19 -1
bptol 8 20 -1
bptol 8 21 -1
bptol 8 22 -1
bptol 8 23 -1
bptol 8 24 -1
bptol 9 15 -1
bptol 9 16 -1
bptol 9 17 -1
bptol 9 18 -1
bptol 9 19 -1
bptol 9 20 -1
bptol 9 21 -1
bptol 9 22 -1
bptol 9 23 -1
bptol 9 24 -1
bptol 10 15 -1
bptol 10 16 -1
bptol 10 17 -1
bptol 10 18 -1
bptol 10 19 -1

bptol 10 20 -1
bptol 10 21 -1
bptol 10 22 -1
bptol 10 23 -1
bptol 10 24 -1
bptol 11 15 -1
bptol 11 16 -1
bptol 11 17 -1
bptol 11 18 -1
bptol 11 19 -1
bptol 11 20 -1
bptol 11 21 -1
bptol 11 22 -1
bptol 11 23 -1
bptol 11 24 -1
bptol 12 15 -1
bptol 12 16 -1
bptol 12 17 -1
bptol 12 18 -1
bptol 12 19 -1
bptol 12 20 -1
bptol 12 21 -1
bptol 12 22 -1
bptol 12 23 -1
bptol 12 24 -1
c ##nodal merging between plate and reaction frame##
bptol 1 5 -1
bptol 1 6 -1
bptol 1 7 -1
bptol 1 8 -1
bptol 1 9 -1
bptol 1 10 -1
bptol 1 11 -1
bptol 1 12 -1

bptol 2 5 -1
bptol 2 6 -1
bptol 2 7 -1
bptol 2 8 -1
bptol 2 9 -1
bptol 2 10 -1
bptol 2 11 -1
bptol 2 12 -1
bptol 3 5 -1
bptol 3 6 -1
bptol 3 7 -1
bptol 3 8 -1
bptol 3 9 -1
bptol 3 10 -1
bptol 3 11 -1
bptol 3 12 -1
bptol 4 5 -1
bptol 4 6 -1
bptol 4 7 -1
bptol 4 8 -1
bptol 4 9 -1
bptol 4 10 -1
bptol 4 11 -1
bptol 4 12 -1
c ##nodal merging between plate, reaction frame and air##
bptol 13 1 -1
bptol 13 2 -1
bptol 13 3 -1
bptol 13 4 -1
bptol 13 5 -1
bptol 13 6 -1
bptol 13 7 -1
bptol 13 8 -1
bptol 11 9 -1

```
bptol 13 10 -1
bptol 13 11 -1
bptol 13 12 -1
bptol 14 1 -1
bptol 14 2 -1
bptol 14 3 -1
bptol 14 4 -1
bptol 14 5 -1
bptol 14 6 -1
bptol 14 7 -1
bptol 14 8 -1
bptol 14 9 -1
bptol 14 10 -1
bptol 14 11 -1
bptol 14 12 -1
st 0.001
endpart merge
c $$$$$$$$$$$$$$$$$$$$$$$$$$$$$$$$$$$$$$$$$$$$
c surface air
c part 25
block
1 2;
1 2;
1 2 3 4 5 6 7;
0 1;
-2 0;
-2 -0.5 -0.1 0 0.1 0.5 2;
mseq i 10;
mseq j 9;
mseq k 7 2 0 0 2 7;
dei 1 2; 1 2; 1 4;
bb 1 1 4 2 1 7 1 ;
mb 1 1 4 2 2 7 y +2
mate 502
```

```
endpart
c part 26
block
1 2;
1 2;
1 2 3 4 5 6 7;
0 1;
-2 0;
-2 -0.5 -0.1 0 0.1 0.5 2;
mseq i 10;
mseq j 9;
mseq k 7 2 0 0 2 7;
dei 1 2; 1 2; 4 7;
bb 1 1 1 2 1 4 2 ;
mb 1 1 1 2 2 4 y +2
mate 503
endpart
c part 27
block
1 2 3;
1 2;
1 2 3 4 5 6 7;
-1 -0.25 0;
-2 0;
-2 -0.5 -0.1 0 0.1 0.5 2;
mseq i 15 5;
mseq j 9;
mseq k 7 2 0 0 2 7;
dei 1 3; 1 2; 1 4;
mb 1 1 4 3 2 7 y +2
bb 1 1 4 3 1 7 3 ;
mate 504
endpart
c part 28
```

block
1 2 3;
1 2;
1 2 3 4 5 6 7;
-1 -0.25 0;
-2 0;
-2 -0.5 -0.1 0 0.1 0.5 2;
mseq i 15 5;
mseq j 9;
mseq k 7 2 0 0 2 7;
dei 1 3; 1 2; 4 7;
mb 1 1 1 3 2 4 y +2
bb 1 1 1 3 1 4 4 ;
mate 505
endpart
c part 29
block
1 41 51 56 60 66;
1 2;
1 2 3 4 5 6 7;
1 2 2.5 3 4 10;
-2 0;
-2 -0.5 -0.1 0 0.1 0.5 2;
dei 1 6; 1 2; 1 4;
mseq j 9;
mseq k 7 2 0 0 2 7;
mb 1 1 4 6 2 7 y +2
bb 1 1 4 6 1 7 5 ;
mate 506
endpart
c part 30
block
1 41 51 56 60 66;
1 2;

1 2 3 4 5 6 7;
1 2 2.5 3 4 10;
-2 0;
-2 -0.5 -0.1 0 0.1 0.5 2;
dei 1 6; 1 2; 4 7;
mseq j 9;
mseq k 7 2 0 0 2 7;
mb 1 1 1 6 2 4 y +2
bb 1 1 1 6 1 4 6 ;
mate 507
c merging between air
bptol 25 26 0.001
bptol 25 27 0.001
bptol 25 28 0.001
bptol 25 29 0.001
bptol 25 30 0.001
bptol 26 27 0.001
bptol 26 28 0.001
bptol 26 29 0.001
bptol 26 30 0.001
bptol 27 28 0.001
bptol 27 29 0.001
bptol 27 30 0.001
bptol 28 29 0.001
bptol 28 30 0.001
bptol 29 30 0.001
c merging between air and water
stp 0.001
endpart merge

VITAE

Keith G. Webster graduated in 2003 from Virginia Tech with a B.S. in Ocean Engineering. The author successfully defended this thesis on January 29, 2007 to complete his Master of Science degree in Ocean Engineering from Virginia Tech. While attending Virginia Tech he worked as an undergraduate research assistant for Dr. Alan Brown and his graduate research assistant John Sajdak (currently Dr. John Sajdak is the Ship Survivability Director for Alion Science and Technology) from August 2002 through May 2003. The author is a member of the Society of Naval Architects and Marine Engineers (SNAME) and the American Society of Naval Engineers (ASNE).